# Regulation of The Carotid Body Type-1 Cell by Lipid Signalling Pathways

A thesis submitted to the Department of Physiology, Anatomy and Genetics, in partial fulfilment of the requirements for the degree of

*Doctor of Philosophy*


**Zaki Alsahafi**

Balliol college, University of Oxford, United Kingdom

Trinity term 2023

# Abstract

Despite several proposed theories, the precise mechanism underlying acute oxygen sensing in type-1 cells of the carotid body remains elusive. This thesis investigates the role of Gq- coupled receptors and PLC signalling molecules in the regulation of carotid body type-1 cells by utilizing $Ca^{2+}$ measurements and single channel electrophysiology. This thesis investigates the involvement of these signalling molecules in hypoxia-induced $[Ca^{2+}]i$ rise and TASK channel inhibition in type-1 cells. In addition, this thesis examines the role of PLC signalling molecules in mediating the effects of metabolic poisons and volatile anaesthetics on TASK channels in type-1 cells. This thesis seeks to address the question as to whether there might be a common signalling pathway mediating all these effects. Specifically, it proposes that lipid signalling may ultimately be central to all these forms of TASK channel regulation.

Following the general introduction and methods chapters, chapter 3 examines the effects of Gq- coupled receptors and PLC signalling molecules on the hypoxia-induced $[Ca^{2+}]i$ rise in type-1 cell. The results show that hypoxia-induced $[Ca^{2+}]i$ rise was sensitive to alterations in Gq-coupled receptors and PLC-signalling molecules, suggesting that these signalling molecules are involved in mediating the hypoxia-induced $[Ca^{2+}]i$ rise in type-1 cells.

Chapter 4, further examines the role of these signalling molecules by looking at their effects on the activity of TASK channels in type-1 cells. This chapter presents novel findings demonstrating the involvement of PLC signalling molecules in mediating the hypoxic inhibition of TASK channels in type 1 cells. It proposes a model for acute oxygen sensing in these cells, incorporating findings from chapters 3 and 4.

Chapter 5 examines the role of PLC signalling molecules in mediating the effects of metabolic inhibitors on TASK channels. Metabolic inhibitors are known to inhibit TASK channels in type-1 cells and other cell types. We further confirmed this and showed that these effects are not likely to be mediated by PLC-produced DAG.

Chapter 6 examines the interactions between DAG and halothane on TASK channels in type-1 cells. We demonstrated that DiC8, a DAG analogue, induced a strong, reversible, and dose-dependent inhibition of TASK channels and inhibited the halothane-induced activation of these channels. These novel findings support the hypothesis that anaesthetics and endogenous ligands may compete for binding sites in sensitive proteins.

In conclusion, this thesis presents novel findings on the role of Gq-coupled receptors and PLC signalling molecules in the regulation of carotid body type-1

cells and suggests that these signalling molecules are involved in mediating the responses of type-1 cells to various endogenous and exogenous stimuli. Additionally, it posits that PLC signalling molecules establish a connection between metabolic function and the modulation of TASK channels by hypoxia in type-1 cells.

## Acknowledgment

I am deeply grateful to my supervisors, **Professor Keith Buckler**, and **Professor Jaideep Pandit.** To Keith, I owe my deepest gratitude. Thank you Keith for granting me the privilege to work in your laboratory. The time and effort you willingly spent teaching me the experimental techniques essential for this thesis have been invaluable. I am profoundly grateful for the time you devoted to review earlier drafts of this thesis, and I will always cherish your insightful comments and unique perspective. Throughout the last four years, I have often sought advice by knocking on Keith's office door, and each time, he has generously shared his wisdom and expertise.

I would also like to express my profound gratitude to Jaideep for his invaluable contribution to this thesis. I have always enjoyed my discussions with Jaideep since our very first meeting in 2019. Jaideep's critical thinking, optimism, dedication, and above all his uplifting remarks at the end of each meeting have consistently motivated and enlightened me.

I would like to thank members of the **Department of Physiology, Anatomy, and Genetics** for their assistance in facilitating this research.
My sincere gratitude goes to **King Saud bin Abdulaziz University for Health Sciences** for granting the PhD scholarship that made this project possible.

Lastly, I am profoundly thankful to my wife **Nouf** for her unwavering love and support throughout this journey.

# Table of contents

# List of Figures

## Chapter 1.



## Chapter 2.

**Chapter 3.**

**Chapter 4.**

## Chapter 5.



## Chapter 6.

**Chapter 7.**

## List of Tables

## Chapter 2.



## Chapter 6.

# List of abbreviation

**[$Ca^{2+}$]i** intracellular $Ca^{2+}$ concentration

**2-AG** 2-Arachidonoylglycerol

**4-AP** 4-aminopyridine

**AHVR** acute hypoxia ventilatory response

**AICAR** 5-Aminoimidazole-4-carboxamide ribonucleotide

**AMPK** adenosine monophosphate activated protein kinase

**AMPK** AMP-activated protein kinase

**ATP** adenosine triphosphate

**BKca** large-conductance $Ca^{2+}$-activated channel

**CGNs** cerebellar granule neurons

**CHO** chinese hamster ovary cells

**CO** carbon monoxide

**COS-cells** fibroblast-like cell lines derived from monkey kidney tissue

**D5919** diacylglycerol Kinase Inhibitor I

**DAG** diacylglycerol

**DiC8** 1,2 dioctanoyl-*sn*-glycerol

**DMSO** dimethyl sulfoxide

**EGTA** ethylene glycol-*bis*(2-aminoethylether)-*N*,*N*,*N*',*N*'-tetraacetic acid

factor (NGF)

**FCCP** carbonyl cyanide 4-(trifluoromethoxy) phenylhydrazone

**GPCR** G-protein-coupled receptors

**$H_2S$** hydrogen sulphite

**HEK293 cells** human Embryonic Kidney (HEK) 293

**HVR** hypoxic ventilatory response

**IP3** inositol triphosphate

**K2P** two pore $K^+$ channel

**Kd** equilibrium dissociation constant

**KO** knock out

**MCI** mitochondrial complex 1

**NaCN** sodium cyanide

**NADH** nicotinamide adenine dinucleotide

**NADPH** nicotinamide adenine dinucleotide phosphate

**nPopen** estimated channel open probability

**OAG** oleoyl-2-acetyl-sn-glycerol

**Olfr78** olfactory receptor-78

**PA** phosphatidic acid

**PAPs** phosphatidic acid phosphatases

**PBS** phosphate-buffered saline

**PIP2** phosphatidylinositol 4,5-bisphosphate

**PKC** protein kinase C

**PLC** phospholipase C

**PMA** phorbol 12-myristate 13-acetate

**PMT** photomultiplier tube

**PNA** peanut agglutinin

**$PO_2$** partial pressure of oxygen

**Rh123** rhodamine 123

**ROS** reactive oxygen species

**SCG** superior cervical ganglion

**SEM** standard error of the mean

**TALK channels** alkaline pH-activated K2P-channels

**TASK** TWIK-related acid-sensing $K^+$ channel

**TEA** tetraethylammonium

**THIK channels** halothane-inhibited K2P-channels

**TRAAK** TWIK-related arachidonic-acid-stimulated $K^+$ channel

**TREK channels** lipid and mechanosensitive K2P-channels

**TREK** TWIK-related $K^+$-channel

**TRESK channels** spinal cord K2P-channel

**TrkA** a cell surface transmembrane receptor tyrosine kinase for nerve growth

**TWIK** tandem of p domains in a weak inward rectifying $K^+$ channel

# Chapter 1. Introduction

## 1.1 The role of chemoreceptors in oxygen homeostasis

Oxygen is essential for cellular metabolism and plays a crucial role in facilitating the optimal functioning of many organs and tissues, including the brain, heart, and muscles. The maintenance of oxygen homeostasis in the body relies on a complex regulatory process that encompasses interactions between the cardiovascular and respiratory systems.

Chemoreceptors play a crucial role in the control of respiration. They detect changes in oxygen, carbon dioxide, and pH levels in the blood and then send this information to the respiratory centres in the brain. The respiratory centres respond by initiating adaptive changes in ventilation, leading to an increase in both the rate and depth of breathing. Moreover, chemoreceptors elicit cardiovascular reactions to enhance the delivery of oxygen to tissues, including vasoconstriction and an increase in heart rate. These coordinated responses strive to maintain oxygen homeostasis and ensure the proper functioning of essential organs. The carotid body conveys sensory information through the glossopharyngeal nerve to the brainstem, specifically the medulla oblongata. This plays a significant role in conditions of carotid body hyperactivity, which results in sympathetic overactivation, leading to hypertension, heart failure, and arrhythmia (Ludbrook, 1990).

## 1.2 Overview of thesis objectives.

This thesis explores the regulatory mechanisms of rat carotid body type-1 cell TASK channels in response to hypoxia, ATP, and $G_{q/11}$ coupled receptors. It also investigates the impact of volatile anaesthetics as significant modulators of TASK channels, highlighting their potential clinical implications. Additionally, this thesis seeks to address the question as to whether there might be a common signalling pathway mediating all these effects. More specifically, I suggest that, ultimately, lipid signalling may be central to all these forms of TASK channel regulation.

In the third chapter, I examined the effects of $G_{q/11}$ and phospholipase C (PLC) activation/inhibition as well as downstream signalling molecules on $Ca^{2+}$ signalling, hypoxia, and muscarinic-evoked $[Ca^{2+}]i$ entry in type-1 cells. In Chapter 4, I directly examined the effects of these signalling molecules on the activity of TASK channels in type-1 cells, first in cell-attached patches and then in the inside-out configuration. The final part of this thesis investigates the interactions between PLC downstream signalling molecules and two other known regulators of TASK channels: metabolic poisons (or ATP) and halothane.

This introduction is divided into four main sections:

(1) The first section focuses on the physiology of the carotid body and the process of chemotransduction in type-1 cells. In this context, I will introduce the central role of TASK channels in mediating cellular excitation in type-1 cells. This section will also discuss contemporary hypotheses as to the nature of the molecular sensor of acute hypoxia in the carotid body.

(2) The second section will review the structure, gating mechanisms, and functional properties of the two-pore domain $K^+$ channels (K2P) in

general. It will also elaborate on the expression, functional, and biophysical properties of TASK channels.

(3) The third section will review the regulation of TASK channels by GPCRs and downstream signalling pathways.

(4) The fourth section of this thesis focuses on the regulation of TASK channels by anaesthetics. The last part of the introduction will focus on the justifications and objectives of the experimental chapters of this thesis.

## 1.3 Carotid body anatomy and excitation by hypoxia

### 1.3.1 Anatomy

The carotid body is a very small organ located at the bifurcation of the common carotid artery, adjacent to the superior cervical sympathetic ganglion (Daly, 1997; Milsom and Burleson, 2007). Its long axis length averages approximately 3 mm in humans, 1.5 mm in cats or dogs, and approximately 750 μm in rats. Its wet weight varies among species, ranging from 13 mg in humans to 600 μg in cats and 60 μg in rats (Heath et al., 1970; Hess, 1975; McDonald, 1981; Verna, 1980; Kumar and Prabhakar, 2012).

The carotid body is highly vascularised and receives the highest blood flow per tissue weight (1000-2000 ml $min^{-1}$ 100 $g^{-1}$) (Barnett et al., 1988; Daly et al., 1954; Prabhakar and Joyner, 2015). In most species, blood supply to the carotid body originates from one artery branching off the dorsolateral aspect of the external carotid artery (McDonald and Laure, 1983; Verna, 1980). In order to regulate the high blood flow, the carotid body possesses a complex vascular structure comprising multiple arteriovenous anastomoses and fenestrated capillaries (McDonald and Laure, 1983; Verna, 1980).

Chemoreceptors of the carotid body are relatively unaffected by acute reductions in blood flow or arterial pressure. This suggests that, within the physiological range, the discharge of chemoreceptors is mainly regulated by $PO_2$ rather than perfusion pressure or total volume of blood flow (Biscoe et al., 1970). However, under pathological conditions, such as chronic heart failure, a sustained reduction in blood flow to the carotid body is involved in the augmentation of peripheral chemoreflex sensitivity (Ding et al., 2012).

Innervation of the carotid body involves a complex network of afferent and efferent neural pathways. It receives afferent sensory innervation from the

carotid sinus nerve, which is a branch of the glossopharyngeal nerve. Ascending pathways of the carotid sinus nerve convey chemoreceptive information to the nucleus tractus solitarius in the dorsal respiratory group. Reciprocal synapses connect sensory nerve endings to type-1 cells, thereby creating an inhibitory feedback loop. When excitatory neural input is activated, type-1 cells release inhibitory transmitters, thereby reducing the sensitivity of the chemoreceptive nerve (Campanucci and Nurse, 2007; McDonald and Mitchell, 1975; Sampson, 1972).

Descending pathways project to type-1 cells as well as the vasculature and can be identified by the expression of neuronal nitric oxide (NO) synthase. NO inhibits transmitter release from type-1 cells and causes vasodilation, resulting in an elevation of blood flow. Therefore, the overall effect of efferent innervation of the carotid body is inhibitory for chemoafferent discharge, which plays an important role in carotid body plasticity in chronic hypoxia (Campanucci and Nurse, 2007; Kumar and Prabhakar, 2012; Wang, 1995). Additionally, sympathetic fibres originating from the superior cervical ganglion innervate the carotid body. This assumes a pivotal role in regulating blood flow and could potentially impact the function of type-1 cells (Felippe et al., 2023).

### 1.3.2 Physiology

The carotid body consists of two types of cells: type-1 and type-2. Type-1 cells, also commonly referred to as “glomus cells”, are oval-shaped in microscopic sections. However, when isolated in vitro, their shape changes to a more spherical shape with a diameter of 8-15 μm in rats (Kumar and Prabhakar, 2012; McDonald and Mitchell, 1975). The number of type-1 cells per carotid body varies among different species, ranging from 12,000 cells in rats to 60,000 cells in cats (Kumar and Prabhakar, 2012; McDonald, 1981; Verna, 1980).

Type-1 cells serve as primary chemoreceptors and are distinguished by their abundance of dense-cored secretory vesicles primarily containing catecholamines, particularly dopamine (Hansen et al., 1982).

In contrast, type-2 cells play a supporting role similar to glial cells in neuronal tissues (Daly, 1997; Milsom and Burleson, 2007). They represent less than 20% of the total cell count of the carotid body (Kock, 1954; Kock and Dunn, 1966). Type-2 cells are smaller than type-1 cells and do not have secretory vesicles (Kumar and Prabhakar, 2012). They are described as unexcitable because they do not respond to hypoxia at the same stimulus levels that stimulate type-1 cells (Duchen et al., 1988; Lopez-Lopez et al., 1989; Pedal et al., 2007; Urena et al., 1989; Xu et al., 2003). Nevertheless, they appear to be involved in carotid body plasticity in chronic hypoxia (Pardal et al., 2007; Platero-Luengo et al., 2014). However, the functional significance of type-2 cells is yet to be fully understood. More recent studies suggest that type-2 cells may contribute to the paracrine signalling within the carotid body. This is supported by findings indicating that type-2 cells express a variety of GPCRs and can be activated by diverse neurotransmitters released from type-1 cells. Additionally, upon stimulation, type-2 cells release ATP, contributing to the phenomenon known as “ATP-induced ATP-release”. This occurs following chemotransduction-induced activation of paracrine signalling within the carotid body (Nurse et al., 2018).

### 1.3.3 Hypoxia evoked events in the carotid body

The carotid body is unique in that even a small reduction in arterial $PO_2$ (e.g., 80-60 mm Hg) is sufficient to instantaneously trigger afferent nerve activation in the carotid body (Biscoe et al., 1970; Parabhkar, 2006).

It is established that the hypoxic chemotransduction process in type-1 cells of the carotid body starts with a reduction of the resting membrane potential, which is primarily maintained by TWIK-related acid-sensitive $K^+$ channels (TASK channels), resulting in membrane depolarisation, which opens voltage-gated $Ca^{2+}$ channels. This, in turn, leads to $Ca^{2+}$ influx and neurosecretion of various neurotransmitters, such as acetylcholine, ATP, adenosine, dopamine, noradrenaline, and serotonin (Buckler, 2015; Gonzalez et al., 1994; Nurse, 2014; Rigual et al., 1984; Rong et al., 2003; Zhang and Nurse, 2004).

Neurotransmitters excite sensory nerve endings on the carotid sinus nerve, which, in turn, activate central respiratory centres, thereby increasing the depth and frequency of breathing. ATP is widely recognised as a crucial neurotransmitter that plays a significant role in the activation of P2X2/3 receptors located on afferent nerve endings in close proximity to type-1 cells (Zhang and Nurse, 2004). Additionally, acetylcholine and adenosine are two important neurotransmitters that are highly expressed in the carotid body type-1 cells and are involved in hypoxia-induced post synaptic excitation (Conde et al., 2012).

A balance between inward and outward currents maintains the resting membrane potential of acutely isolated type-1 cells at -50 to -60 mV (Buckler, 2000, 2012, 2015; Buckler and Vaughan-Jones, 1994). Nevertheless, the background $K^+$ current in type-1 cells is significantly inhibited in response to hypoxia (by 50 to 80%) and/or acidosis (by 50 to 60%) (Buckler, 1994; Buckler et al., 2000). This $K^+$ current was originally characterised by its acid sensitivity, voltage insensitivity, and resistance to $K^+$ channel blockers (TEA and 4-AP) (Buckler, 1997, 2000).

The molecular identity of the background or leak current of type-1 cells remained a mystery until the TASK channel (TASK-1) was first cloned and described (Duprat et al., 1997). Two years later, the TASK 3 channel was cloned (Rajan et al., 2000). TASK channels consist of four transmembrane domains and two pore domains. They are expressed in neurons, cardiac myocytes, and vascular smooth muscle cells, where they participate in regulating circadian rhythm, heart rate, and pulmonary vascular tone (Bayliss et al., 2001; Decher et al., 2011; Gurney et al., 2003; Jones et al., 2002; Karschin et al., 2001; Olschewski et al., 2006; Putzke et al., 2007; Sirois et al., 2000; Steinberg et al., 2015). TASK channels produce $K^+$ currents that exhibit all the characteristics of background conductance. These currents are characterised by their voltage insensitivity, resistance to classical $K^+$ channel blockers (TEA and 4-AP), and pH sensitivity (Buckler, 1997; Buckler et al., 2000; Duprat et al., 1997). TASK 1 and TASK 3 channels have been reported to form heterodimers in certain expression systems. The co-expression of TASK1 and TASK3 channels in Xenopus oocytes resulted in a current with intermediate pH sensitivity (Czirjak and Enyedi, 2002).

The kinetic properties of the background or leak current of the type-1 cell were similar to those of the TASK channel in terms of their mild inward rectification, flickery openings of short duration, inhibition by zinc, quinidine, and bupivacaine, and activation by halothane. These similarities have led to the suggestion that the oxygen-sensitive current of the type-1 cell is carried by TASK channels. This was later supported by pharmacological and genetic studies (Buckler, 1997, 2000; Kim et al., 2009a; Turner and Buckler, 2013b).

Although TASK channel inhibition is the primary cause of cellular depolarization and excitation in response to both hypoxia and acidosis in type-1 cells, other channels may also contribute, such as high-threshold voltage-gated $Ca^{2+}$ channels that become active at potentials higher than -50 mV (Buckler and

Vaughan-Jones, 1994). Hypoxia-evoked $Ca^{2+}$ entry into type-1 cells is largely mediated by L- and N-type $Ca^{2+}$ channels (Silva and Lewis, 1995).

In addition to TASK channels and $Ca^{2+}$ channels, type-1 cells also express $Cl^-$ channels, voltage-gated $Na^+$ channels, voltage-gated (delayed rectifier) $K^+$ channels, and an uncharacterised background $Na^+$ conductance (Buckler, 1997; Buckler, 2015; Carpenter and Peers, 1997, 2001; Duchen et al., 1988; Lopez-Lopez et al., 1997; Urena et al., 1989). Furthermore, TREK channels were also implicated in the acute oxygen sensitivity of type-1 cells (Yamamoto and Taniguchi, 2005; Kreneisz et al., 2009). Furthermore, other researchers have proposed the participation of transient receptor potential (TRP) channels and other non-selective $Ca^{2+}$-activated currents in the hypoxic chemotransduction process in the carotid body type-1 cells (Kumar et al., 2006; Kim et al., 2015).

Although the inhibition of TASK-like $K^+$ channels in response to hypoxia is widely accepted, it is still unclear how $PO_2$ levels are linked to the activity of these channels in type-1 cells. Two experiments were conducted to investigate the underlying mechanisms of hypoxia-induced inhibition of TASK-like $K^+$ channels in type-1 cells and to determine whether these channels are directly sensitive to oxygen. The first experiment involved expressing TASK channels in other cell types, such as HEK cells, and determining whether they maintained their sensitivity to oxygen. When the human TASK-1 channel was expressed in HEK-293 cells, it was found that its activity was modulated by reductions in $PO_2$. This suggests that TASK channels are directly sensitive to oxygen (Lewis et al., 2001). However, later research failed to replicate these findings and demonstrated that TASK channels remained largely unaffected by reductions in $PO_2$ (Buckler and Honore, 2004; Buckler, 2015).

The second experiment was conducted on the excised patches of type-1 cells. If TASK channels are directly sensitive to oxygen, they should be able to maintain responsiveness to oxygen even when isolated from the cellular environment in excised patches. Buckler et al. (2000) reported that TASK channels rundown after patch excision and lose their sensitivity to oxygen. These two experiments demonstrate that TASK channels are not directly sensitive to oxygen and that cellular constituents are necessary for their functionality. Consequently, type-1 cells may contain cytosolic signalling molecules or cofactors that confer oxygen sensitivity to TASK channels.

### 1.3.4 Oxygen sensing hypotheses

Several hypotheses have emerged over the years regarding the identity of the $O_2$ sensor in type-1 cells, which will be discussed in the following section. In 1972, Mills and Jobsis demonstrated that reduction in cytochrome a3 (complex IV) occurs simultaneously with chemoreceptor discharge in the carotid body of cats. They proposed that cytochromes in the carotid body mitochondria might have a lower affinity for oxygen than those found in other cells. Later, in 1992, Duchen and Biscoe demonstrated that type-1 cells exhibit changes in mitochondrial NADH levels when $PO_2$ falls below 60 mmHg, in contrast to other tissues such as chromaffin cells, where this change occurs only when $PO_2$ drops below 5 mmHg. They suggested that mitochondria in type-1 cells can modify respiratory function across the physiologically relevant range of $PO_2$ (Duchen and Biscoe, 1992a, b).

More recent findings have demonstrated that the mitochondria of type-1 cells have a gene expression profile that is distinct from that of other cell types. Specifically, genes encoding COX4I2 and COX8b, which are atypical isoforms of the more widely distributed COX4I1 and COX8A subunits found in

mitochondrial complex IV, were highly expressed in type-1 cells (Fernández-Agüera et al., 2015; Gao L et al., 2017; Moreno-Domínguez et al., 2020). Mice with genetic deletions of NduFs2, a subunit of mitochondrial complex I, and COX4I2 have demonstrated compromised oxygen sensitivity in the carotid body (Fernández-Agüera et al., 2015; Moreno-Domínguez et al., 2020). Consequently, a model has been proposed suggesting that the distinctive metabolic profile represented by these genes is likely responsible for the acute oxygen-sensing capabilities of type-1 cells (Ortega-Sáenz and López-Barneo, 2020). Furthermore, it has recently been discovered that a novel subunit of mitochondrial complex VI, known as HIGD1C, is predominantly expressed in type-1 cells. Mutant mice lacking the Higd1c protein exhibit impaired oxygen sensitivity and diminished responses to metabolic toxins (Timòn-Gòmez et al., 2022).

Metabolic inhibitors, such as rotenone, cyanide, FCCP, and oligomycin, significantly inhibit the oxygen-sensitive background $K^+$ current in type-1 cells and evoke a $Ca^{2+}$ influx; therefore, they mimic the effects of hypoxia. Moreover, the effects of hypoxia and metabolic inhibitors on type-1 cells are mutually exclusive, suggesting that they share the same mechanism of action (Wyatt and Buckler, 2004).

Additionally, metabolic inhibitors have been shown to modulate all three forms of TASK channels, including TASK1, TASK3, and TASK1/TASK3 heterodimers, in TASK-knockout (KO) mice (Turner and Buckler, 2013b). The remaining question, however, is: what is the link between metabolic function and chemotransduction in type-1 cells?

### 1.3.5 Potential oxygen-mediated signalling pathways within type 1 cells

#### A possible role of ATP

Varas et al. (2007) demonstrated that TASK-like $K^+$ channels in carotid body type-1 cells are strongly activated by MgATP in inside-out patches. Therefore, MgATP could be the link between metabolic function and $O_2$ sensing in type-1 cells. Under normoxic conditions, TASK channel activity is maintained by normal levels of MgATP. However, under hypoxic conditions, low MgATP levels inhibit TASK channels. Although MgATP can stimulate TASK channels in type-1 cells, there is no known nucleotide binding site in the primary sequence of TASK channels, and there are no reports of cloned TASK1 or TASK3 channels being MgATP-sensitive (Buckler, 2015). Thus, a MgATP-dependent cytosolic signalling molecule may be required to link MgATP levels to TASK channel activity.

#### A possible role of AMPK

In response to hypoxia, mitochondrial electron transport is suppressed, leading to an increase in the AMP/ATP ratio. This triggers the activation of AMP-activated protein kinase (AMPK). Once activated, AMPK phosphorylates ion channels, causing cell depolarisation and neurosecretion. Therefore, AMPK has been proposed to link reductions in $PO_2$ to TASK channels inhibition and the subsequent depolarization of type-1 cells. In isolated type-1 cells, the application of AICAR, an AMPK activator, inhibited $O_2$ sensitive $K^+$ currents, depolarised the plasma membrane, induced voltage-gated $Ca^{2+}$ entry, and increased sensory afferent discharge. Therefore, it mimics the key aspects of the hypoxic response in these cells. In contrast, the AMPK antagonist compound C

reverses the effects of AICAR and hypoxia on type-1 cells (Evans et al., 2005; Wyatt et al., 2007). It has also been shown that the TASK3 channel expressed in HEK293 cells was inhibited by AICAR and this was antagonised by compound C, whereas the TASK1 channel was insensitive to AICAR (Dallas et al., 2009). These findings led to the hypothesis that AMPK mediates the hypoxic inhibition of TASK channels in type-1 cells. Later pharmacological research, however, called this into question. First, the results with AMPK activators and inhibitors could not be replicated. Kreneisz et al. (2004) reported that AICAR had no effect on TASK channels expressed in HEK293 cells. Another study also failed to find any AICAR or compound C effect on TASK channels or the hypoxic inhibition of these channels in isolated rat type-1 cells (Kim et al., 2014). Second, there is uncertainty regarding the selectivity of both compound C and AICAR, as some of their cellular effects have been found to be independent of AMPK (Emerling et al., 2007; Guigas et al., 2007). Furthermore, AMPK deletion did not result in any reduction in hypoxia-evoked afferent discharge from the carotid body (Mahmoud et al., 2016). Therefore, it is unlikely that AMPK is involved in the hypoxic chemotransduction process in type-1 cells.

**A possible role of LKB1**

Recent findings have demonstrated that deletion of the gene encoding LKB1, a kinase that operates upstream of AMPK and activates it in response to metabolic stresses, such as hypoxia, in type-1 cells has significant effects on carotid body function. Specifically, the absence of LKB1 suppressed carotid body basal afferent discharge, attenuated its afferent input responses to hypoxia and hypercapnia, and blocked hypoxia-evoked $Ca^{2+}$ entry in type-1 cells.

Based on these results, a proposed model of acute oxygen sensing suggests that the baseline sensitivity of the carotid body to hypoxia and

hypercapnia is determined by the level of LKB1 expression. It is thought that the interaction between LKB1 and AMPK signalling pathways is critical for detecting and integrating signals within a hypoxia-responsive circuit downstream of the carotid body (MacMillan et al., 2022).

**A possible role of ROS**

Both genetic and pharmacological studies have revealed the important role of mitochondrial complex I (MCI) in the $O_2$ sensitivity of type-1 cells. Pharmacological inhibition or genetic disruption of MCI abolished the hypoxic response of type-1 cells (Fernandez-Aguera et al., 2015; Ortega-Saenz et al., 2003; Wyatt and Buckler, 2004). Moreover, restoration of mitochondrial NADH dehydrogenase activity in MCI-deficient mice completely restores the hypoxic response of type-1 cells (Jimènes-Gómez et al., 2023). Therefore, a proposed model of acute $O_2$ sensing suggests that reduced cytochrome C oxidase activity under hypoxic conditions leads to a slowdown or reversion of MCI with NADH accumulation and ROS production. These changes in cellular metabolism and redox state modulate ion channels, ultimately resulting in membrane depolarisation (Ortega-Sáenz et al., 2020).

However, there is data contradicting the involvement of ROS in oxygen sensing. Papreck et al. (2012) reported that hydrogen peroxide only affected TASK channels when it was applied at a high non-physiological concentration. Moreover, in mouse carotid body preparations, the production of ROS during hypoxia either increased or decreased with no clear consistency (Bernardini et al., 2014). Furthermore, a substantial portion of the hypoxia-evoked chemoafferent discharge in rats carotid body persists after the administration of antioxidants that target mitochondrial ROS production (Swiderska et al., 2021). This underscores the involvement of signalling pathways other than ROS in the

hypoxia signalling cascade within the carotid body. In addition, TASK channel inhibition can be maintained even in the complete absence of oxygen (Buckler and Vaughan-Jones, 1994a; Buckler and Turner, 2013). Therefore, it is unlikely that ROS are essential for the hypoxic chemotransduction process in type-1 cells.

## A possible role of gaseous signalling molecules

Another possibility has arisen from studies utilising gaseous signalling molecules such as hydrogen sulphide ($H_2S$) and carbon monoxide (CO). The effects of $H_2S$ and CO mimic those of hypoxia. They depolarise type-1 cells by inhibiting background $K^+$ currents and TASK channels (Barbe et al., 2002; Buckler, 2012). However, $H_2S$ and CO can also inhibit mitochondrial metabolism. Therefore, the effects of $H_2S$ and CO on type-1 cells may be secondary to their effects on metabolic function (Buckler, 2015). While certain studies suggest the involvement of CO and $H_2S$ in oxygen sensing, divergent findings have been reported by others. The production of CO and $H_2S$ is mediated by hemeoxygenase -2 (HO-2) and cystathionine y-lyase (CSE), respectively. It has been proposed that hypoxia inhibits the production of CO, which leads to the activation of CSE, promoting $H_2S$ production (Rakoczy and Wyatt, 2018). However, mice lacking HO-2 maintain normal carotid body hypoxic sensitivity (Ortega-Saenz et al., 2006). Additionally, Kim et al. (2015) reported that inhibiting $H_2S$ production has no effect on TASK channels. Furthermore, the knockout of the enzymes involved in $H_2S$ production had no effect on carotid body oxygen sensitivity (Wang et al., 2017).

## A possible role of Olfr78

Chang et al. (2015) proposed that the olfactory receptor Olfr78 is the $O_2$ sensor responsible for mediating the acute oxygen sensitivity of type-1 cells. Olfr78 is highly and selectively expressed in type-1 cells and found to be activated by lactate (Chang et al., 2015; Zhou et al., 2016). Chang et al. (2015) reported that Olfr78 knockout mice have a lower hypoxic ventilatory response than wild-type mice. Therefore, they proposed a model of acute oxygen sensing in type-1 cells in which lactate accumulation under hypoxic conditions activates the Olfr78 receptor, which depolarises type-1 cells. However, subsequent research conducted by Chang's group and others failed to replicate these findings and reported that Olfr78 knockout mice exhibit a normal ventilatory response to hypoxia (Torres-Torrelo et al., 2018; Chang et al., 2018). Moreover, acutely isolated type-1 cells respond to hypoxia when continuously superfused with lactate-free hypoxic solutions. Therefore, it is unlikely that the hypoxic response of type-1 cells is mediated by lactate accumulation.

Later research suggested that Olfr78 plays a significant role in sensing and responding to a wide range of low $O_2$ levels in the carotid body. However, this was independent of lactate and did not contribute to the response to severe hypoxia (Peng et al., 2020). It has been recently proposed that Olfr78 activation is mediated by the production of $H_2S$ under hypoxic conditions (Peng et al., 2023).

## 1.4 K2P channels

### 1.4.1 Structure, functional properties, and gating of K2P channels

TASK channels are members of the two-pore domain potassium (K2P) channels. K2P is the most recently discovered group of mammalian $K^+$ channels. In mammals, 15 KCNK genes encoding K2P channels are expressed in various tissues, including the brain, heart, lung, kidney, and carotid body (Goldstein et al., 2001; Goldstein et al., 2005).

Eukaryotic K2P channels have been subdivided into six distinct subfamilies based on their structural and functional properties (Enyedi and Czirja, 2010; Goldstein et al., 2001; Renigunta et al., 2015):

1- TWIK channels - weakly inwardly rectifying
   TWIK-1 (K2P 1.1; KCNK1)
   TWIK-2 (K2P 6.1; KCNK6)
   TWIK-3 (K2P 7.1; KCNK7)

2- TREK channels - lipid and mechanosensitive
   TREK-1 (K2P 2.1; KCNK2)
   TREK-2 (K2P 10.1; KCNK10)
   TRAAK (K2P 4.1; KCNK4)

3- TASK channels - acid pH- inhibited
   TASK-1 (K2P 3.1; KCNK3)
   TASK-3 (K2P 9.1; KCNK9)

TASK-5 (K2P 15.1; KCNK15)

4- TALK channels - alkaline pH-activated

TASK-2 (K2P 5.1; KCNK5)

TALK-1 (K2P 16.1; KCNK16)

TALK-2 (K2P 17.1; KCNK17)

5- THIK channels - halothane inhibited

THIK-1 (K2P 13.1; KCNK13)

THIK-2 (K2P 12.1; KCNK12)

6- TRESK channels - spinal cord

TRESK (K2P 18.1; KCNK18)

K2P channels are frequently implicated in modulating the resting membrane potential and are commonly referred to as “leak”, “background”, or “open rectifier” channels. These terms refer to the current-to-voltage relationship of K2P channels, which is reasonably well described by the Goldman-Hodgkin-Katz (GHK) equation. Under physiological conditions (where intracellular $K^+$ concentration is higher than extracellular $K^+$ concentration), the ideal GHK $K^+$ rectifying channel is expected to exhibit strong outward rectification. On the other hand, when the concentration of $K^+$ is symmetrical, the rectification disappears and the current-to-voltage relationship should be nearly linear (Renigunta et al., 2015; Goldstein et al., 2001).

Crystallographic analysis of TRAAK and TWIK-1 channels has revealed the crystal structure of K2P channels (Brohawn et al., 2012; Miller and Long, 2012). Unlike other classical tetrameric $K^+$ channels, functional K2P channels appear to exist as dimers of subunits, each of which has four transmembrane domains (M1-M4), two pore regions (P1 and P2), and two extracellular cap

helices (C1 and C2), see Figure 1.1. The two subunits appear to assemble in a simple anti-parallel manner (Brohawn et al., 2012; Miller and Long, 2012; Renigunta et al., 2015).

The presence of the cap helix above the selectivity filter of K2P channels may explain their resistance to classical $K^+$ channel blockers, including pore-blocking toxins from the extracellular side (Brohawn et al., 2012; Steinberg et al., 2015). Further analysis of the crystal structure of TRAAK channels, utilising a higher resolution, revealed an unusual aspect of K2P pore domain architecture. Brohawn et al. (2013) reported that the C1 and M1 helices had undergone domain swapping, resulting in their relocation to the opposite side of the channel. The same phenomenon has also been reported in other K2P channels (Dong et al., 2015). However, the functional significance of this phenomenon remains to be determined (Renigunta et al., 2015).

Although commonly described as “leak” channels that are constitutively open at rest, many K2P channels are gated and regulated by a wide range of physiological and pharmacological regulatory inputs (Renigunta et al., 2015). Similar to other $K^+$ channels, K2P channels are thought to have two main gating mechanisms: an inactivation (or c-type) gate at the selectivity filter in close proximity to the extracellular side of the channel (upper gate) and an activation gate at the intracellular entrance of the channel (lower gate) (Mathie et al., 2010). The crystal structures of the mechanosensitive K2P channels TRAAK and TREK2 have revealed a unique mechanism for gating in K2P channels. These channels have been crystallised in two different confirmations: “up”, where the central cavity is open and the channel is conductive, and “down”, where the central cavity is blocked by lipid acyl chains and the channel is nonconductive (Brohawn, 2015; Brohawn et al., 2012, 2013, 2014; Lolicato et al., 2014; Miller et al., 2012). Piechotta et al. (2011) utilised high-affinity pore blockers of K2P channel in conjunction with systematic scanning mutagenesis

to investigate the pore structure and gating mechanisms of TREK-1 channels. They demonstrated that TREK-1 channels exist in an “open-state” configuration, and the primary gating mechanism is located at or within the selectivity filter and does not involve movement of the helix bundle crossing.

The most recent advances in K2P channels gating show that the opening and closing of the TASK1 channel pore are controlled by a lower ‘X-gate’. This gate is formed by interactions between the two crossed C-terminal M4 transmembrane helices at the vestibule entrance. This unusual conformation is formed by bending M4 on either side of a six-residue sequence (VLRFMT) (Rödström et al., 2020). The VLRFMT region has previously been shown to be critical for the regulation of TASK channels by anaesthetics and neurotransmitters (Patel et al., 1999; Tally and Bayliss, 2002; Veale et al., 2007). Mutations at the ‘X-gate’ of the TASK1 channel increased channel open probability, impaired sevoflurane-induced activation, GPCRs-mediated inhibition in the cell-attached mode, and DiC8-induced inhibition in excised patches (Rödström et al., 2020; Sörmann et al., 2022).

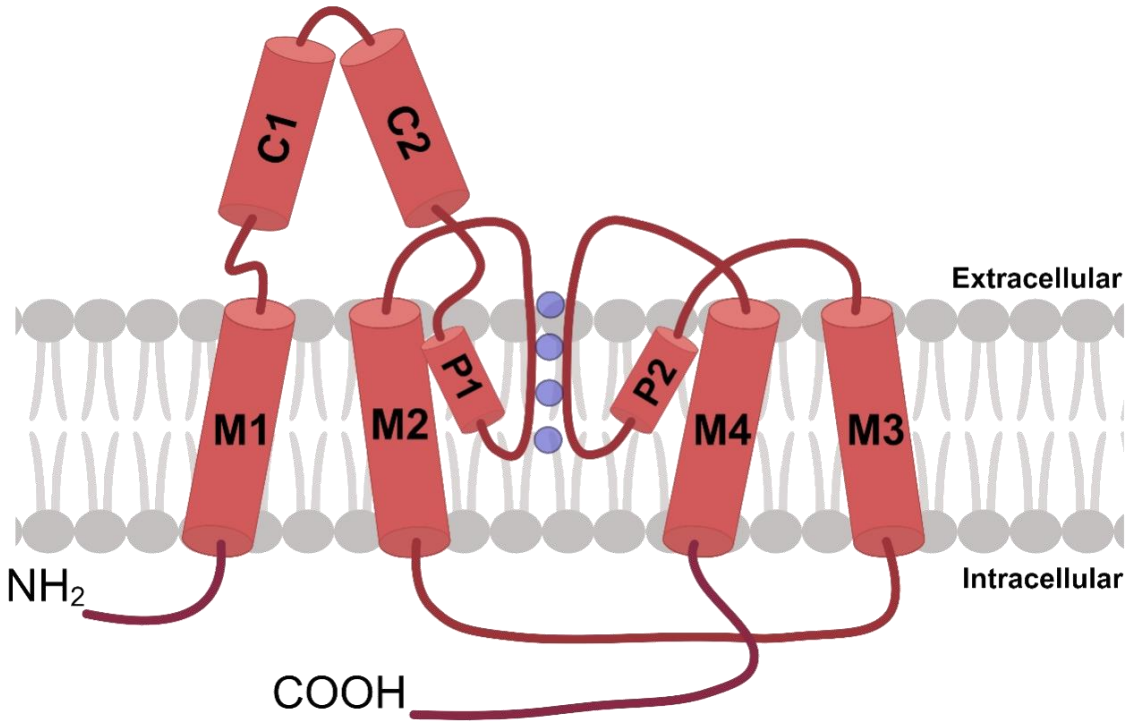


**Figure 1.1: General structure of K2P channels.** These channels comprise of four transmembrane domains (M1-M4), two pore-forming domains (P1 and P2) and two extracellular cap helices (C1 and C2). Picture based on (Renigunta et al., 2015).

### 1.4.2 Properties of TASK channels

In 1997, Buckler made a significant discovery regarding the hypoxic chemotransduction process in type-1 cells of the carotid body. He demonstrated the presence of a background or leak potassium current that is sensitive to changes in oxygen levels in these cells (Buckler, 1997).

As discussed in Section 1.3.3, this $K^+$ current was shown to be carried by TASK channels. Further characterisation of the TASK-like $K^+$ current in rat carotid body type-1 cells showed a dependency on $Mg^{2+}$. Earlier recordings were made in the presence of extracellular $Mg^{2+}$, where the main channel conductance was about ~14-16 pS, which doubled in the absence of extracellular $Mg^{2+}$ to 28 pS (Buckler et al., 2000; Buckler, 2015; Williams and Buckler, 2004). $Mg^{2+}$ dependency had previously been observed in cloned TASK 3 channels but not in cloned TASK 1 channels (Musset et al., 2006; Rajan et al., 2000). This led to the suggestion that the primary background $K^+$ channel in type-1 cells may be a heterodimer of TASK 1 and TASK 3. Kim et al. (2009a) confirmed this by using various $Mg^{2+}$ concentrations and selective inhibitors of TASK 1 or TASK 3. They found that TASK-like $K^+$ channels in rat carotid body type-1 cells are composed of TASK 1, TASK 3, and TASK 1/3 heteromers. Evidence in favour of heterodimerization in mouse carotid body type-1 cells was provided in this lab by utilising genetic studies. The principal form of single-channel activity of type-1 cells in wild-type mice was absent in both TASK1 knockout and TASK3 knockout mice. In the absence of TASK1 channels in $Task1^{-/-}$ mice, a larger conductance TASK3-like channel was observed. Conversely, in $Task3^{-/-}$ mice lacking TASK3 channels, a smaller conductance TASK1-like channel was observed. In double knockout mice, both TASK1 and TASK3 channels, as well as the wild type channel, were absent.

Moreover, in mice, TASK1, TASK3, and TASK1/3 heterodimer channels are all inhibited by hypoxia. However, TASK3 shows less hypoxic inhibition than TASK1 or TASK1/3 (Turner and Buckler, 2013b).

In summary, it is generally accepted that in rats and mice, the main form of the $O_2$-sensitive $K^+$ current in carotid body type-1 cells is predominantly carried by the TASK1/3 heteromeric channel. However, in humans, only TASK1 has been confirmed (Fagerlund et al., 2010; Kim et al., 2009a; Mkrtchian et al., 2012; Turner and Buckler, 2013b).

With regard to the pharmacological modulation of TASK channels, these channels are inhibited by barium, quinidine, anandamide, and methanandamide (Buckler et al., 2000; Enyedi and Czirjak, 2010; Kim et al., 2009a; Veale et al., 2007). Ruthenium and $Zn^{2+}$ inhibit only TASK3 (Czirjak and Enyedi, 2003, 2010; Kim et al., 2009a). Additionally, there are a number of newer, much more selective TASK channel inhibitors, such as A1899, PK-THPP, ML 365, BAY1000493, and A293 (Coburn et al., 2012; Cotton et al., 2013; Decher et al., 2021; Flaherty et al., 2014; Kiper et al., 2015; Streit et al., 2011). In type-1 cells, the inhibition of TASK channels by A1899, PK-THPP, and ML365 leads to membrane depolarization, which in turn facilitates a substantial $Ca^{2+}$ influx. These observations provide further evidence supporting the essential role of TASK channels in the chemotransduction process in type-1 cells (O'Donohoe et al., 2018).

In wild-type carotid body type-1 cell patches, TASK 1 appears to have a lower conductance than TASK 3. This difference in single-channel conductance was used by Kim et al. (2009a) to classify currents as TASK1, TASK 3, or TASK1/3. However, given that the channel activity of type-1 cells is usually high and most patches contain multiple channels, it is difficult to classify channels based solely on their conductance states. Moreover, it is common to

observe transitions between different conductance states during an open event; therefore, we in this laboratory believe that visual inspection is not sufficient to differentiate between simultaneous openings of multiple channels or transitions between different conductance states of the same channel. In Figure 1.2, a recording of native carotid body TASK channel activity clearly shows the variations in channel openings amplitude and the difficulty of classifying TASK channels based on this.

However, careful kinetic analysis of carotid body TASK channels activity shows that these channels have fast flickery kinetics with short bursts of rapid openings. The estimated mean open time was 0.3 ms, which was followed by a short closed time of 0.1 ms and a burst duration of 1.7 ms. The long closed state ranges from 2 to 30 ms, as shown in Figure 1.3 (Williams and Buckler, 2004).

Although other, as yet unidentified, ion channels in type-1 cells may contribute to hypoxia-induced depolarization, it is generally accepted that TASK1, TASK3, and TASK1/3 heterodimers produce the main $O_2$-sensitive background $K^+$ current of type-1 cells. Throughout this thesis, TASK1, TASK3, and TASK1/3 channels will be referred to as carotid body TASK channels.

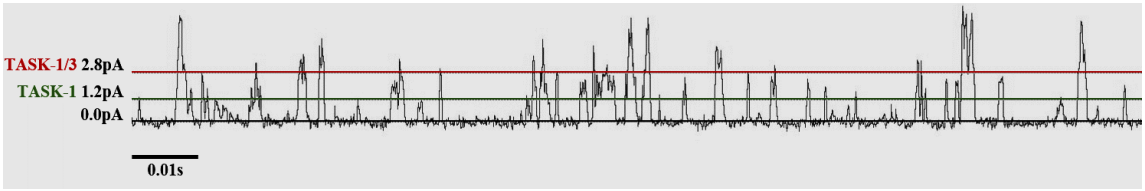


**Figure 1.2: An example trace of cell-attached single channel recording from rat carotid body type-1 cell demonstrating the typical TASK channels activity.** The trace obtained in this study. Bath Tyrode 100mM $k^+$, pipette potential 140Mm $K^+$.

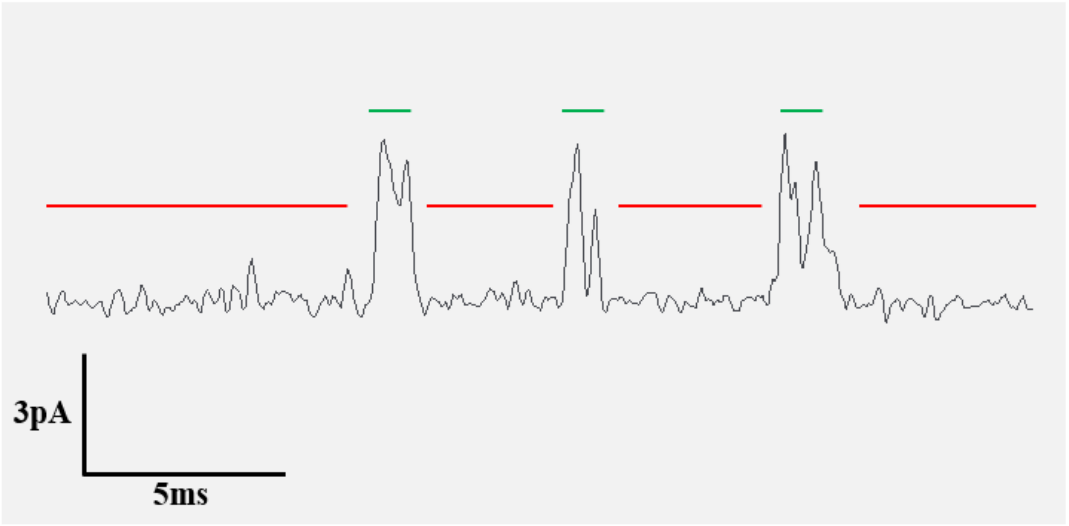


**Figure 1.3: Single channel kinetics of rat type-1 cell TASK channels.** An example trace obtained in this study. The long closed states of the channel is indicated with the red line. The channel openings are indicated with the green line. Recording filtered at 5 KHz.

## 1.5 TASK channels regulation by GPCRs

A common feature in tissues that express endogenous TASK channels is that these channels/currents are regulated by G-protein-coupled receptors (GPCRs). Typically, TASK channels are inhibited by hormones and neurotransmitters that stimulate GPCRs, specifically the G proteins of the αq/11 subclass. Inhibition of TASK channels by GPCRs has been reported in both native cell types and heterologous expression systems coexpressing TASK channels and Gq coupled receptors (Bayliss et al., 2001; Chemin et al., 2003; Chen et al., 2006; Czirják et al., 2000, 2001; Hopwood and Trapp, 2005; Kettunen et al., 2003; Larkman and Perkins, 2005; Lindner et al., 2011; Meuth et al., 2003; Millar et al., 2000; Perrier et al., 2003; Sirois et al., 2002; Talley et al., 2000). Numerous neurotransmitters, signalling through GqPCRs, have been identified within the carotid body. For example, angiotensin II (Ang II) has been demonstrated to augment the frequency of carotid body chemoreceptor discharge (Allen, 1998; Peng et al., 2011). Additionally, serotonin (5-HT) is released from type-1 cells in the carotid body under normoxic conditions, with an increase observed in response to hypoxia (Zhang et al., 2000, 2003; Yokoyama et al., 2015). Acetylcholine (Ach) is another transmitter signalling through GqPCRs. Application of Ach has been shown to excite the carotid body type-1 cells (Bairam et al., 2006; Shirahata et al., 2003).

When a ligand binds to $G_{q/11}$PCRs, it induces a conformational change followed by the activation of phospholipase C (PLC). The activated PLC hydrolyses plasma membrane phosphatidylinositol-4,5-biphosphate (PIP2) into inositol-1,4,5-triphosphate (IP3) and diacylglycerol (DAG). IP3 induces $Ca^{2+}$ release from the sarcoplasmic/endoplasmic reticulum (SR/ER) secondary to IP3 receptor activation. This, along with an increase in intracellular DAG levels, can

activate another signalling molecule: protein kinase C (PKC), see Figure 1.4 (Kadamur et al., 2013; Litosch, 2016; Weis and Kobilka, 2018).

Although it is widely accepted that TASK channels are inhibited by GqPCR, the underlying mechanism of this inhibition is poorly understood. Two possible mechanisms have been proposed for the GqPCR-mediated inhibition of TASK channels: a direct action of activated Gαq protein on TASK channels or actions of downstream signalling molecules (PIP2, DAG, and IP3).

**Direct Actions of Gαq Protein**

Evidence in favour of a direct action of the Gαq protein on TASK channels came from experiments conducted by Chen et al. (2006). They demonstrated that TASK channels were inhibited by activating a Gαq mutant protein that is deficient in PLC activation, by activating Gαq in inside-out patches where PLC cannot be activated, and by activating Gαq when PIP2, the PLC substrate, was depleted. Based on these findings, they concluded that TASK channels are directly activated by Gαq independent of subsequent PLC activation.

**PLC activation**

However, contradicting the results of Chen et al. (2006), PLC activation was shown to inhibit TASK channels expressed in oocytes (Czirjak et al., 2001). Several other studies have provided insights into the effects of U73122, a PLC inhibitor, on TASK channels in different cell types. Notably, in carotid body type-1 cells, U73122 was found to activate TASK-like currents (Ortiz and Varas, 2010). Similarly, in COS-7 cells co-expressing TASK channels and glutamate receptors, U73122 reduced the inhibitory effect of glutamate on TASK1 and TASK3 channels (Chemin et al., 2003). Additionally, U73122

reduced the inhibitory effect of carbachol on TASK1 channels in oocytes co-expressing TASK1 and M1 receptors (Czirjak et al., 2001). In CHO cells co-transfected with human TASK3 and M1 receptors, U73122 effectively blocked the muscarinic inhibition of TASK channels (Wilke et al., 2014). Moreover, U73122 effectively blocked endothelin-induced inhibition of TASK channels in rat cardiomyocytes (Schiekel et al., 2013).

**PIP2 depletion**

PIP2, the PLC substrate, has been implicated in the regulation of many ion channels. Previous research has shown that voltage-gated and inward-rectifier $K^+$ channels activity depends on PIP2 level (Rjasanow et al., 2015; Suh et al., 2006). Further research was conducted to investigate the regulation of TASK channels by PIP2. Incubation of oocytes expressing the TASK1 channel with wortmannin, which at a micromolar concentration inhibits phosphatidylinositol 3-kinase and subsequently reduces PIP2 levels, inhibited the baseline activity of TASK1 and slowed down its recovery after muscarinic receptor stimulation (Czirjak et al., 2001). Lopes et al. (2005) demonstrated that TASK channels expressed in Xenopus oocytes were activated by PIP2, inhibited by PIP2 scavengers, and their recovery from agonist-induced inhibition was dependent on PIP2 resynthesis. PIP2 regulation of TASK channels was also reported by Chemin et al. (2003). They demonstrated that PIP2 depletion strongly inhibited TASK channels in the cell-attached mode, whereas PIP2 application reactivated these channels in the inside-out mode. However, it remains unclear whether the PIP2 levels achieved in these experiments by the application of exogenous PIP2 or PIP2 scavengers correlate with the physiological level of PIP2.

By utilising advanced genetically encoded tools to alter PIP2 levels while monitoring TASK channels activity, Linder et al. (2011) provided evidence against the regulation of these channels by PIP2. They demonstrated that TASK channels expressed in CHO cells were insensitive to PIP2 depletion and that PIP2 resynthesis is not required for TASK channels recovery post receptor-mediated inhibition. Furthermore, TASK channels in thalamic neurons have been shown to be insensitive to changes in PIP2 (Bista et al., 2015).

**IP3**

Another possible signalling molecule that can mediate GPCRs inhibition of TASK channels is IP3. Previous research showed that IP3 injections did not affect TASK1 channels (Czirjak et al., 2001). Moreover, depleting intracellular $Ca^{2+}$ stores or reducing cytoplasmic $Ca^{2+}$ levels did not affect receptor-mediated inhibition of TASK1 (Wilke et al., 2014). TASK3 currents were also insensitive to intracellular application of $Ca^{2+}$ in inside-out patches (Kim et al., 2000). Furthermore, the application of EGTA did not affect TASK channels or their inhibition by glutamate (Chemin et al., 2003). Therefore, IP3 is unlikely to be involved in the regulation of TASK channels by GPCRs.

**DAG**

Some emerging evidence suggests that DAG is essential for maintaining the baseline activity of TASK channels and for their inhibition by GPCRs. DAG is a fusogenic lipid that is known to act as a second messenger in cell signalling. It can be produced by several mechanisms, including PLC activation and phosphatidic acid phosphatases (PAPs) activity. PAPs are enzymes that play a pivotal role in the synthesis of phospholipids. The activity of these enzymes is

dependent on $Mg^{2+}$ (Wu and Carman, 1994). It has been shown that ATP inhibits PAPs activity by binding to $Mg^{2+}$ (Humble and Berglund, 1991). Multiple metabolic pathways are involved in DAG metabolism, including hydrolysis by DAG-lipases, resulting in the formation of monoacylglycerols such as endocannabinoid 2-arachidonoyl glycerol (2-AG), as well as ATP-dependent phosphorylation by DAG-kinases, leading to the production of phosphatidic acid (PA) (Eichmann and Lass, 2015; Prentki and Madiraju, 2008; Tafesse et al., 2006; Wu and Carman, 1994).

It has been shown that TASK channels were dose-dependently inhibited by the application of 1-oleoyl-2-acetyl-sn-glycerol (OAG), a DAG analogue/ PKC activator, in rat carotid body type-1 cells and thalamic neurons (Ortiz and Varas, 2010; Bista et al., 2015). Furthermore, the application of the membrane-permeable DAG analogue 1,2- dioctanoyl-sn-glycerol (DiC8) to CHO cells expressing TASK channels or to cerebellar granule neurons resulted in reversible, dose-dependent inhibition of these channels. Increasing DAG metabolism by overexpressing DAG-lipases or DAG-kinases in CHO cells co-expressing TASK channels and M1 receptors resulted in a reduction of receptor-mediated inhibition. This indicates that TASK channels inhibition by GPCRs is likely mediated by DAG (Wike et al., 2014).

The TASK 3 channel expressed in Xenopus oocytes was inhibited by the application of DiC8 to the cytoplasmic face of the patch in inside-out recordings. This suggests that DiC8 may directly affect TASK channels. Furthermore, mutations that deleted the VLRFLT region of the TASK 3 channel blocked DiC8-induced inhibition of this channel. This further supports the direct regulation of TASK channels by DAG (Wilke et al., 2014). Furthermore, Sormann et al. (2022) demonstrated that mutations disrupting the lower ‘X-gate’ of the TASK1 channel impaired GPCRs sensitivity and blocked DiC8-induced inhibition in excised patches.

## DAG-mediated activation of PKC

Apart from its direct effect on TASK channels, DAG functions as a signalling molecule that can initiate downstream pathways, including the activation of PKC. Previous research has investigated the role of PKC in the regulation of TASK channels; however, the results have been inconclusive and contradictory. It has been shown that inhibiting PKC activity by the application of chelerythrine, a selective PKC inhibitor, enhances the basal activity of TASK channels and blocks their muscarinic inhibition (Ortiz and Varas, 2010). However, contrasting findings were reported by Czirjak et al. (2000). They reported that altering PKC levels did not affect TASK1 channel activity or its inhibition by angiotensin II in Xenopus oocytes co-expressing TASK-1 and angiotensin II receptor. These findings were further supported by Chemin et al. (2003), who demonstrated that neither PKC inhibition with staurosporine, a non-selective inhibitor of protein kinases, nor PKC activation by phorbol ester, a potent activator of PKC, affected the baseline activity of TASK channels or their inhibition by glutamate. Similarly, in rat cardiomyocytes, the inhibition of PKC did not affect the regulation of TASK channels by GPCRs (Schiekel et al., 2013). Moreover, removal of all potential PKC phosphorylation sites in the human TASK3 channel had no effect on its inhibition by GPCRs (Veale et al., 2007). Therefore, with diverse findings and conflicting views, the role of PKC in regulating TASK channels is yet to be fully understood.

## Possible mechanisms of TASK channel inhibition

Ion channels can be inhibited either by a change in their gating mechanisms or by a reduction in their surface expression (Wickman and Clapham, 1995). It has been proposed that internalisation of TASK channels is a possible mechanism for their regulation by GPCRs. Internalisation of the

TASK1 channel in response to the activation of the muscarinic M1 receptor or TrkA, a receptor for nerve growth factor, was reported in adrenal medullary cells and its cloned cell line PC12 (Matsuoka et al., 2013; Matsuoka and Inoue, 2017; Inoue et al., 2020). Dynasore, a dynamin inhibitor, reduced muscarinic agonist-induced inhibition of the TASK1 channel and blocked the translocation of TASK-like immunoreactive material from the plasma membrane to the cytoplasm. These findings suggest that the muscarinic agonist-induced inhibition of TASK1 is mediated by clathrin-dependent endocytosis. This was blocked by inhibiting PLC or PKC activity, indicating that the PLC-PKC signalling pathway is crucial for the muscarinic-induced internalisation of the TASK1 channel (Matsuoka and Inoue, 2017). Once activated, PKC activates the non-receptor tyrosine kinase, Src, which phosphorylates a tyrosine residue at the C-terminus of TASK1. This phosphorylation induces a conformational change in the C-terminus of TASK1, exposing a dileucine motif downstream of the fourth transmembrane domain. This enables the binding of the adaptor protein AP-2 to the dileucine motif, which triggers clathrin-dependent endocytosis (Inoue et al., 2020). The TASK3 channel, on the other hand, has not been shown to internalise upon muscarinic stimulation because its C-terminus lacks tyrosine phosphorylation sites (Matsuoka and Inoue, 2017).

**Summary**

Although there is compelling evidence that TASK channels are regulated by PLC downstream signalling molecules, it remains unclear which signalling molecules (PIP2, DAG, PKC, or IP3) and how (a change in gating or a reduction in surface expression) mediate GPCRs-induced inhibition of these channels.

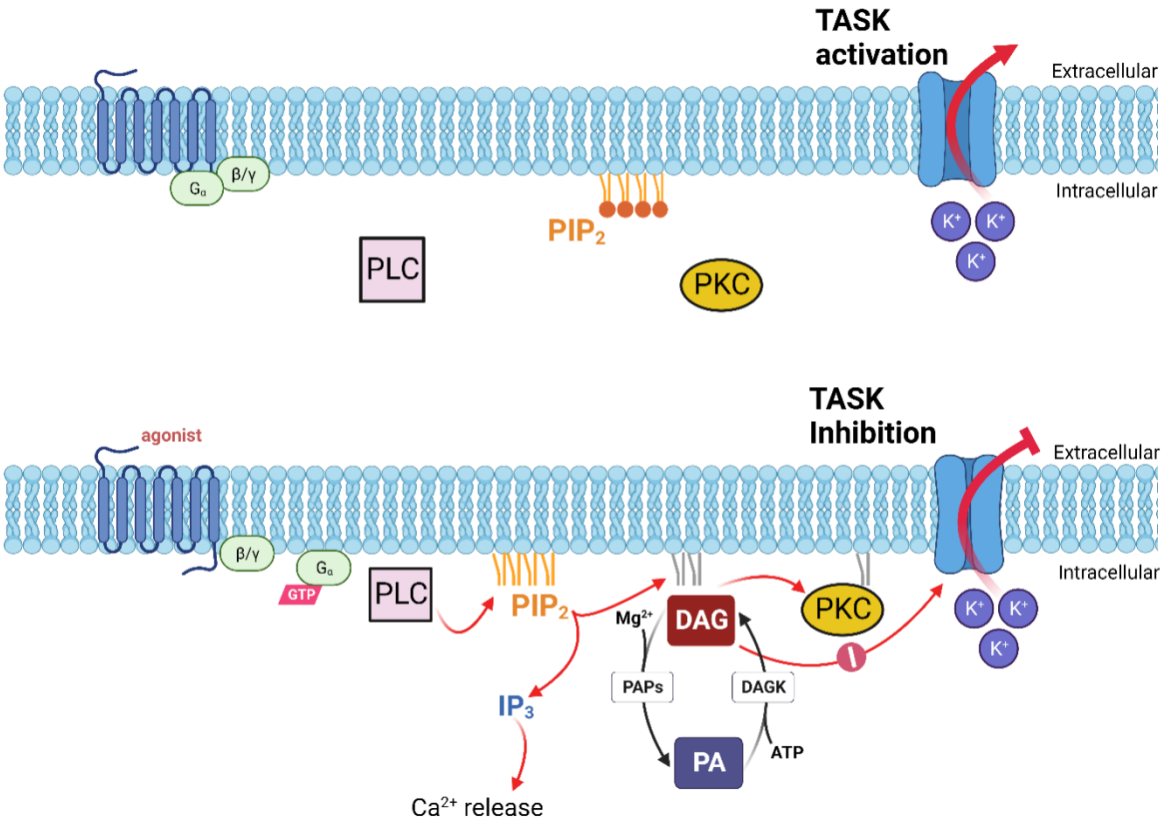


**Figure 1.4: Schematic presentation of the GPCRs signalling pathways.** Activated Gαq receptor activates PLC signalling molecules resulting in TASK channel inhibition.

## 1.6 TASK channels regulation by anaesthetics

One of the main side effects of volatile anaesthetics is the suppression of the ventilatory response to hypoxia and hypercapnia (Hirshman et al., 1977; Idle et al., 1999; Knill and Gelb, 1978). This is mediated in part by direct effects on the carotid body. Davies et al. (1982) showed that the general anaesthetic halothane reduces the hypoxic and hypercapnic responses of the carotid body. Given that normal carotid body hypoxic and hypercapnic responses involve the modulation of TASK channels, research was undertaken by this laboratory to explore the actions of volatile anaesthetics on type-1 cell TASK channels activity. Initially, halothane was identified as a potent stimulant of the background TASK-like potassium current in the carotid body and other tissues (Berg et al., 2004; Buckler et al., 2000; Pandit et al., 2010; Putzke et al., 2007). Subsequent investigations have revealed that both halothane and isoflurane can activate TASK channels and suppress hypoxia-evoked $Ca^{2+}$ entry in type-1 cells of the carotid body. Notably, halothane has demonstrated a more profound effect than isoflurane in these regards (Pandit et al., 2010). This differential sensitivity to halothane and isoflurane at the single channel level reflects their effects on inhibiting the human hypoxic ventilatory response (Pandit, 2002; Pandit et al., 2010).

Stimulation of TASK channels by volatile anaesthetics has also been reported in heterologous expression systems (Berg et al., 2004; Patel et al., 1999; Putzke et al., 2007). Linden et al. (2006, 2007) used TASK1 and TASK 3 knockout mice to examine the role of TASK channels in mediating the hypnotic effect of volatile anaesthetics. TASK1 knockout and TASK3 knockout mice showed reduced sensitivity to the hypnotic effects of halothane and isoflurane. Nevertheless, Pang et al. (2009) demonstrated that the sensitivity to halothane in TASK1 knockout mice was comparable to that in wild-type mice, but it was

reduced in TASK3 knockout mice. Therefore, the possibility of different halothane sensitivity among TASK channels cannot be ruled out.

Although it is generally accepted that TASK channels are activated by volatile anaesthetics, little is known about the underlying molecular bases of this activation. Patel et al. (1999) reported that the VLRFMT region, located at the beginning of the cytoplasmic C-terminus of the TASK-1 channel, is critical for halothane-induced activation. The same region, referred to as the 'halothane response element', has been shown to be essential for the activation of the TASK3 channel by halothane and for receptor-mediated inhibition of TASK channels (Tally and Bayliss, 2002; Veale et al., 2007). Therefore, the VLRFMT region appears to be important for both endogenous and exogenous regulation of TASK channels.

Another important region for the anaesthetic activation of TASK channels was identified by Andres-Enguix et al. (2007). They utilised site-directed mutagenesis and chimeric channel constructs to investigate the mechanisms underlying anaesthetics-induced activation of TASK channels. In human TASK channels and TASK channels cloned from Lymnaea stagnalis (Ly), where the anaesthetic sensitive $K^+$ current was first discovered, a mutation of a single amino acid, 159, located in the region between the cytoplasmic end of TM2 and the middle of TM3, inhibited anaesthetics-induced activation of both channels. Moreover, TASK3 channel activity was increased by the occupancy of amino acid 159 in both LyTASK3 and human TASK3 (Conway and Cotten, 2012).

To summarise, two regions of TASK channels have been shown to be critical for the anaesthetics-induced activation of these channels: a potential binding site at the end of TM2 and another binding site at the beginning of the C-terminus.

## 1.7 Questions addressed in this thesis

Several observations from previous research are of particular interest to this thesis. In excised patches of type-1 cells, TASK channels undergo a rapid rundown (decline in their basal activity) and lose their sensitivity to $O_2$. This indicates that cellular constituents are crucial for the functioning of these channels. Following this rundown, TASK channels can be reactivated by MgATP, suggesting that the activity of these channels is dependent on MgATP. It has been established that TASK channels are inhibited by a wide range of metabolic inhibitors. The effects of these inhibitors and hypoxia on TASK channels are mutually exclusive, implying that metabolic function is the convergence point of these two pathways. Furthermore, TASK channels have been shown to be regulated by Gq-coupled receptors and PLC signalling molecules. Notably, the metabolism of several PLC signalling molecules is ATP-dependent.

On the basis of these findings, in Chapters 3 and 4, I sought to determine whether Gq-coupled receptors and PLC signalling molecules are involved in mediating the oxygen sensitivity of TASK channels in type-1 cells. In Chapter 5, I sought to determine the role of PLC in mediating the inhibitory effects of metabolic inhibitors on TASK channels.

Previous research has shown that a specific domain at the C-terminus of TASK channels is necessary for their activation by anaesthetics and inhibition by DAG. Therefore, in Chapter 6, I extended my research to examine the interactions between DAG and halothane on TASK channels in type-1 cells.

# CHAPTER 2. Materials and Methods

## 2.1 Isolation of carotid body type-1 cells

### 2.1.1 Explanation for choice of rat pups

In rats, the carotid body can be easily identified as a round-shaped cluster of cells, usually below or attached to the SCG in close proximity to the internal branch of the common carotid artery. Younger rats (P11-P14) have less connective tissue, which allows for easier identification of the carotid body. On the other hand, in mice, dissecting the carotid body is challenging as it appears to be dispersed amongst several islands of cells (Slingo, 2013).

The process of isolating type-1 cells is affected by several factors, including enzymes concentration, incubation time in the enzymatic solution, and mechanical trituration. Carotid bodies dissected from younger rats require low enzymatic concentrations and a short incubation time, which improves the quality of the enzymatic digestion process. Therefore, rat pups (P11-P14) were chosen for this thesis to investigate the regulation of carotid body type-1 cells. Healthy type-1 cells were obtained on a relatively stable basis throughout my project (8-12 cells from 2 rat pups per day). During this developmental stage (P11-P14), the carotid body's sensitivity to hypoxia is fully established. Hypoxic responses are evident in the carotid body of new born rats as early as 1-2 days of age. (Kholwadwala and Donnelly, 1992). Only male rat pups were used in this study to exclude any sex related variations.

### 2.1.2 Surgery

Carotid bodies were excised from Sprague-Dawley rat pups (11- 14 days old) under non-recovery anaesthesia. The rats were first placed in an induction chamber to deliver isoflurane (5% isoflurane in $O_2$, air flow rate of 5 litres/min). Once a loss of righting reflex had been established, the rats were placed on the

surgical table in the supine position, and a nose cone was used to maintain 5% isoflurane delivery at 500 ml/min. From this supine position, the upper limbs were fixed in extension using a tape. The depth of anaesthesia was then tested using the pedal withdrawal reflex. Once a surgical plane of anaesthesia had been established (e.g., loss of the pedal withdrawal reflex) a longitudinal incision was then made in the neck area, the skin was flapped bilaterally, and the salivary glands were removed. The mylohyoid, sternomastoid, sternohyoid, and clavotrapezius muscles, as well as the surrounding fibrous tissue, were removed to expose the carotid artery and its two branches, see Figure 2.1. Then, a ligature was tied at the most caudal point of the carotid artery, followed by two cuts at the most caudal and rostral points to dissect the carotid bifurcation. Once the carotid bifurcation was dissected, it was then transferred to a culture dish containing ice-cold low $Ca^{2+}$ low $Mg^{2+}$ DPBS (GIBCO). This was done to slow metabolism and minimise cell death. A similar procedure was done to dissect the other carotid bifurcation, and the rats were decapitated while still under terminal anaesthesia. All animal procedures were approved by the University of Oxford's Local Ethical Review Process and conducted in accordance with project and personal licences issued under the UK Animals (Scientific Procedures) Act 1986.

The carotid bifurcations were then transferred to a silicone elastomer plate (Sylgard, Dow corning). While still in the ice-cold DPBS, the two branches of the carotid artery were fixed by small stainless-steel pins with the SCG facing down. From this position, connective tissue and the occipital artery were removed. Then the carotid bifurcation was flipped to expose the SCG, which was then carefully removed. At this point, the carotid body could be identified and excised, see Figure 2.2. Carotid bodies were then kept in another dish containing low $Ca^{2+}$ low $Mg^{2+}$ DPBS.

On a typical day of experiments, four carotid bodies were dissected from two rat pups. Once all carotid bodies had been excised, they were incubated in a warmed HAMS-F12 (Sigma) containing collagenase (0.6 mg/ml, CLS-1 Worthington) and trypsin (0.25 mg/ml, Sigma) at 37°C and 5% $CO_2$ in air for 22-24 minutes, depending on the age of the rat (older rats require a longer incubation period). Collagenase and trypsin were weighed in a 15 mL tube 10-15 minutes prior to the surgery. Once all carotid bodies were dissected, 10 ml of the warmed culture medium was added to the same tube and mixed, and 2 ml syringe connected to a filter (0.22 μm Merck Millipore Ltd. Carrigtwohill, Ireland) was used to add 2 ml of the enzymatic solution to a small dish to which the carotid bodies were transferred. At the end of the first incubation period, a fine forceps was used to gently tease the carotid bodies apart, increasing the surface area and facilitating the enzymatic digestion process. The carotid bodies were then returned to the incubator for an additional 2-4 minutes. At the end of the second incubation period, the carotid bodies were transferred to a culture dish containing enzyme-free modified culture medium (refer to Table 2.1) and gently agitated using a 200 μl pipette set at 30 μl to wash off the enzymatic solution. Then, they were transferred to another dish containing the modified culture medium, but with the addition of trypsin inhibitor (250 μg/ml, Sigma-Aldrich). From this dish, 210 μl of media was added to a transparent 10 ml tube, followed by another 30 μl containing the carotid bodies. Using small, medium, and large (125-370 μm) fire-polished glass Pasteur pipettes, the carotid bodies were gently triturated under direct microscopic vision until the tissue was fully dispersed. The trituration process took about 3-4 minutes and started with the large glass Pasteur pipette, then the medium one, and ended with the smaller glass Pasteur pipette. Approximately 30 μl of the primary cell culture was then plated onto each of 4-8 6 mm glass coverslips that had been previously coated with 0.01% poly-D-lysine. Cells were then incubated for 2 hours at 37°C with

5% $CO_2$ to allow them to settle and adhere to the coverslip before additional modified cell culture medium was added to the culture dish.

Coverslips were coated with poly-D-lysine on the same day by adding 30 µl of 0.01% poly-D-lysine (Sigma-Aldrich, Gillingham, Dorset, UK) to each coverslip for 5 min. The coverslips were then washed with water and air dried. Two rat pups typically provide sufficient type-1 cells to permit 7-12 recordings to be made/attempted in a day.

**Figure 2.1 Microscopic view of the carotid bifurcation.**

The carotid bifurcation is highlighted with the yellow circle. Adjacent anatomical structures are labelled.

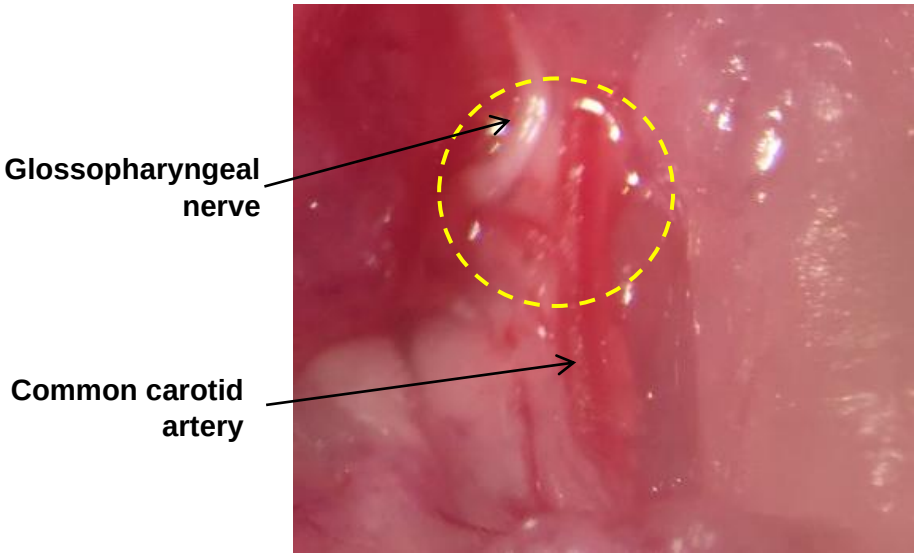


**Figure 2.2 Ex vivo dissection of the carotid body**. The carotid body is highlighted with the red circle.

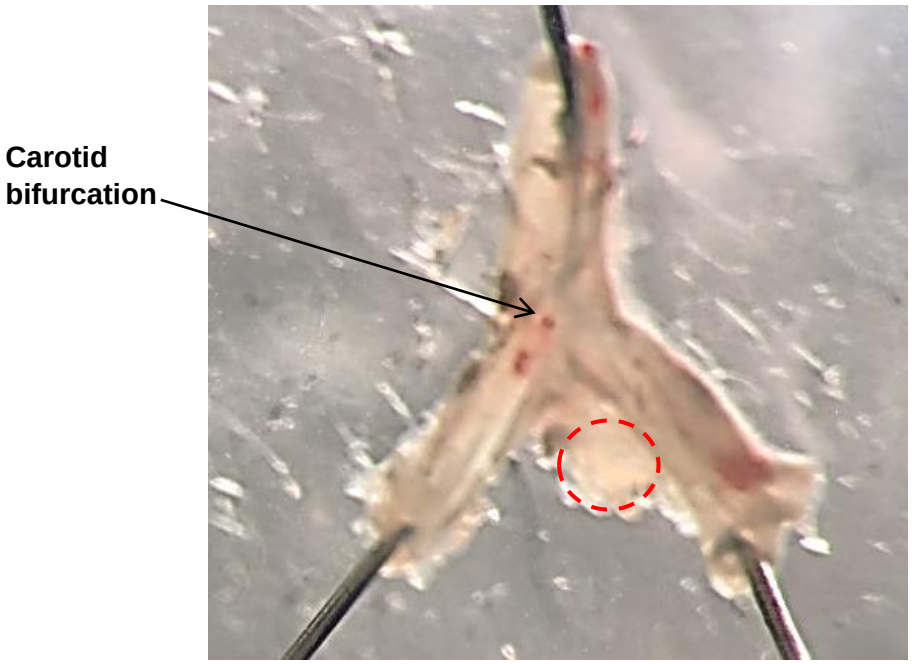

**Table2.1 Constituents of modified culture medium for isolated type-1 cells**

| Ingredient | Volume (ml) |
|---|---|
| Nutrient mixture F12 in Dulbecco's Modified Eagle Medium (F12/DMEM) | 50 |
| Fetal bovine serum | 5 |
| Penicillin streptomycin | 0.5 |
| Insulin (10 mg/ml) | 0.02 |

### 2.1.3 Staining of type-1 cells

Various carotid body cells can be observed at the end of the enzymatic dissociation process, including type-1, type-2, fibroblasts, and blood cells. Isolated type-1 cells can easily be identified as single, small, round-shaped cells of ~10 µm diameter or clusters of 2-5 cells, which typically appear phase bright under phase contrast microscopy with a 10x objective.

In some experiments, rhodamine-tagged peanut agglutinin (PNA) was used to label type-1 cells to aid identification. Kim et al. (2009b) established that rhodamine-PNA binds to rat carotid body type-1 cells within one hour of exposure without altering their physiological response.

Coverslips containing dissociated carotid bodies were treated with Rhodamine-PNA (2 µl/ml) for one hour. When excited at 485 nm, PNA-labelled type-1 cells were stained a bright orange colour.

## 2.2 Solutions

The primary solution used in my thesis is a $CO_2$-$HCO_3^-$ buffered standard Tyrode solution. It contains the following:

**Table2.2 Standard Tyrode solution**

| Ingredient | Concentrations (mM) |
|---|---|
| NaCl | 117 |
| KCl | 4.5 |
| $MgCl_2$ | 1 |
| $NaHCO_3$ | 23 |
| Glucose | 11 |
| $CaCl_2$ | 2.5 |

Two main variations were made to this solution as needed, which will be clarified in each chapter:

1- A high $K^+$ solution (70 or 100 mM) was prepared by increasing KCl and reducing NaCl.
2- A $Ca^{2+}$-free solution was prepared by omitting $CaCl_2$ and adding 1mM EGTA as a calcium chelating agent.

Tyrodes were equilibrated with 5% $CO_2$ in 95% air (normoxic solution) or 5% $CO_2$ in 95% $N_2$ (hypoxic solution) for 10-15 minutes before placing coverslips in the recording chamber. The bottles containing Tyrode solution were placed in a water bath heated to ~38ºC to achieve a temperature of 37ºC in the experimental bath.

## 2.3 Explanation for the choice of the hypoxic stimulus

In this thesis, a strong hypoxic stimulus was induced by equilibrating Tyrode solution with a combination of 5% $CO_2$ and 95% $N_2$, resulting in oxygen levels of 1.5-3 mmHg in the cell perfusion chamber. The oxygen tension in the cell perfusion chamber was assessed using an optical sensor (Presence, Regensburg, Germany).The use of such a powerful hypoxic stimulus was intended to maximise the hypoxic signal. Importantly, despite the severity of this stimulus, it had no discernible effect on non-oxygen sensitive tissues, such as the superior cervical ganglia (SCG) (Buckler and Turner, 2013a).

## 2.4 Description of the perfusion system

### 2.4.1 Rig setup

The perfusion system used in this thesis can be described as a semi-closed or airtight system, which enables precise control of oxygen tension in the recording chamber. An illustration of the cell perfusion system is shown in Figure 2.3. Glass bottles containing Tyrode solution (0.2-2 L) were placed in a water bath where the temperature was maintained at 38 ºC. The glass bottles were fitted with a plastic bung/stopper having two holes drilled in the top: one 5 mm hole to allow the insertion of a glass gas distribution tube (DWK Life Sciences Limited, Stoke-on-Trent, UK), and a smaller 1.6 mm hole through which a 1.5 mm stainless steel tube (medical grade) was inserted to allow solutions to be aspirated from the bottle.

Gas was delivered from pressurised gas cylinders (British Oxygen Company (BOC), Surrey, UK) fitted with two-stage gas pressure regulators (set

to 5-10 psi) through 4 mm bore copper and/or plastic tubing to the gas dispersion tubes in the bottles. The flow rate was controlled using rotameters or simple needle valves (GASARC, Essex, UK) in order to maintain a steady stream of bubbles emerging from the gas dispersion tubes at a typical gas flow rate of 100 – 200 ml/min. Gases were supplied premixed by (BOC) to our chosen proportions of $O_2$, $CO_2$, and $N_2$ to provide either hypoxic or normoxic gas mixtures. Solutions were equilibrated with the gas mixture of choice for at least 15 minutes prior to use.

The aspiration stainless steel tube, which was placed in a glass bottle, was connected through stainless steel tubing (articulated with short sections of Pharmed plastic tubing (Copley, Leicester, UK) to a two/three way tap that directed solution outflow to the experimental chamber or to a waste circuit. The operation of the tap was controlled by a remote lever and control rod, enabling one input solution to be directed to the experimental chamber and the other to waste (and for this arrangement to be switched within seconds). See Figures 2.4 and 2.5. Stainless steel tubes bringing solution into the Faraday cage were grounded at the point of entry.

Solutions were delivered to the recording chamber by gravity and were subsequently aspirated from the downstream end of the recording chamber through a fine stainless steel tube using a peristaltic vacuum pump. This aspiration tube was electrically shielded by a layer of plastic tubing and then an earthed outer stainless steel tube (which does not come into contact with the saline). Solutions aspirated through this tube were also electrically isolated using a dropper arrangement.

**Figure 2.3 Perfusion system** To equilibrate Tyrode solution with various gas mixtures, gas passes from gas cylinders through plastic tubing to gas regulators then to the gas dispersion tube immersed in a glass bottle. The equilibrated solution travels through a narrow-bore metal aspiration tube connected through a plastic tubing to the experimental bath and then to the waste. The flow of the solution in this system is continuous and driven by gravity and a peristaltic pump.

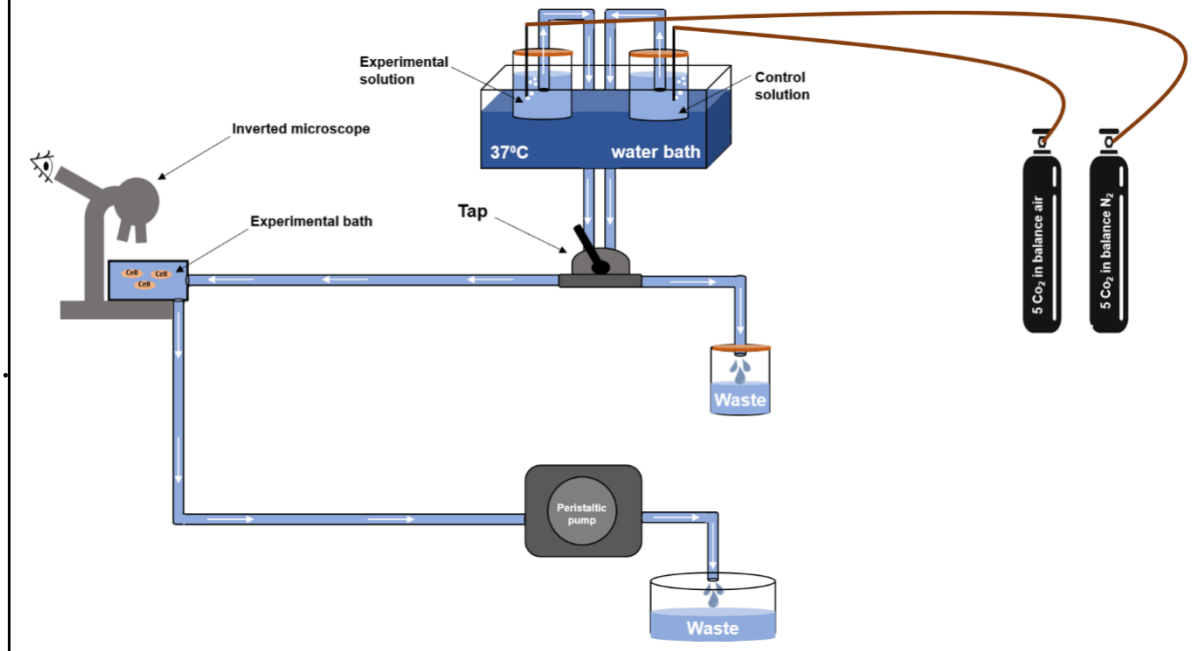

**Figure 2.4 Experimental bath** Superfusate switch, experimental bath, heater, waste outflow, Ag/AgCL grounding electrodes and aspiration tube are indicated with the arrows. Experimental bath volume is ~100 µl. Groundings for electrophysiology experiments can be seen.

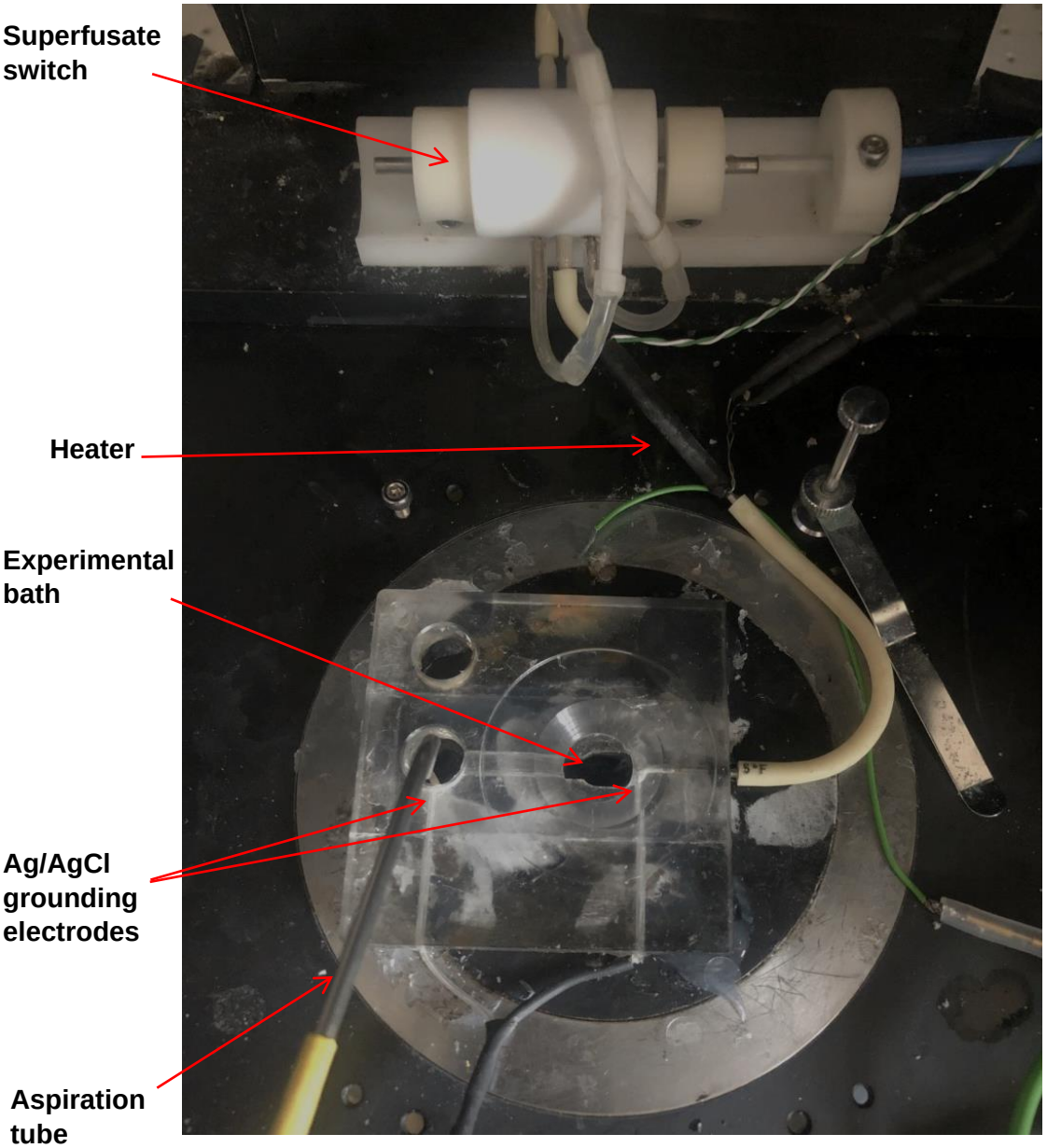

**Figure 2.5 Mechanism of the rapid switching system.** Two lines were connected to the switch at the input point. The line in the middle runs to the bath then to the aspirated waste outflow, while the solution from the other input line flows passively into a separate waste bottle (outside of the Faraday cage). The switch is mechanically controlled, panel (A) the switch is pulled outward, causing the red line to be delivered to the bath while the blue line is directed to waste. Panel (B) when the switch is pushed inward, the blue line is delivered to the bath while the red line passes to waste. Note that with the red line directed to the bath the entire contents of the blue line can be flushed through the system using a syringe attached to the waste outflow and vice versa when the blue line is directed to the bath. This arrangement allows an unlimited number of different solutions to be used in one experiment.

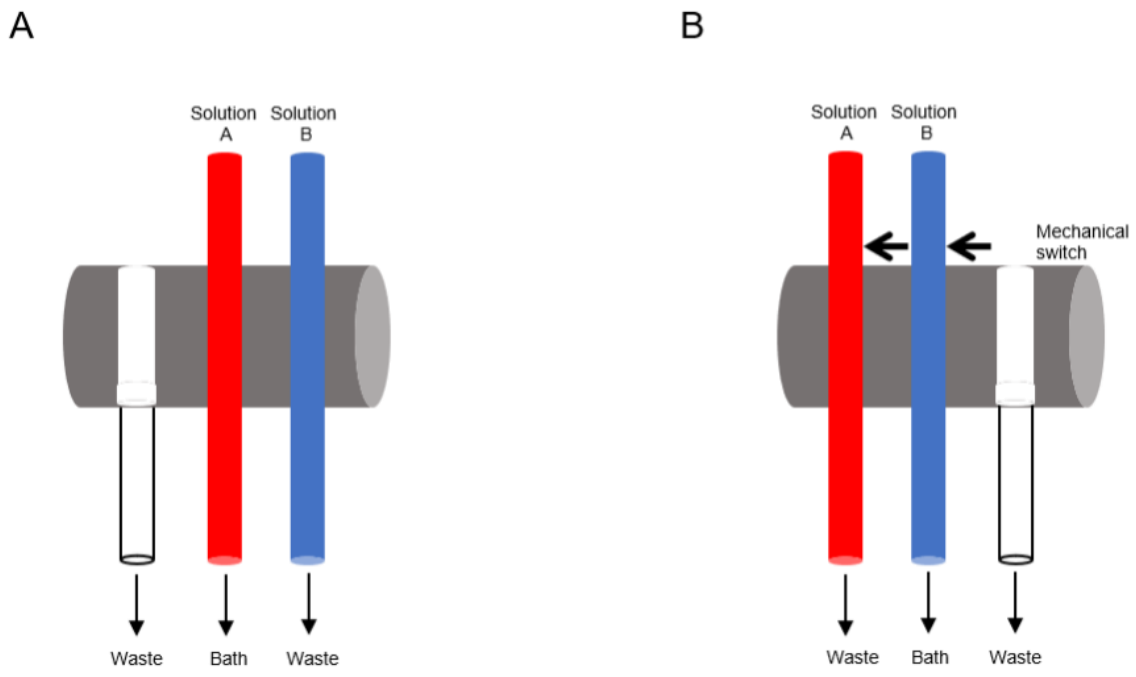

### 2.4.2 Rig setup for anaesthetics experiments

The rig setup for anaesthetics experiments was similar to that used in other experiments, with the exception that the gas supply was first passed through a vaporiser to be equilibrated with two concentrations of halothane (1% and 2%), before it was connected through a narrow-bore nylon tubing (BS5409) to a gas dispersion tube (Corning, High Wycombe, UK) immersed in a glass bottle (0.2 L) containing Tyrode solution.

To ensure accurate delivery of the anaesthetics to the recording chamber, the concentration in the bottle's headspace gas was continuously measured using an infrared gas analyser (Capnomac Ultima, Datex, Sevenoaks, UK). When the halothane vaporiser was set at 2%, the gas analyser reading of the halothane concentration in the bottle was 1.9-2%. A schematic illustration of the experimental setup for the anaesthetic's experiments is shown in Figure 2.6.

**Figure 2.6 Perfusion system for anaesthetics experiments.** To equilibrate the gas mixture with the desired halothane concentration, gas passes from the gas cylinder to a rotameter via a plastic tubing then to halothane vaporisers. The vaporiser output was connected through nylon tubing to the gas dispersion tube immersed in a glass bottle. The concentration in the bottle was continuously monitored using an infrared gas analyser.

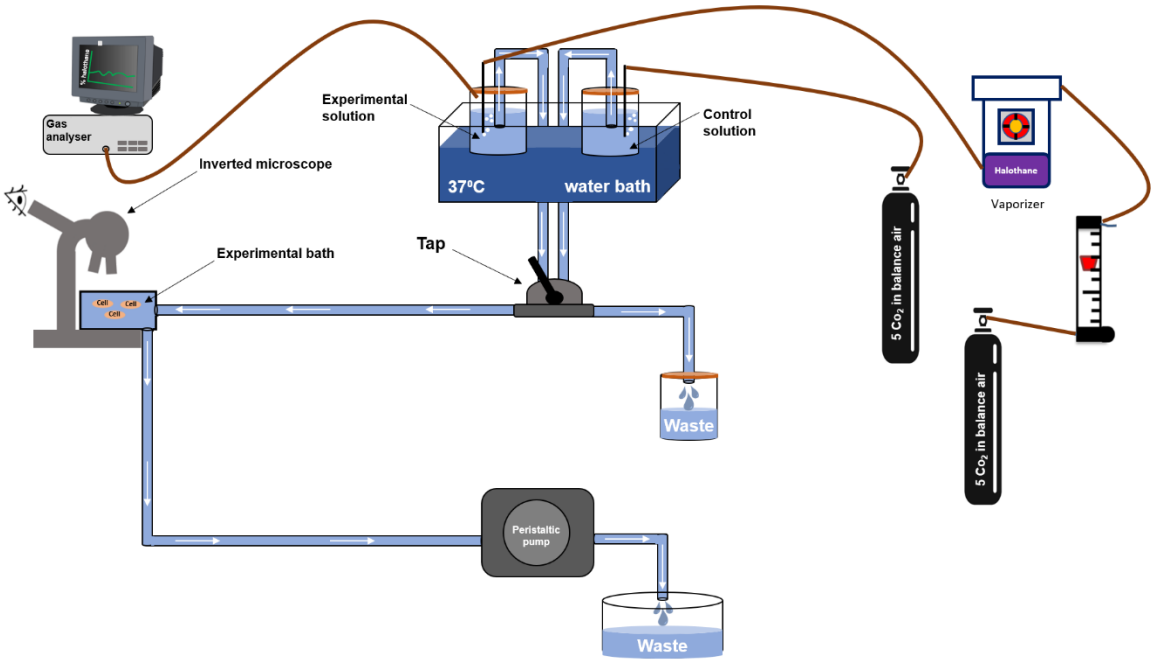

## 2.5 Challenges with accurate anaesthetics delivery

The delivery of volatile anaesthetics to isolated cells placed in a recording chamber poses different challenges. First, the high volatility of these substances can result in a loss of concentration between the vaporiser, the bottle, and the recording chamber. Second, type-1 cells need to be supplied with a continuous flow of solutions equilibrated with $O_2$ to maintain their functionality. Therefore, minimising the reduction in the anaesthetic concentration becomes even more challenging. Third, some experiments involve the application of anaesthetics before and after the application of a pharmacological agent. Therefore, it is important to maintain a relatively stable concentration of anaesthetics throughout this process.

Our laboratory has previously designed a system for the accurate delivery of anaesthetics in a recording chamber with a continuous flow of solutions. The primary objective of this system is to minimise the loss of concentration as the anaesthetic travels from the vaporiser to the recording chamber and to ensure that its concentration is relatively stable throughout the course of the experiment. This system has previously been described and tested (Huskens et al., 2016).

## 2.6 Chemicals and pharmacological agents

Chemical and pharmacological agents were dissolved in the Tyrode solution to achieve the desired final concentration. Agents concentrations and suppliers are listed in each chapter.

## 2.7 Measurements of intracellular $Ca^{2+}$

### 2.7.1 Dye loading of isolated type-1 cells

Isolated rat carotid body type-1 cells were loaded with indo-1 acetoxymethyl (AM) dye (Molecular Probes, Leiden, The Netherlands). A stock solution was prepared by dissolving 5 μg of Indo-1AM in 50 μl of DMSO. Then, 5 μl was added to 2 ml of the modified culture medium to achieve a final concentration of 2.5 μM/l. Cells were incubated in this loading solution for one hour at room temperature before being transferred to the experimental chamber. Once a cell takes up the AM form of Indo-1, the acetoxymethyl ester appears to be cleaved by intracellular esterase, leaving the calcium sensing form (Indo-1) trapped inside the cell.

Indo-1 was preferred over other $Ca^{2+}$ indicators for the following reasons:

1- Indo-1 fluoresces brightly at low excitation intensity, which helps to avoid problems such as photobleaching or NADH autofluorescence.
2- Indo-1 has a higher $Ca^{2+}$ dissociation constant ($K_D$) than other $Ca^{2+}$ indicators, such as quin2. This higher $K_D$ enables a better temporal resolution of changes in intracellular $[Ca^{2+}]i$ (Jackson et al., 1987).
3- Indo-1 has a dual emission peak: one at 475 nm in a $Ca^{2+}$-free medium and another at 405 nm in the presence of $Ca^{2+}$. From these two peaks, taking the ratio of the intensities at two excitation wavelengths directly correlates with intracellular $[Ca^{2+}]i$. This reduces problems associated with other single-wavelength $Ca^{2+}$ indicators, such as uneven dye loading and variations in optical path length (due to differences in cell thickness), which can affect fluorescence intensity independent of $[Ca^{2+}]i$ changes.

### 2.7.2 Instrument setup

An inverted microscope (Nikon Diaphot 200, Tokyo, Japan) was adapted for use as a micro-fluorimeter. A 100-W xenon lamp (Nikon, Tokyo, Japan) was used as a fluorescence excitation light source filtered at 350 ± 5 nm (close to the excitation maximal for Indo-1). Emitted fluorescent light was split using a dichroic mirror of 450 nm, passed through bandpass emission filters centred on 405 ± 16 and 495 ± 10 nm, and measured by a pair of tri-alkali cooled photomultiplier tubes (PMT) (Thorn EMI, London, UK). PMT output was sent to a current-to-voltage converter and then digitised at 250 Hz using a CED 1401 (CED, Cambridge, UK). Indo-1 signals were averaged at 0.5 second intervals for a sampling rate of 2 Hz. The setup of the inverted microscope is illustrated in Figure 2.7.

**Figure 2.7 Plan view of inverted microscope setup**. For $Ca^{2+}$ recording with Indo-1 dye, Indo fluorescence was induced by excitation at 340 nm and recorded at 405 ± 16 nm and 495 ± 10 nm and excitation filter of 340 nm was used. Dichroic were long pass at 390 nm (cameras) and 450 nm (between PMTs). Red line represents excitation light, and blue is the omitted light.

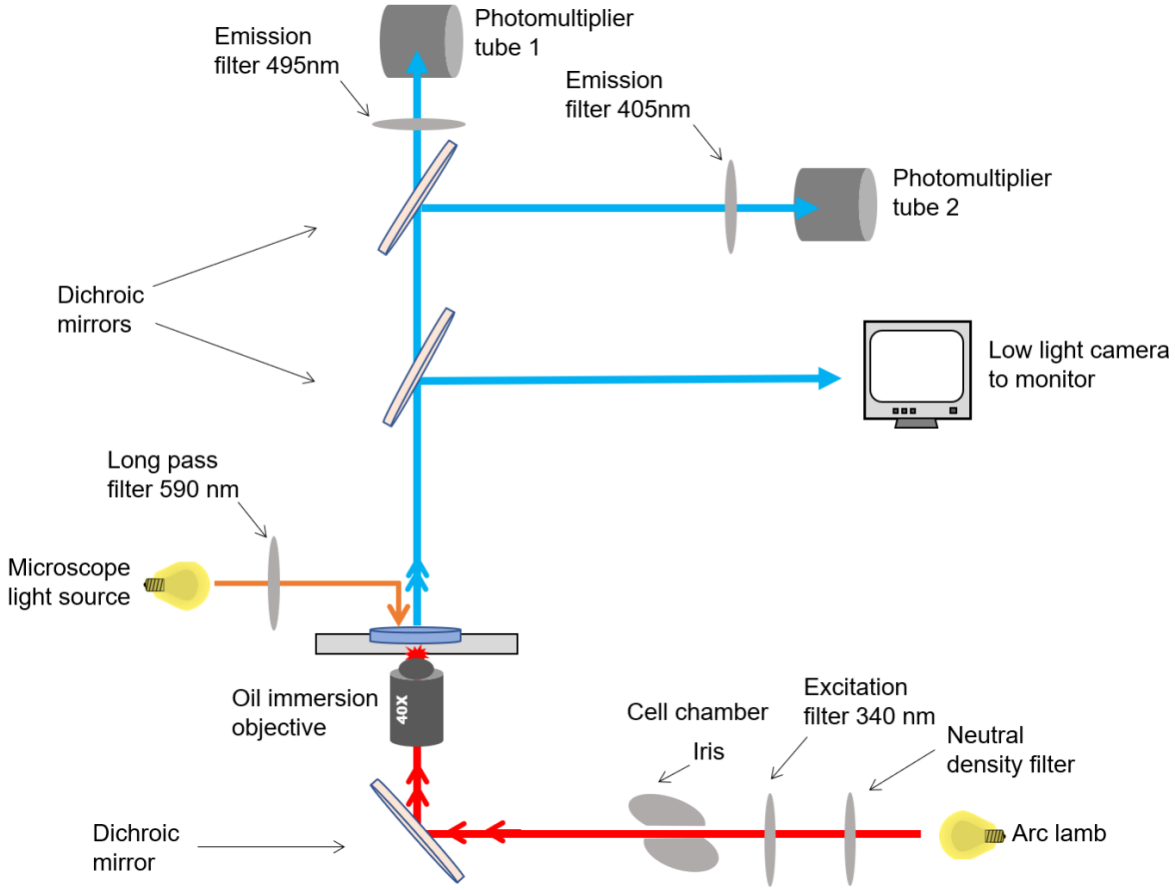

### 2.7.3 In vitro calibration of $[Ca^{2+}]i$

In order to convert fluorescence output to $[Ca^{2+}]i$, a two-point ionomycin calibration was done. Coverslips containing freshly isolated type-1 cells were loaded with indo-1 dye for one hour before they were transferred to a $Ca^{2+}$ - free medium with 10 μM ionomycin and 10 mM EGTA as a chelating agent. After thirty minutes, one coverslip was placed in the recording chamber with a continuous flow of a $Ca^{2+}$ - free medium (without ionomycin). Once type-1 cells were microscopically identified, the background signal was zeroed, and the solution was switched to a $Ca^{2+}$ - free medium with 10 μM ionomycin. This enables the determination of the Rmin and F495 free values. Next, the solution was switched to 10 mM $Ca^{2+}$ to determine the Rmax and F495 values.

The equation for calcium calibration is as follows:

$$[Ca^{2+}] = K_d \, x \, \frac{\text{F495 free}}{\text{F495 bound}} \quad x \quad \frac{\text{R-Rmin}}{\text{Rmax - R}}$$

Where R represents the fluorescence intensity ratio at 405 nm to fluorescence at 495 nm, R min represents the fluorescence ratio of the $[Ca^{2+}]$ free form of indo1, R max is the fluorescence ratio of calcium-bound indo-1, F495 free is the fluorescence intensity measured at 495 nm in $[Ca^{2+}]$ free solution, F495 bound is the fluorescence intensity measured at 495 nm in $[Ca^{2+}]$ max solution, and $K_D$ is the dissociation constant for $Ca^{2+}$ of indo1, approximately 230 nM (Jackson et al., 1987). These ratios were then averaged and used to calibrate the $Ca^{2+}$ signal in subsequent experiments.

### 2.7.4 Analysis of $[Ca^{2+}]i$ recordings

$Ca^{2+}$ recording of isolated rat carotid body type-1 cells starts with 40 seconds recording of baseline $Ca^{2+}$ level, then a brief hypoxic challenge (<20 seconds) was applied by switching the Tyrode solution equilibrated with normoxic gas mixture to the one equilibrated with hypoxic gas mixture, which increased the $Ca^{2+}$ signal. Next, the solution was switched back to the normoxic solution for 30-40 seconds before applying any agent of interest (Agent X). Then hypoxia was applied again in the presence of agent X. Calcium responses were evaluated by measuring the peak calcium response induced by hypoxia and muscarinic agonists. This approach was chosen as both hypoxia and muscarinic agonists were applied for a short time until a response was observed. In cases where other pharmacological agents were applied for a longer time (40-60 sec), their impact on type-1 cells' $[Ca^{2+}]i$ was determined by averaging the calcium levels 10 seconds after the application of each agent until the agent was removed. The data was reported by comparing the first hypoxic response to the hypoxic response in the presence of agent x (see Figure 2.8).

The agent X effect was calculated as:

$$\text{Agent X effect} = \frac{[Ca^{2+}]i \text{ hypoxia with agent X} - [Ca^{2+}]i \text{ baseline}}{[Ca^{2+}]i \text{ hypoxia} - [Ca^{2+}]i \text{ baseline}} X\ 100$$

And consequently, agent X % depression = 100 - agent X effect.

**Figure 2.8 Illustration of $Ca^{2+}$ signal analysis.** The red arrow indicates the hypoxic $Ca^{2+}$ response under baseline conditions. The green arrow indicates the second hypoxic $Ca^{2+}$ response in the presence of agent X. The orange arrow indicates the difference between the first and the second hypoxic $Ca^{2+}$ response (% depression).

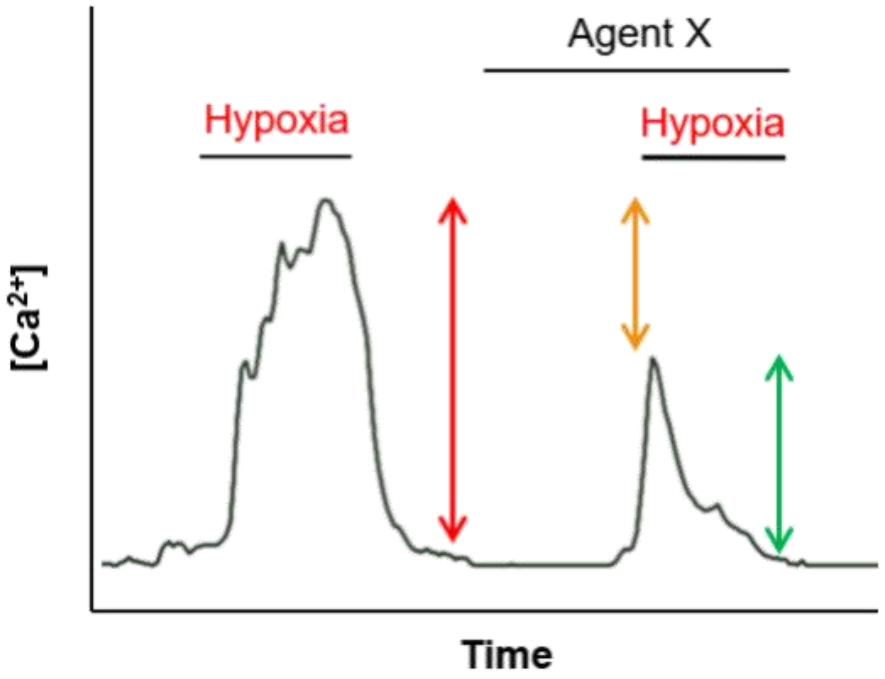

## 2.8 Electrophysiology

### 2.8.1 Pipette and pipette filling solution

To record single-channel activity, borosilicate glass capillaries (Harvard Apparatus Ltd., Kent, UK) were first pulled using a vertical puller (Narishige, Tokyo, Japan), then coated with Sylgard (Dow Croning, Wiseburge, Germany) to reduce the pipette conductance. Then, just prior to being used, the pipette tip was fire-polished to enable a stronger seal to the patched cell. The pipette was then filled with a high $K^+$ solution containing (in mM: 140 KCl, 1 $MgCl_2$, 1 EGTA, 10 HEPES, 10 TEA, 5 4-AP, pH 7.4 at 37ºC). The classical $K^+$ channels blockers, TEA and 4-AP, were added to the solution to block the activity of other $K^+$ channels.

### 2.8.2 Software and data acquisition

Axopatch 200B (Molecular Devices LLC, Sunnyvale, US) was used to perform cell-attached patch clamp recordings. Clamp current was filtered at 5 kHz, recorded, and digitised at 20 kHz using a CED 1401 and Spike 10 software (Cambridge Electronic Designs, Cambridge, UK). Voltage clamp protocols were also generated via the Spike 10 software for subsequent analysis of the recorded data.

### 2.8.3 Voltage clamp protocol

Once a healthy type-1 cell was identified, a previously pulled and sylgard-coated borosilicate pipette was briefly fire-polished, filled with the

electrode filling solution, and then placed in the micromanipulator. By carefully approaching the cell of interest, a seal was attempted. Upon successful formation of a good seal (>5 GΩ), the standard Tyrode solution was switched to a high $K^+$ (100 mM) Tyrode, and a positive potential of +100 mV was applied. The combination of a +100 mV pipette potential, 100 mM $K^+$ extracellular, and 140 mM $K^+$ pipette filling solution caused the activity of TASK channels to be shown as an inward current, which made it easy to define channel openings and thus enabled accurate measurements of TASK channel activity. In addition, the highly negative membrane potential across the patch helps to silence other voltage-gated channels in the patch. Once a stable activity of TASK channels was obtained, a brief hypoxic challenge (< 20 seconds) was applied to confirm the identity of the cell.

For inside-out recordings, after obtaining a GΩ seal, the high $K^+$ solution was switched to an intracellular solution containing: in mM (120 KCl, 5 $MgCl_2$, 10 EGTA, 10 Glucose, 23 $KHCO_3$; pH adjusted with KOH to 7.2 at 32ºC). Then the electrode was pulled away from the cell. A small piece of cell membrane will eventually separate from the cell surface, forming a vesicle on the tip of the pipette without compromising the G seal. Then the pipette tip was briefly passed through the air-water interface to burst the vesicle and enter inside-out mode.

### 2.8.4 Data analysis of patch clamp recordings

The number of ion channels can vary among different patches. Therefore, channel activity was defined by nPopen, where n represents the number of ion channels in the patch, and Popen represents the probability of a channel being open at any given time. The first step in nPopen analysis is to determine the main conductance state for each recording. This is done by constructing a

frequency all-points histogram. Most of the frequency all-points histograms contained one broad peak representing the amplitude of a single channel opening. The threshold for a single channel opening was set below this level, typically at 50%. Subsequently, multiple openings are defined as 150%, 250%, etc., of this threshold. These values were then added together and indexed to the number of measurements in the patch. To put it another way, the script used to calculate nPopen assigns each point one of the following values: 0 (baseline), 1 (single opening), 2 (double opening), or 3 (triple opening), etc. This is then added together and divided by the number of measurements taken. The nPopen is the average value of this. The percentage change in nPopen was determined using the following formula:

Percentage change = ((nPopen under Condition A - nPopen under Control) / nPopen under Control) * 100

Normalising channel activity to the control level of channel activity for each patch helps to eliminate a major source of variability in nPopen due to variation in the number of channels present in any given patch.

**Figure 2.9 nPopen analysis example.** All point frequency histogram of type-1 cell TASK channel activity. In this example, the main conductance amplitude is 2.5 pA. The 50% threshold is shown **(A)**. Screen capture of nPopen analysis. Currents above the 50% threshold (1.25 pA in this example) were counted as channel openings **(B)**.

**(A)**

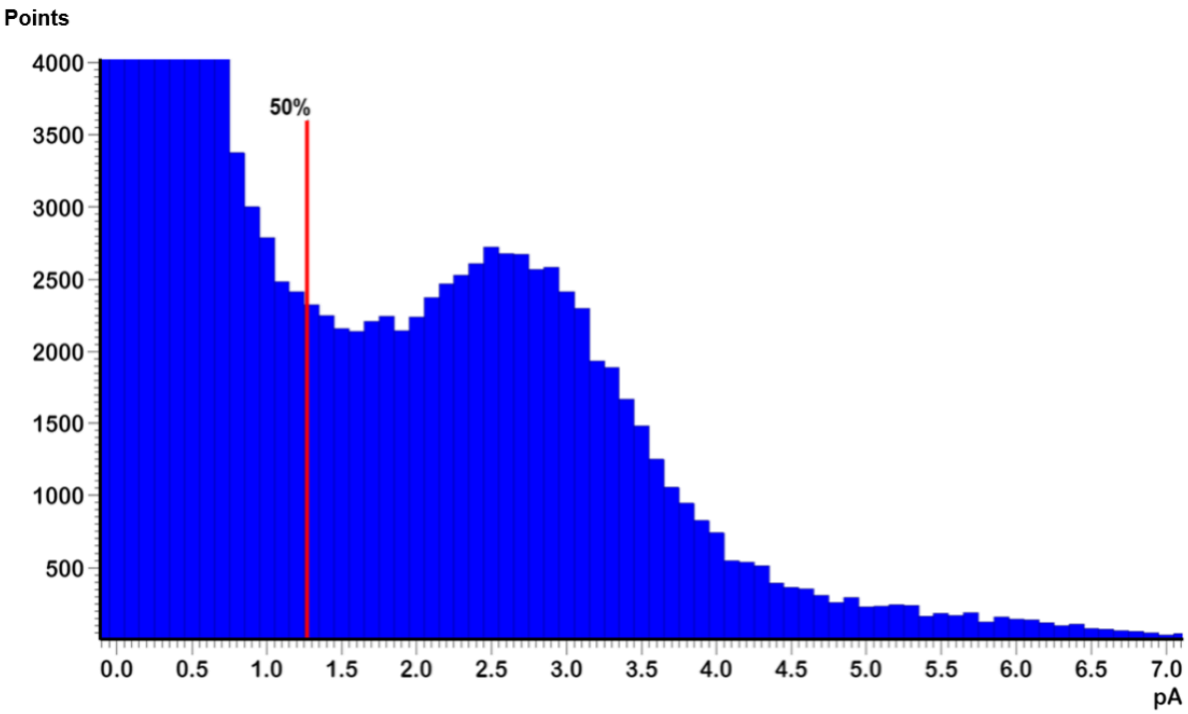


**(B)**

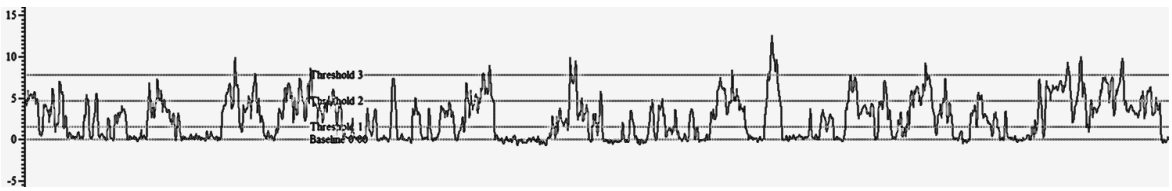

## 2.9 Statistics

Data are reported as the average value ± standard error of the mean. A paired t-test was used to determine the significance when two agents or two different concentrations of the same agent were applied to the same cell. Where more than two groups were compared, an ANOVA test was used. In each chapter, a more detailed description of the statistics used will be listed.

# Chapter. 3 The role of PLC signalling molecules in mediating hypoxia and muscarinic agonists evoked $[Ca^{2+}]i$ rise in type-1 cell

## 3.1 Introduction

As described in Chapter 1, the type-1 cell of the carotid body responds to hypoxia with an inhibition of background TASK-like $K^+$ currents, which decreases background potassium conductance and depolarises the membrane. This activates voltage-gated calcium channels ($Ca^{2+}{}_v$), resulting in $Ca^{2+}$ influx and neurosecretion (Buckler and Vaughan-Jones, 1994a; Buckler, 1997; Turner and Buckler, 2013; Buckler, 2015). Therefore, the inhibition of TASK channels is a major step in the hypoxia transduction cascade in type-1 cells. However, how exactly TASK channels sense a reduction in $PO_2$ has remained a mystery for decades.

Previous studies have provided crucial insights for our current research. First, mitochondrial inhibitors have been recognised for their potent stimulation of the carotid body, as evidenced by various studies (Heymans et al., 1931; Anichkov and Belen'kii, 1963; Krylov and Anichkov, 1968; Mills and Jobsis, 1971; Duchen and Biscoe, 1992a,b). Additionally, a broad spectrum of metabolic inhibitors has been found to inhibit background TASK-like $K^+$ channels in rat carotid body type-1 cells, as well as all three forms of TASK channels (TASK1, TASK3, and TASK1/TASK3 heterodimers) in TASK KO mice (Williams and Buckler, 2004; Wyatt and Buckler, 2004; Turner and Buckler, 2013b). This, along with the observation that the effects of metabolic inhibitors and hypoxia on TASK channels in type-1 cells are mutually exclusive, suggests that mitochondrial metabolism serves as the convergence point for both pathways (Wyatt and Buckler, 2004; Buckler, 2012, 2015).

Second, in patch clamp recordings of acutely isolated type-1 cells, an interesting observation emerges: In cell-attached patches, TASK channels are inhibited by hypoxia. However, in the inside-out mode, these channels undergo

a rapid rundown in activity after patch excision and lose their sensitivity to oxygen. This suggests that the functionality and $O_2$ sensitivity of TASK channels in type-1 cells are likely maintained by cytosolic signalling molecules or cofactors (Williams and Buckler, 2004; Buckler and Honore, 2004; Buckler, 2015). Following the rundown phase, TASK channels can be reactivated by applying millimolar concentrations of MgATP, indicating a potential dependence on MgATP. Nevertheless, it is worth noting that neither cloned TASK1 nor TASK3 channels have been reported to exhibit direct sensitivity to MgATP, nor have any recognised nucleotide binding sites been identified in the primary sequence of these channels. Taking together, these observations suggest that a MgATP-dependent signalling molecule is required to confer oxygen sensitivity to TASK channels (Buckler et al., 2000; Buckler and Honore, 2004; Buckler, 2015).

Third, in neonatal mice, RNA sequencing revealed that type-1 cells overexpress multiple genes encoding molecules known to be involved in GPCRs signalling (Zhou et al., 2016). This highlights the potential importance of GPCRs signalling pathways in regulating type-1 cells, particularly their responses to hypoxia.

Fourth, as discussed in Chapter 1, TASK channels in type-1 cells, other cell types, and heterologous expression systems are regulated by PLC downstream signalling molecules. Furthermore, the activity of many membrane lipid kinases (e.g., DAG kinase) is ATP-dependent (Xia and Yang, 2005; Han et al., 2008).

Based on the high expression of GPCRs in type-1 cells, the regulation of TASK channels by PLC signalling molecules, which are subject to ATP-dependent metabolism, and the apparent MgATP dependence of the oxygen sensor in type-1 cells, I formulated a hypothesis. I propose that PLC signalling

molecules could function as oxygen sensors, modulating the activity of TASK channels in response to hypoxia in type-1 cells.

I started by examining the effects of PLC signalling molecules on type-1 cell $[Ca^{2+}]i$ and hypoxia-evoked $[Ca^{2+}]i$ entry. This enabled me to efficiently assess the effects of various pharmacological agents in a relatively short timeframe before progressing to subsequent patch clamping experiments. Additionally, examining the effects of PLC signalling molecules at the cellular level might provide vital clues as to the mechanisms of the hypoxia transduction cascade in type-1 cells.

This chapter starts by examining the effects of three muscarinic agonists on $[Ca^{2+}]i$ in type-1 cells. Next, I investigated the source of muscarinic agonist-evoked $[Ca^{2+}]i$ entry. Then, I examined the effects of various pharmacological agents that either inhibit or activate PLC and downstream signalling molecules on hypoxia and muscarinic agonist-evoked $[Ca^{2+}]i$ entry.

## 3.2 Methods

All experiments were performed in accordance with the UK Animals (Scientific Procedures) Act, 1986.

**Cell isolation:**

The detailed method of carotid body dissection has been described in Chapter 2, Section 2.1.2. Briefly, under terminal anaesthesia, carotid bodies were dissected from rat pups (P11-P14). Carotid bodies were digested enzymatically and mechanically to isolate type-1 cells. Cell suspension was then plated onto poly-D-lysine treated coverslips then kept in the incubator for two hours before being topped up with modified culture medium. All recordings took place within 5-6 hours after the surgery.

**Calcium imaging:**

Rat type-1 cells were loaded with Indo-1-AM at room temperature and incubated for 1 hour. The detailed method of calcium imaging is described in Chapter 2, Section 2.7. Indo-1 dye was excited using a xenon lamp light source filtered through a 340 ± 5 nm bandpass filter. Emitted Indo-1 fluorescence was filtered at 405 ± 10 nm and 495 ± 15 nm using bandpass filters and measured using photomultiplier tubes (PMT). The PMT output was transmitted to a current to voltage converter, then digitised using a CED Power 1401, and recorded using Spike 2 software (CED, Cambridge, UK).

**Solutions:**

Coverslips were placed in the recording chamber and continuously superfused with warmed (37º) Tyrode solution (in mM: 117 NaCl, 4.5 KCl, 1 $MgCl_2$, 23 $NaHCO_3$, 11 Glucose). The Tyrode solution was equilibrated with either normoxic gas mixture (5% $CO_2$, balance air) or hypoxic gas mixture (5% $CO_2$, balance $N_2$).

**Recording protocol:**

Healthy type-1 cells were identified first by their appearance and then by their response to a brief hypoxic stimulus. Then methacholine chloride was applied before the application of the pharmacological agents of interest. After 50-60 seconds, hypoxia and then methacholine chloride were applied in the presence of the agent of interest, and then the cell was allowed to recover in control solution.

**Drugs**:

All drugs were appropriately reconstituted prior to dissolution in Tyrode solution. U73122, U3343, DiC8, and calphostin C were obtained from Sigma-Aldrich. Indo-1 AM was obtained from Calbiochem. FR900359 was obtained from Cayman Chemical. M-3m3fbs and o-3m3fbs were obtained from Biotechne-Tocris. The concentrations of the administered drugs were determined either based on the EC50 values specific to each drug, prior usage in similar studies, or a combination of both approaches.

**Statistical analysis of $[Ca^{2+}]i$ recordings in type-1 cells:**

N numbers denote separate recordings from a distinct cell/s on different coverslips. Statistical significance was assessed using Student's t tests. A p value $< 0.05$ was taken as statistically significant. Where more than two groups were compared, an ANOVA test was used.

## 3.3 Results

In this study, type-1 cells were first classified as such by visual inspection. Single cells with a diameter of ~ 5 μm or clusters of 2-3 cells were selected. The cells were then challenged with a brief hypoxic stimulus to further confirm their identity. Only cells that responded to hypoxia with a rise in $[Ca^{2+}]i$ were selected for further study. In some experiments, rhodamine-conjugated peanut agglutinin (PNA) was used to aid in identifying type-1 cells (see Methods, Chapter 2). Once a PNA-labelled cell was found, a brief hypoxic challenge was applied to confirm its identity.

### 3.3.1 Effects of muscarinic agonists on type-1 cell $[Ca^{2+}]i$

First, I wanted to establish that a wide range of muscarinic agonists can evoke a $[Ca^{2+}]i$ rise in type-1 cells. The application of methacholine chloride (300 μM), muscarine chloride (50 μM), and oxotremorine (100 μM) induced a rapid and reversible rise in $[Ca^{2+}]i$ (n = 6, Figure 3.1). To determine whether this response is mediated by the release of $Ca^{2+}$ from internal stores or through $Ca^{2+}$ influx, I studied the effects of both $Ca^{2+}$ removal and the addition of a non-selective antagonist of $Ca^{2+}$ entry ($Ni^{2+}$). The methacholine chloride-evoked $[Ca^{2+}]i$ rise was largely (but not completely) reduced in $Ca^{2+}$ -free medium ( $Ca^{2+}$ excluded from the bathing medium and 1 mM EGTA was added) (see Figures 3.2A and B $\Delta$ $[Ca^{2+}]i$ control *vs.* $Ca^{2+}$ -free conditions: 468.5 ± 85.5 *vs.* 60 ± 42.5, n = 8, p = 0.001).

Additionally, the $[Ca^{2+}]i$ response to methacholine chloride was reduced by 2 mM $Ni^{2+}$ (Figures 3.2C and D $\Delta$ $[Ca^{2+}]i$ control *vs.* with 2 mM $Ni^{2+}$: 445.5 ± 54.3 *vs.* 97.9 ± 24.5, n = 7, $p < 0.001$). Taken together, these observations suggest that the methacholine chloride-evoked $[Ca^{2+}]i$ rise is mediated by $Ca^{2+}$

influx and, to a lesser extent, by $Ca^{2+}$ release from internal stores. In contrast, $Ca^{2+}$ response to hypoxia is almost entirely mediated by voltage-gated $Ca^{2+}$ influx (Buckler and Vaughan-Jones, 1994; Urena et al., 1994). Methacholine chloride was used as a positive control to activate Gq11-coupled receptors in subsequent experiments.

**Figure 3.1 Effects of muscarinic agonists on [$Ca^{2+}$]i in type-1 cells**

Recordings of [$Ca^{2+}$]i in isolated type-1 cells showing responses to muscarinic agonists **(A)**. Mean Δ [$Ca^{2+}$]i responses to methacholine chloride (300 µM), muscarine chloride (100 µM), and oxotremorine ( 50 µM) **(B)**. (n = 6, no statistical difference between the agents (ANOVA p = 0.86). Error bars indicate S.E.M.

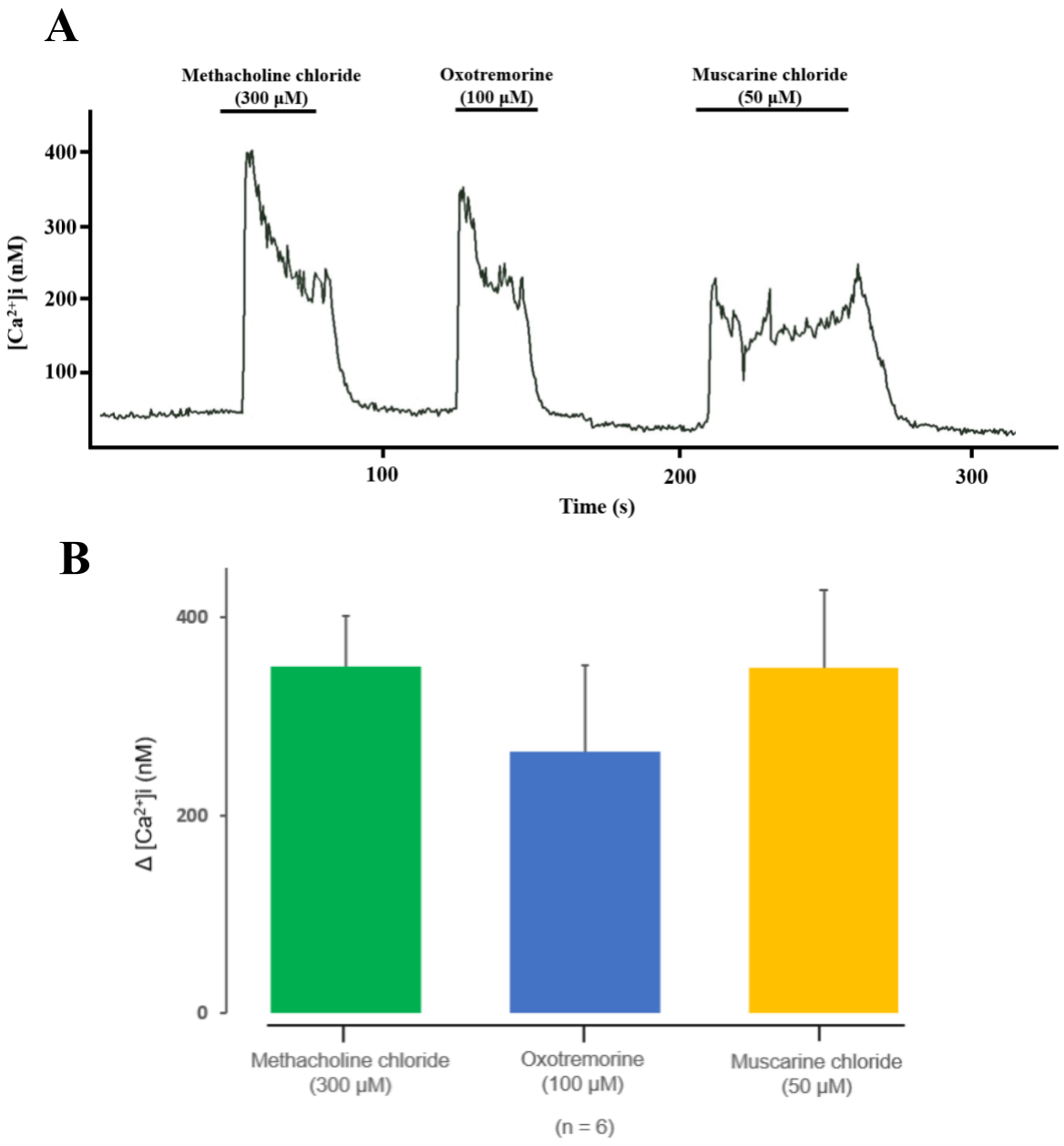

**Figure 3.2 Methacholine chloride evoked $[Ca^{2+}]i$ rise is dependent upon $Ca^{2+}$ influx**

Effects of removal of extracellular $Ca^{2+}$ (+ 1 mM EGTA) on type-1 cells $[Ca^{2+}]i$ response to methacholine chloride (300 µM) **(A)**. Quantitative effects of methacholine chloride response in $Ca^{2+}$-free conditions **(B)**. Effects of 2 mM $Ni^{2+}$ on methacholine chloride evoked $[Ca^{2+}]i$ **(C)**. Quantitative effects of 2 mM $Ni^{2+}$ on methacholine chloride evoked $[Ca^{2+}]i$ **(D)**. Note that both $Ca^{2+}$ removal and the application of 2 mM $Ni^{2+}$ significantly reduced methacholine chloride evoked $[Ca^{2+}]i$. Error bars indicate S.E.M. Statistical significance was assessed using a paired Student's t-test.

**A**

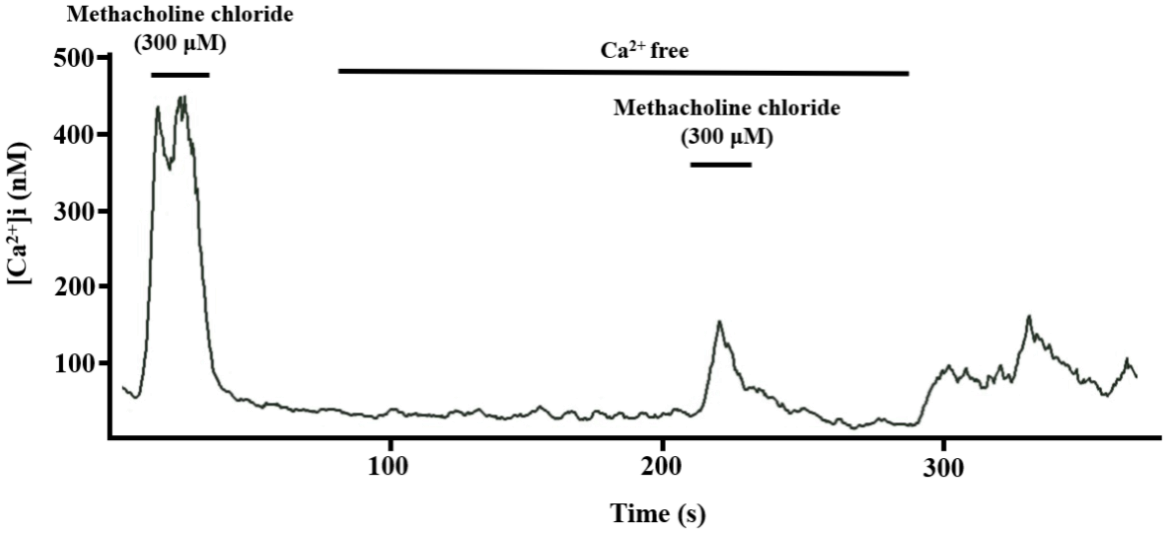

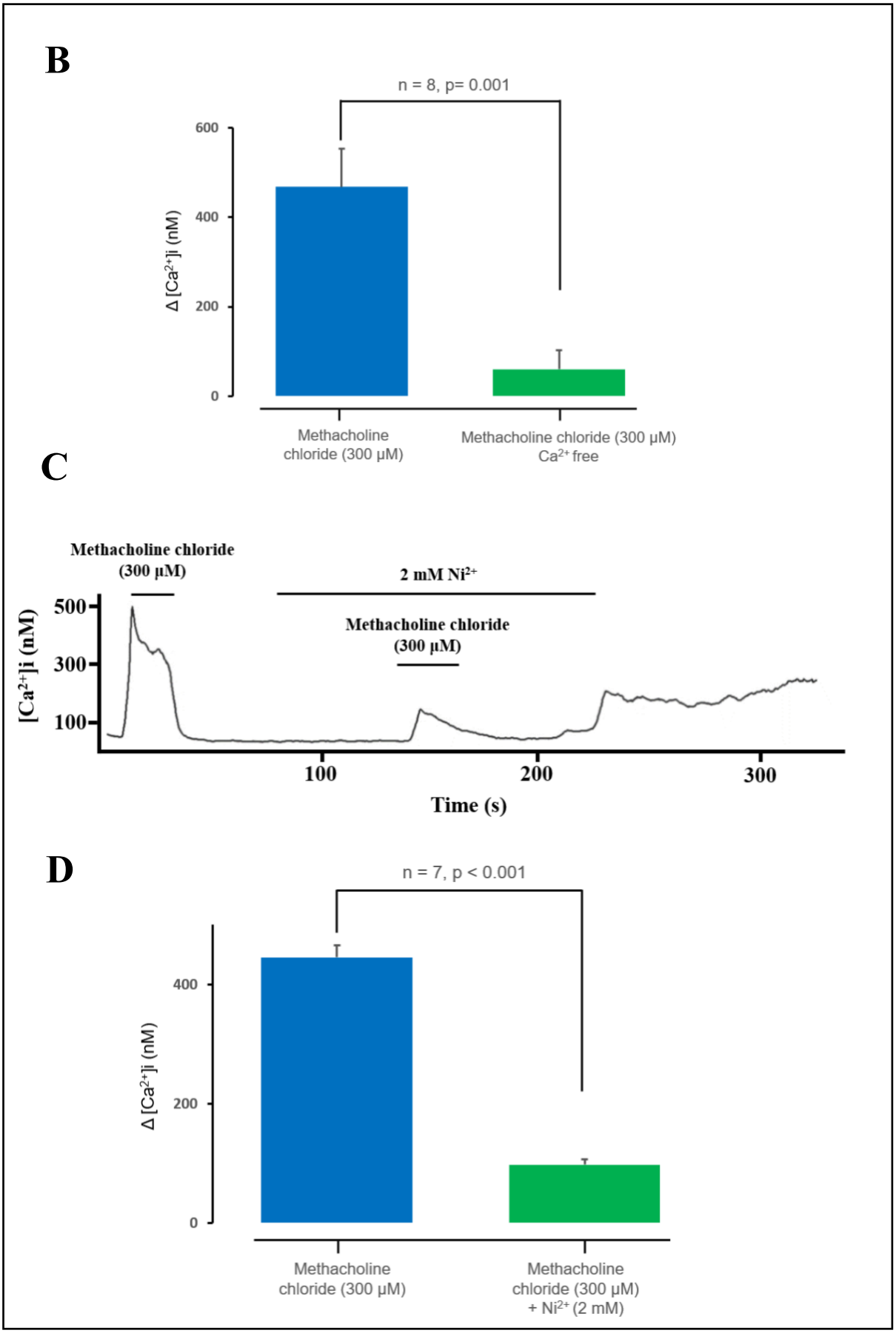
B
n = 8, p= 0.001
600
400
200
0
Δ [Ca2+]i (nM)
Methacholine chloride (300 µM)
Methacholine chloride (300 µM) Ca2+ free
C
Methacholine chloride (300 µM)
2 mM Ni2+
Methacholine chloride (300 µM)
500
300
100
[Ca2+]i (nM)
100
200
300
Time (s)
D
n = 7, p < 0.001
400
200
0
Δ [Ca2+]i (nM)
Methacholine chloride (300 µM)
Methacholine chloride (300 µM) + Ni2+ (2 mM)

### 3.3.2 Effects of the Gq inhibitor FR900359 on hypoxia and methacholine chloride evoked $[Ca^{2+}]i$ rise

To test whether Gq- coupled receptors are involved in mediating hypoxia and methacholine chloride-evoked $[Ca^{2+}]i$ transients, a specific inhibitor of the Gq protein, FR900359, was applied. Application of FR900359 (1 μM) had no effect on baseline levels of $[Ca^{2+}]i$ but inhibited hypoxia (see Figures 3.3A and B Δ $[Ca^{2+}]i$ hypoxia *vs.* hypoxia plus FR900359: 678.6 ± 195.5 *vs.*128.4 ± 19.7, compare red bar *vs.* yellow bar, n = 10, p = 0.006) and methacholine chloride (300 μM)- induced $[Ca^{2+}]i$ (see Figures 3.3A and B Δ $[Ca^{2+}]i$ methacholine chloride 300 μM *vs.* methacholine chloride 300 μM plus FR900359: 238.6 ± 105.8 *vs.*11.3 ± 9.7, compare blue bar *vs.* green bar, n = 5, p = 0.03). FR900359 had no effect on the high $K^+$ (100 mM) evoked $[Ca^{2+}]i$ transients. Its effects on hypoxia and methacholine chloride were irreversible.

**Figure 3.3 Effects of the Gq inhibitor FR900359 (1 μM) on $[Ca^{2+}]i$ in type-1 cells** Recordings of **[**$Ca^{2+}$]i in isolated type-1 cells showing their responses to hypoxia and methacholine chloride (300 μM) in control and with FR900359 **(A)**. Quantitative effects of 1 μM FR900359 on hypoxia and methacholine chloride evoked $[Ca^{2+}]i$ transients **(B)**. Note that FR900359 inhibited both hypoxia and methacholine chloride evoked $[Ca^{2+}]i$. Error bars indicate S.E.M. The signal was saturated in response to high $K^+$, resulting in an abrupt truncation of the signal. Statistical significance was assessed using a paired Student's t-test.

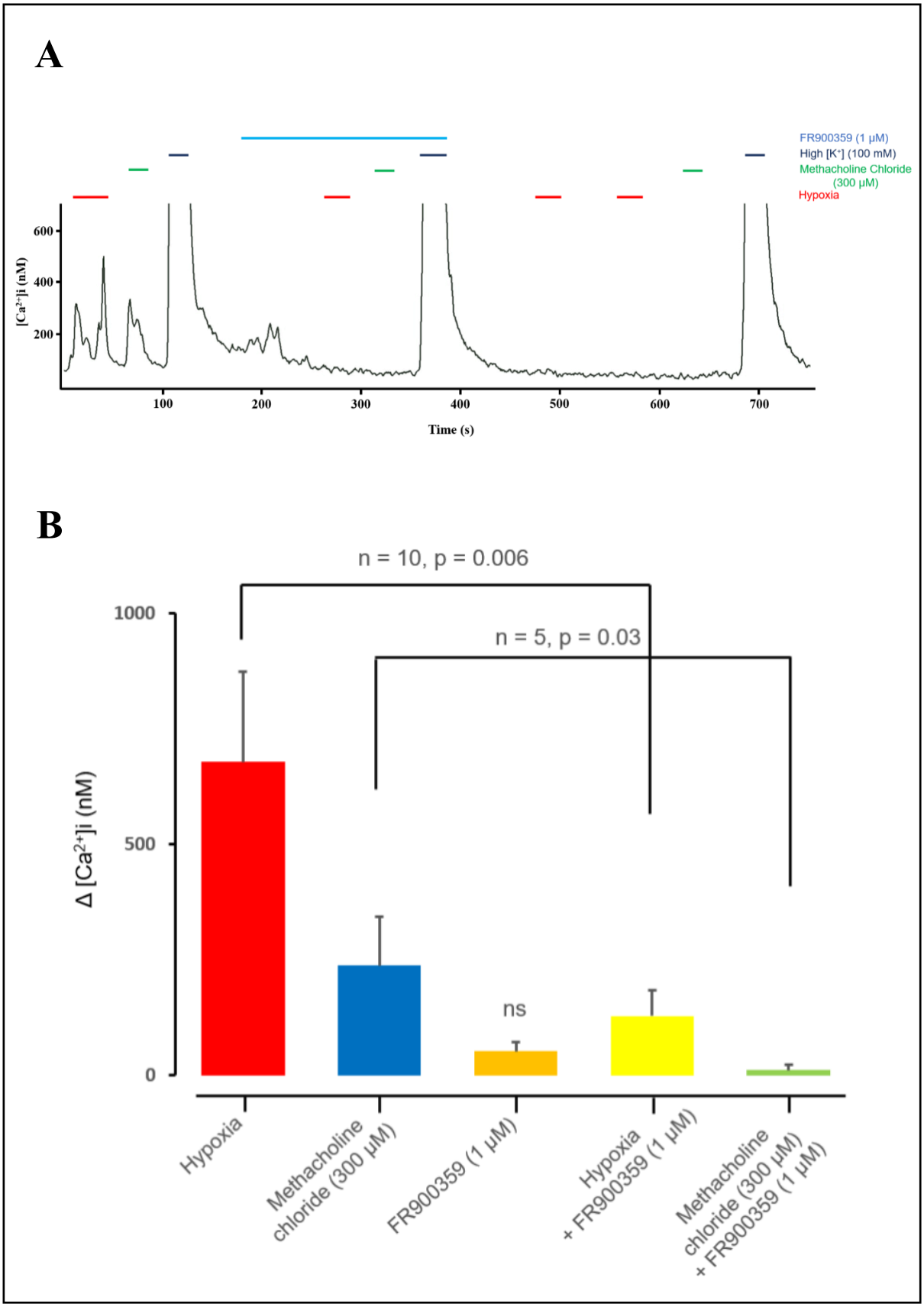
A
FR900359 (1 μM)
High [K+] (100 mM)
Methacholine Chloride (300 μM)
Hypoxia
[Ca2+]i (nM)
600
400
200
100
200
300
400
500
600
700
Time (s)
B
n = 10, p = 0.006
n = 5, p = 0.03
1000
500
0
Δ [Ca2+]i (nM)
ns
Hypoxia
Methacholine chloride (300 μM)
FR900359 (1 μM)
Hypoxia + FR900359 (1 μM)
Methacholine chloride (300 μM) + FR900359 (1 μM)

### 3.3.3 Effects of the PLC inhibitor U73122 on hypoxia and methacholine chloride evoked $[Ca^{2+}]i$ rise

Next, I investigated the role of PLC in hypoxia and methacholine chloride-evoked $[Ca^{2+}]i$ transients. U73122, a widely used inhibitor of phosphoinositide-specific PLC, was applied at three different concentrations: 5 μM, 1 μM and 100 nM. Application of 5 μM U73122 had no effect on baseline levels of $[Ca^{2+}]i$ but inhibited hypoxia (see Figures 3.4A and D Δ $[Ca^{2+}]i$ hypoxia *vs.* hypoxia plus U73122: 635.4 ± 100 nM *vs.* 8.6 ± 4.6 nM, compare red bar *vs.* yellow bar, n = 10, $p < 0.001$) and methacholine chloride evoked $[Ca^{2+}]i$ transients (see Figures 3.4A and D Δ $[Ca^{2+}]i$ methacholine chloride 300 μM *vs.* methacholine chloride 300 μM plus U73122: 499 ± 112.5 nM *vs.* 3.6 ± 1.9 nM, compare blue bar *vs.* green bar, n = 7, $p < 0.001$). However, in a selected subset of our experiments, U73122 blocked or reduced the high $K^+$ (100 mM) evoked $[Ca^{2+}]i$ transients, indicating that it induced some off-target effects (n = 7). I reduced U73122 to a lower concentration (1 μM) in an effort to uncouple its effect on high $K^+$ from its effect on hypoxia. At this concentration, U73122 inhibited hypoxia and methacholine chloride-evoked $[Ca^{2+}]i$ transients (see Figures 3.4B and E Δ $[Ca^{2+}]i$ hypoxia *vs.* hypoxia plus U73122: 563.4 nM ± 135.6 *vs.* 68.6 ± 13.3 nM, compare red bar *vs.* yellow bar, n = 9, p = 0.003; methacholine chloride 300 μM *vs.* methacholine chloride 300 μM plus U73122: 331.5 ± 84.5 nM *vs.* 75.5 ± 22, compare blue bar *vs.* green bar, n = 5, p = 0.001). However, at this concentration, U73122 still reduced the high $K^+$-evoked $[Ca^{2+}]i$ transients (n = 4).

I then reduced the concentration of U73122 even further to 100 nM.

A similar inhibition of hypoxia and methacholine chloride-evoked $[Ca^{2+}]i$ transients was observed (see Figures 3.4C and F Δ $[Ca^{2+}]i$ hypoxia *vs.* hypoxia plus U73122: 595.8 nM ± 162.3 *vs.* 103.4 nM ± 32.5, compare red bar *vs.* yellow bar, n = 8, $p < 0.01$; methacholine chloride 300 μM vs. methacholine

chloride 300 μM plus U73122: 321.1 ± 39.5 nM *vs.* 94.4 ± 46.4 nM, compare blue bar *vs.* green bar, n = 5, p = 0.03). However, U73122 still reduced the high $K^+$-evoked $[Ca^{2+}]i$ transients at this concentration.
U73343, the U73122 control compound, had no effect on hypoxia and methacholine chloride-evoked $[Ca^{2+}]i$ transients (see Figures 3.5A and B, n = 5).

These data suggest that PLC activity is involved in the modulation of type-1 $[Ca^{2+}]i$ responses to hypoxia and muscarinic agonists. It is unclear, however, whether these effects are mediated by TASK channels, voltage-gated $Ca^{2+}$ channels, or both.

**Figure 3.4: Effects of the PLC inhibitor U73122 (5 µM, 1 µM, and 100 nM) on [$Ca^{2+}$]i in type-1 cells** Recordings of [$Ca^{2+}$]i in isolated type-1 cells showing responses to hypoxia and methacholine chloride (300 µM) in control and in the presence of three different concentrations of U73122 (5 µM **(A)**, 1 µM **(B),** and 100 nM **(C)**). Quantitative effects of U73122 on hypoxia and methacholine chloride evoked [$Ca^{2+}$]i at 5 µM **(D)**, 1 µM **(E),** and 100 nM **(F)**. Note that in all three concentrations, U73122 inhibited the high [$K^+$] (100 mM)-evoked [$Ca^{2+}$]i transients. Error bars indicate S.E.M. The signal was saturated in response to high $K^+$, resulting in an abrupt truncation of the signal. Statistical significance was assessed using a paired Student's t-test.

**A**

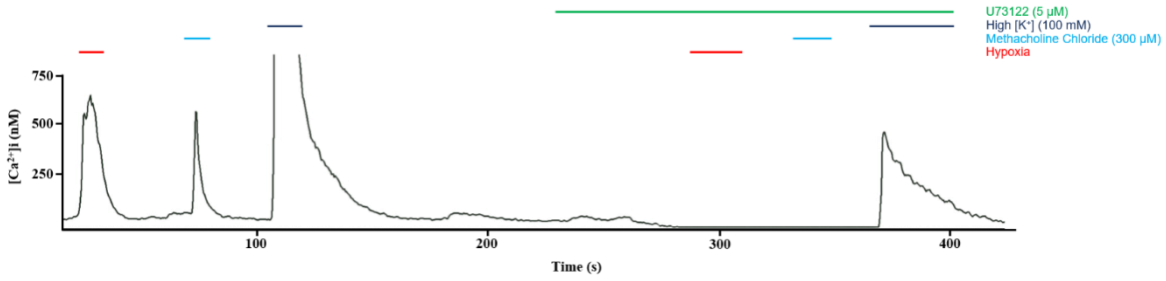


**B**

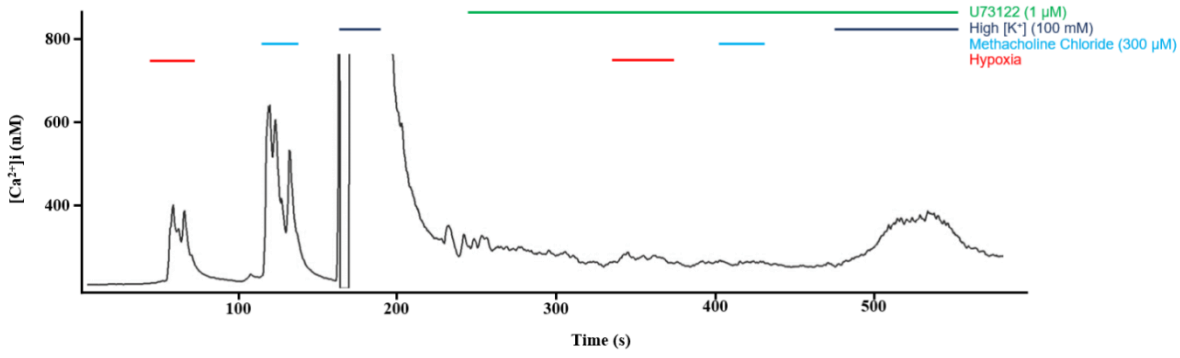

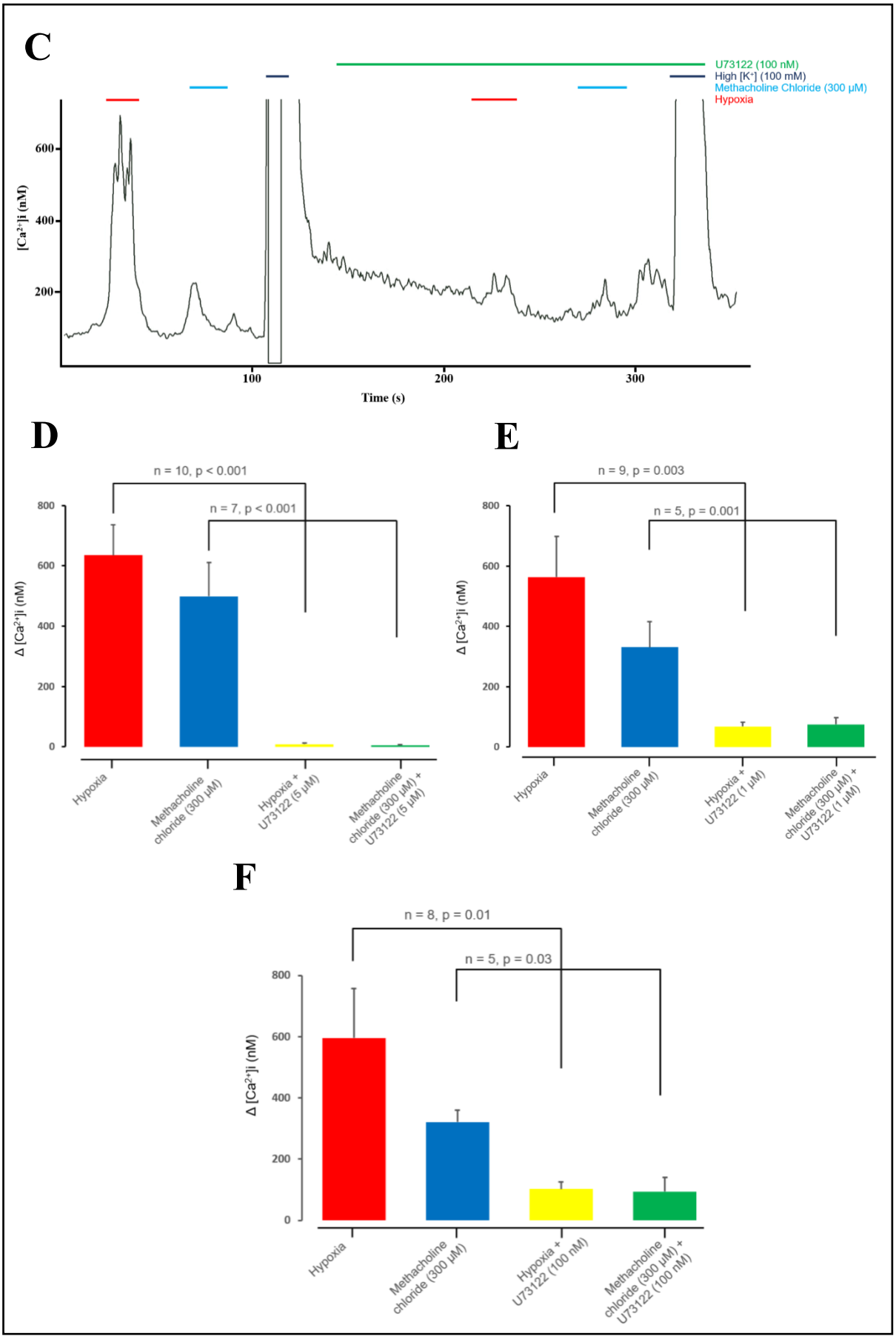
C
U73122 (100 nM)
High [K+] (100 mM)
Methacholine Chloride (300 µM)
Hypoxia
[Ca2+]i (nM)
600
400
200
100
200
300
Time (s)
D
n = 10, p < 0.001
n = 7, p < 0.001
Δ [Ca2+]i (nM)
800
600
400
200
0
Hypoxia
Methacholine chloride (300 µM)
Hypoxia + U73122 (5 µM)
Methacholine chloride (300 µM) + U73122 (5 µM)
E
n = 9, p = 0.003
n = 5, p = 0.001
Δ [Ca2+]i (nM)
800
600
400
200
0
Hypoxia
Methacholine chloride (300 µM)
Hypoxia + U73122 (1 µM)
Methacholine chloride (300 µM) + U73122 (1 µM)
F
n = 8, p = 0.01
n = 5, p = 0.03
Δ [Ca2+]i (nM)
800
600
400
200
0
Hypoxia
Methacholine chloride (300 µM)
Hypoxia + U73122 (100 nM)
Methacholine chloride (300 µM) + U73122 (100 nM)

**Figure 3.5: Effects of U73343, the U73122 control compound, (5 µM) on [$Ca^{2+}$]i in type-1 cells** Recordings of [$Ca^{2+}$]i in isolated type-1 cells showing responses to hypoxia and methacholine chloride (300 µM) in control and in the presence of U73343 (5 µM) **(A)**. Quantitative effects of U73343 on hypoxia and methacholine chloride evoked [$Ca^{2+}$]i transients **(B).** Error bars indicate S.E.M. Statistical significance was assessed using a paired Student's t-test.

**A**

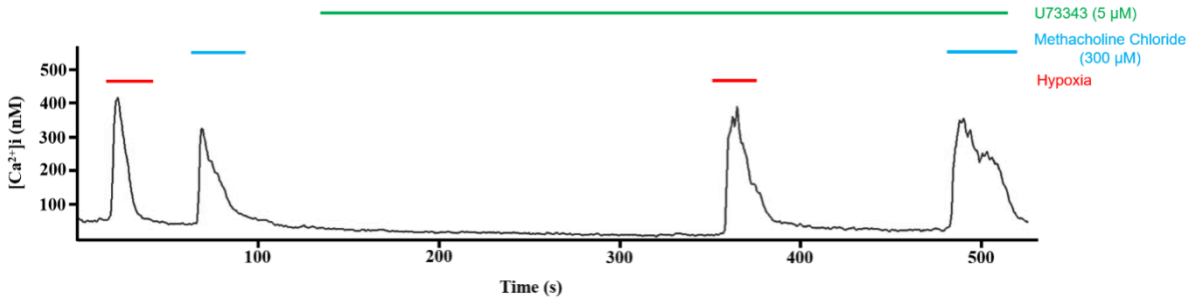


**B**

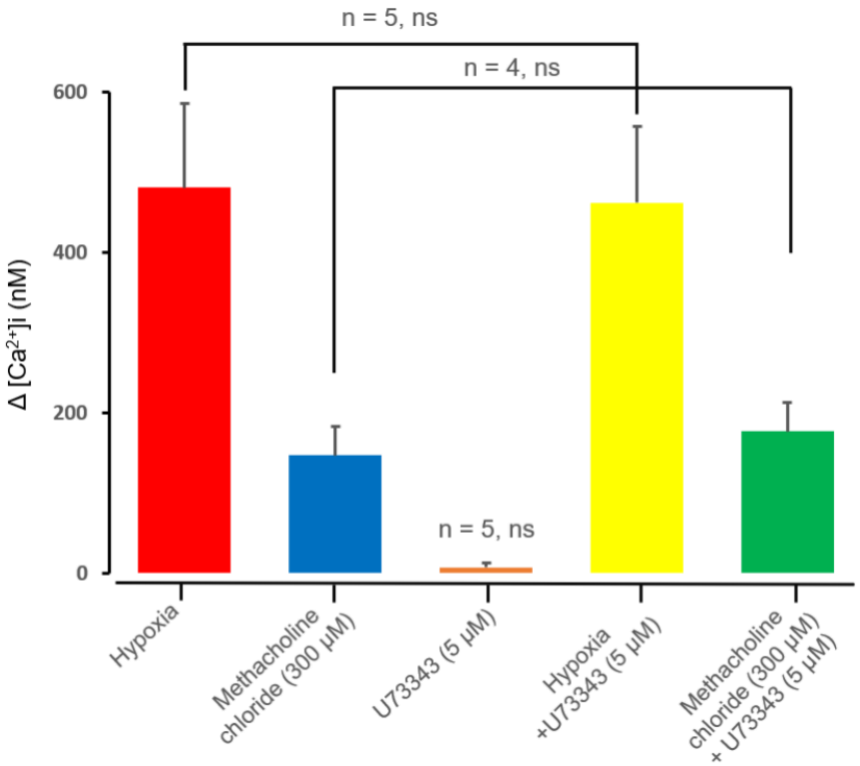

### 3.3.4 Effects of the PLC activator m-3m3fbs on hypoxia and methacholine chloride evoked $[Ca^{2+}]i$ rise

In search of other practical methods to further examine the effects of PLC on type-1 cell $[Ca^{2+}]i$ responses, I used the PLC activator m-3m3fbs. M-3m3fbs (10 and 20 μM) induced a significant dose-dependent reversible increase in baseline levels of $[Ca^{2+}]i$ (see Figures 3.6A (i and ii) and B (i and ii), $[Ca^{2+}]i$ control *vs.* m-3m3fbs at 10 μM 57.9 ± 6.9 nM *vs.* 92.5 ± 14 nM, n = 5, $p < 0.007$; at 20 μM: 69.2 ± 4.7 nM *vs.* 154.5 ± 22 nM, n = 7, p = 0.009). However, the effects of m-3m3fbs on hypoxia and methacholine chloride-induced $[Ca^{2+}]i$ transients were not significant at either concentration (see Figures 3.6C and D Δ $[Ca^{2+}]i$ hypoxia *vs.* hypoxia plus m-3m3fbs at 10 μM: 454.6 ± 24.7 nM *vs.* 293.6 ± 40.2 nM, compare red bar *vs.* yellow bar, n = 5, p = 0.06; hypoxia *vs.* hypoxia plus m-3m3fbs at 20 μM: 506.5.2 ± 28.7 nM *vs.* 446.8 ± 25.2 nM, compare red bar *vs.* yellow bar, n = 7, p = 0.13; methacholine chloride 300 μM *vs.* methacholine chloride 300 μM plus m-3m3fbs at 10 μM: 326.25 ± 41.7 nM *vs.* 258.7 ± 37.7 nM, compare blue bar *vs.* green bar, n = 4, p = 0.29; methacholine chloride 300 μM *vs.* methacholine chloride 300 μM plus m-3m3fbs at 20 μM: 305.9 ± 17.2 nM *vs.* 317.5 ± 19 nM, compare blue bar *vs.* green bar, n = 4, p = 0.14). However, the small n number in these experiments may result in insufficient statistical power to detect the effects of m-3m3fbs on type-1 cells $[Ca^{2+}]i$ responses.

O-3m3fbs, the m-3m3fbs control compound, had no effect on baseline levels of $[Ca^{2+}]i$, hypoxia, and methacholine chloride-evoked $[Ca^{2+}]i$ transients (see Figures 3.7A and B, n = 5 for hypoxia and 3 for methacholine chloride). Taken together, these results suggest that baseline $[Ca^{2+}]i$ levels in type-1 cells are sensitive to PLC activation.

**Figure 3.6: Effects of the PLC activator m-3m3fbs (10 and 20 µM) on [$Ca^{2+}$]i in type-1 cells** Recordings of [$Ca^{2+}$]i in isolated type-1 cells showing responses to hypoxia (i) and methacholine chloride (ii) (300 µM) in control and in the presence of m-3m3fbs 10 µM **(A)** and 20 µM **(B)**. Quantitative effects of m-3m3fbs on hypoxia and methacholine chloride evoked [$Ca^{2+}$]i transients at 10 µM **(C)** and 20 µM **(D)**. Note that m-3m3fbs (10 and 20 µM) induced spiking of [$Ca^{2+}$]i. Error bars indicate S.E.M. Statistical significance was assessed using a paired Student's t-test.

**A**

(i)

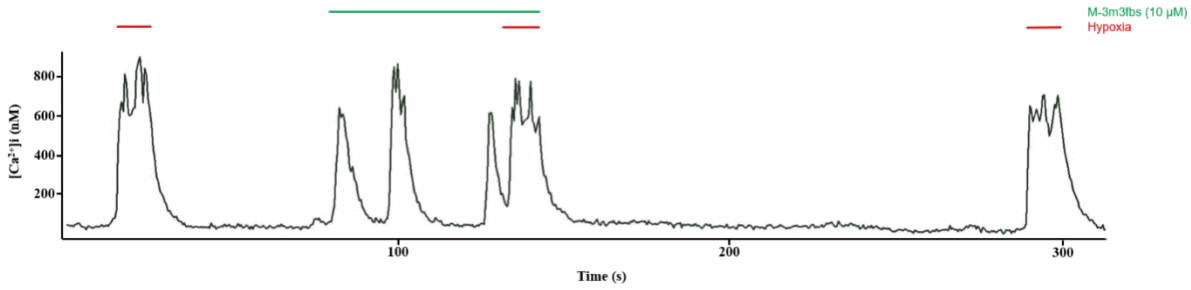


(ii)

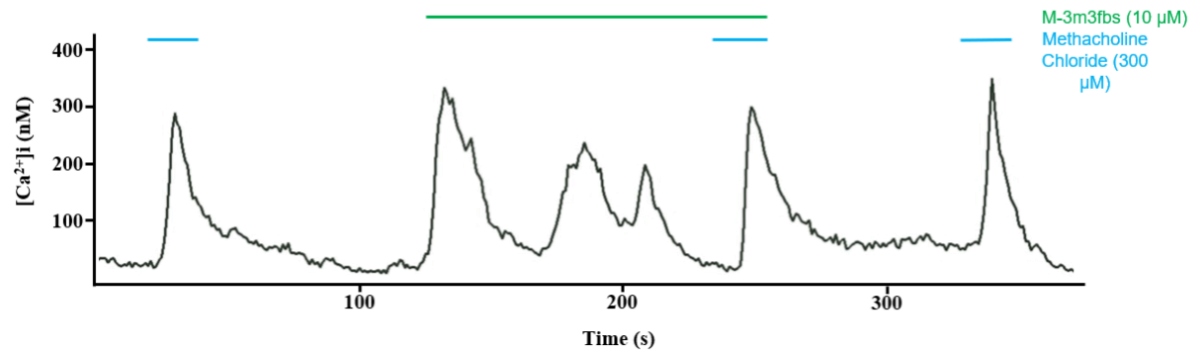

**B**

(i)

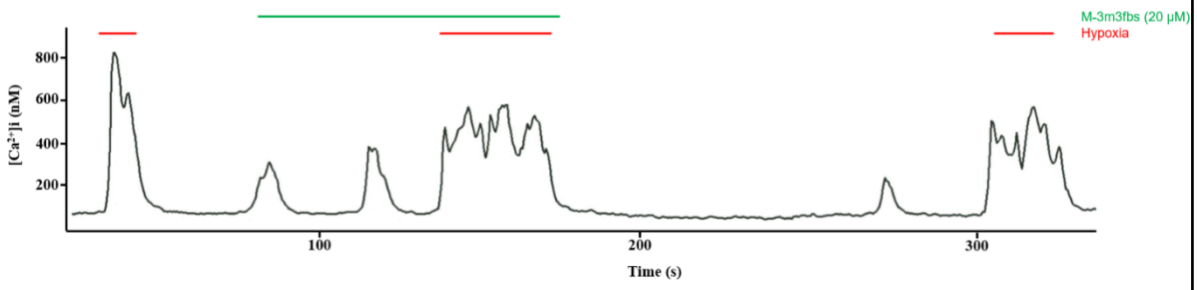
M-3m3fbs (20 μM)
Hypoxia
800
600
400
200
[Ca²⁺]i (nM)
100
200
300
Time (s)

(ii)

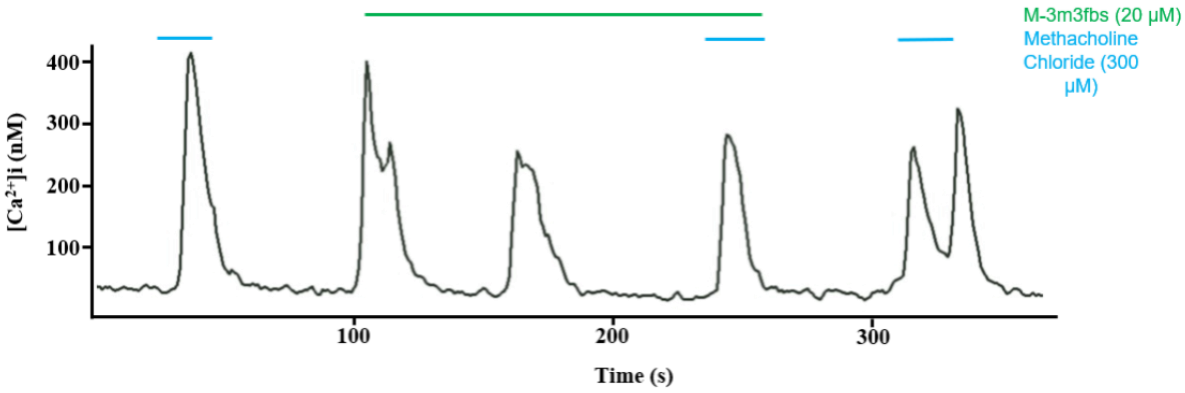
M-3m3fbs (20 μM)
Methacholine Chloride (300 μM)
400
300
200
100
[Ca²⁺]i (nM)
100
200
300
Time (s)

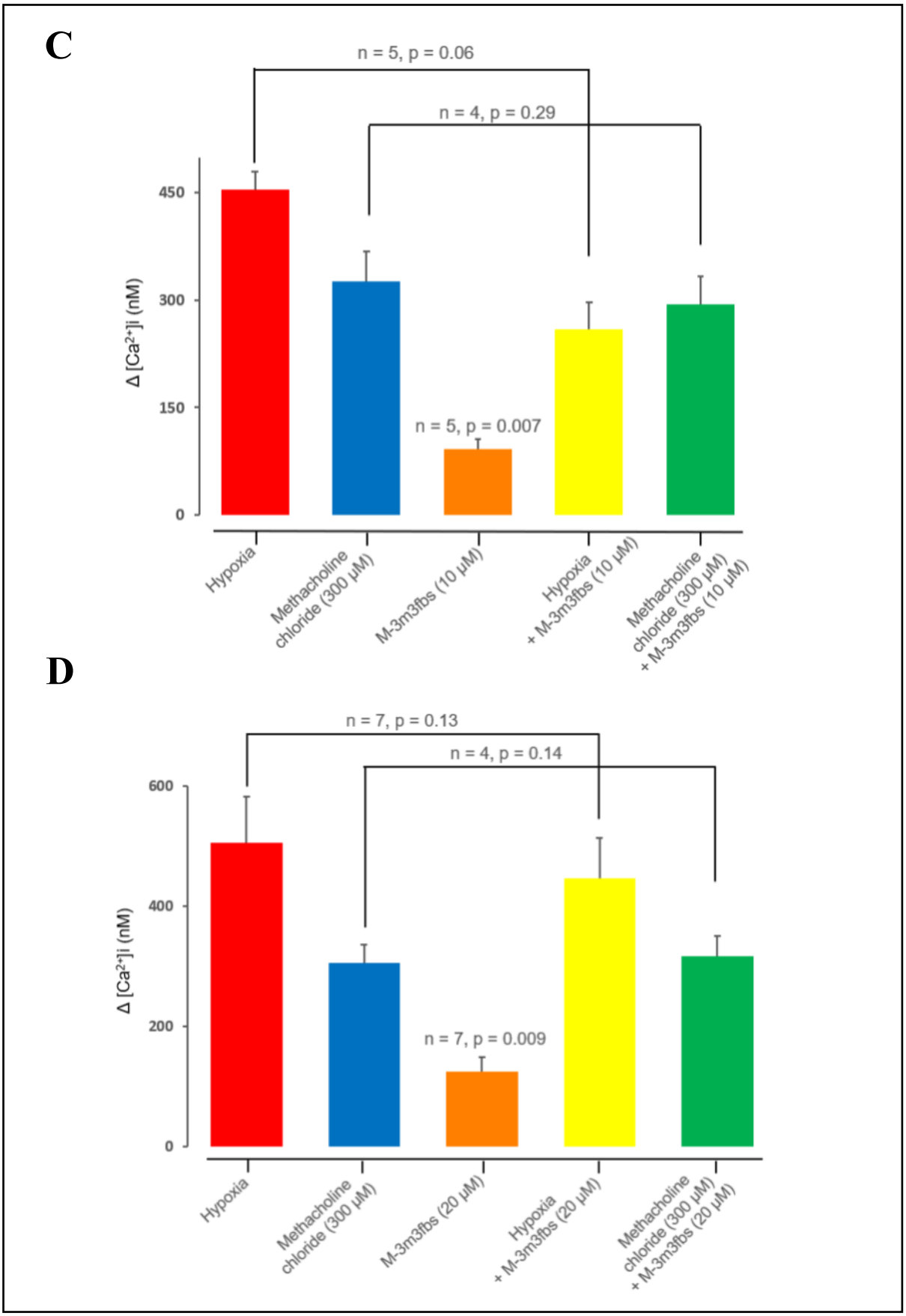
C
n = 5, p = 0.06
n = 4, p = 0.29
n = 5, p = 0.007
Δ [Ca2+]i (nM)
450
300
150
0
Hypoxia
Methacholine chloride (300 µM)
M-3m3fbs (10 µM)
Hypoxia + M-3m3fbs (10 µM)
Methacholine chloride (300 µM) + M-3m3fbs (10 µM)
D
n = 7, p = 0.13
n = 4, p = 0.14
n = 7, p = 0.009
Δ [Ca2+]i (nM)
600
400
200
0
Hypoxia
Methacholine chloride (300 µM)
M-3m3fbs (20 µM)
Hypoxia + M-3m3fbs (20 µM)
Methacholine chloride (300 µM) + M-3m3fbs (20 µM)

**Figure 3.7: Effects of o-3m3fbs, the m-3m3fbs control compound, (10 µM) on [$Ca^{2+}$]i in type-1 cells.** Recordings of [$Ca^{2+}$]i in isolated type-1 cells showing responses to hypoxia (i) and methacholine chloride (ii) (300 µM) in control and in the presence of o-3m3fbs (10 µM) **(A)**. Quantitative effects of o-3m3fbs on hypoxia and methacholine chloride evoked [$Ca^{2+}$]i transients **(B).** Error bars indicate S.E.M. Statistical significance was assessed using a paired Student's t-test.

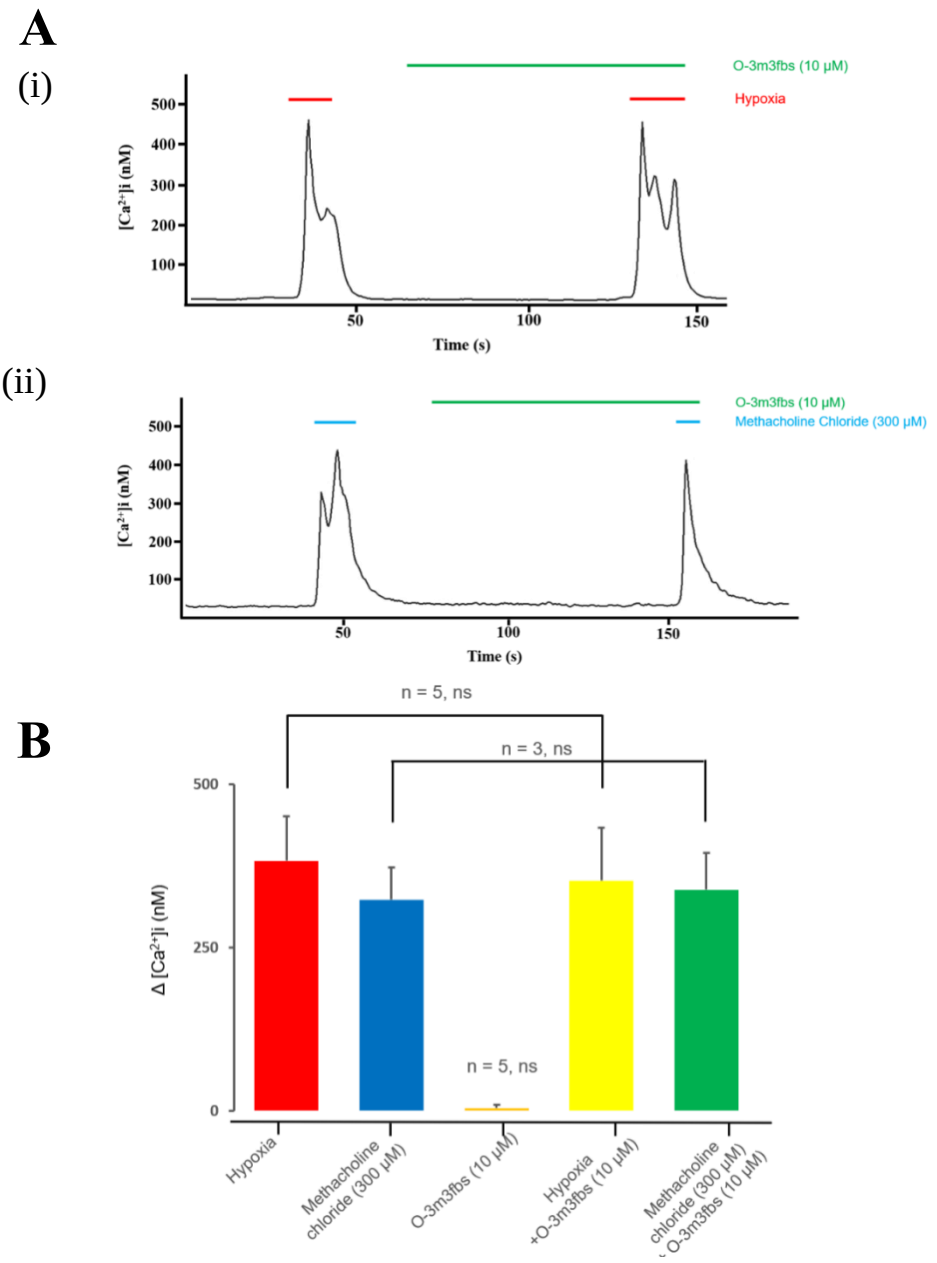

### 3.3.5 Effects of the membrane-permeable short-chain DAG analogue 1,2 dioctanoyl-*sn*-glycerol (DiC8) on hypoxia and methacholine chloride evoked $[Ca^{2+}]i$ rise

To determine the effects of signalling molecules downstream of PLC on $[Ca^{2+}]i$ responses of type-1 cells, I first investigated the effects of DAG. Application of the DAG analogue DiC8 (5 μM) induced a rise in type-1 cell $[Ca^{2+}]i$ (see Figures 3.8A and C, $[Ca^{2+}]i$ control *vs.* DiC8: 63.8 ± 7.5 nM *vs.* 238.3 ± 30.1 nM, n = 8, $p < 0.001$) and augmented hypoxia (see Figures 3.8A and C Δ $[Ca^{2+}]i$ hypoxia *vs.* hypoxia plus DiC8 (5 μM): 392 ± 89 nM *vs.* 654 ± 144.4 nM, compare red bar *vs.* yellow bar, n = 8, $p < 0.01$) and methacholine chloride-evoked $[Ca^{2+}]i$ transients (see Figures 3.8B and C Δ $[Ca^{2+}]i$ methacholine chloride (300 μM) *vs.* methacholine chloride (300 μM) plus DiC8 (5 μM): 192.7 ± 42.8 nM *vs.* 411.9 ± 86.1 nM, compare blue bar *vs.* green bar, n = 7, $p < 0.01$). These results indicate that DAG is involved in hypoxia and muscarinic agonist-evoked $[Ca^{2+}]i$ transients.

**Figure 3.8: Effects of the DAG analogue DiC8 (5 μM) on $[Ca^{2+}]i$ in type-1 cells.** Recordings of **[**$Ca^{2+}$] in isolated type-1 cells showing responses to hypoxia **(A)** and methacholine chloride (300 μM) **(B)** in control and in the presence of DiC8. Quantitative effects of 5 μM DiC8 on hypoxia and methacholine chloride-evoked $[Ca^{2+}]i$ transients **(C)**. Note that DiC8 induced spiking of the $[Ca^{2+}]i$ and augmented both hypoxia and methacholine chloride evoked $[Ca^{2+}]i$ transients. Error bars indicate S.E.M. Statistical significance was assessed using a paired Student's t-test.

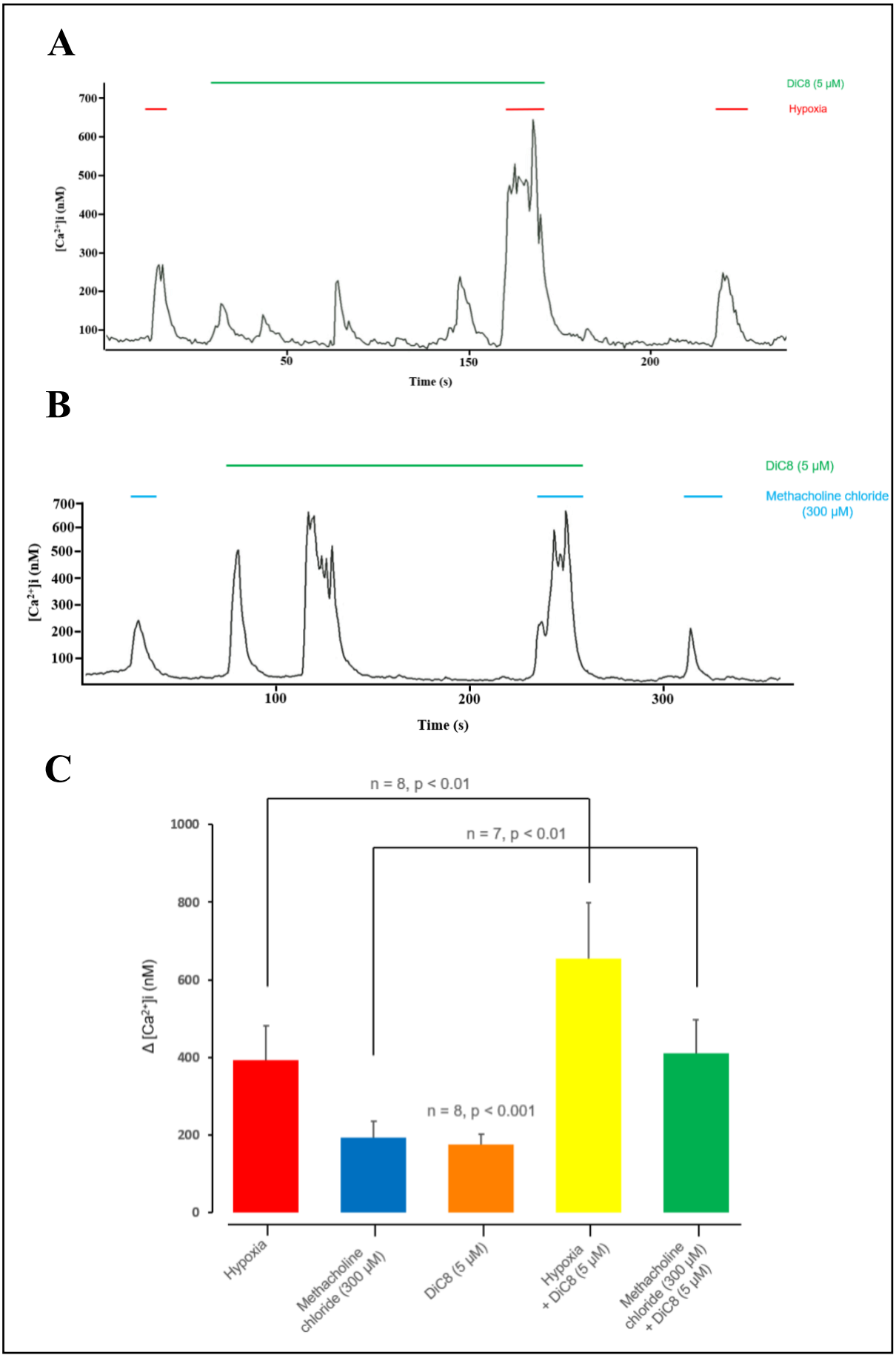
A
DiC8 (5 µM)
Hypoxia
[Ca2+]i (nM)
Time (s)
B
DiC8 (5 µM)
Methacholine chloride (300 µM)
[Ca2+]i (nM)
Time (s)
C
n = 8, p < 0.01
n = 7, p < 0.01
n = 8, p < 0.001
Δ [Ca2+]i (nM)
Hypoxia
Methacholine chloride (300 µM)
DiC8 (5 µM)
Hypoxia + DiC8 (5 µM)
Methacholine chloride (300 µM) + DiC8 (5 µM)

### 3.3.6 Effect of the PKC inhibitor Calphostin C on hypoxia and methacholine chloride evoked $[Ca^{2+}]i$

Finally, the PKC inhibitor calphostin C was employed to determine whether PKC is involved in mediating hypoxia and methacholine chloride-induced $[Ca^{2+}]i$ transients in type-1 cells. Application of calphostin C (50 nM) had no effect on baseline levels of $[Ca^{2+}]i$ but inhibited both hypoxia and methacholine chloride-induced $[Ca^{2+}]i$ transients (see Figures 3.9A, B, and C $\Delta$ $[Ca^{2+}]i$ hypoxia *vs.* hypoxia plus calphostin C: 617 nM ± 178.2 *vs.* 203.7 nM ± 111, compare red bar *vs.* yellow bar, n = 6, p = 0.004; methacholine chloride 300 µM *vs.* methacholine chloride 300 µM plus calphostin C: 309.6 nM ± 146.7 *vs.* 86.5 nM ± 18.2, compare blue bar *vs.* green bar, n = 4, p = 0.03). These results indicate that hypoxia and methacholine chloride-induced $[Ca^{2+}]i$ transients in type-1 cells are sensitive to changes in PKC levels.

**Figure 3.9: Effects of the PKC inhibitor calphostin C (50 nM) on $[Ca^{2+}]i$ in type-1 cells.** Recordings of **[**$Ca^{2+}$] in isolated type-1 cells showing responses to hypoxia **(A)** and methacholine chloride (300 µM) **(B)** in control and in the presence of calphostin C. Quantitative effects of 50 nM Calphostin C on hypoxia and methacholine chloride-evoked $[Ca^{2+}]i$ **(C)**. Error bars indicate S.E.M. Statistical significance was assessed using a paired Student's t-test.

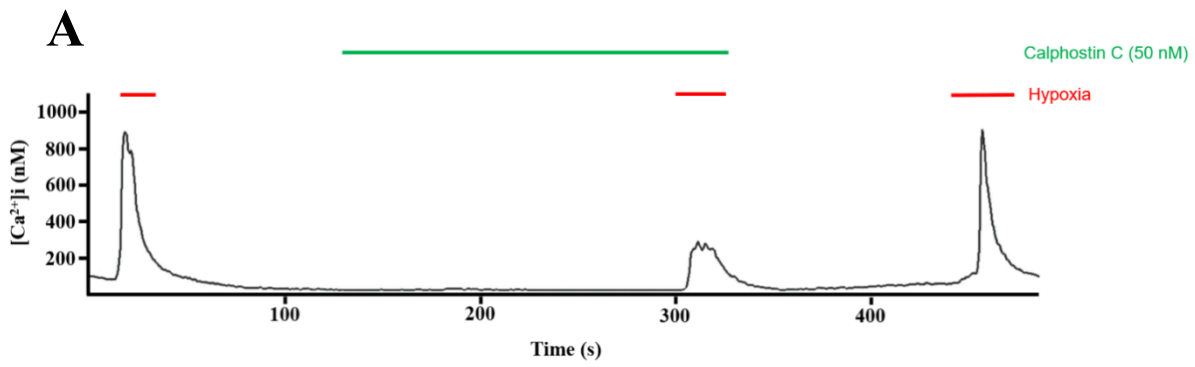

**B**

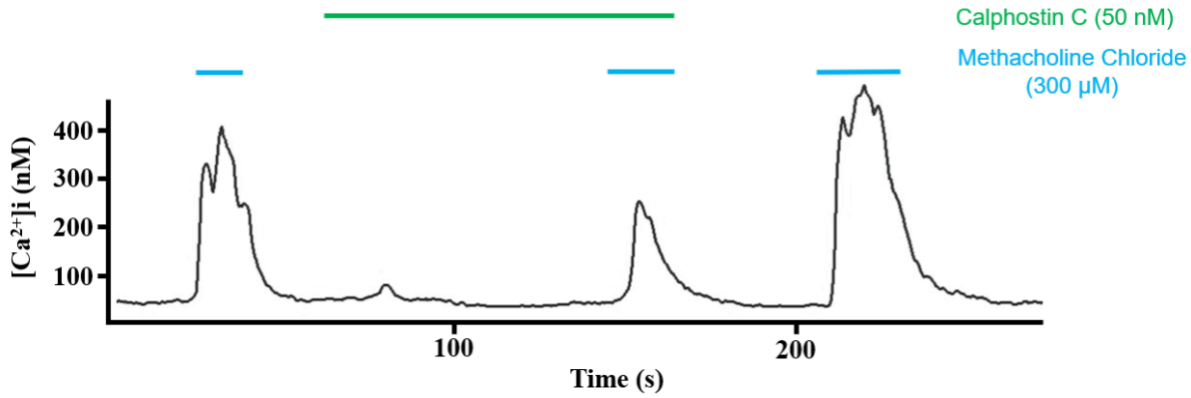
Calphostin C (50 nM)
Methacholine Chloride
(300 µM)
[Ca2+]i (nM)
400
300
200
100
100
200
Time (s)

**C**

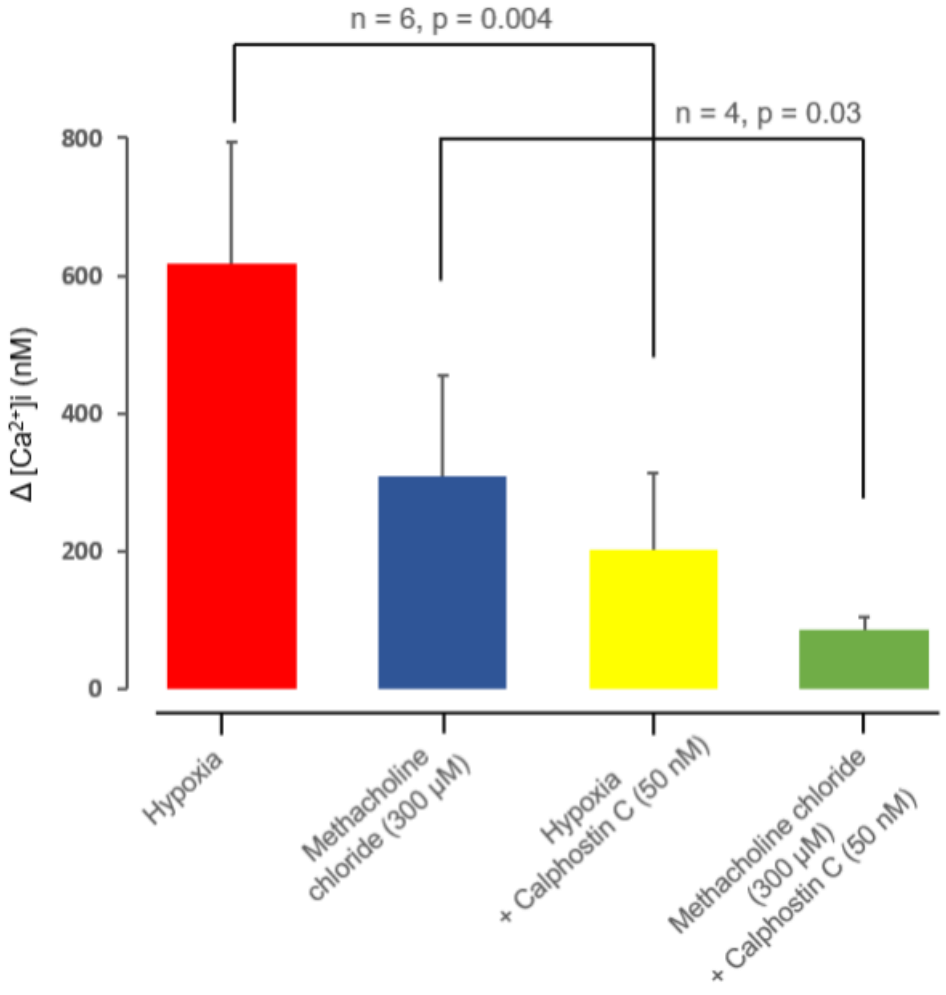
n = 6, p = 0.004
n = 4, p = 0.03
Δ [Ca2+]i (nM)
800
600
400
200
0
Hypoxia
Methacholine chloride (300 µM)
Hypoxia + Calphostin C (50 nM)
Methacholine chloride (300 µM) + Calphostin C (50 nM)

## 3.4 Discussion

In this chapter, I investigated the effects of Gq- coupled receptors and PLC signalling molecules on hypoxia and muscarinic agonist-evoked $[Ca^{2+}]i$ rise in carotid body type-1 cells. The findings presented in this chapter demonstrate novel actions of these signalling molecules on type-1 cell $Ca^{2+}$ responses. I will first discuss the main findings of this chapter, followed by a general discussion and the technical limitations of this study.

I demonstrated that methacholine chloride-evoked $[Ca^{2+}]i$ rise is significantly but not completely inhibited by blocking $Ca^{2+}$ entry and in $Ca^{2+}$-free medium. These observations suggest that methacholine chloride evoked $[Ca^{2+}]i$ rise is predominantly mediated by $Ca^{2+}$ influx. This aligns with prior studies that demonstrated the inhibition of muscarinic-agonist-induced $[Ca^{2+}]i$ rise in carotid body type-1 cells after pre-incubation in a $Ca^{2+}$-free medium (Dasso et al., 1997). Additionally, the results presented in this chapter are with agreement with those of Ortiz and Varas (2007) who reported that muscarinic agonists inhibit the carotid body typ-1 cell TASK channels in a PLC-dependent mechanism. In addition to the PLC-dependent regulation of TASK channels, muscarinic agonists can induce a decrease in cyclic AMP levels, resulting in the activation of protein kinase A (Thompson, 2010). It is thought that PLC signalling and cAMP act independently. However, certain muscarinic agonists may activate both pathways resulting in increased levels of DAG, IP3, and cAMP levels (Michal et al., 2001).

An unanticipated result of this study was that hypoxia-evoked $[Ca^{2+}]i$ rise was inhibited by the application of the Gq inhibitor FR900359. This implies that baseline Gq activity is required for the hypoxic $[Ca^{2+}]i$ response and, most likely, for subsequent neurosecretion. In principle, this could result from a direct

effect of Gq inhibition and/or inhibition of PLC signalling molecules. This will be investigated further in the following chapter, which will look at the effects of Gq inhibition on TASK channel activity in type-1 cells.

The second finding of this study is that the PLC inhibitor U73122 reduced hypoxia-evoked $[Ca^{2+}]i$ rise, indicating that this response is sensitive to PLC activity. However, significant concern arose regarding the specificity of this compound, as it appeared to produce some off-target effects. Specifically, in certain experiments, U73122 either blocked or inhibited high $K^+$-evoked $[Ca^{2+}]i$ rise, suggesting that U73122 may directly or indirectly inhibit voltage-gated calcium channels. Notably, it has been shown that U73122 inhibits $Ca^{2+}$ influx through PLC-independent mechanisms in activated neutrophils (Wang, 1996). Furthermore, U73122 attenuated receptor-mediated inhibition of voltage-gated $Ca^{2+}$ channels in sympathetic neurons in bullfrogs (Wu et al., 2002).

U73122 is a commonly used PLC inhibitor known to target multiple isoforms of PLC (Smith et al., 1990). Although previous reports confirmed the ability of this compound to inhibit PLC activity, they also highlighted the potential for off-target effects. To mitigate this concern, a low concentration of U73122 is recommended (Horowitz et al., 2005). In this study, I tested three different concentrations of U73122 (5 µM, 1 µM, and 100 nM). However, I encountered challenges in fully distinguishing the effect of U73122 on the hypoxia-evoked $[Ca^{2+}]i$ rise from its effect on the high $K^+$- evoked $[Ca^{2+}]i$ rise. However, I observed that the high $K^+$- evoked $[Ca^{2+}]i$ rise was less inhibited at lower concentrations of U73122 (100 nM). To strengthen the evidence of U73122's specificity, I also employed U73343, the U73122 control compound, which had no effect on the $[Ca^{2+}]i$ responses of type-1 cells.

In addition to U73122, I used the PLC activator m-3m3fbs (10 and 20 µM) to further investigate the role of PLC in mediating hypoxia and

methacholine chloride-evoked $[Ca^{2+}]i$ rise. M-3m3fbs had no significant effect on either response, but at the two concentrations used, m-3m3fbs caused $[Ca^{2+}]i$ spiking. On the other hand, o-3m3fbs, the m-3m3fbs control compound, did not affect $Ca^{2+}$ responses or baseline $[Ca^{2+}]i$ levels in type-1 cells.

The next step of this study was to investigate the effects of PKC on hypoxia and methacholine chloride-evoked $[Ca^{2+}]i$ rise in type-1 cells. The PKC inhibitor calphostin C inhibited both responses, suggesting that PKC is involved in mediating $Ca^{2+}$ responses in type-1 cells. It has been previously reported that PKC activity is involved in the hypoxia-induced activation of L-type $Ca^{2+}$ channels in the carotid body type-1 cells (Summers et al., 2000).

The fourth finding of this study is that DiC8, a DAG analogue, elicited $[Ca^{2+}]i$ spikes and augmented both hypoxia and methacholine chloride-induced $[Ca^{2+}]i$ rise. This suggests that hypoxia and methacholine chloride-induced $[Ca^{2+}]i$ rise is sensitive to changes in DAG levels. However, it is crucial to note that DiC8's effect on type-1 cells $[Ca^{2+}]i$ is not necessarily mediated by TASK channels and may include other pathways (e.g., $Ca^{2+}$ channels). Notably, DiC8 has been shown to activate L-type $Ca^{2+}$ channels in guinea pig pyramidal neurons (Doerner and Alger, 1992). Remarkably, the DiC8-induced $[Ca^{2+}]i$ transients were lower than the hypoxia-induced $[Ca^{2+}]i$ transients, suggesting the potential involvement of other pathways in mediating hypoxia-induced $[Ca^{2+}]i$ transients. However, it is difficult to determine whether the applied concentration of DiC8 is relevant to the physiological levels of DAG in the carotid body type-1 cells.

In summary, the findings presented in this chapter demonstrate novel actions of Gq- coupled receptors and PLC signalling molecules on hypoxia and methacholine chloride- evoked $[Ca^{2+}]i$ rise in type-1 cells. I will investigate this further in the next chapter, which will look at the effects of these molecules on

the activity of TASK channels in type-1 cells and conclude with an overall discussion of the findings of both chapters.

However, what remains to be determined is how PLC signalling molecules fit into the hypoxia chemotransuction process in type-1 cells and whether they are affected by reductions in $PO_2$ levels. More research using advanced tools to track changes in PLC signalling molecules activity under normoxic and hypoxic conditions, as well as more controlled pharmacological agents with fewer side effects, would be an essential next step to confirm the involvement of these molecules in the hypoxia signalling cascade in type-1 cells.

## 3.5 Limitations and technical challenges:

There are two main limitations of this study that will be addressed and discussed. First, I exclusively used pharmacological agents to activate or inhibit Gq or PLC signalling molecules without monitoring their intracellular activity. To address this issue, methacholine chloride was used as a positive control. Given that the effects of methacholine chloride are mediated by Gq -coupled receptors, examining the effects of the applied pharmacological agents on the methacholine chloride-evoked $[Ca^{2+}]i$ rise can confirm their efficacy. Furthermore, where possible, I used the negative control compounds of the applied agents to further confirm their specificity.

A second limitation of this study is that the applied pharmacological agents must be dissolved in Tyrode solution while being continuously bubbled with normoxic or hypoxic gas mixtures. Therefore, it was challenging to

maintain their concentration in the bottle throughout the experiment (3-5 hours). To address this problem, I first monitored the effects of each agent throughout the experiment and observed any variations between recordings made at the beginning of the experiment and those made hours later. If the effect of an agent remained constant, there was likely no concentration loss during the experiment. On the other hand, if the effect of an agent appeared to reduce, I replaced the Tyrode solutions with fresh solutions every 1 to 2 hours. Furthermore, before adding amphipathic agents such as DiC8, Tyrode solutions were bubbled with either normoxic or hypoxic gas mixtures through a gas dispersion tube for 10-15 minutes. Then, the drug was added, and the gas dispersion tube was removed from the solution and kept just above the solution's surface to minimise concentration loss (Buckler and Honore, 2005).

# Chapter. 4 The role of PLC signalling molecules in the regulation of TASK channels and in mediating the hypoxic and muscarinic response of these channels in type-1 cell

## 4.1 Introduction

TASK channels are known to be modulated by neurotransmitters that signal through GPCRs, specifically the G proteins of the αq/11 subclass. Ion channels can be regulated either directly by activated Gαq or indirectly by their downstream signalling molecules (Wickman and Clapham, 1995). As discussed in Chapter 1, TASK channels regulation by PLC signalling molecules has been previously reported in various native cell types and is readily reconstituted in heterologous expression systems when recombinant TASK is co-expressed with Gq-coupled receptors. However, little is known about the regulation of TASK channels in type-1 cells by PLC downstream signalling molecules. It has previously been reported that type-1 cells TASK-like $K^+$ channels are activated by PLC and PKC inhibition and inhibited by PKC activation (Ortiz and Varas, 2010).

Previous studies have indicated that cellular constituents are essential for the baseline activity and oxygen sensitivity of TASK channels in type-1 cells. Furthermore, the activity of these channels has been shown to be MgATP-dependent (Buckler, 2015; Buckler and Honore, 2004; Williams and Buckler, 2004). Additionally, TASK channels expressed in COS-7 cells or HEK293 cells remain unaffected by hypoxia, despite some conflicting reports in the literature (Honore and Buckler, 2004, 2005; Lewis et al., 2001). This highlights the cell-type specificity and unique regulatory mechanisms that govern TASK channel responses to changes in oxygen levels. Additionally, it underscores the importance of investigating these channels within the specific context of type-1 cells to achieve a comprehensive understanding of their behaviour.

As discussed in Chapters 1 and 3, previous research suggested that mitochondrial processes may underlie the oxygen sensitivity of type-1 cells. However, the link between mitochondrial function and TASK channel

regulation is unknown, but it probably involves ATP (Buckler, 2015; Wyatt and Buckler, 2004; Williams and Buckler, 2004).

Because PLC signalling molecules can regulate TASK channels and their metabolism appears to be ATP-dependent, they emerge as potential candidates to bridge the gap between mitochondrial activity and TASK channel oxygen sensitivity (Han et al., 2008; Xia and Yang, 2005).

To determine the role of Gq-coupled receptors and PLC signalling molecules in the regulation of TASK channels in type-1 cells, this chapter sought to clarify a number of questions. The first part of this chapter focuses on the regulation of TASK channels in type-1 cells by Gq- coupled receptors. As previously discussed in Chapter 3, Gq-coupled receptors are highly expressed in type-1 cells, which suggests that GPCRs may play a role in the oxygen sensitivity of these cells (Zhou et al., 2015). Furthermore, mutations disrupting the lower "X" gate of TASK channels result in overactive channels with impaired sensitivity to GPCRs (Sormann et al., 2022). This suggests that the baseline activity of TASK channels is controlled by GPCRs. Additionally, the results presented in the third chapter of this thesis show that Gq inhibition blocked both hypoxia and methacholine chloride-evoked $[Ca^{2+}]i$ rise. However, this inhibition of hypoxia-induced $[Ca^{2+}]i$ transients is not necessarily mediated by TASK channels (e.g., $Ca^{2+}$ channels). Therefore, I wanted to examine the effect of Gq inhibition on type-1 cells TASK channels.

The second part of this chapter examines the effects of PLC and its downstream signalling molecules on the activity of TASK channels in type-1 cells. Although the regulation of TASK channels by PLC and its downstream signalling molecules is widely accepted, the underlying mechanisms of channel regulation are poorly understood (see Chapter 1). Therefore, I sought to determine the role of PLC and its downstream signalling molecules in the regulation of TASK channels in type-1 cells. To achieve this, I applied pharmacological agents to acutely isolated type-1 cells to alter PLC signalling

molecules and measured the activity of TASK channels in the cell-attached configuration under control and hypoxic conditions. For comparison, I also examined the effects of these agents on TASK channels responses to methacholine chloride.

The final part of this chapter dives into the role of PLC signalling molecules in regulating the activity of TASK channels in excised patches of type-1 cells. Prior research has shown that TASK channels in type-1 cells undergo a rapid rundown in activity following patch excision. After this rundown, these channels can be partially reactivated by millimolar doses of MgATP, suggesting that the activity of these channels is ATP-dependent (Buckler, 2015; Varas et al., 2007; Williams and Buckler, 2004). However, it was observed that even after MgATP application, channel activity did not return to the baseline level. This suggests that other cytosolic factors are necessary for the activity of the TASK channel. Furthermore, the absence of known nucleotide binding sites in the primary sequence of TASK channels and the lack of reports of cloned TASK1 or TASK3 being sensitive to MgATP prompted us to hypothesise that the rundown of these channels might be caused by DAG accumulation following patch excision (Buckler, 2015). Considering that DAG induces a strong inhibition of these channels and that the activity of DAG kinase (DAGK) is ATP-dependent, it is conceivable that the reactivation of TASK channels by MgATP is mediated by the activation of DAGK. This activation inhibits DAG levels and, as a result, activates these channels.

To test this hypothesis, I initially examined the effects of reducing DAG levels by applying a PLC inhibitor in the cell-attached mode before excising the patch on the rundown of TASK channels after patch excision. Subsequently, I investigated the effects of applying a DAGK inhibitor on MgATP reactivation of TASK channels after patch excision.

## 4.2 Methods

All experiments were performed in accordance with the UK Animals (Scientific Procedures) Act, 1986.

**Cell isolation:**

For the extended procedure, refer to Chapter 2, Section 2.1.2. Briefly, carotid body bifurcations were dissected from rat pups (P11-P14). They were then digested enzymatically and mechanically, resulting in a single cell suspension. Primary cell cultures were plated onto coverslips pre-treated with Poly-D-lysine and incubated for 2 hours. Recordings took place within 5-6 hours of plating.

**Electrophysiology:**

Cell-attached and inside-out recordings were performed using an Axopatch 200B (Molecular Devices LLC, Sunnyvale, US). Sylgard-coated and fire-polished borosilicate pipettes (Harvard Apparatus Ltd., Kent, UK) were used. For the extended procedures, refer to Chapter 2, Section 2.8. In short, coverslips containing isolated type-1 cells were placed in the recording chamber and continuously superfused with warmed Tyrode solution. Tyrode solutions were continuously bubbled with either normoxic (5% $CO_2$, balance air) or hypoxic gas mixture (5% $CO_2$, balance $N_2$). Seal formation was attempted with a borosilicate pipette containing a high $K^+$ solution (140 mM). Upon the formation of a good seal (> 5 GΩ), the Tyrode solution was switched to either a high $K^+$ solution for the cell-attached mode or an intracellular solution for the inside-out mode. Then, a positive pipette potential of +100 mV was applied.

For inside-out recordings, once a G seal was obtained, the electrode was pulled away from the cell. A small piece of cell membrane will eventually

separate from the cell surface, forming a vesicle on the tip of the pipette without compromising the G seal. The pipette tip was then briefly passed through the air-water interface to burst the vesicle and enter the inside-out mode. The 'intracellular solution' used for recording from inside-out patches contained: in mM (120 KCl, 5 $MgCl_2$, 10 EGTA, 10 Glucose, 23 $KHCO_3$; pH adjusted with KOH to 7.2 at 32ºC). In experiments with 5 mM $K_2ATP$, this was added directly on the day of the experiment to the intracellular solution, and pH was re-adjusted with KOH to 7.2. In these experiments, to maintain free intracellular $Mg^{2+}$ at 3 mM where $K_2ATP$ was used, the intracellular $Mg^{2+}$ was raised to 10 mM (to allow for the formation of 5 mM MgATP in solution).
Voltage clamp protocol, data acquisition, and data analysis were performed using Spike 10 software (Cambridge Electronics Design, Cambridge, UK).
The background $K^+$ channel of type-1 cells exhibited inward currents with brief, flickering openings under the recording conditions of this study.

**Experimental protocol for the measurements of TASK channels activity in type-1 cell:**

The channel activity was analysed using 20s sections of recording collected at least 10s after any solution exchange. Single channel activity was defined by nPopen. For this, an all-points histogram was constructed using a 20s section of data to determine the main conductance state. Then, a 50% opening threshold was set for nPopen analysis. The change in channel activity was reported as an increase or decrease in nPopen relative to the control.

**Drugs:**

Following cell identification, type-1 cells were subjected to superfusion with the Tyrode solution, both in the presence and absence of the drug under

investigation, using the cells as their own controls. The drugs were applied to cells for a duration of 50-60 seconds, and a similar wash period followed the exposure to allow any reversible effects to subside. All drugs were appropriately reconstituted prior to dissolution in Tyrode solution. U73122, U3343, K2ATP, D5919, DiC8, EGTA, Tetraethylammonium (TEA), 4-aminopyridine (4-AP), and calphostin C were obtained from Sigma/Aldrich. Indo-1 AM was obtained from Calbiochem. FR900359 was obtained from Cayman Chemical. M-3m3fbs and o-3m3fbs were obtained from Biotechne/Tocris. LY290042 was obtained from Abcam, Cambridge, UK. The concentrations of the administered drugs were determined either based on the EC50 values specific to each drug, prior usage in similar studies, or a combination of both approaches.

**Statistical analysis of TASK channels recordings:**

N numbers denote separate recordings from a distinct cell/s on different coverslips. The percentage change in nPopen was determined using the following formula:

Percentage change = ((nPopen under Condition A - nPopen under Control) / nPopen under Control) * 100

Normalising channel activity to the control level of channel activity for each patch helps to eliminate a major source of variability in nPopen due to variation in the number of channels present in any given patch. Mean normalised nPopen values were used to assess statistical significance using a paired Student's t-test. p value $< 0.05$ was considered statistically significant.

Note that in some graphs, data are presented as % change of channel activity and in others it is presented as % inhibition of channel activity, which is simply the inversion of the y-axis. This method of presentation was employed to emphasise the effects of hypoxia and methacholine, which are inhibitory.

## 4.3 Results

In this study, cell-attached and inside-out patch clamp recordings were obtained from acutely isolated type-1 cells (n = 109). Cells were classified as such when they responded to hypoxia with an inhibition of background TASK-like $k^+$ currents. Cells that did not respond to a brief hypoxic stimulus were not studied further.

### 4.3.1 The role of Gq- coupled receptors in the regulation of TASK channels in type-1 cell

The TASK channel activity observed under control conditions (as described in the methods section, pipette +100 mV and 140 mM $K^+$ and in Tyrode 100 mM $K^+$) often displayed brief flickery inward currents. Under these conditions, most all-points frequency histograms show a single but broad peak at around 2.87 ± 0.03 pA (number of cell-attached patch clamp recordings obtained in this chapter = 94), suggesting one main open state, which has been previously shown to represent the heterodimeric TASK1/3 channel predominant in rat type-1 cells (Kim et al., 2009; Turner and Buckler, 2013b). Once a stable recording of channel activity was obtained, a brief hypoxic stimulus (<20s) was applied to confirm the identity of the cell. Hypoxia induced a reversible inhibition of channel activity by 46.4 ± 2.5% (n = 9; $p<0.001$). Once the hypoxic stimulus was removed, channel activity rapidly recovered to baseline. Then, after ~20s, methacholine chloride (300 μM) was applied for less than 20s. This induced a reversible inhibition of channel activity by 34.9 ± 4.7 (n = 6; p=0.01). However, in a selected subset of our experiments, methacholine chloride had no effect on channel activity (n = 3 of 9 recordings). It is possible that, in some cells, muscarinic receptors were damaged during the enzymatic

cell isolation process, or perhaps, in some patches, there were not enough muscarinic receptors. I cannot rule out the possibility of variations in muscarinic sensitivity among type-1 cells.

To investigate the role of Gq- coupled receptors in the regulation of TASK channels, the Gq inhibitor FR900359 was applied to acutely isolated type-1 cells. Application of 1 μM FR900359 had no significant effect on baseline channel activity (see Figures 4.1A, B, and D; orange bar; n = 9; p = 0.19) and hypoxia-mediated inhibition of channel activity in cell-attached patches (see Figures 4.1B and D; compare red and yellow bars; n = 9; p = 0.23) but blocked methacholine chloride (300 μM) induced inhibition of channel activity (see Figures 4.1B and D; compare blue and green bars; methacholine chloride *vs.* methacholine chloride plus FR900359: 34.9 ± 4.7 *vs.* 8.7 ± 3.7%; n = 6; p = 0.01).

A representative all-points histogram in Figure 4.1C reveals that FR900359 induced a small insignificant inhibition of channel activity (n = 9; p = 0.19). Inhibition of the methacholine chloride response by FR900359 confirms the drug inhibitory actions on Gq- coupled receptors. Therefore, our results suggest that Gq- coupled receptors are not involved in the regulation of the baseline activity of TASK channels or their inhibition by hypoxia in type-1 cells.

**Figure 4.1. Effects of the Gq inhibitor FR900359 (1 μM) on TASK channels activity in rat carotid body type-1 cell** Three representative traces of single-channel recordings for control (i), FR900359 (ii), and post washout (iii) **(A)**. Four representative traces of single channel recordings for hypoxia (i), hypoxia plus FR900359 (ii), methacholine chloride (iii), and methacholine chloride plus FR900359 (iv) **(B)**. Representative all-points histogram from the same recording, control in blue and FR900359 in red. Histogram was generated from a selected 20s of both control and FR900359 application. Bin width was 0.1 pA **(C)**. Comparison of inhibitory effects of hypoxia, methacholine chloride 300 μM, 1 μM FR900359, hypoxia and methacholine chloride 300 μM plus 1 μM FR900359 on channel activity. Data are expressed as percentage inhibition of nPopen in the presence of hypoxia, methacholine chloride, and FR900359 relative to control (means ± SEM) **(D)**. The traces were recorded with a pipette potential of +100 mV, 140 mM $K^+$ in pipette solution and 100 mM $K^+$ in Tyrode solution.

Bar shows 0.01 s timescale; vertical bar shows 10 pA current. Statistical significance was assessed using a paired Student's t-test.

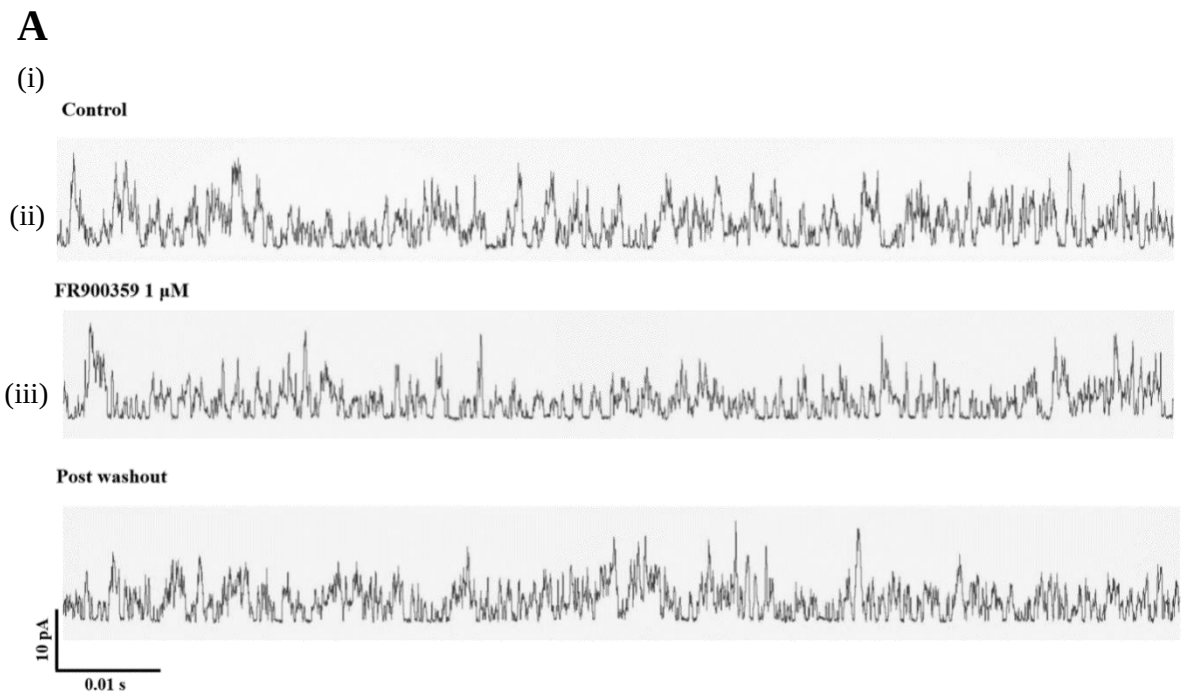

**B**

(i) **Hypoxia**

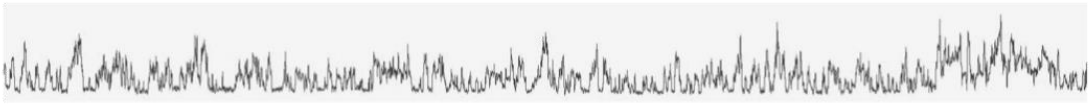

(ii) **Hypoxia + FR900359 1 µM**

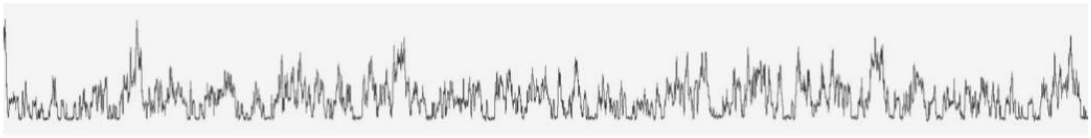

(iii) **Methacholine chloride 300 µM**

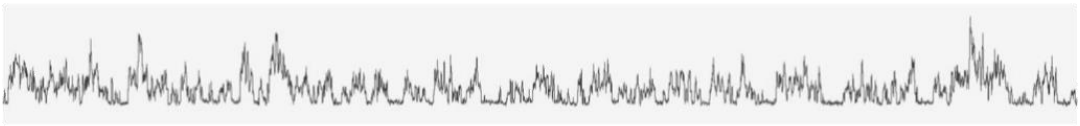

(vi) **Methacholine chloride 300 µM + FR900359 1 µM**

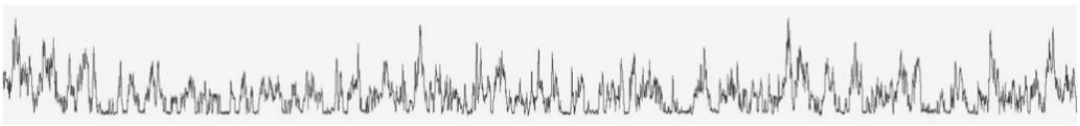


**C**

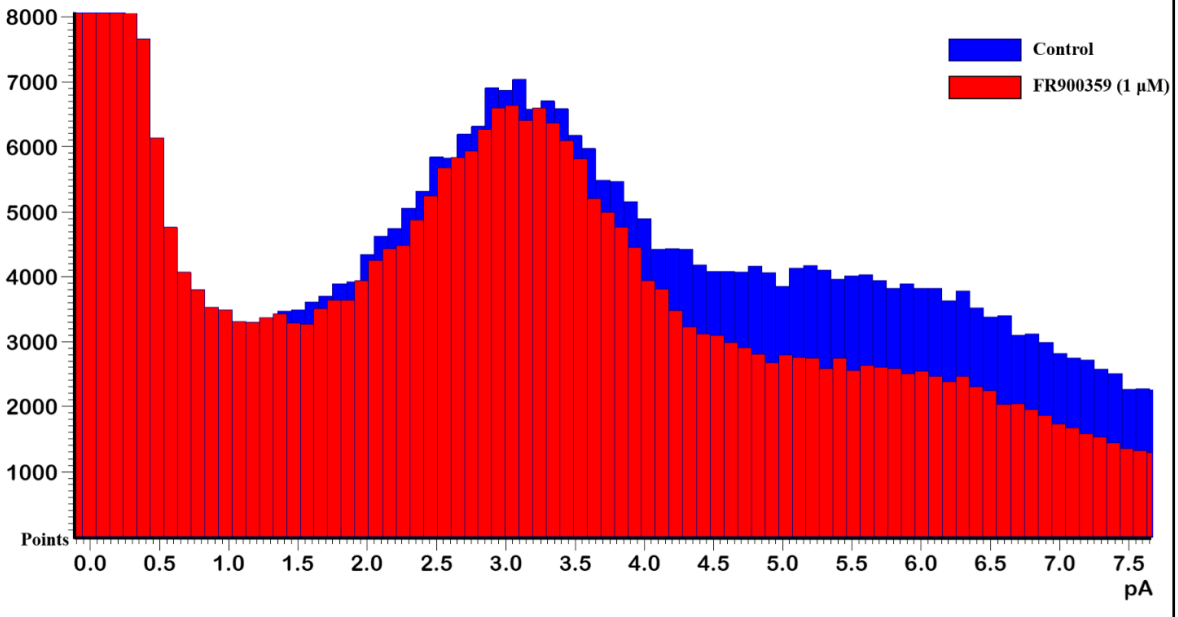

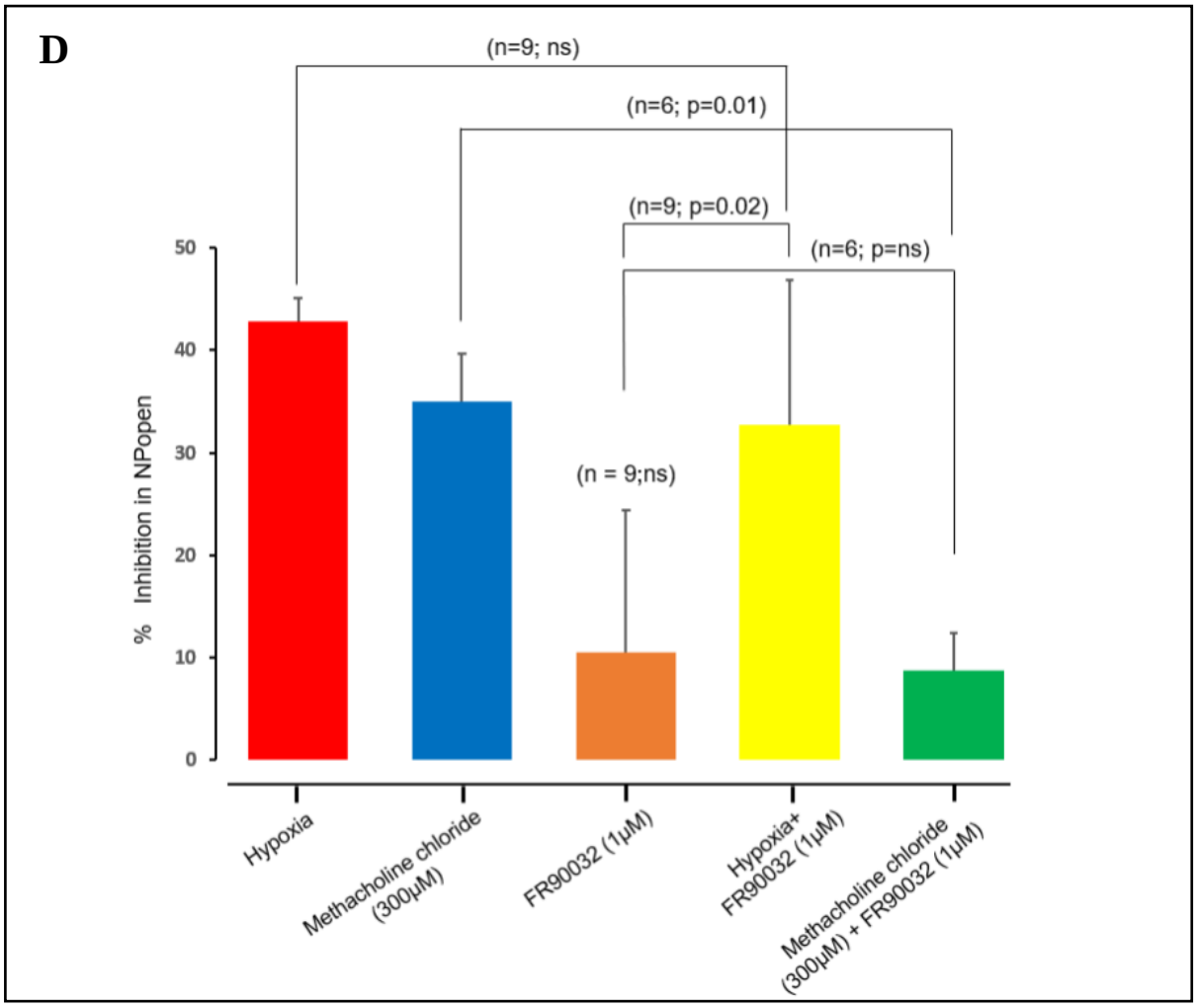
D
(n=9; ns)
(n=6; p=0.01)
(n=9; p=0.02)
(n=6; p=ns)
(n = 9;ns)
% Inhibition in NPopen
50
40
30
20
10
0
Hypoxia
Methacholine chloride (300μM)
FR90032 (1μM)
Hypoxia+ FR90032 (1μM)
Methacholine chloride (300μM) + FR90032 (1μM)

### 4.3.2 The role of PLC in the regulation of TASK channels in type-1 cell

Next, I sought to determine the role of PLC in the regulation of background TASK channels in type-1 cells. I started by examining the effects of PLC inhibition on TASK channels. Application of the PLC inhibitor U73122 (0.5 μM) induced a strong activation of channel activity in cell-attached patches by 64.8 ± 8.3% (see Figures 4.2A and D; orange bar; n = 10; $p < 0.001$). Figure 4.2C shows a typical all-points histogram for channel activity upon application of U73122 (0.5 μM). This suggests that TASK channel activity in type-1 cells is likely suppressed by the products of constitutive PLC activity. Subsequently, I investigated the effects of U73122 on hypoxia and methacholine chloride-induced inhibition of TASK channel. Application of 0.5 μM U73112 completely abrogated methacholine chloride (300 μM) induced inhibition of channel activity (see Figures 4.2B and D; compare blue bar *vs.* green bar; n = 6; $p = 0.01$). The effects of U73112 on hypoxia-regulated channel activity were more complex. Inhibition of channel activity persisted in the presence of hypoxia (compare yellow bar with orange bar). The combination of channel activation by U73112 and inhibition by hypoxia, however, effectively cancelled each other out (yellow bar). In consequence, under the conditions used in Chapter 3 to measure $Ca^{2+}$ responses, the combination of both hypoxia and 0.5 μM U73112 would not change TASK activity appreciably, so there would be no membrane depolarisation or subsequent rise in $Ca^{2+}$.

Subsequently, I increased the concentration of U73122 to 5 μM to examine if this higher dose could effectively block the hypoxic inhibition of background TASK channels in type-1 cells. Application of 5 μM U73122 induced an even stronger activation of channel activity in cell-attached patches by 115.12 ± 25.5 % (see Figures 4.3A, C, and D; orange bar; n = 9; $p < 0.001$). In the presence of 5 μM U73112, neither hypoxia nor methacholine had a significant effect on

channel activity (see Figures 4.3B and D; compare yellow bar *vs*. orange bar and green bar *vs*. orange bar).

U73343, the U73122 control compound, had no significant effect on channel activity in cell-attached patches (see Figures 4.4A, B, C, and D; n = 4; p = 0.15).

To further examine the effects of PLC on TASK channels activity, I applied the PLC activator m-3m3fbs to isolated type-1 cells. Application of 20 μM m-3m3fbs induced a strong reversible inhibition of channel activity in cell-attached patches by 48 ± 9 % (see Figures 4.5A, C, and D, orange bar; n = 6; p < 0.001). In the presence of m-3m3fbs, hypoxia and methacholine chloride had no statistically significant additional effect on TASK channels (see Figures 4.5B and D; m-3m3fbs *vs.* m-3m3fbs plus hypoxia (orange bar *vs.* yellow bar): 48 ± 9 *vs.* 64.8 ± 8.4%, n = 6, p = 0.21; m-3m3fbs *vs.* m-3m3fbs plus methacholine chloride (orange bar *vs.* green bar): 48 ± 9 *vs.* 57 ± 12.5%, n = 5, p = 0.31; see Figures 4.5B and D).

O-3m3fbs, the m-3m3fbs control compound, had no significant effect on TASK channels in cell-attached patches (see Figures 4.6A, B, C, and D; n = 4; p = 0.09).

Taken together, these results demonstrate that PLC is involved in the regulation of TASK channels in type-1 cells and their inhibition by hypoxia and muscarinic agonist.

**Figure 4.2. Effects of the PLC inhibitor U73122 (0.5 μM) on TASK channels activity in rat carotid body type-1 cell**

Three representative traces of single-channel recordings for control (i), U73122 (ii), and post washout (iii) **(A)**. Four representative traces of single channel recordings for hypoxia (i), hypoxia plus U73122 (ii), methacholine chloride (iii), and methacholine chloride plus U73122 (iv) **(B)**. Representative all-points histogram from the same recording, control in blue and U73122 in red **(C)**. Histogram was generated from a selected 20s of both control and U73122 application. Bin width was 0.1 pA. Comparison of the effects of hypoxia, methacholine chloride (300 μM), U73122, hypoxia and methacholine chloride 300 μM plus U73122 on channel activity. Data are expressed as percentage change of nPopen in the presence of hypoxia, methacholine chloride, and U73122 relative to control (means ± SEM) **(D)**. The traces were recorded with a pipette potential of +100 mV, 140 mM $K^+$ in pipette solution and 100 mM $K^+$ in Tyrode solution. Bar shows 0.05 s timescale; vertical bar shows 10 pA current. Statistical significance was assessed using a paired Student's t-test.

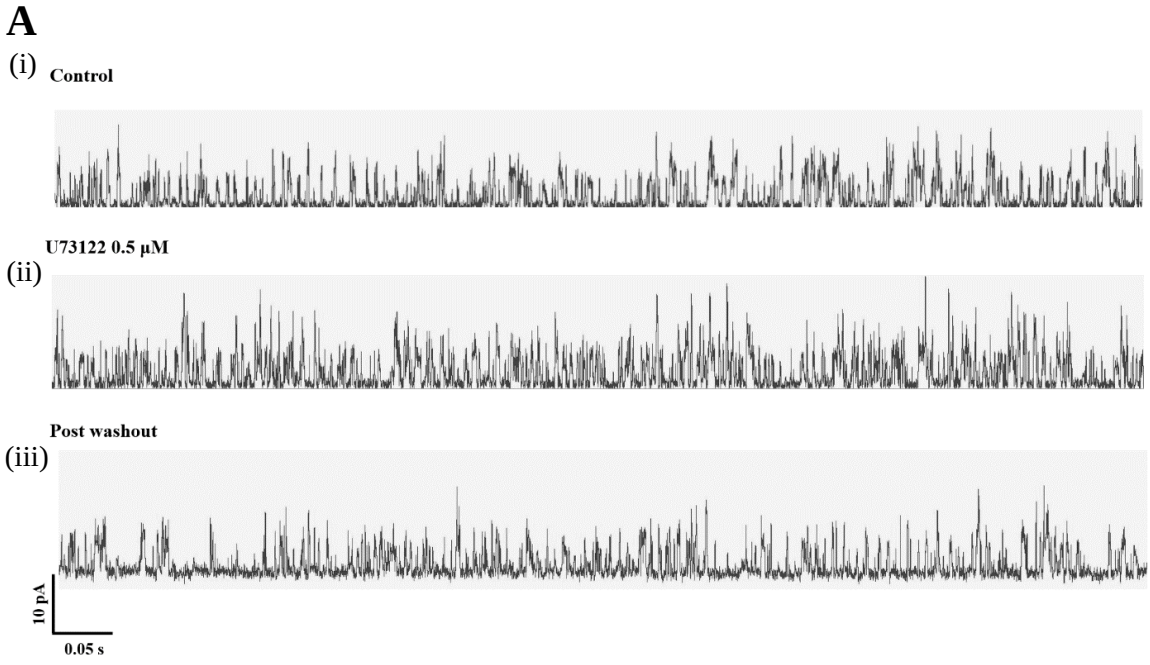

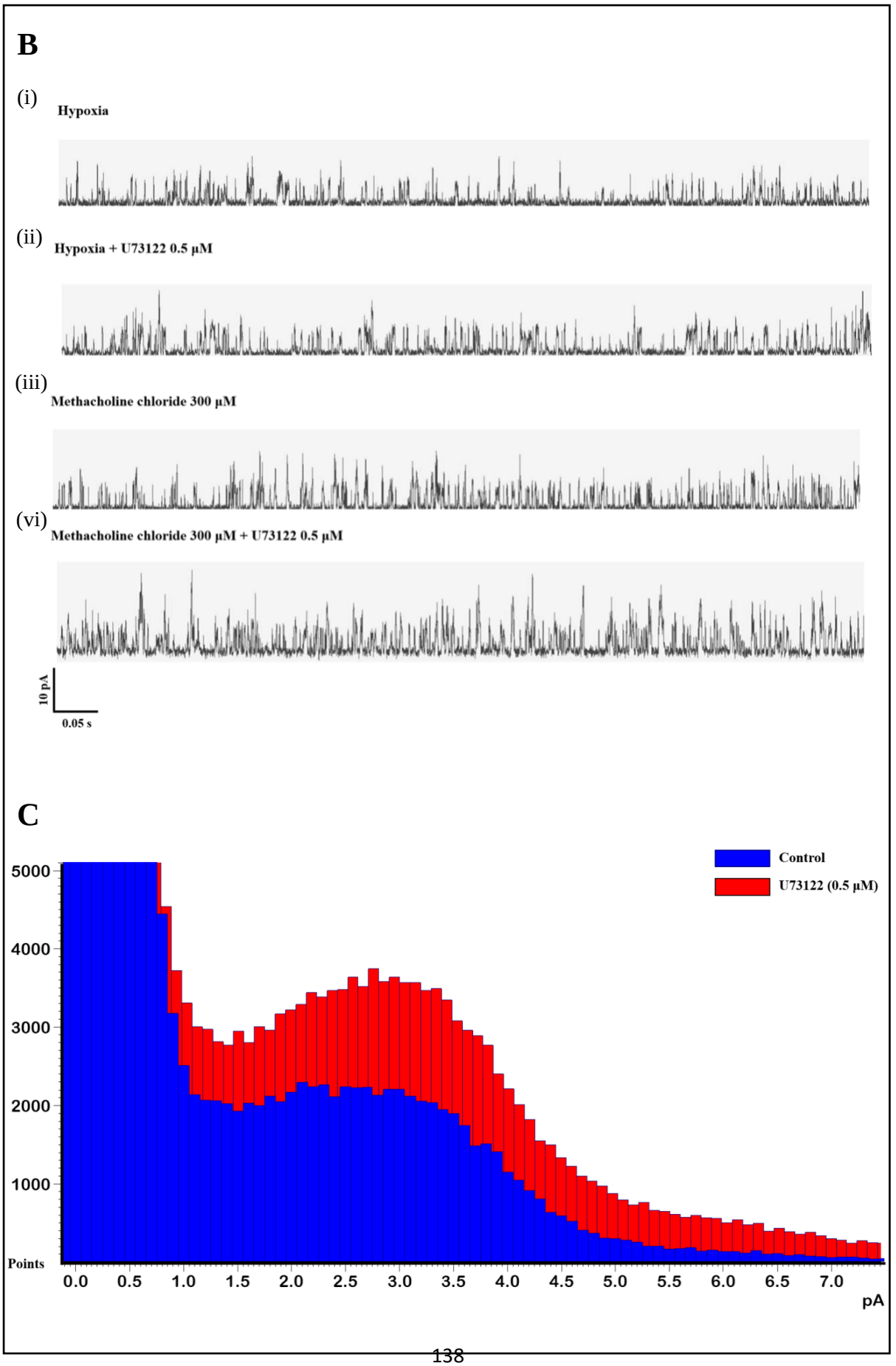
B
(i)
Hypoxia
(ii)
Hypoxia + U73122 0.5 µM
(iii)
Methacholine chloride 300 µM
(vi)
Methacholine chloride 300 µM + U73122 0.5 µM
10 pA
0.05 s
C
Control
U73122 (0.5 µM)
5000
4000
3000
2000
1000
Points
0.0
0.5
1.0
1.5
2.0
2.5
3.0
3.5
4.0
4.5
5.0
5.5
6.0
6.5
7.0
pA

**D**

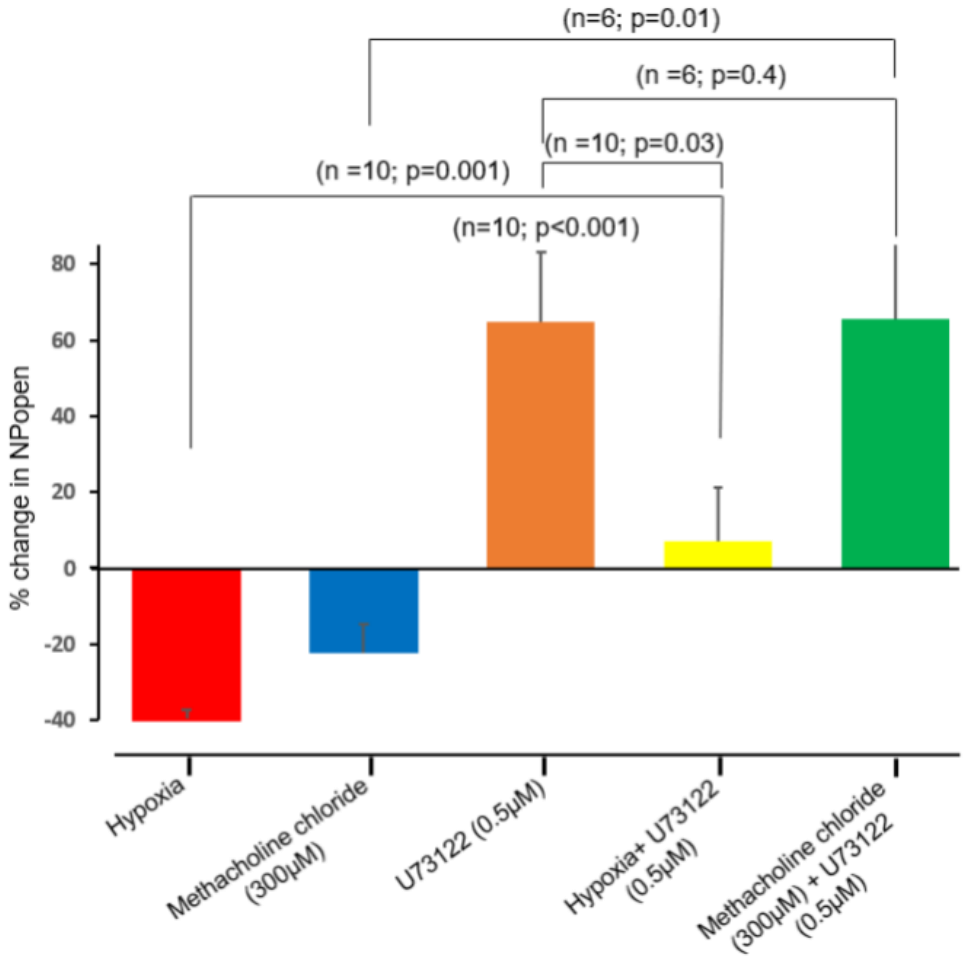
(n=6; p=0.01)
(n =6; p=0.4)
(n =10; p=0.03)
(n =10; p=0.001)
(n=10; p<0.001)
% change in NPopen
80
60
40
20
0
-20
-40
Hypoxia
Methacholine chloride (300μM)
U73122 (0.5μM)
Hypoxia+ U73122 (0.5μM)
Methacholine chloride (300μM) + U73122 (0.5μM)

**Figure 4.3 Effects of the PLC inhibitor U73122 (5 μM) on TASK channels activity in rat carotid body type-1 cell** Three representative traces of single-channel recordings for control (i), U73122 (ii), and post washout (iii) **(A)**. Four representative traces of single channel recordings for hypoxia (i), hypoxia plus U73122 (ii), methacholine chloride (iii), and methacholine chloride plus U73122 (iv) **(B)**. Representative all-points histogram from the same recording, control in blue and U73122 in red. Histogram was generated from a selected 20s of both control and U73122 application. Bin-width was 0.1pA **(C)**. Comparison of the effects of hypoxia, methacholine chloride 300 μM, U73122, hypoxia and methacholine chloride 300 μM plus U73122 on channel activity. Data are expressed as percentage change of nPopen in the presence of hypoxia, methacholine chloride, and U73122 relative to control (means ± SEM) **(D)**. The traces were recorded with a pipette potential of +100 mV, 140 mM $K^+$ in pipette solution and 100 mM $K^+$ in Tyrode solution. Bar shows 0.05 s timescale; vertical bar shows 10 pA current. Statistical significance was assessed using a paired Student's t-test.

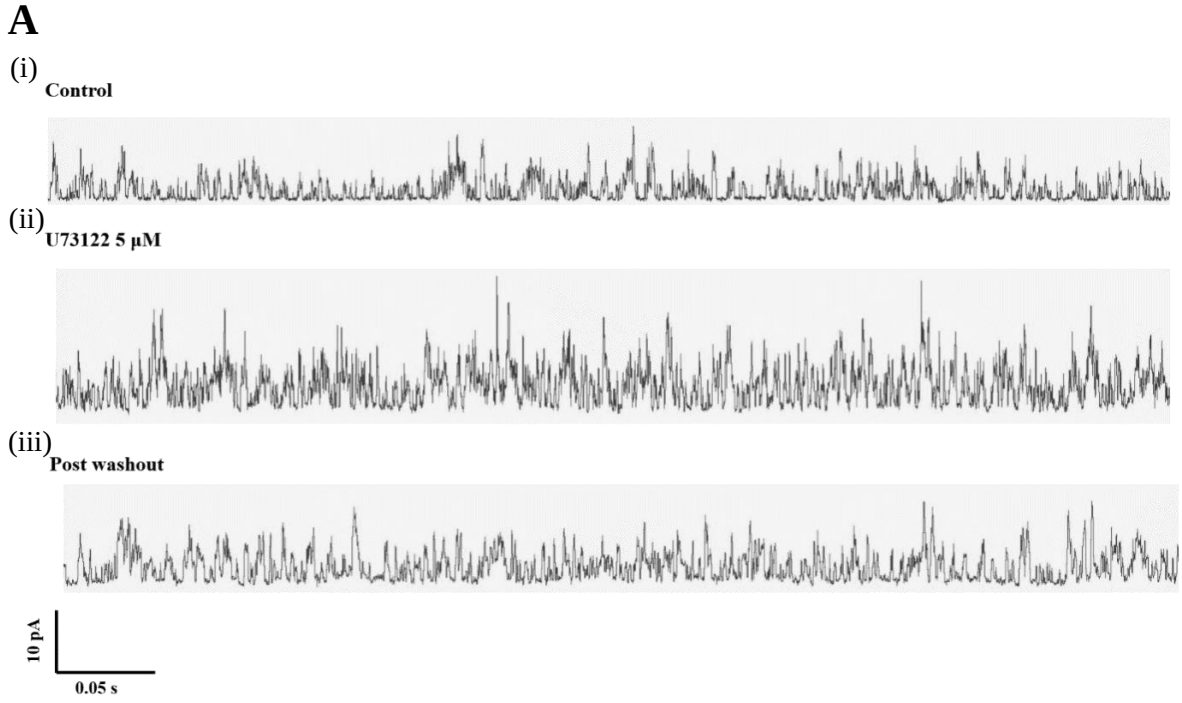

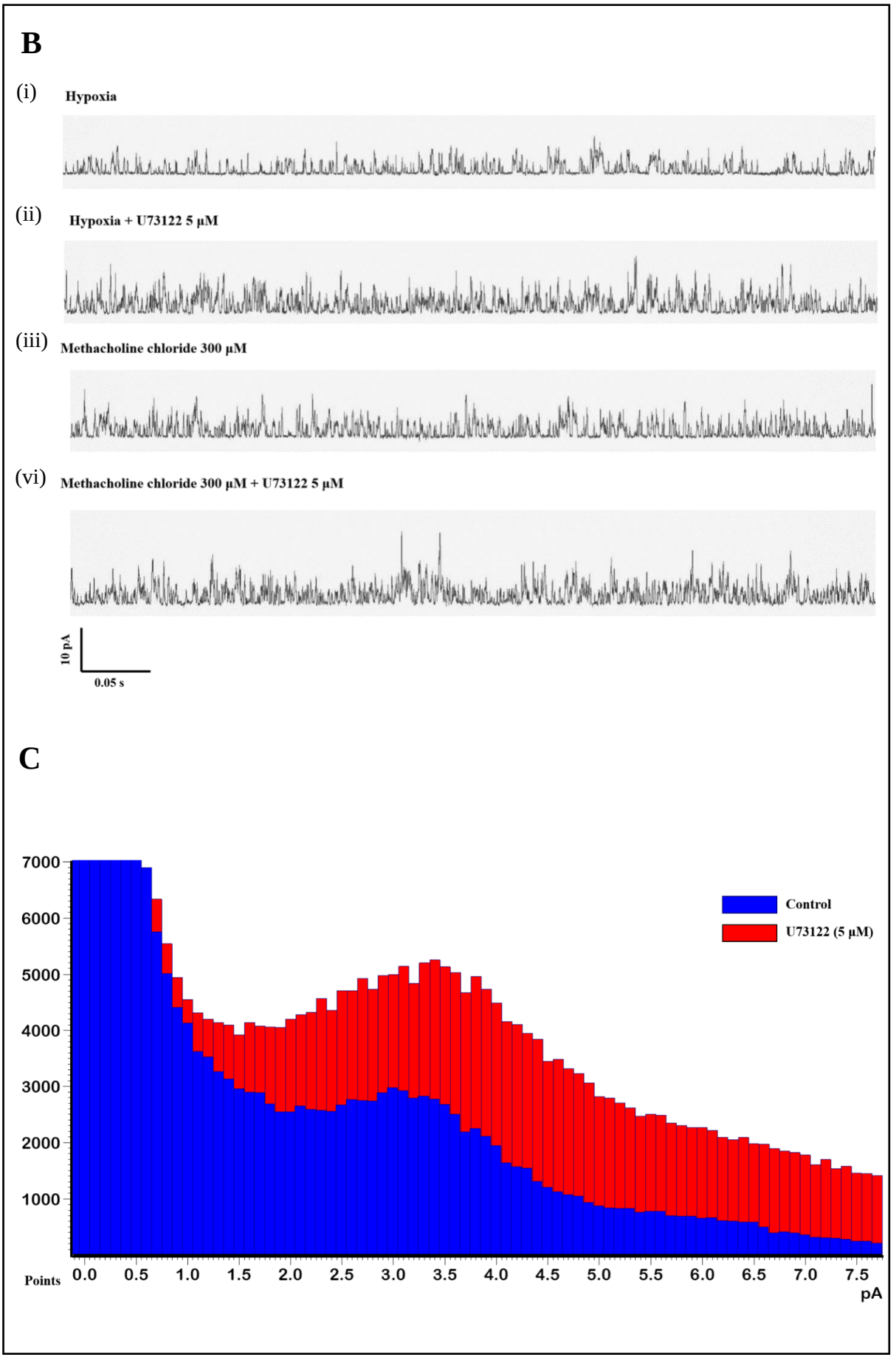
B
(i)
Hypoxia
(ii)
Hypoxia + U73122 5 µM
(iii)
Methacholine chloride 300 µM
(vi)
Methacholine chloride 300 µM + U73122 5 µM
10 pA
0.05 s
C
7000
6000
5000
4000
3000
2000
1000
Points
0.0
0.5
1.0
1.5
2.0
2.5
3.0
3.5
4.0
4.5
5.0
5.5
6.0
6.5
7.0
7.5
pA
Control
U73122 (5 µM)

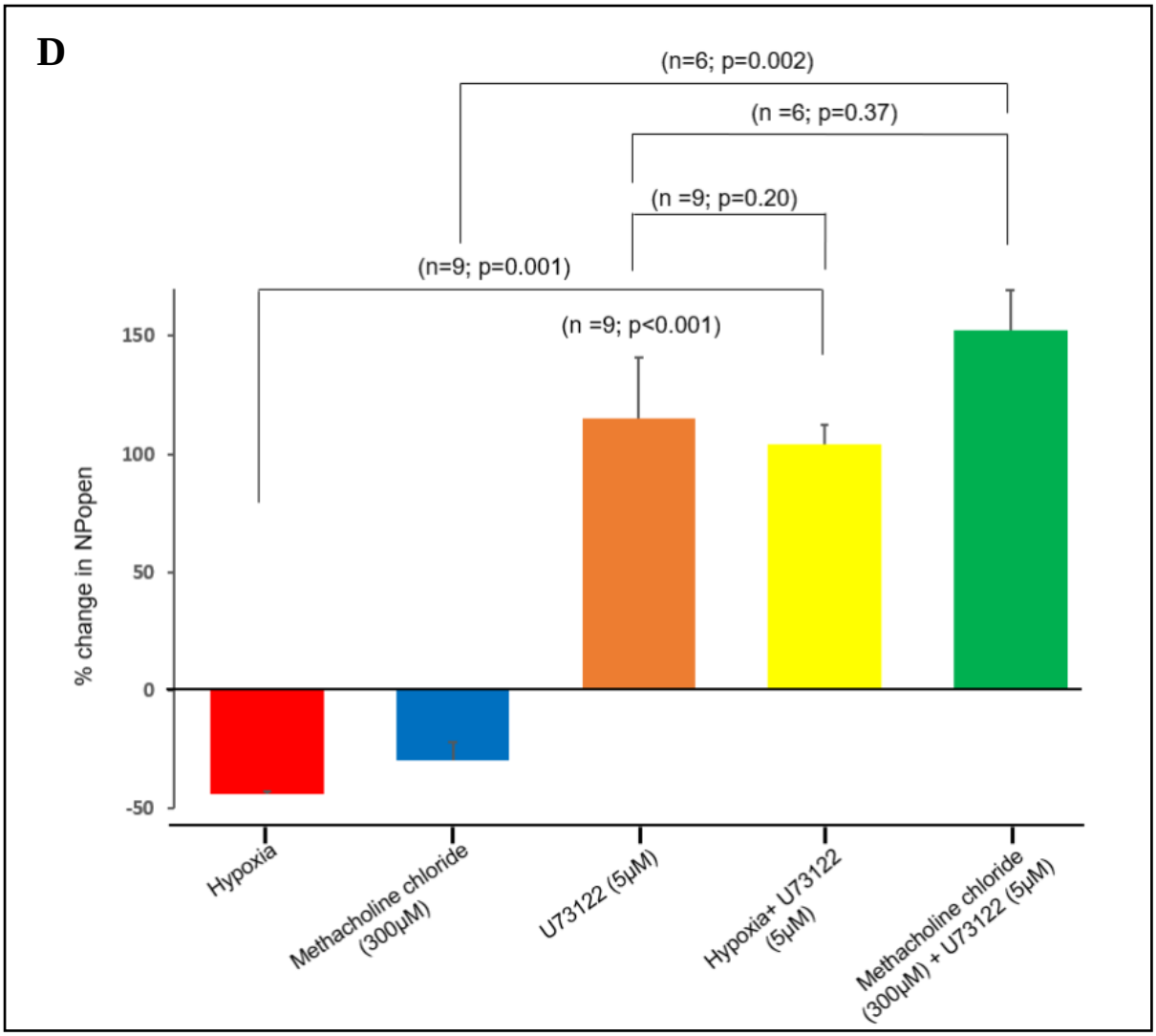
D
(n=6; p=0.002)
(n =6; p=0.37)
(n =9; p=0.20)
(n=9; p=0.001)
(n =9; p<0.001)
% change in NPopen
150
100
50
0
-50
Hypoxia
Methacholine chloride (300μM)
U73122 (5μM)
Hypoxia+ U73122 (5μM)
Methacholine chloride (300μM) + U73122 (5μM)

**Figure 4.4 Effects of U73343 (5 μM), the U73122 control compound, on TASK channels activity in rat carotid body type-1 cell** Three representative traces of single-channel recordings for control (i), U73343 (ii), and post washout (iii) **(A)**. Four representative traces of single channel recordings for hypoxia (i), hypoxia plus U73343 (ii), methacholine chloride (iii), and methacholine chloride plus U73343 (iv) **(B)**. Representative all-points histogram from the same recording, control in blue and U73343 in red. Histogram was generated from a selected 20s of both control and U73343 application. Bin-width was 0.1pA **(C)**. Comparison of the effects of hypoxia, methacholine chloride 300 μM, U73343, hypoxia and methacholine chloride 300 μM plus U73343 on channel activity. Data are expressed as percentage change of nPopen in the presence of hypoxia, methacholine chloride, and U73343 relative to control (means ± SEM) **(D)**. The traces were recorded with a pipette potential of +100 mV, 140 mM $K^+$ in pipette solution and 100 mM $K^+$ in Tyrode solution. Bar shows 0.02 s timescale; vertical bar shows 10 pA current. Statistical significance was assessed using a paired Student's t-test.

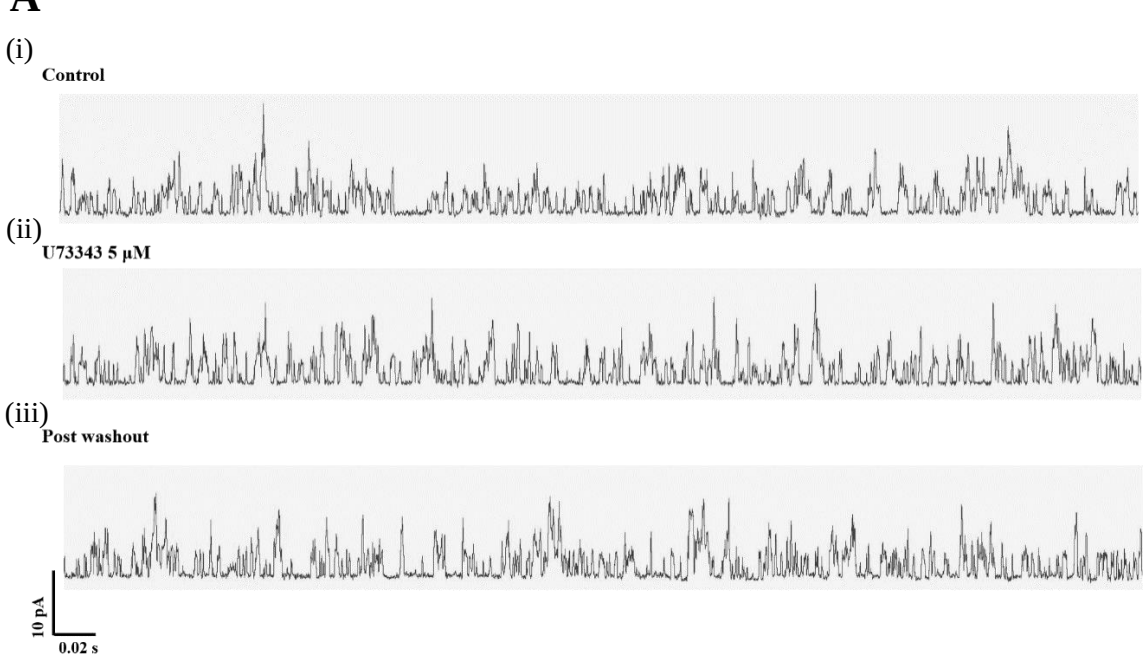

**B**

(i) **Hypoxia**

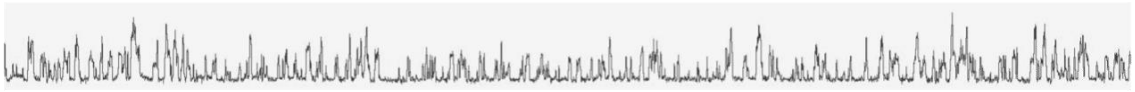

(ii) **Hypoxia + U73343 5 µM**

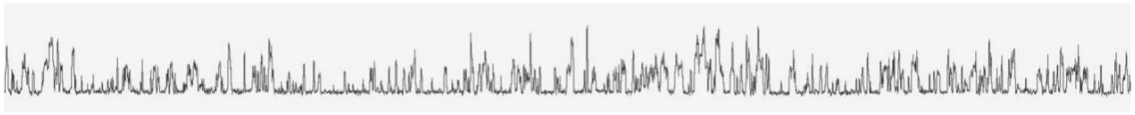

(iii) **Methacholine chloride 300 µM**

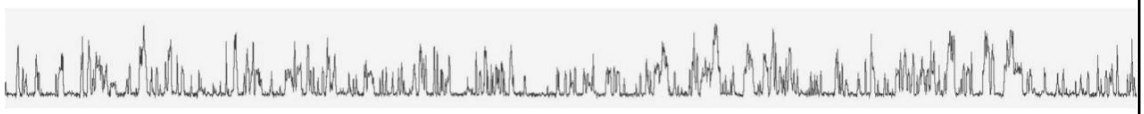

(vi) **Methacholine chloride 300 µM + U73122 5 µM**

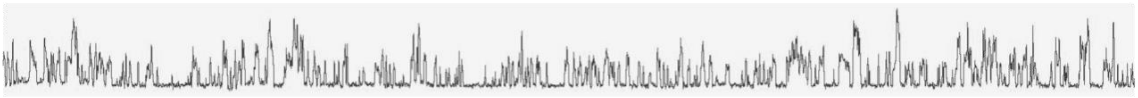


**C**

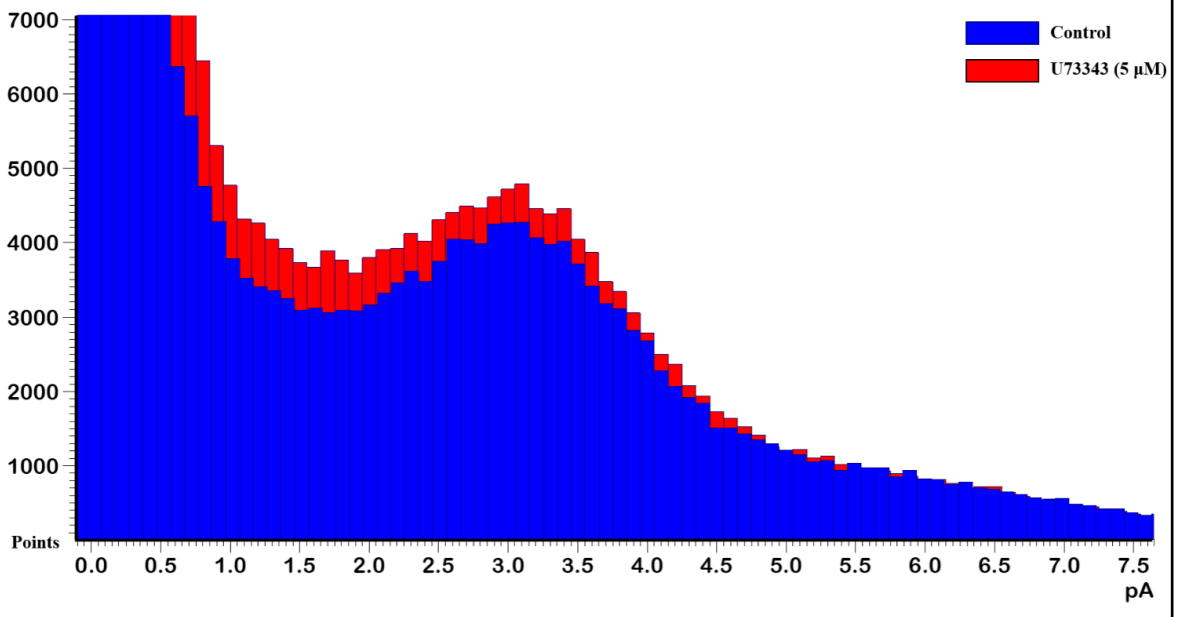

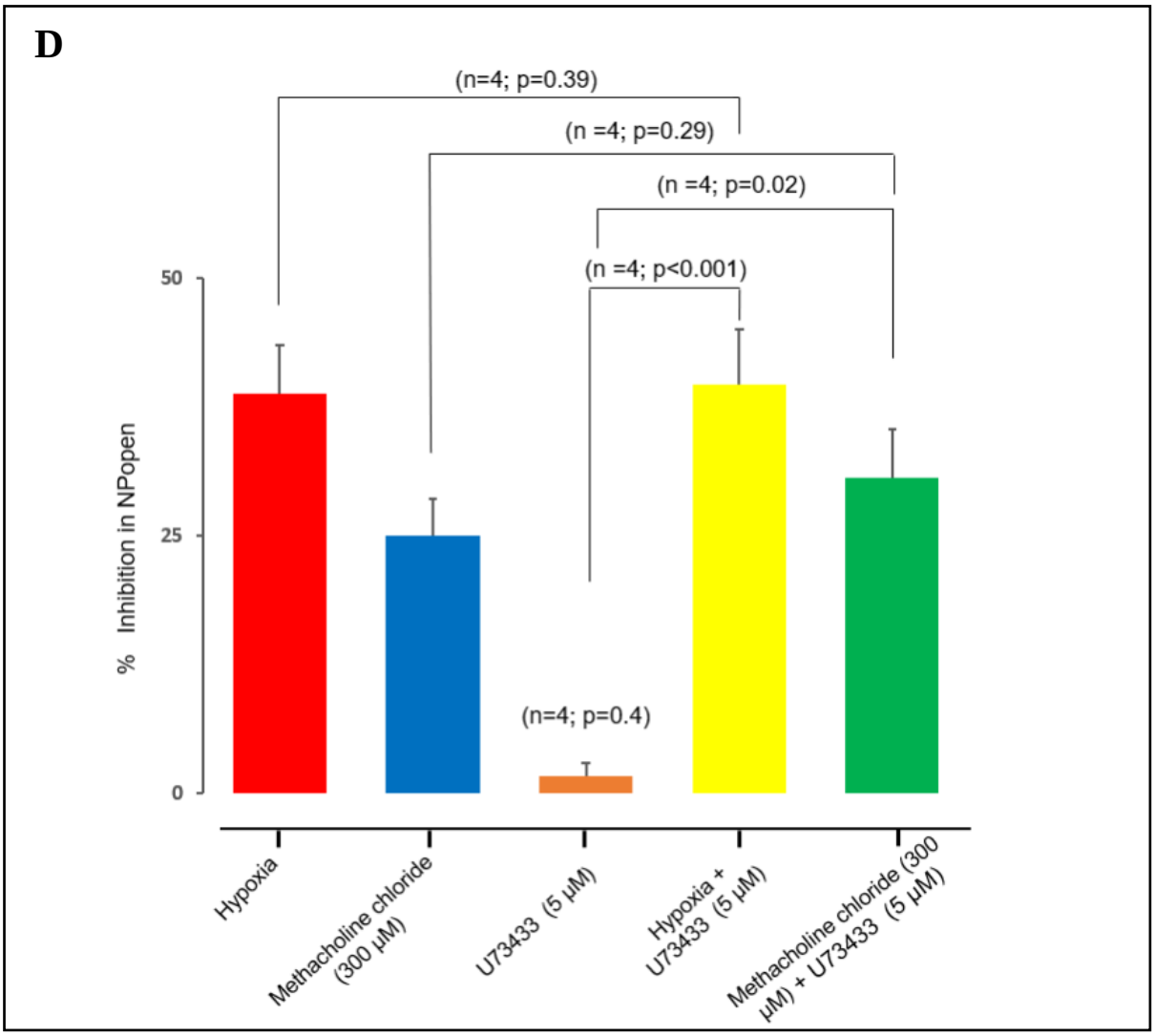
D
(n=4; p=0.39)
(n =4; p=0.29)
(n =4; p=0.02)
(n =4; p<0.001)
(n=4; p=0.4)
% Inhibition in NPopen
50
25
0
Hypoxia
Methacholine chloride (300 µM)
U73433 (5 µM)
Hypoxia + U73433 (5 µM)
Methacholine chloride (300 µM) + U73433 (5 µM)

**Figure 4.5 Effects of the PLC activator m-3m3fbs (20 μM), on TASK channels activity in rat carotid body type-1 cell** Three representative traces of single-channel recordings for control (i), m-3m3fbs (ii), and post washout (iii) **(A)**. Four representative traces of single channel recordings for hypoxia (i), hypoxia plus m-3m3fbs (ii), methacholine chloride (iii) and methacholine chloride plus m-3m3fbs (iv) **(B)**. Representative all-points histogram from the same recording, control in blue and m-3m3fbs in red. Histogram was generated from a selected 20s of both control and m-3m3fbs application. Bin-width was 0.1pA **(C)**. Comparison of inhibitory effects of hypoxia, methacholine chloride 300 μM, m-3m3fbs, hypoxia and methacholine chloride 300 μM plus m-3m3fbs on channel activity. Data are expressed as percentage inhibition of nPopen in the presence of hypoxia, methacholine chloride, and m-3m3fbs relative to control (means ± SEM) **(D)**. The traces were recorded with a pipette potential of +100 mV, 140 mM $K^+$ in pipette solution and 100 mM $K^+$ in Tyrode solution. Bar shows 0.02 s timescale; vertical bar shows 10 pA current. Statistical significance was evaluated utilizing a paired Student's t-test.

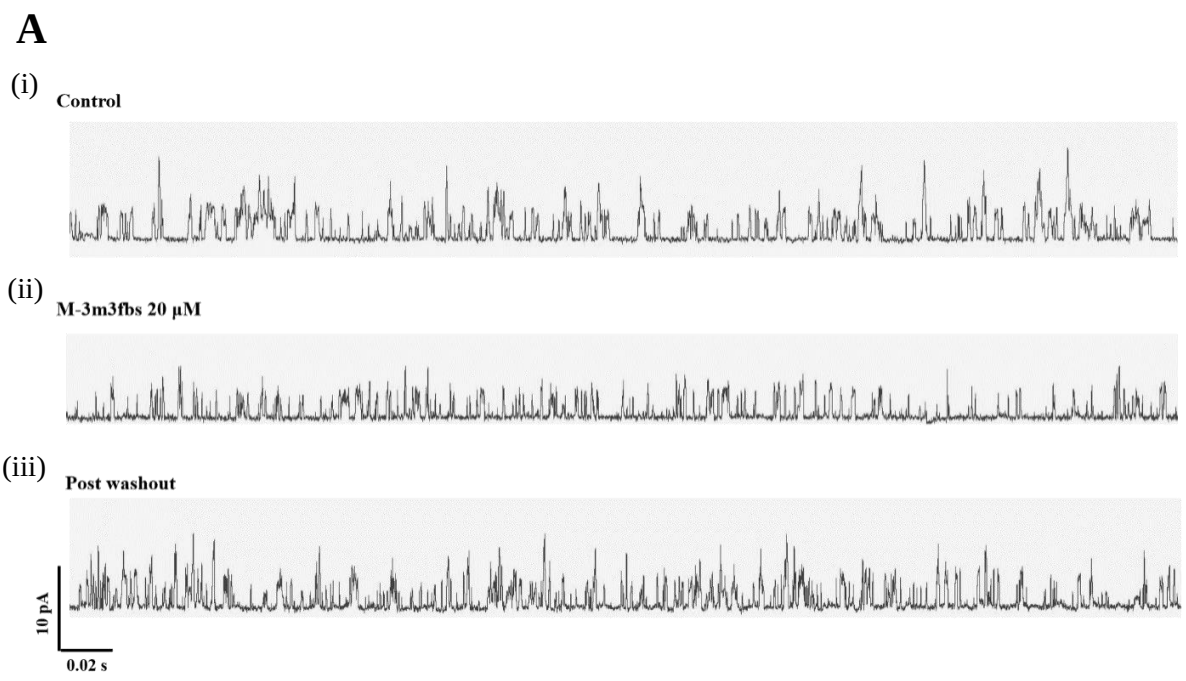

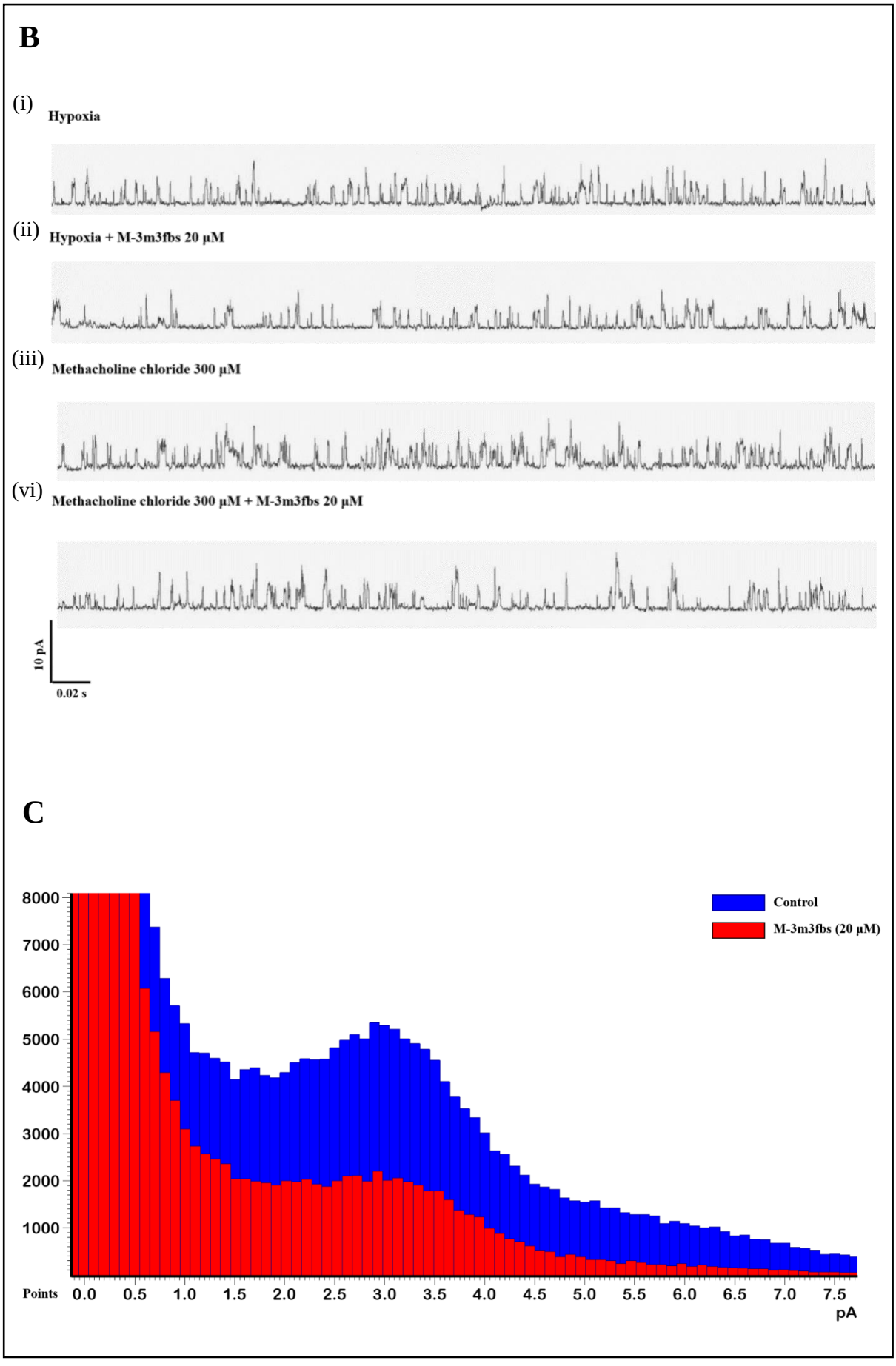
B
(i)
Hypoxia
(ii)
Hypoxia + M-3m3fbs 20 µM
(iii)
Methacholine chloride 300 µM
(vi)
Methacholine chloride 300 µM + M-3m3fbs 20 µM
10 pA
0.02 s
C
Control
M-3m3fbs (20 µM)
8000
7000
6000
5000
4000
3000
2000
1000
Points
0.0
0.5
1.0
1.5
2.0
2.5
3.0
3.5
4.0
4.5
5.0
5.5
6.0
6.5
7.0
7.5
pA

**D**

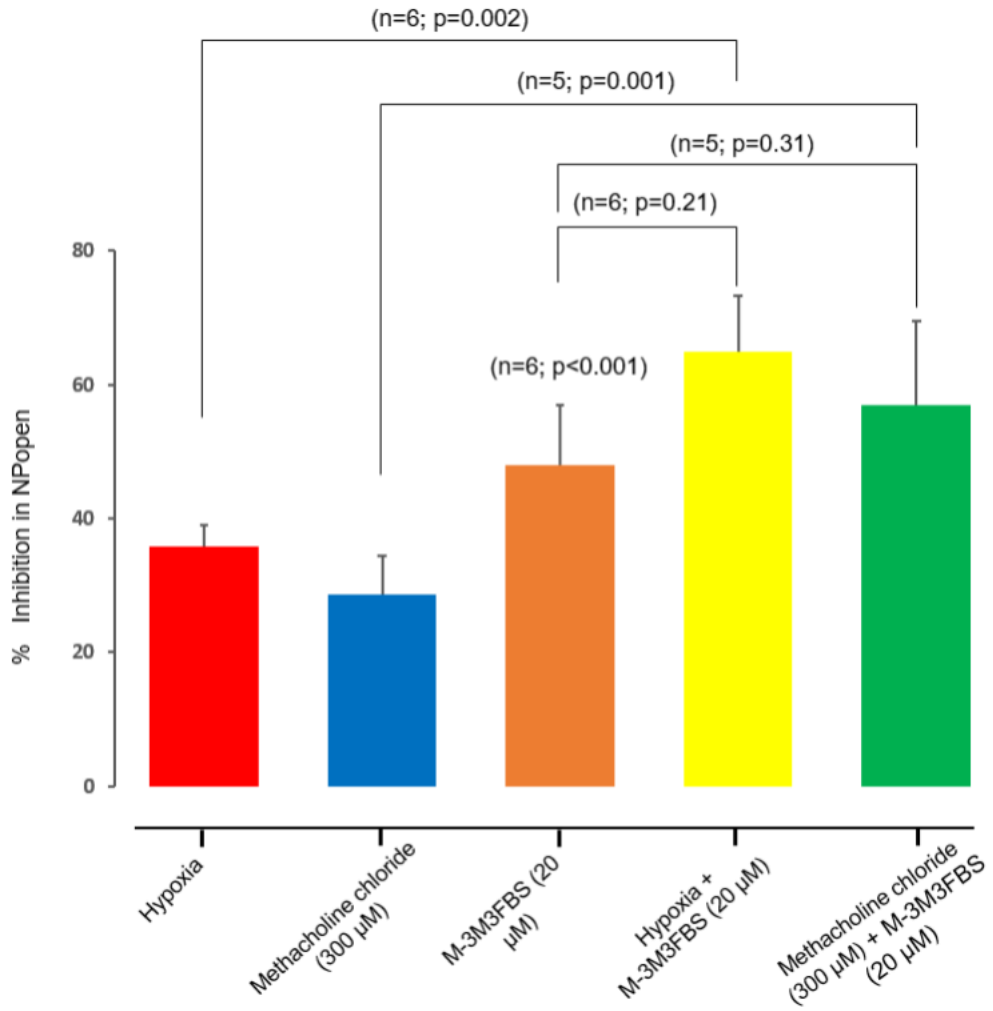
(n=6; p=0.002)
(n=5; p=0.001)
(n=5; p=0.31)
(n=6; p=0.21)
(n=6; p<0.001)
% Inhibition in NPopen
80
60
40
20
0
Hypoxia
Methacholine chloride (300 µM)
M-3M3FBS (20 µM)
Hypoxia + M-3M3FBS (20 µM)
Methacholine chloride (300 µM) + M-3M3FBS (20 µM)

**Figure 4.6 Effects of o-3m3fbs (20 μM), the m-3m3fbs control compound, on TASK channels activity in rat carotid body type-1 cell**

Three representative traces of single-channel recordings for control (i), o-3m3fbs (ii), and post washout (iii) **(A)**. Four representative traces of single channel recordings for hypoxia (i), hypoxia plus o-3m3fbs (ii), methacholine chloride (iii), and methacholine chloride plus o-3m3fbs (iv) **(B)**. Representative all-points histogram from the same recording, control in blue and o-3m3fbs in red. Histogram was generated from a selected 20s of both control and o-3m3fbs application. Bin-width was 0.1pA **(C)**. Comparison of inhibitory effects of hypoxia, methacholine chloride 300 μM, o-3m3fbs and hypoxia and methacholine chloride 300 μM plus o-3m3fbs on channel activity. Data are expressed as percentage inhibition of nPopen in the presence of hypoxia, methacholine chloride, and o-3m3fbs relative to control (means ± SEM) **(D)**. The traces were recorded with a pipette potential of +100 mV, 140 mM $K^+$ in pipette solution and 100 mM $K^+$ in Tyrode solution. Bars shows 0.02 s timescale; vertical bar shows 10 pA current. Statistical significance was evaluated utilizing a paired Student's t-test.

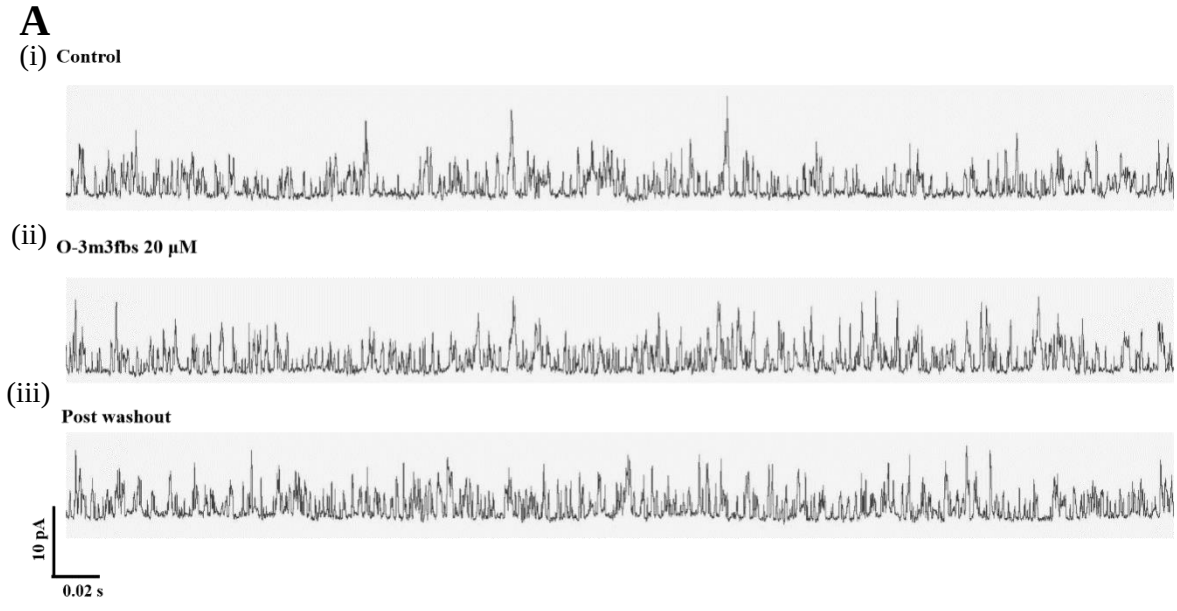

**B**

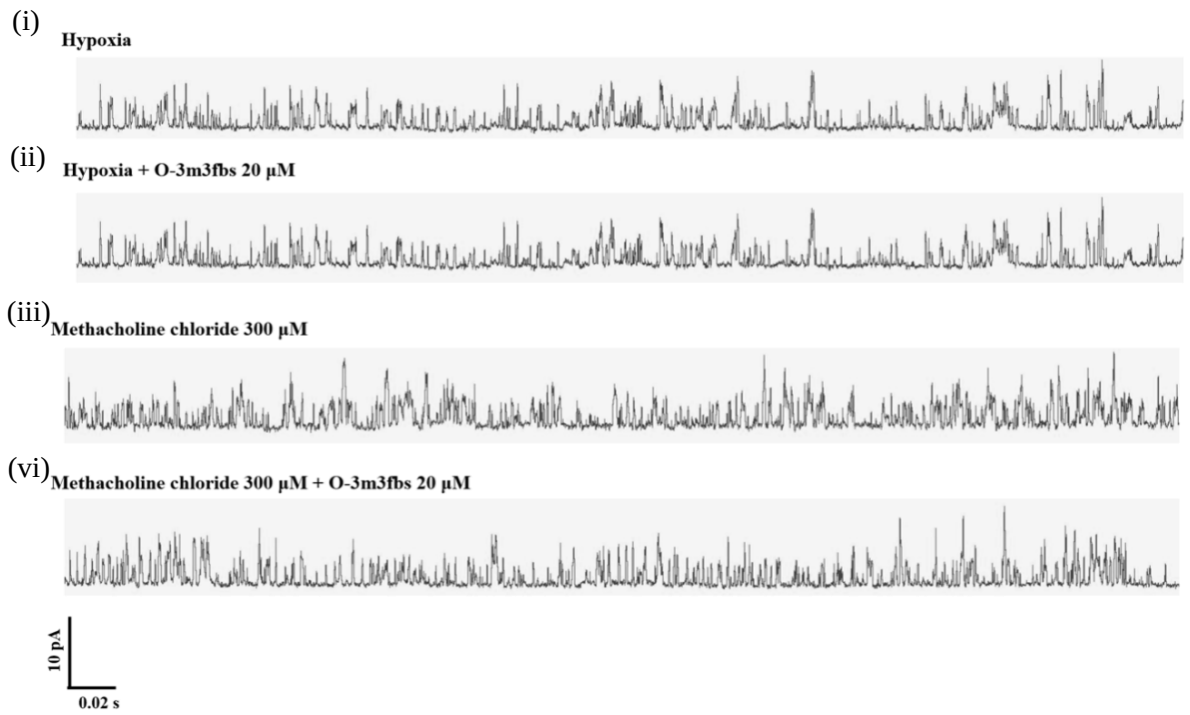
(i)
Hypoxia
(ii)
Hypoxia + O-3m3fbs 20 µM
(iii)
Methacholine chloride 300 µM
(vi)
Methacholine chloride 300 µM + O-3m3fbs 20 µM
10 pA
0.02 s

**C**

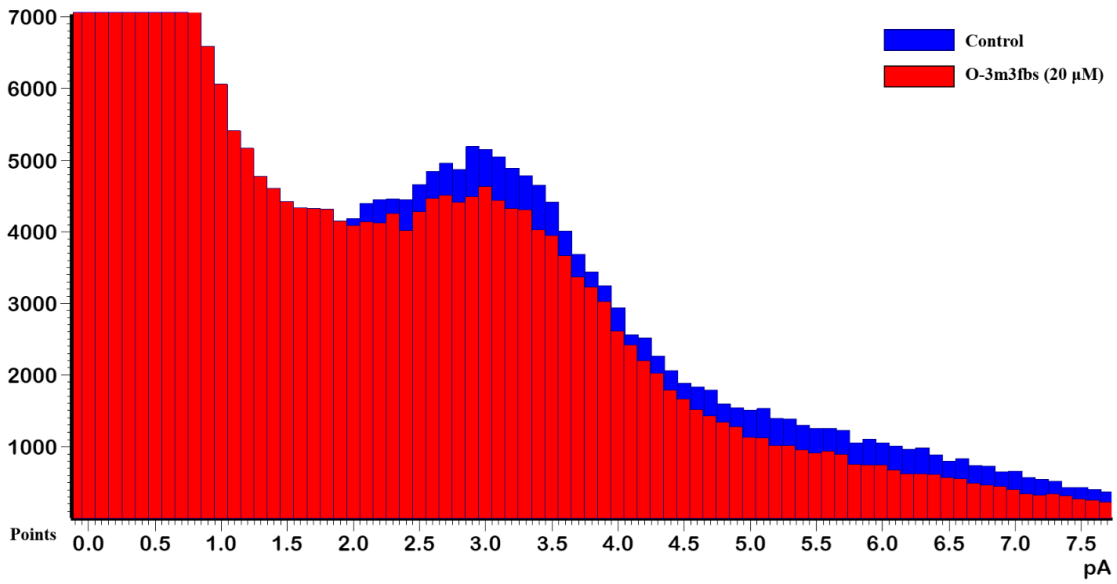
Control
O-3m3fbs (20 µM)
7000
6000
5000
4000
3000
2000
1000
Points
0.0
0.5
1.0
1.5
2.0
2.5
3.0
3.5
4.0
4.5
5.0
5.5
6.0
6.5
7.0
7.5
pA

**D**

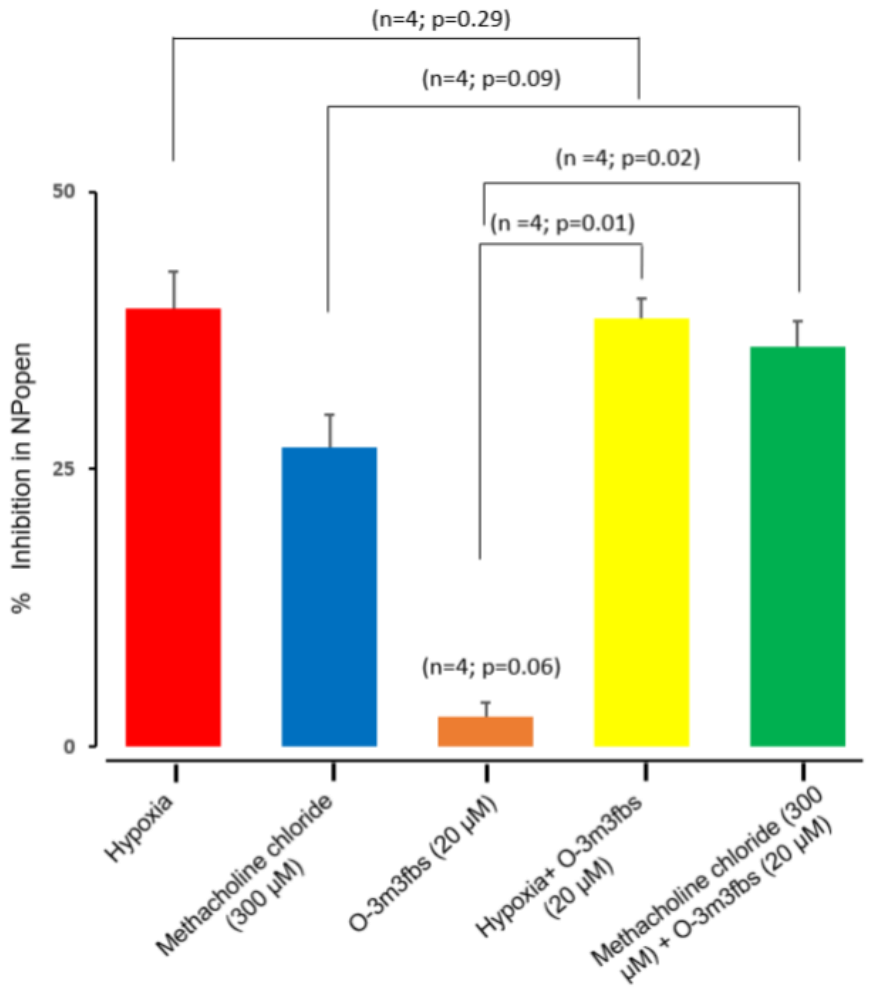
(n=4; p=0.29)
(n=4; p=0.09)
(n =4; p=0.02)
(n =4; p=0.01)
(n=4; p=0.06)
50
25
0
% Inhibition in NPopen
Hypoxia
Methacholine chloride (300 µM)
O-3m3fbs (20 µM)
Hypoxia+ O-3m3fbs (20 µM)
Methacholine chloride (300 µM) + O-3m3fbs (20 µM)

### 4.3.3 The role of DAG in the regulation of TASK channels in type-1 cell

To determine the role of DAG in the regulation of TASK channels in type-1 cells, I applied the DAG analogue DiC8 to acutely isolated type-1 cells. DiC8 is a short-chain membrane-permeable DAG analogue that has been widely used to assess the impact of DAG on cell signalling mechanisms. Application of 5 μM DiC8 induced a strong, reversible, and maximal (see Chapter 6, Figure 6.1) inhibition of channel activity in cell-attached patches by 69.3 ± 3.9% (see Figures 4.7A, B, and D; n = 10; $p < 0.001$). Figure 4.7C shows a typical all-points histogram of channel activity upon DiC8 application, note the decline in frequency at all levels of channel current.

When DiC8 was co-applied with hypoxia or methacholine chloride, there was no additional effect on TASK channels activity, as defined by nPopen (DiC8 orange bar *vs.* DiC8 plus hypoxia yellow bar: 69.3 ± 3.9 *vs.* 67.3 ± 3.8%, n = 10, p = 0.36; DiC8 orange bar *vs*. DiC8 plus methacholine chloride green bar: 69.3 ± 3.9 *vs.* 66.2 ± 9.8%, n = 8, p = 0.45; see Figures 4.7B and D).

DAG signalling is generally thought to be terminated by diacylglycerol kinases (DGKs), which phosphorylate DAG to produce phosphatidic acid. Therefore, I further studied the effects of DAG on TASK channels by applying a DAGK inhibitor (D5919). This inhibitor is expected to reduce DAG phosphorylation and consequently increase DAG levels where there is constitutive PLC activity. Application of 10 μM D5919 inhibited channel activity in cell-attached patches, as defined by nPopen by 45.8 ± 6.7% (see Figures 4.8A, B, and D; orange bar, n = 9; $p < 0.001$). This concentration was applied to ensure a maximal inhibition of DAGK activity (Lingelem et al., 2021). IFigure 4.8C shows a typical all-points histogram for the channel activity upon D5919 (10 μM) application, note the reduction in open-channel current over the whole amplitude range, which is consistent with a nearly uniform suppression of background TASK channel activity at all conductance levels. In the presence of D5919, hypoxia and

methacholine chloride had no additional effect on TASK channels activity, as defined by nPopen (D5919 orange bar *vs.* D5919 plus hypoxia yellow bar: 45.8 ± 6.7 *vs.* 49.6 ± 7.7%, n = 9, p = 0.43; D5919 orange bar *vs.* D5919 plus methacholine chloride green bar: 45.8 ± 6.7 *vs.* 56.9 ± 9.9%, n = 6, p = 0.19; see Figures 4.8 B and D).

What emerges from these results is that DAG is involved in the regulation of the baseline activity of TASK channels in type-1 cells and the inhibition of these channels by hypoxia and muscarinic agonist.

**Figure 4.7 Effects of DiC8 (5 μM), a DAG analogue, on TASK channels activity in rat carotid body type-1 cell** Three representative traces of single-channel recordings for control (i), DiC8 (ii), and post washout (iii) **(A)**. Four representative traces of single channel recordings for hypoxia (i), hypoxia plus DiC8 (ii), methacholine chloride (iii), and methacholine chloride plus DiC8 (iv) **(B)**. Representative all-points histogram from the same recording, control in blue and DiC8 in red. Histogram was generated from a selected 20s of both control and DiC8 application. Bin-width was 0.1pA **(C)**. Comparison of inhibitory effects of hypoxia, methacholine chloride 300 μM, DiC8, hypoxia and methacholine chloride 300 μM plus DiC8 on channel activity. Data are expressed as percentage inhibition of nPopen in the presence of hypoxia, methacholine chloride, and DiC8 relative to control (means ± SEM) **(D)**. The traces were recorded with a pipette potential of +100 mV, 140 mM $K^+$ in pipette solution and 100 mM $K^+$ in Tyrode solution. Bars shows 0.02 s timescale; vertical bar shows 10 pA current. Statistical significance was evaluated utilizing a paired Student's t-test.

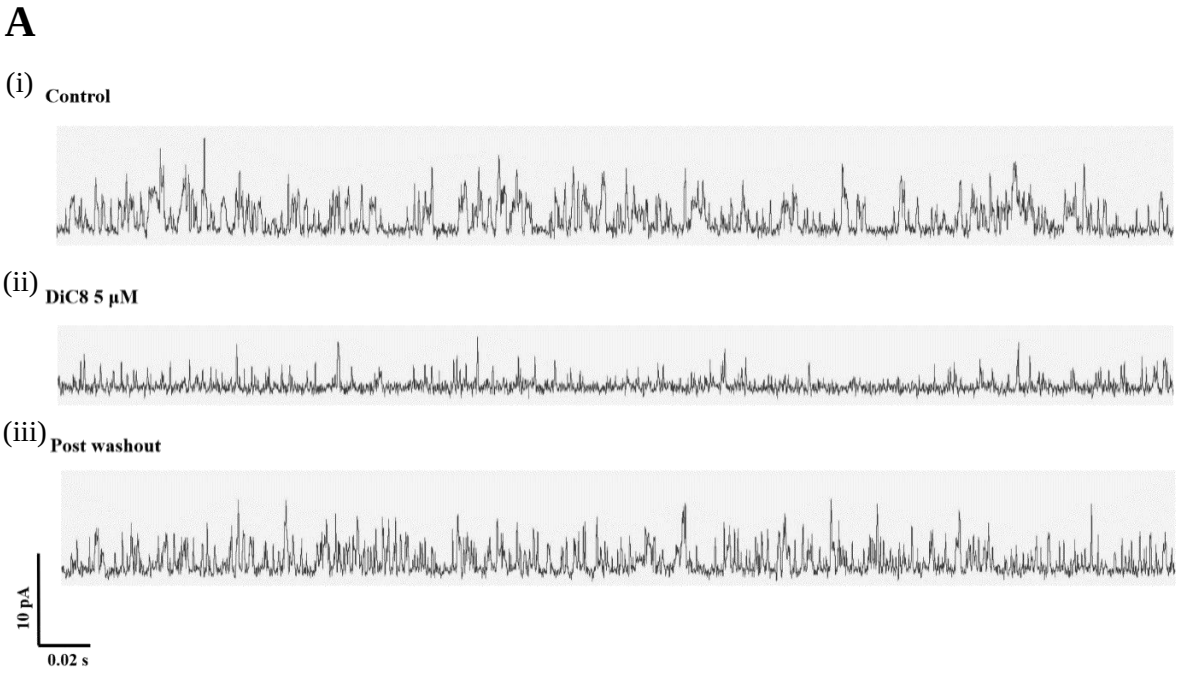

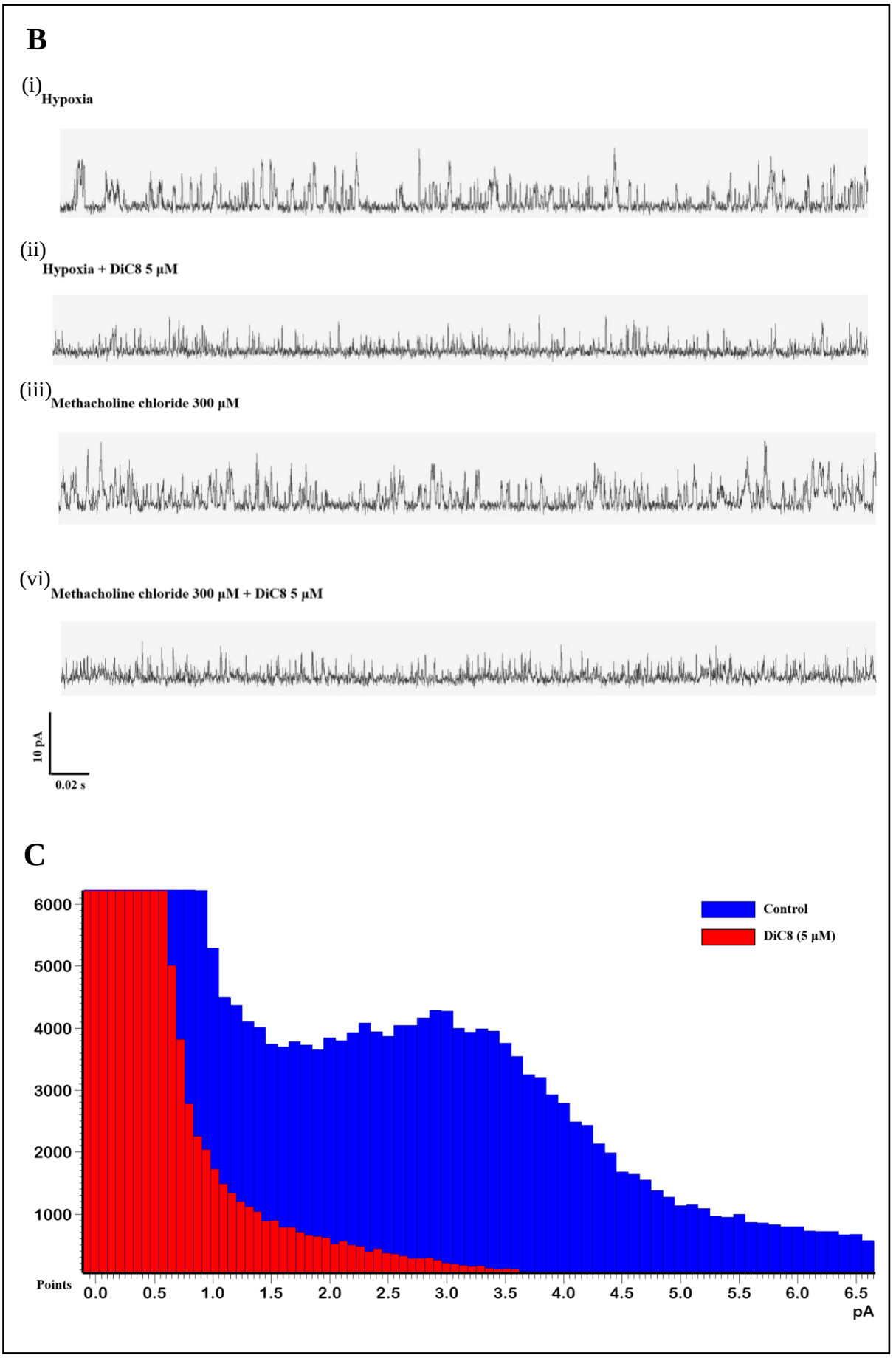
B
(i) Hypoxia
(ii) Hypoxia + DiC8 5 µM
(iii) Methacholine chloride 300 µM
(vi) Methacholine chloride 300 µM + DiC8 5 µM
10 pA
0.02 s
C
Control
DiC8 (5 µM)
6000
5000
4000
3000
2000
1000
Points
0.0
0.5
1.0
1.5
2.0
2.5
3.0
3.5
4.0
4.5
5.0
5.5
6.0
6.5
pA

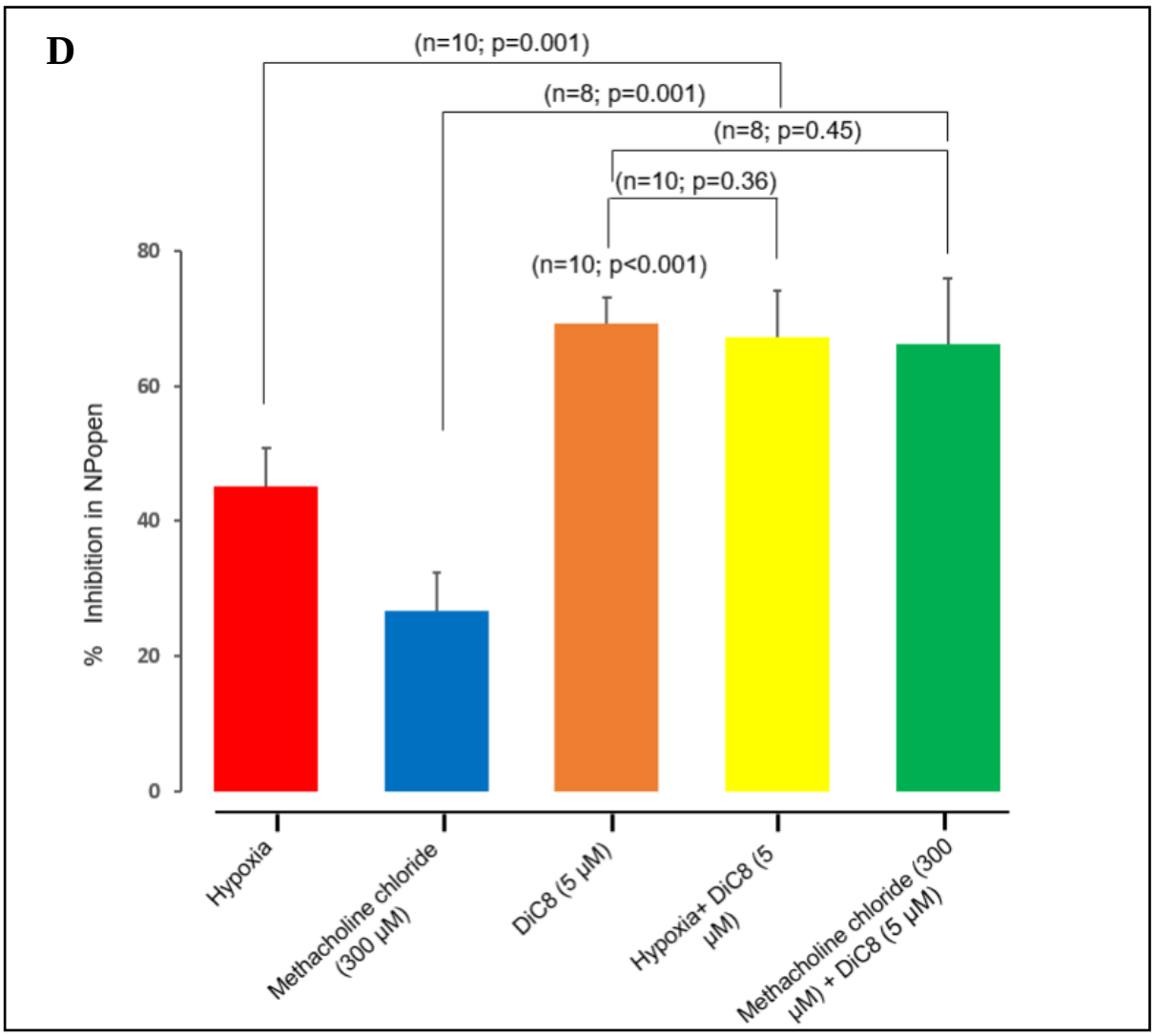
D
(n=10; p=0.001)
(n=8; p=0.001)
(n=8; p=0.45)
(n=10; p=0.36)
(n=10; p<0.001)
% Inhibition in NPopen
80
60
40
20
0
Hypoxia
Methacholine chloride (300 µM)
DiC8 (5 µM)
Hypoxia+ DiC8 (5 µM)
Methacholine chloride (300 µM) + DiC8 (5 µM)

**Figure 4.8 Effects of D5919 (10 μM), a DAG kinase inhibitor, on TASK channels activity in rat carotid body type-1 cell** Three representative traces of single-channel recordings for control (i), D5919 (ii), and post washout (iii) **(A)**. Four representative traces of single channel recordings for hypoxia (i), hypoxia plus D5919 (ii), methacholine chloride (iii), and methacholine chloride plus D5919 (iv) **(B)**. Representative all-points histogram from the same recording, control in blue and D5919 in red. Histogram was generated from a selected 20s of both control and D5919 application. Bin-width was 0.1pA **(C)**. Comparison of inhibitory effects of hypoxia, methacholine chloride 300 μM, D5919, hypoxia and methacholine chloride 300 μM plus D5919 on channel activity. Data are expressed as percentage inhibition of nPopen in the presence of hypoxia, methacholine chloride, and D5919 relative to control (means ± SEM) **(D)**. The traces were recorded with a pipette potential of +100 mV, 140 mM $K^+$ in pipette solution and 100 mM $K^+$ in Tyrode solution. Bar shows 0.02 s timescale; vertical bar shows 10 pA current. Statistical significance was evaluated utilizing a paired Student's t-test.

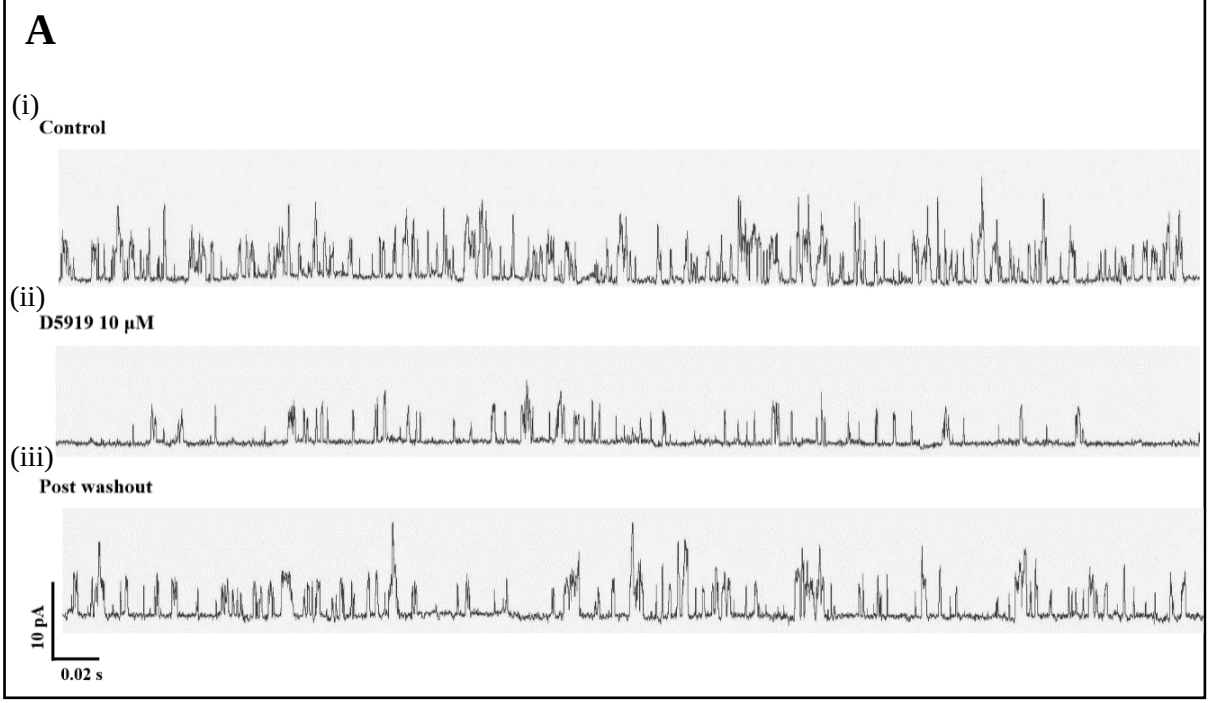

**B**

(i) **Hypoxia**

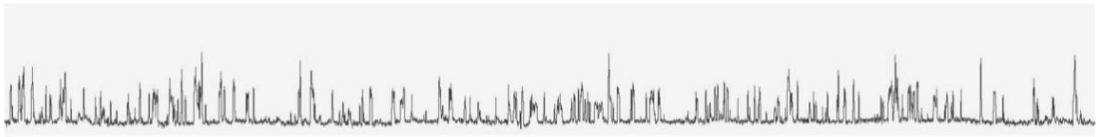

(ii) **Hypoxia + D5919 10 µM**

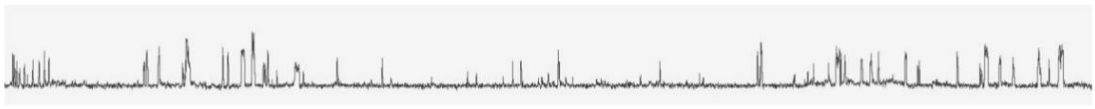

(iii) **Methacholine chloride 300 µM**

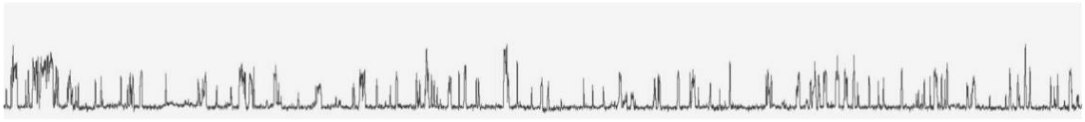

(iv) **Methacholine chloride 300 µM + D5919 10 µM**

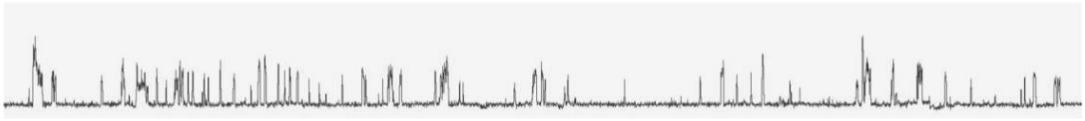

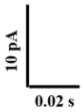


**C**

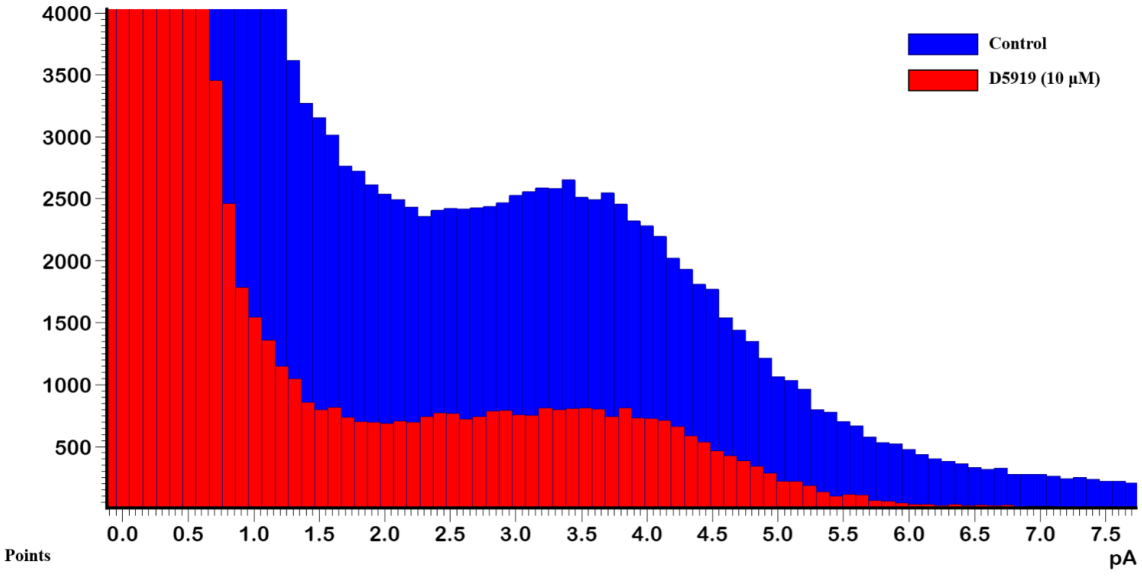

**D**

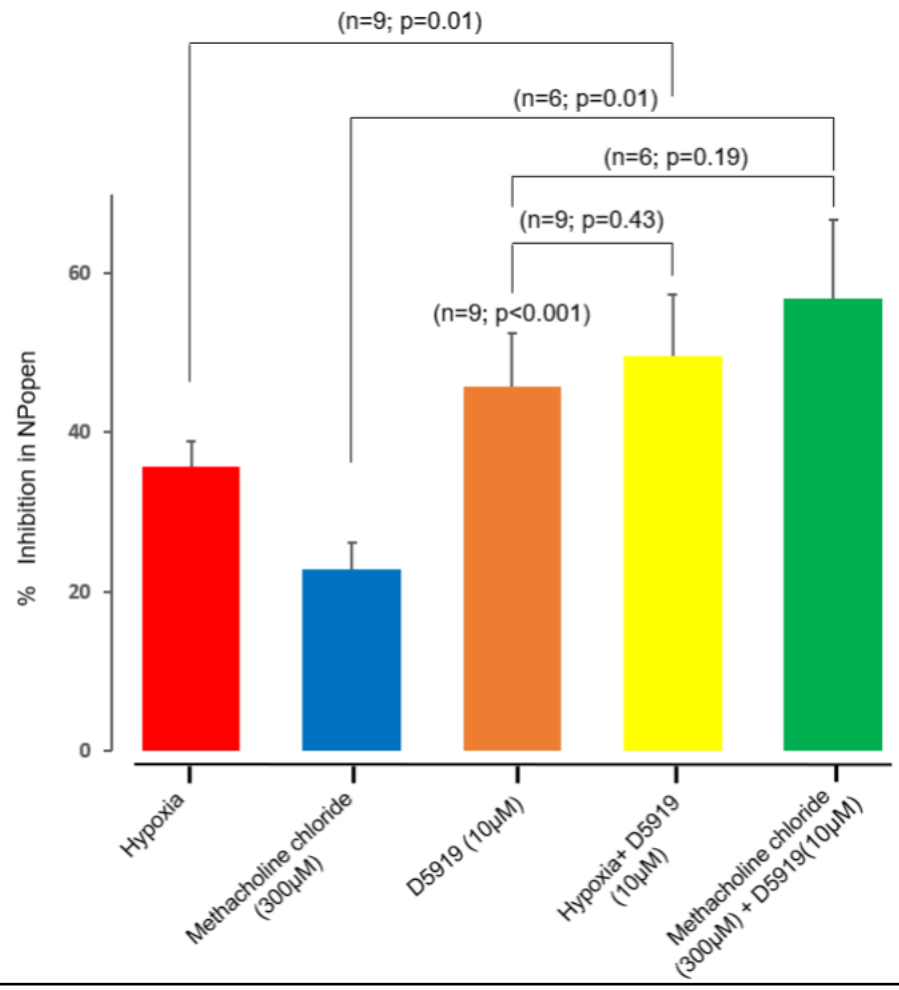
(n=9; p=0.01)
(n=6; p=0.01)
(n=6; p=0.19)
(n=9; p=0.43)
(n=9; p<0.001)
% Inhibition in NPopen
0
20
40
60
Hypoxia
Methacholine chloride (300µM)
D5919 (10µM)
Hypoxia+ D5919 (10µM)
Methacholine chloride (300µM) + D5919(10µM)

### 4.3.4 The role of PKC in the regulation of TASK channels in type-1 cell

Next, I examined the effects of PKC on the activity of TASK channels in type-1 cells. I applied a highly selective inhibitor of PKC, calphostin C, to acutely isolated type-1 cells. Application of 50 nM calphostin C did not affect channel activity in cell-attached patches (Figures 4.9A, C, and D, orange bar; n = 8; p = 0.20). It also had no significant effect on hypoxia (red bar *vs.* yellow bar; n = 8; p = 0.44) or methacholine chloride (300 μM) induced inhibition of channel activity (blue bar *vs.* green bar; n = 7; p = 0.12); see Figures 4.9B and D. Figure 4.9C shows a typical all-points histogram for the channel activity upon calphostin C application. These findings suggest that PKC is not involved in the regulation of TASK channels in type-1 cells.

**Figure 4.9 Effects of calphostin C (50 nM), a PKC inhibitor, on TASK channels activity in rat carotid body type-1 cell** Three representative traces of single-channel recordings for control (i), calphostin C (ii), and post washout (iii) **(A)**. Four representative traces of single channel recordings for hypoxia (i), hypoxia plus calphostin C (ii), methacholine chloride (iii), and methacholine chloride plus calphostin C (iv) **(B)**. Representative all-points histogram from the same recording, control in blue and calphostin C in red. Histogram was generated from a selected 20s of both control and calphostin C application. Bin-width was 0.1pA **(C)**. Comparison of inhibitory effects of hypoxia, methacholine chloride 300 μM, calphostin C, hypoxia and methacholine chloride 300 μM plus calphostin C on channel activity. Data are expressed as percentage inhibition of nPopen in the presence of hypoxia, methacholine chloride, and calphostin C relative to control (means ± SEM) **(D)**. The traces were recorded with a pipette potential of +100 mV, 140 mM $K^+$ in pipette solution and 100 mM $K^+$ in Tyrode solution. Bar shows 0.05 s timescale; vertical bar shows 5 pA current. Statistical significance was evaluated utilizing a paired Student's t-test.

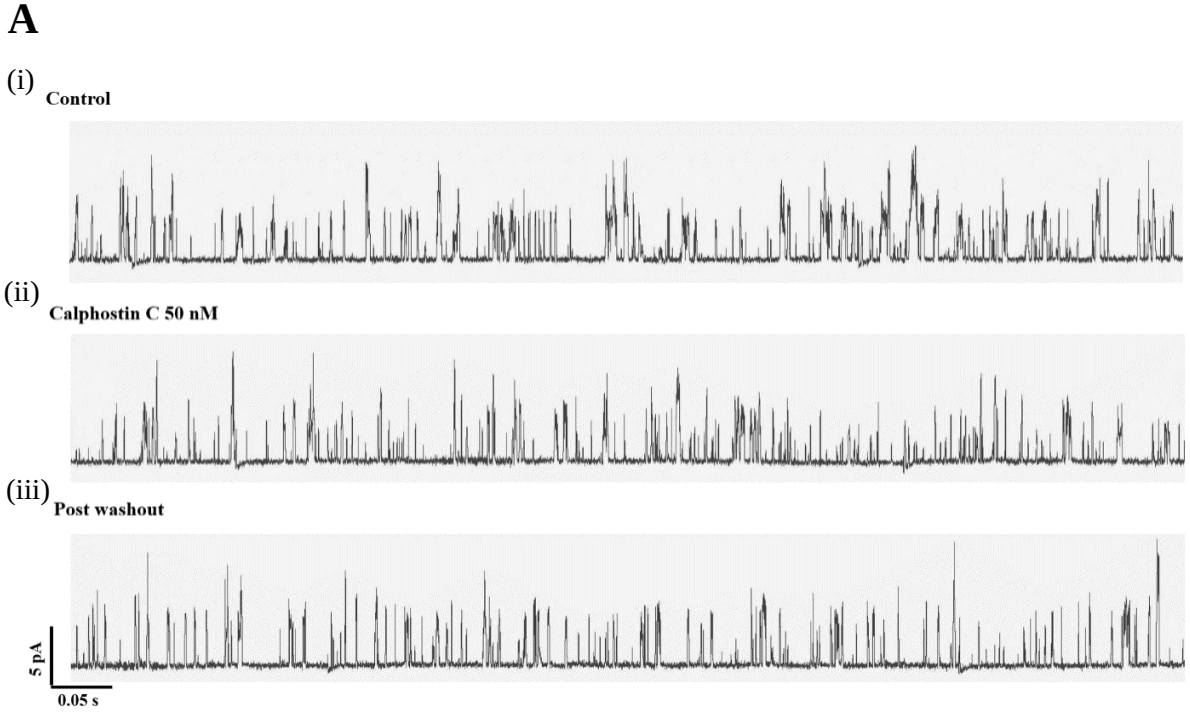

**B**

(i) Hypoxia

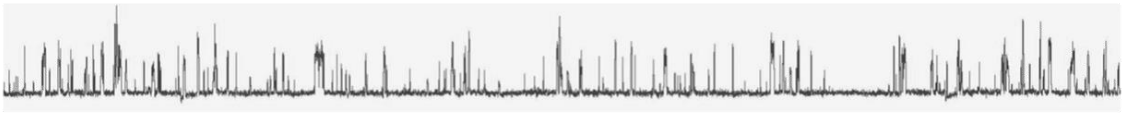

(ii) Hypoxia + Calphostin C 50 nM

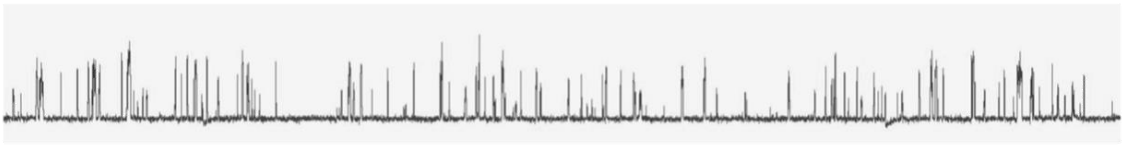

(iii) Methacholine chloride 300 µM

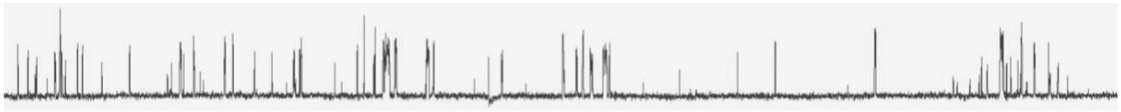

(iv) Methacholine chloride 300 µM + Calphostin C 50 nM

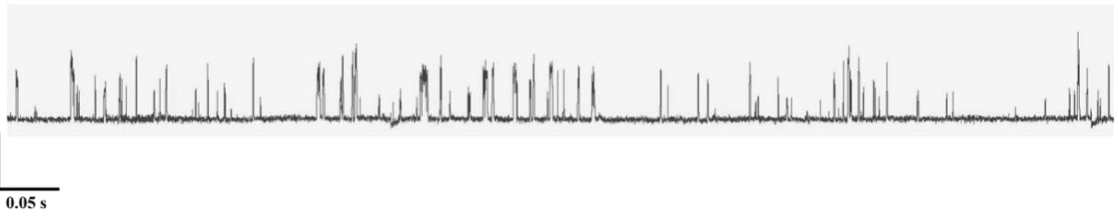


**C**

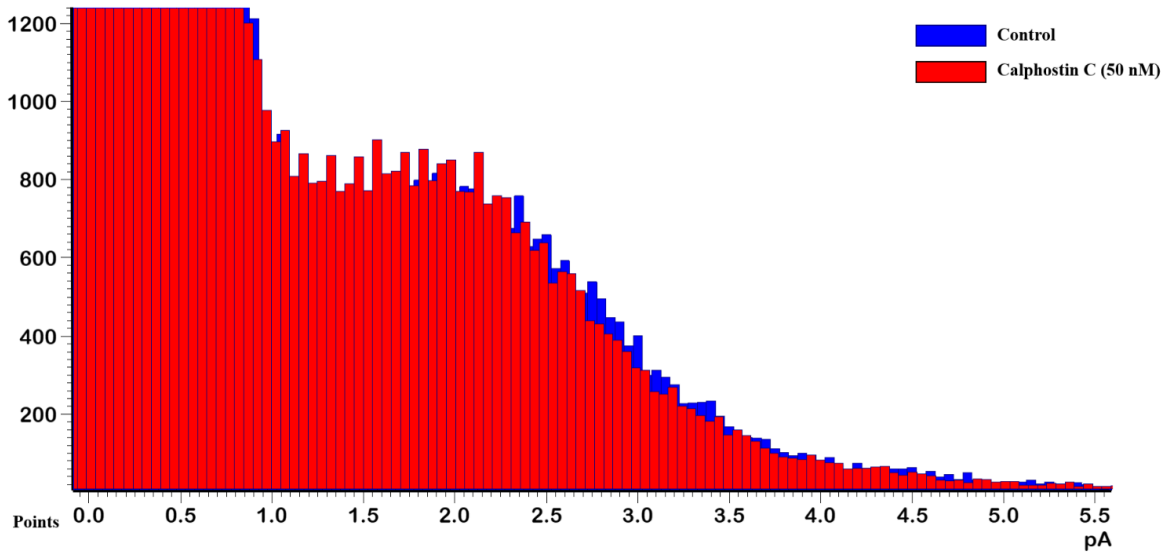

**D**

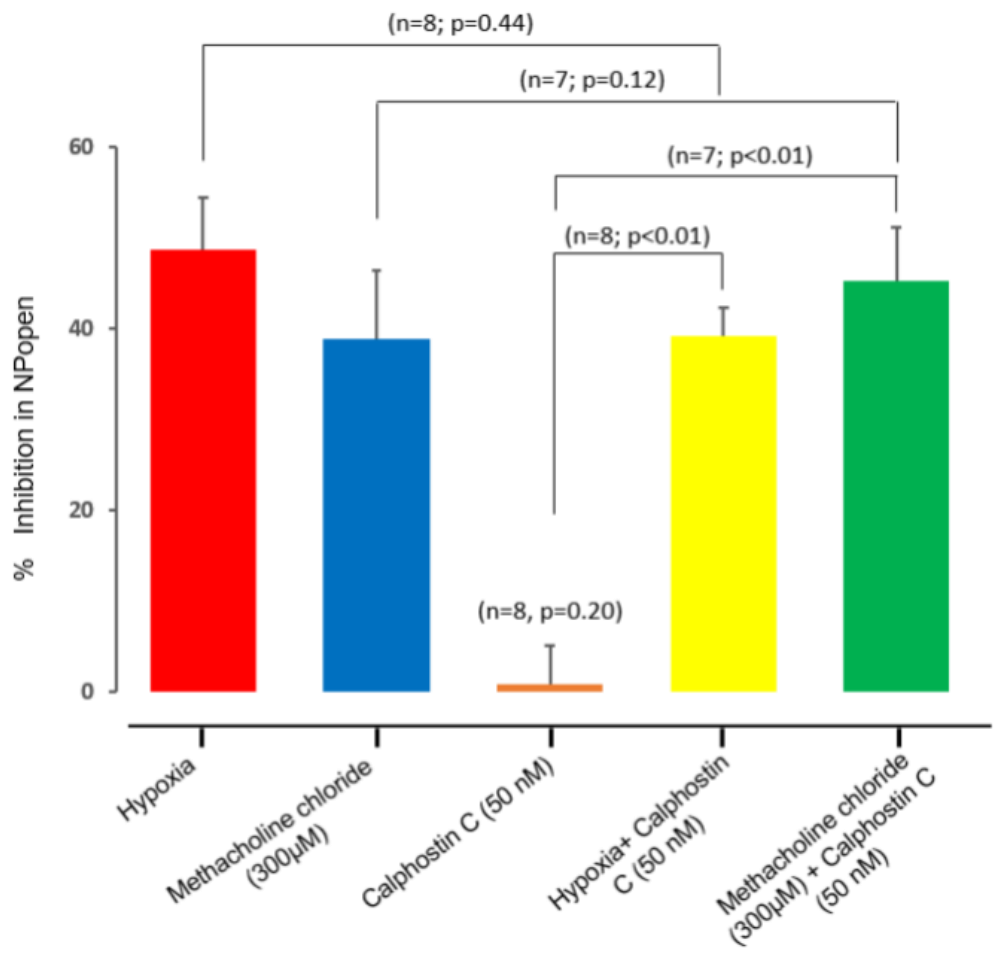
(n=8; p=0.44)
(n=7; p=0.12)
(n=7; p<0.01)
(n=8; p<0.01)
(n=8, p=0.20)
% Inhibition in NPopen
60
40
20
0
Hypoxia
Methacholine chloride (300μM)
Calphostin C (50 nM)
Hypoxia+ Calphostin C (50 nM)
Methacholine chloride (300μM) + Calphostin C (50 nM)

### 4.3.5 The role of IP3 in the regulation of TASK channels in type-1 cell

To investigate the effects of IP3 on TASK channels, I applied the PI3 kinase inhibitor LY290042 to acutely isolated type-1 cells. LY290042 is a highly selective inhibitor of phosphatidylinositol 3-kinase, thus increasing endogenous IP3 levels. Application of 10 μM LY290042 inhibited channel activity in cell-attached patches by 13.7 ± 7% (see Figures 4.10A, C, and D, orange bar; n = 8; p = 0.04). Figure 4.11C shows a typical all-points histogram for channel activity upon LY290042 application. LY290042 had no significant effect on hypoxic inhibition (see Figures 4.10B and D; red bar *vs.* yellow bar; n = 8; p = 0.18), but slightly enhanced methacholine chloride (300 μM) induced inhibition of channel activity from 30.8 ± 2.94 to 36.4 ± 4.9% (see Figures 4.10B and D; blue bar *vs.* green bar; n = 7; p = 0.03).

These results indicate that IP3 is only involved in the muscarinic inhibition of TASK channels in type-1 cells.

**Figure 4.10 Effects of LY290042 (10 μM), a PI3K inhibitor, on TASK channels activity in rat carotid body type-1 cells** Three representative traces of single-channel recordings for control (i), LY290042 (ii), and post washout (iii) **(A)**. Four representative traces of single channel recordings for hypoxia (i), hypoxia plus LY290042 (ii), methacholine chloride (iii), and methacholine chloride plus LY290042 (iv) **(B)**. Representative all-points histogram from the same recording, control in blue and LY290042 in red. Histogram was generated from a selected 20s of both control and LY290042 application. Bin-width was 0.1pA **(C)**. Comparison of inhibitory effects of hypoxia, methacholine chloride 300 μM, LY290042, hypoxia and methacholine chloride 300 μM plus LY290042 on channel activity. Data are expressed as percentage inhibition of nPopen in the presence of hypoxia, methacholine chloride, and LY290042 relative to control (means ± SEM) **(D)**. The traces were recorded with a pipette potential of +100 mV, 140 mM $K^+$ in pipette solution and 100 mM $K^+$ in Tyrode solution. Bars shows 0.05 s timescale; vertical bar shows 10 pA current. Statistical significance was evaluated utilizing a paired Student's t-test.

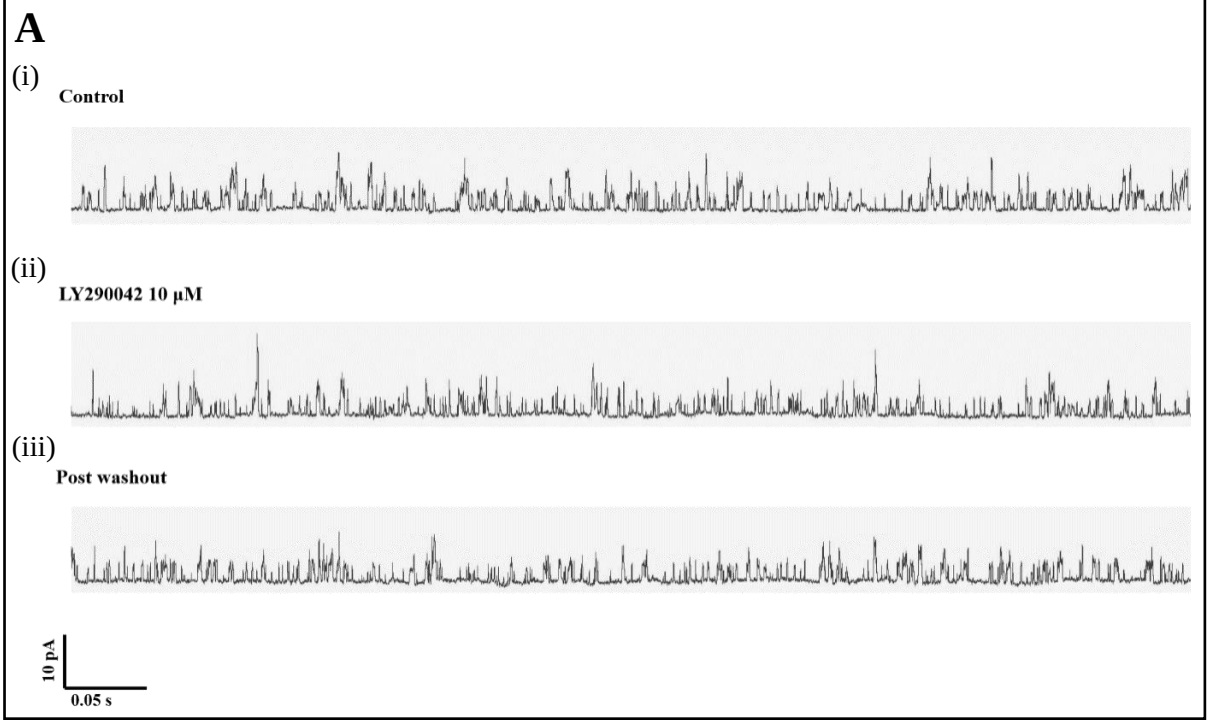

**B**

(i) **Hypoxia**

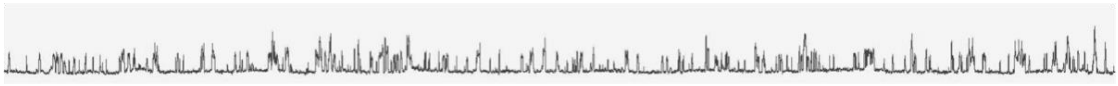

(ii) **Hypoxia + LY290042 10 µM**

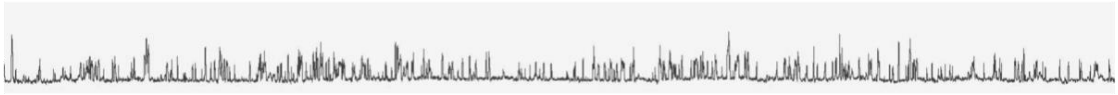

(iii) **Methacholine chloride 300 µM**

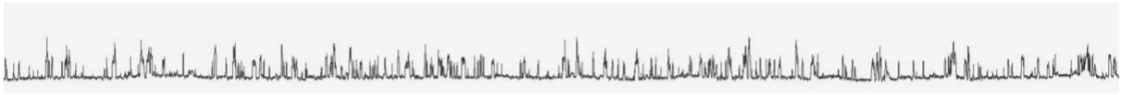

(iv) **Methacholine chloride 300 µM + LY290042 10 µM**

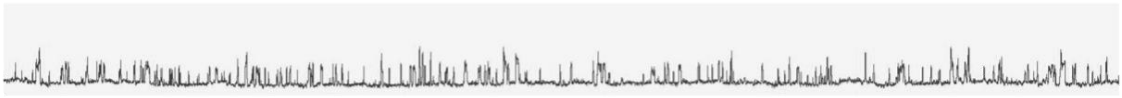

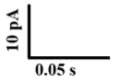


**C**

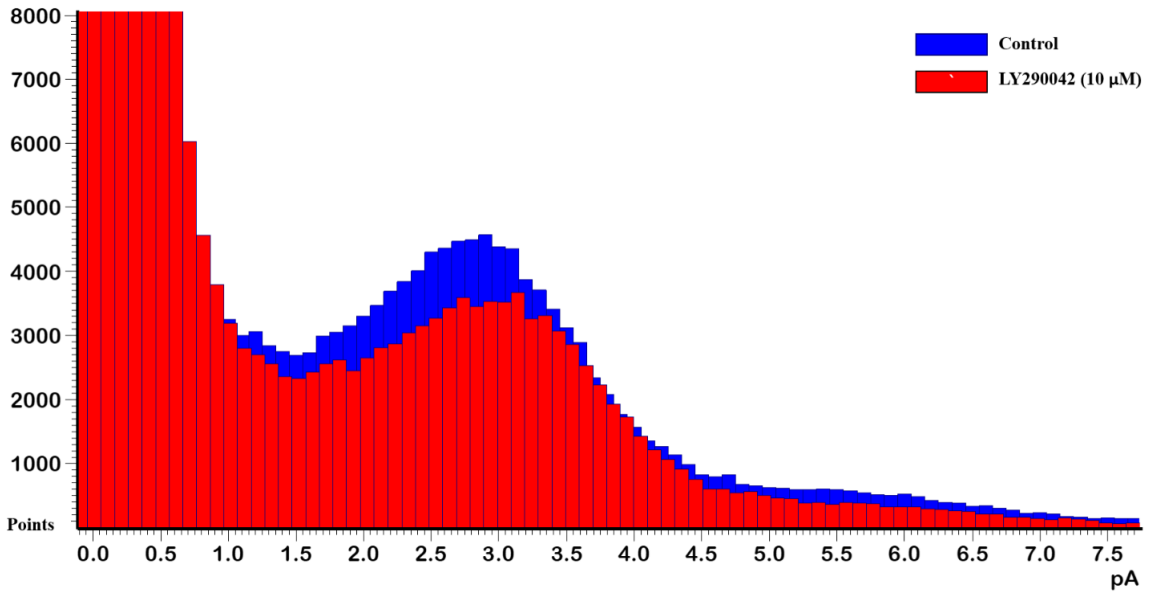

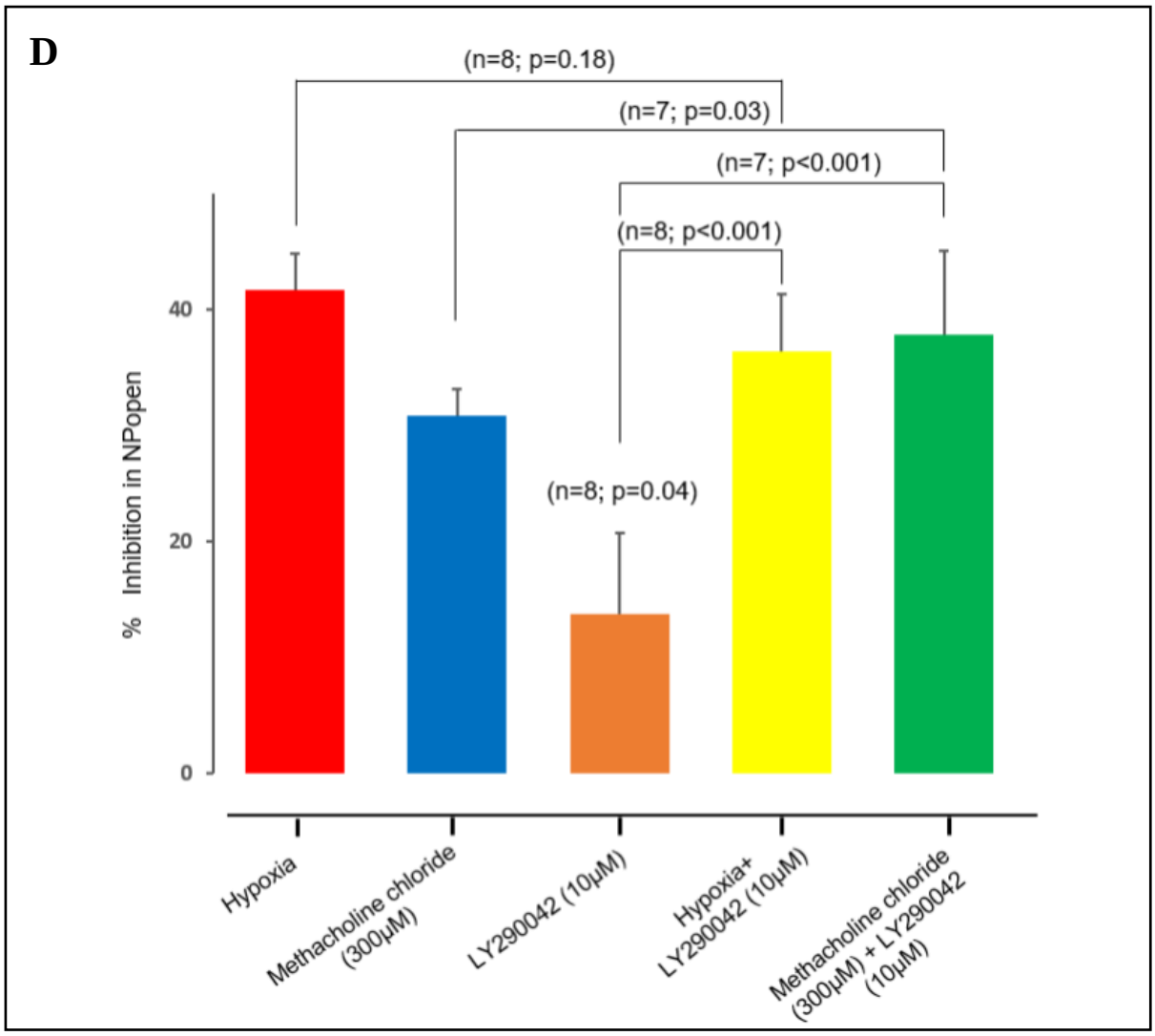
D
(n=8; p=0.18)
(n=7; p=0.03)
(n=7; p<0.001)
(n=8; p<0.001)
(n=8; p=0.04)
% Inhibition in NPopen
40
20
0
Hypoxia
Methacholine chloride (300μM)
LY290042 (10μM)
Hypoxia+ LY290042 (10μM)
Methacholine chloride (300μM) + LY290042 (10μM)

### 4.3.6 The role of DAG in the regulation of TASK channels activity in excised patches of type-1 cell

It has been previously reported that type-1 cells TASK channels exhibit a rapid rundown in activity following patch excision. Here, I sought to determine whether this rundown in channel activity is mediated by DAG accumulation. Given what appears to be constitutive PLC activity in these cells, I reasoned that the loss of ATP upon patch excision would be expected to instantly inhibit DAG kinase activity, resulting in DAG accumulation in the membrane. First, I confirmed the observation that TASK channels rundown in excised patches of type-1 cells (see Figures 4.11A and D; n = 5). Next, I applied a PLC inhibitor (U73122, 5 μM) for 40-50 seconds to reduce endogenous DAG levels before excising the patch. Application of 5 μM U73122 induced a strong activation of TASK channels in cell-attached patches by 97.7 ± 21.8% (see Figures 4.11B and E; n = 5; p = 0.005). However, this had no significant effect on TASK channels rundown after patch excision (see Figures 4.11B, C, and E; seconds post patch excision: % inhibition of nPopen control *vs.* U73122: 10: 88.11 ± 2.6 *vs.* 92.4 ± 3% (n = 5; p = 0.37); 20: 95.9 ± 0.7% *vs.* 96.4 ± 0.9% (n = 5; p = 0.10); 30: 97.2 ± 0.6% *vs.* 97.6 ± 0.9% (n = 5; p = 0.31).

These data indicate that the rundown of TASK channels in excised patches of type-1 cells is unlikely to be caused by DAG accumulation from constitutive PLC activity.

**Figure 4.11 Effects of U73122 (5 μM), a PLC inhibitor, on channel activity in excised patches** Representative single-channel recording showing rundown of TASK channels activity upon patch excision of a cell-attached patch to form an inside-out patch in two experiments one in control over approximately 2.2 minutes **(A),** and the other post U73122 application over approximately 1.2 minutes **(B)**. Two representative traces from the same experiments in A and B, over approximately 0.6 seconds showing TASK channels activity in inside-out patches. Note that in these traces, inward currents through channel openings are shown as upward deflections from baseline **(C)**. Average time course of rundown post patch excision. Mean ± S.E.M. nPopen determined over 20s intervals relative to nPopen determined over entire cell-attached period prior to patch excision in control (n=5) **(D)** and in the presence of U73122 (n=5) **(E)**. The traces were recorded with a pipette potential of +100 mV, 140 mM $K^+$ in pipette solution and 152 mM $K^+$ in Tyrode solution. Tyrode solution was switched to an intracellular solution ~10s prior to patch excision. N represents the number of recordings obtained from different type-1 cells.

**A**

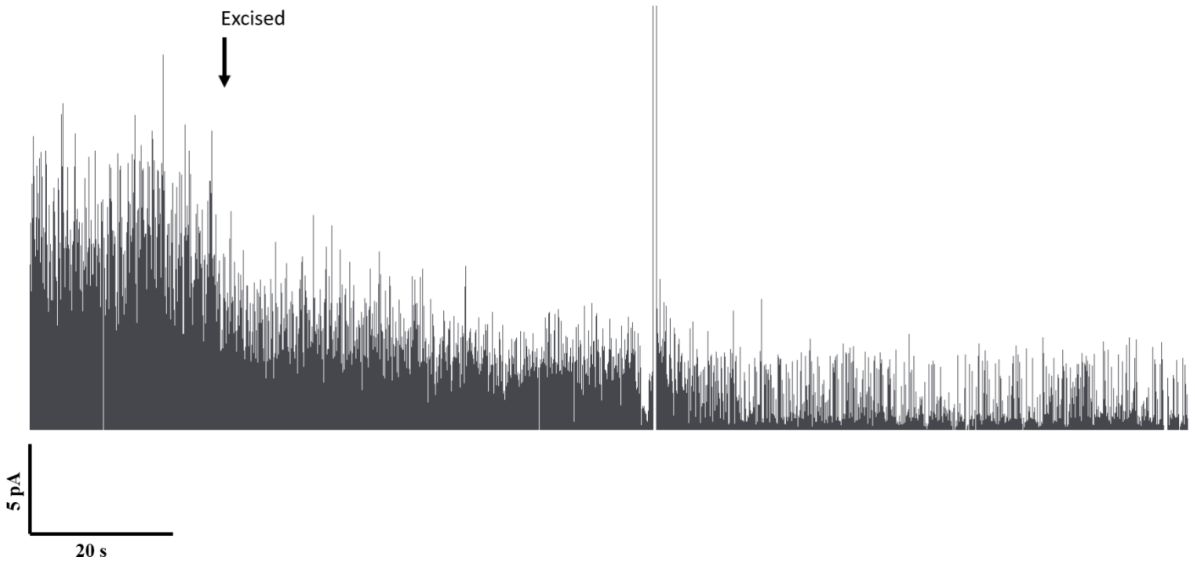

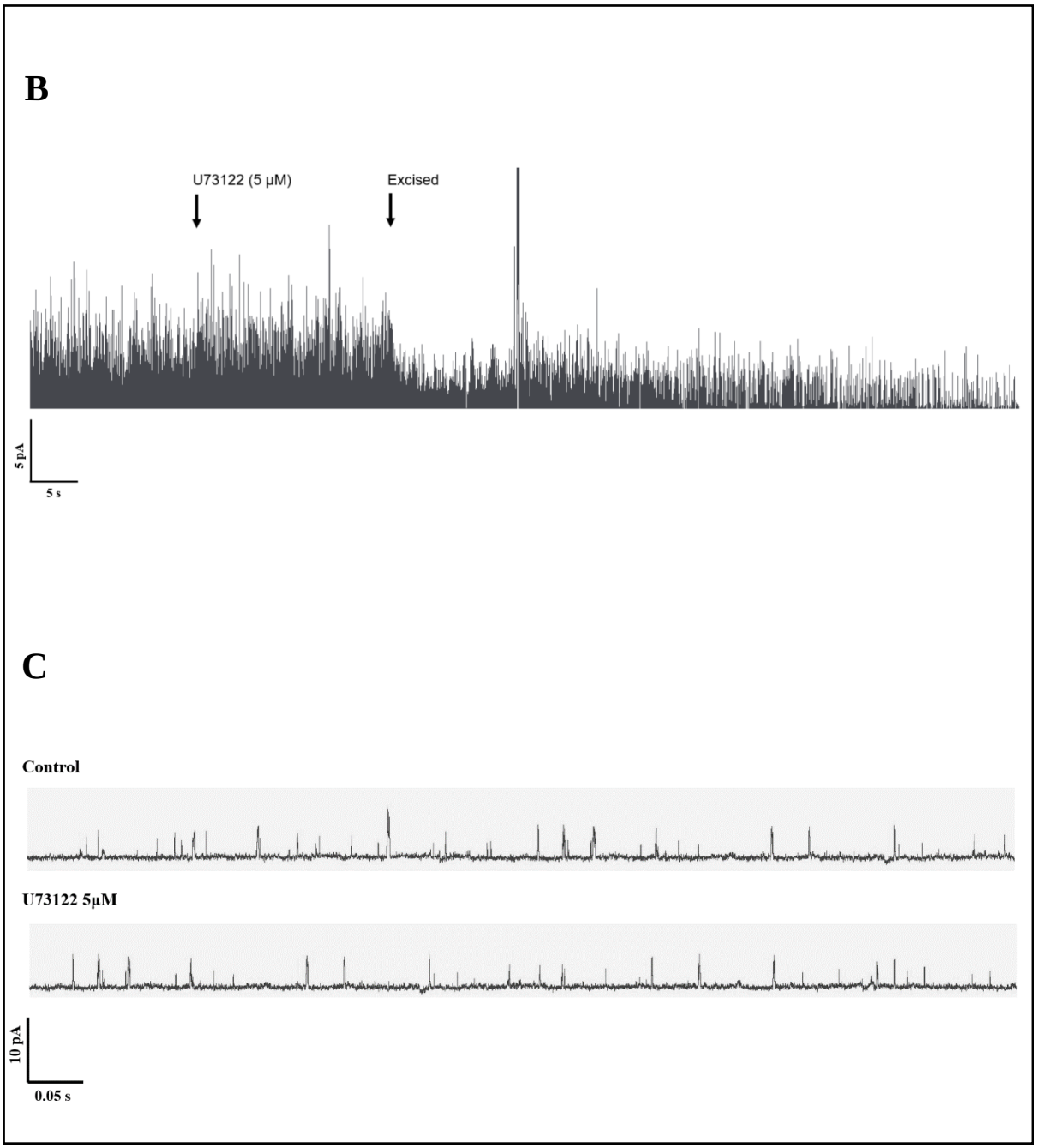
B
U73122 (5 μM)
Excised
5 pA
5 s
C
Control
U73122 5μM
10 pA
0.05 s

**D**

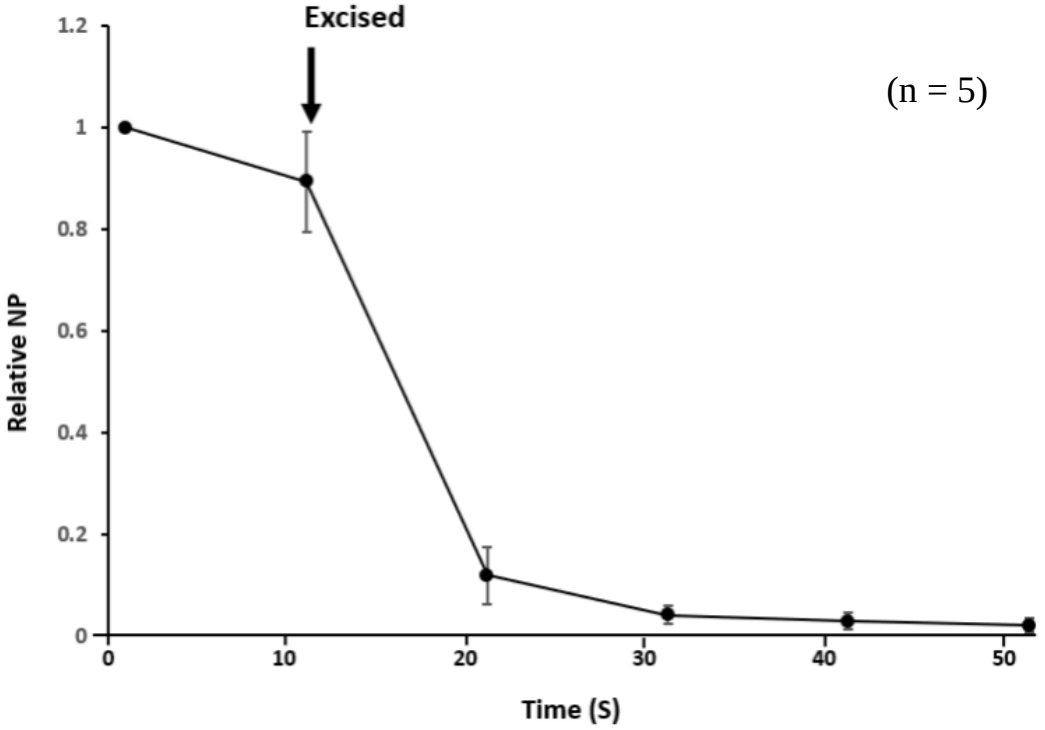
Excised
(n = 5)
Relative NP
Time (S)
1.2
1
0.8
0.6
0.4
0.2
0
0
10
20
30
40
50

**E**

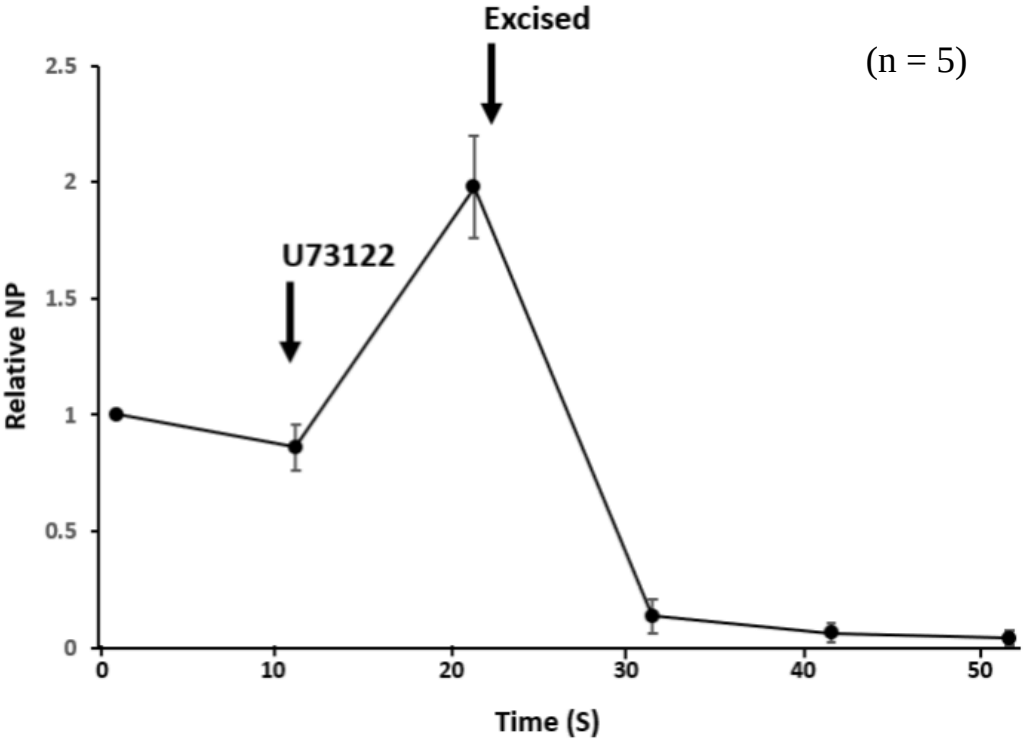
Excised
(n = 5)
U73122
Relative NP
Time (S)
2.5
2
1.5
1
0.5
0
0
10
20
30
40
50

### 4.3.7 The role of DAG in mediating MgATP reactivation of TASK channels in excised patches of type-1 cell

Earlier studies have reported that the application of millimolar levels of MgATP can reactivate TASK channels after patch excision (Williams and Buckler, 2004; Varas et al., 2007). Here, I wanted to determine whether this reactivation is mediated by DAGK activation, given that the activity of DAG kinase is ATP-dependent, which subsequently reduces DAG levels in the membrane. First, I applied 5 mM MgATP after patch excision. This induced a strong reactivation of TASK channels in inside-out patches by 297.7 ± 67.7 % (see Figures 4.12A, B, and C, blue bar; $n = 5$; $p < 0.01$). Relative nPopen before patch excision was 0.91 ± 0.09, which decreased to 0.27 ± 0.11 after patch excision in the presence of 5 mM MgATP. D5919 was then applied in the presence of 5 mM MgATP. This had no effect on the reactivation of TASK channels by MgATP: % increase in nPopen: MgATP vs. MgATP plus D5919: 297.7 ± 67.7 vs. 336.5 ± 53 (see Figures 4.12A, B, and C, green bar; $p = 0.19$; $n = 5$). These results suggest that DAG kinase is not involved in MgATP reactivation of TASK channels.

**Figure 4.12 Effects of D5919 (10 µM), a DAG kinase inhibitor, on MgATP reactivation of channel activity in excised patches** Representative single channel recording showing rundown of TASK channels activity upon patch excision of a cell-attached patch to form an inside-out patch in presence of MgATP (5 mM) and D5919 (10 µM) **(A)**. Single-channel recording from an inside-out patch in control, in presence of MgATP, and in the presence of MgATP plus D5919. Note that in these traces inward currents through channel openings are shown as upward deflections from baseline **(B)**. Percentage increase in nPopen in inside-out patch clamp recordings of type-1 cells. At least 20 seconds of data was used for each nPopen calculation, which was done 20 seconds after any solution change. Data are expressed as % increase in nPopen during the application of MgATP and MgATP plus D5919 relative to control nPopen post patch excision **(C)**. The traces were recorded with a pipette potential of +100 mV, 140 mM $K^+$ in pipette solution and 152 mM $K^+$ in Tyrode solution. Tyrode solution was switched to an intracellular solution ~10s prior to patch excision. N represents the number of recordings obtained from different type-1 cells. Statistical significance was evaluated utilizing a paired Student's t-test.

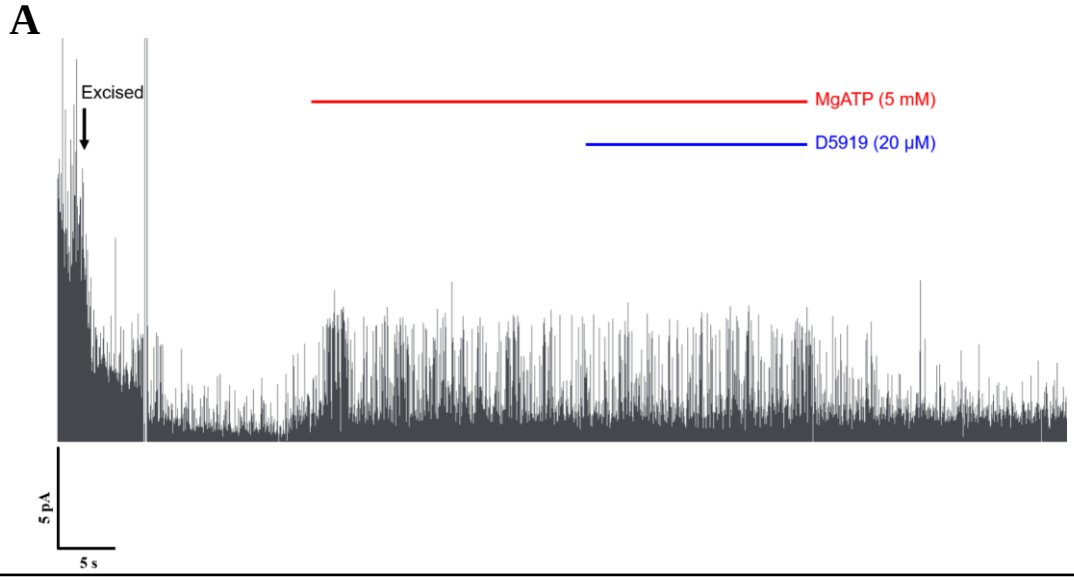

**B**

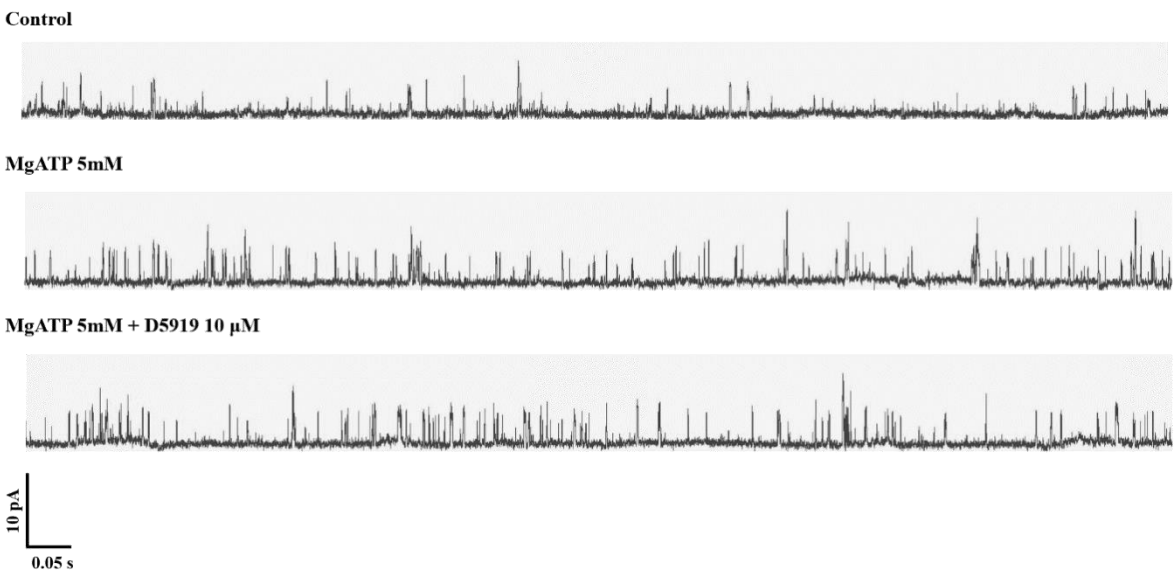
Control
MgATP 5mM
MgATP 5mM + D5919 10 µM
10 pA
0.05 s

**C**

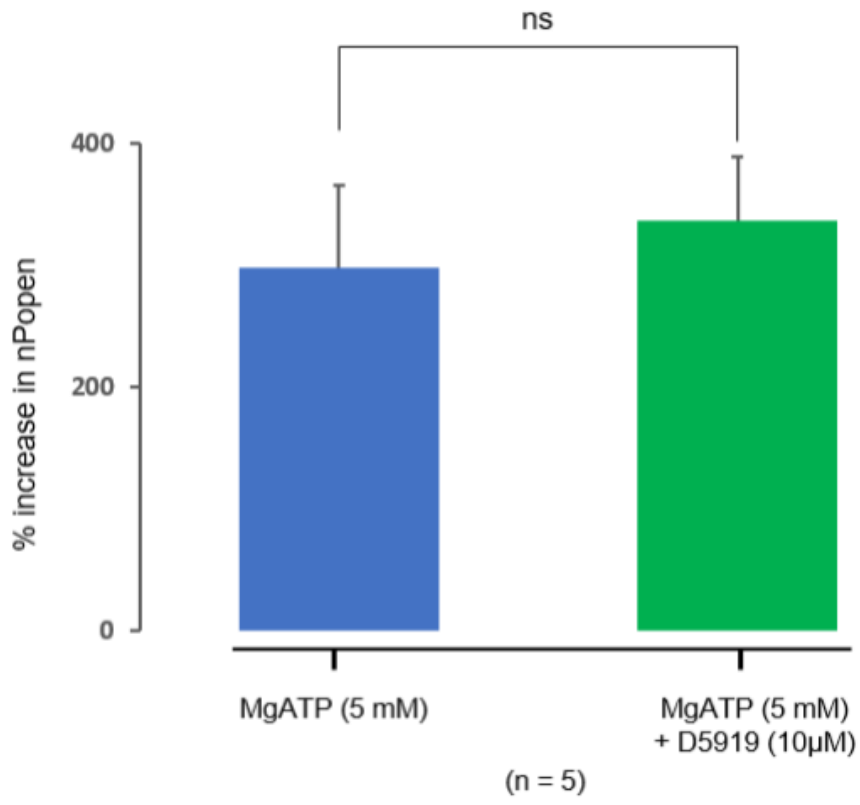
ns
400
200
0
% increase in nPopen
MgATP (5 mM)
MgATP (5 mM)
+ D5919 (10µM)
(n = 5)

## 4.4 Discussion

The main findings of this chapter are that PLC and DAG are involved in the regulation of TASK channels and the inhibition of these channels by hypoxia in type-1 cells. First, I will discuss the key results of this chapter, followed by a proposed mechanism for acute oxygen sensing in type-1 cells. Then, I will discuss the limitations and technical challenges of this chapter, followed by suggestions for future follow-up experiments.

The first finding is that the application of the Gq protein inhibitor FR900359 did not affect the baseline activity of TASK channels or the hypoxic inhibition of these channels in type-1 cells. Only a few Gq protein modulators have been described in the literature to date. FR900359 is a natural product that selectively inhibits Gq proteins. The most plausible mechanism by which FR900359 influences Gq-mediated signalling is by decreasing guanine nucleotide dissociation (GDI), most likely by stabilising the GDP-bound form of the α subunit (Tietze et al., 2019). In this study, I assessed the efficacy of FR900359 by examining its impact on methacholine chloride-induced inhibition of TASK channels. The observation that this was reduced by the application of FR900359 confirms the inhibitory actions of this drug on Gq- mediated signalling.

The role of Gq- coupled receptors in the regulation of TASK channels is poorly understood. The little we know comes from studies conducted in heterologous expression systems, where the channel activity may not represent what occurs in more sophisticated native cells. TASK channels expressed in HEK293 cells were directly inhibited by Gq activation in both cell-attached and inside-out configurations (Chen et al., 2006). More recent evidence has demonstrated that the open probability of TASK channels is linked to their Gaq

sensitivity (Sormann et al., 2022). The observation that Gq inhibition had no impact on the baseline activity or hypoxic inhibition of TASK channels in type-1 cells suggests that: a) there is little constitutive activation of Gq-coupled receptors in isolated type-1 cells; and b) the effects of hypoxia are not mediated through Gq coupled receptors.

The second finding is that altering PLC activity influenced the baseline activity of TASK channels as well as the inhibition of these channels by hypoxia and muscarinic agonist in type-1 cells. PLC inhibition by U73122 induced a strong activation of TASK channels and blocked both hypoxia- and methacholine chloride-mediated inhibition, whereas its control compound, U73343, had no significant effect on these responses. These findings align with those of earlier studies conducted in both type-1 cells and other cell types (Czirjak et al., 2001; Ortiz and Varas, 2010; Wike et al., 2014). Furthermore, they suggest that the activity of TASK channels in type-1 cells is controlled by constitutive PLC activity.

U73122 is a widely used PLC inhibitor that has been used to study the role of PLC activity in various cell types. The specificity of U73122 has, however, been called into question by some. Several side effects have been reported for not only U73122 but also its control compound, U73343. For example, Horowitz et al. (2005) reported that some effects of U73122 were due to the sequestration of PIP2 and alkylation. Boyd et al. (2000) reported that U73122 did not affect the muscarinic inhibition of TASK-like currents in cerebellar granule neurons (CGNs). Similarly, in HEK293 cells expressing TASK 3 channels, U73122 was found to have no effect on the inhibition of TASK 3 channels by Gaq (Chen et al., 2006). On the other hand, U73433, the inactive analogue of U73122, downregulated TASK channels expressed in COS-7 cells (Chemin et al., 2003). Furthermore, U73433 inhibited TASK

channels in rat cardiomyocytes (Schiekel et al., 2013). Previous research has confirmed that U73122 exhibits a potent inhibition of PLC activity. To minimise its potential side effects, it is recommended to use the lowest effective concentration and limit the application time (Horowitz et al., 2005).

I decided to further investigate the involvement of PLC in the regulation of TASK channels using the PLC activator m-3m3fbs. M-3m3fbs inhibited TASK channels strongly and reversibly, whereas its control compound, o-3m3fbs, had no effect on the activity of these channels. Furthermore, when hypoxia or methacholine chloride was combined with m-3m3fbs, there was no additional effect on TASK channels. These results agree with those of Wike et al. (2014), who first established that m-3m3fbs did, in fact, activate PLC and then demonstrated that this activation inhibited TASK3 channels expressed in CHO cells.

The regulation of TASK channels by PLC could be attributed to either depletion of PIP2, production of IP3 and DAG, or both mechanisms. However, using sophisticated genetic tools, Lindner et al. (2011) conducted experiments demonstrating that neither PIP2 depletion nor inhibition of PIP2 resynthesis following receptor-mediated depletion affected the activity of TASK channel. Furthermore, TASK channels in thalamic neurons have been shown to be insensitive to changes in PIP2 (Bista et al., 2015). Thus, it is more likely that PLC regulation of TASK channels is mediated by downstream signalling molecules (IP3 and DAG) than by PIP2 depletion.

The third finding of this chapter is that TASK channels in type-1 cells are modulated by perturbations in intracellular DAG levels. The application of either a DAG analogue, DiC8, or a DAG kinase inhibitor, D5919, resulted in robust and reversible inhibition of TASK channels. Interestingly, when hypoxia

or methacholine chloride were applied in the presence of either DiC8 or D5919, they did not produce any additional effect on TASK channels. The observation that a DAGK inhibitor was sufficient to elicit a strong inhibition of TASK channels implies that physiological plasma membrane concentrations of native DAG species are adequate to modulate TASK channels. Although D5919 is known to be a potent inhibitor od DAGK, it has been reported that this compound also functions as an antagonist of serotonin receptors (Boroda et al., 2017). This is a novel result and further confirms the findings of earlier studies that reported DAG regulation of TASK channels in other cell types and heterologous expression systems (Bista et al., 2015; Sormann et al., 2022; Wike et al., 2014). The regulation of TASK channels by DAG in type-1 cells poses two unresolved questions: First, the impact of hypoxia on intracellular DAG levels in type-1 cells remains uncertain. Hypoxia could potentially increase intracellular DAG levels by activating PLC or reduce DAG degradation by inhibiting DAGK activity. Significant activation of PLC in hypoxia seems unlikely, however, for the following reason: receptor mediated activation of PLC generates sufficient IP3 to bring about a rapid release of $Ca^{2+}$ from internal stores in type 1 cells, but this is never seen in hypoxia (the $Ca^{2+}$ response to hypoxia can be blocked simply by voltage clamping type-1 cells to their resting membrane potential) (Buckler and Vaughan-Jones, 1994a; Urena et al., 1994).

The most likely model therefore is that under normoxic conditions there is constitutive PLC activity generating a small stream of DAG, this DAG is then phosphorylated to phosphatidic acid, sufficient DAG remains however to maintain some small tonic inhibition of TASK channel. In hypoxia, DAGK becomes inhibited by falling ATP levels, and so DAG levels rise, TASK channel is more profoundly inhibited, the cell membrane depolarises, and $Ca^{2+}$ floods into the cell. In this model, there is a dependency on continued DAG

production by PLC under hypoxic conditions but no need for an actual increase in PLC activity.

Second, the precise mechanism by which DAG inhibits TASK channels is yet to be fully understood. It is unclear whether this inhibition involves the direct binding of DAG to TASK channels or if additional downstream signalling molecules, such as PKC, are required. Previous research has shown that DAG analogues directly inhibit TASK channels in inside-out patches where cytoplasmic proteins are not retained (Sormann et al., 2022; Wike et al., 2014). Therefore, direct binding is likely the mechanism by which DAG inhibits TASK channels. Then, the remaining question is: What are the potential DAG-binding sites in TASK channels?

It has previously been shown that a six-amino acid motif (VLRFMT in TASK 1 and VLRFLT in TASK 3) is essential for the regulation of TASK channels by GPCRs (Talley et al., 2002; Veale et al., 2007). Wike et al. (2014) reported that the same region is also critical for DAG-induced inhibition of TASK channels. The issue, therefore, becomes: Is this motif a necessary gating element or a DAG-binding site?

Given that DAG is a membrane-resident lipid, it would be necessary for putative DAG-binding sites in TASK channels to be closely associated with or even partially inserted into the membrane. The VLRFLT motif is located at the boundary between the plasma membrane and the cytosol, which satisfies the prerequisite for DAG binding (Wike et al., 2014). Interestingly, the VLRFLT motif is contained within the closed structure of the cytoplasmic X-gate, which has recently been described in TASK channels (Rödström et al., 2020). Thus, DAG inhibition of TASK channels may be mediated by DAG binding to the VLRFMT motif, which stabilises the closed state of the X-gate.

The fourth finding is that PKC inhibition had no effect on the activity of TASK channels in type-1 cells. This is consistent with the findings of Czirjak et al. (2000), who reported that altering PKC levels did not affect the baseline activity of the TASK1 channel or angiotensin II-induced inhibition of this channel in Xenopus oocytes co-expressing TASK-1 and angiotensin II receptor. These findings were further supported by Chemin et al. (2003), who demonstrated that neither PKC inhibition with staurosporine, a non-selective inhibitor of protein kinases, nor PKC activation by phorbol ester, a potent activator of PKC, affected the baseline activity of TASK channels or glutamate-mediated inhibition of these channels. Similarly, in rat cardiomyocytes, PKC inhibition did not affect the regulation of TASK channels by GPCRs (Schiekel et al., 2013). Moreover, removal of all potential PKC phosphorylation sites in the human TASK3 channel had no effect on GPCRs-induced inhibition of this channel (Veale et al., 2007). Other studies, however, have demonstrated that PKC regulates TASK channels, refer to Chapter 1, Section 1.5 (Besana et al., 2004; Ortiz and Varas, 2010). The conflicting results observed in previous studies could potentially be attributed to variations in experimental techniques and the use of different pharmacological agents in each investigation. For example, Ortiz and Varas (2010) subjected isolated carotid body type-1 cells to a 15-minute incubation with calphostin C, while in this study, calphostin C was applied for less than a minute without prior incubation. Alternatively, TASK channels may exhibit different levels of sensitivity to PKC in different cell types.

The fifth finding is that increasing IP3 levels by the application of an IP3 kinase inhibitor, LY290045, induced a small but significant inhibition of TASK channels and augmented muscarinic agonist-induced inhibition. However, LY290045 had no effect on the hypoxic inhibition of TASK channels. These

results contradict prior research, which suggested that alterations in IP3 levels did not affect TASK channels (Czirjak et al., 2001; Wike et al., 2014). It should be noted, however, that in those studies, IP3 was directly injected into Xenopus oocytes expressing either TASK1 or TASK3 channels. Therefore, whether the IP3 levels achieved in these studies correlate with the physiologically relevant IP3 levels in type-1 cells remains unclear.

In the final section of this chapter, I investigated the activity of TASK channels in the excised patches of type-1 cells. Surprisingly, I found that neither DAG nor PLC appeared to play a role in the rundown of these channels following patch excision or in their reactivation by MgATP. Prior research has shown that TASK channels in type-1 cells experience a decline in activity and lose their sensitivity to oxygen after patch excision in inside-out recordings. Post patch excision, these channels can be reactivated by the application of MgATP (Buckler et al., 2000; Buckler and Honore, 2004; Buckler, 2015; Varas et al., 2007). Furthermore, hypoxia has been shown to reduce intracellular levels of MgATP (Buckler et al., 2000; Varas et al., 2007). My results showed that both PLC and DAG can regulate TASK channels activity in type-1 cells. Given that DAG is a membrane-resident signalling molecule, it is reasonable to assume that DAG will remain attached to TASK channels in inside-out patches. Additionally, DAG degradation by DAGK is ATP-dependent (Han et al., 2008). DAG kinases utilise ATP as a phosphate donor to catalyse the phosphorylation of DAG to generate phosphatidic acid (Ma et al., 2019). Thus, I hypothesised that in inside-out patches, the rundown of TASK channels is due to DAG accumulation and that MgATP reactivation of these channels is mediated by activating DAGK, which reduces DAG levels, leading to the disinhibition of TASK channels. However, neither reducing DAG levels by inhibiting PLC activity prior to patch excision nor inhibiting DAGK activity post patch excision affected the rundown of TASK channels or their reactivation by

MgATP. These findings suggest that the rundown of TASK channels after patch excision is unlikely to be mediated by DAG accumulation and that the reactivation of these channels by MgATP does not involve DAGK activation.

There are two possible explanations for our results. First, applying a PLC inhibitor to reduce DAG production before patch excision only targets one pathway of DAG production, leaving other mechanisms, such as PAPs, still capable of generating DAG (Eichmann and Lass, 2015; Prentki and Madiraju, 2008). Consequently, DAG produced under PLC inhibition might have been sufficient to inhibit TASK channels post patch excision. Second, in the absence of any estimations of MgATP levels in type-1 cells, it remains uncertain whether the applied MgATP in this study (5 mM) corresponds with physiological MgATP levels in type-1 cells. As a result, the administered MgATP may have been substantially higher than normal MgATP levels, possibly leading to strong activation of DAGK despite the presence of the DAGK inhibitor. Despite these uncertainties, our finding that MgATP activated TASK channels in excised patches of type-1 cells highlights the sensitivity of these channels to MgATP. However, two key questions remain to be addressed: 1) Does the activation of TASK channels by MgATP result from direct interactions between MgATP and these channels, 2) Does this phenomenon play a role in the hypoxia signalling cascade within type-1 cells? Additional research focussing on measuring hypoxia-evoked $[Ca^{2+}]i$ entry and TASK channel inhibition in type-1 cells under clamped intracellular MgATP conditions could provide further insights into this issue (Holmes et al., 2022).

In summary, the results presented in this chapter indicate the involvement of PLC and DAG in regulating TASK channels and their inhibition under hypoxic conditions in cell-attached patches of type-1 cells. The observation that agents targeting PLC or DAG affect the $Ca^{2+}$ and TASK channels responses to severe

hypoxia (1.5-3 mmHg) suggests: 1) these signalling molecules are involved in mediating the carotid body type-1 cells response to severe hypoxia, 2) If the mechanisms involved in mediating the carotid body responses to severe hypoxia also contribute to the carotid body responses at moderate or mild hypoxia, this would suggest that the same signalling molecules are involved in mediating CB responses across all levels of hypoxia. However, what we already know about the chemotransduction process in the carotid body suggests the involvement of different pathways in mediating responses to varying levels of hypoxia, see Prabhakar (2006). For example, $H_2S$ has been shown to be involved in mediating the carotid body responses to hypoxia but not anoxia (Peng et al., 2020).

On the other hand, PLC produced DAG appears not to be involved in the rundown of TASK channels in type-1 cells after patch excision. The reasons behind the decline in TASK channel activity in excised patches and the exact mechanism by which MgATP reactivates these channels remain uncertain.

### 4.4.1 Proposed model of acute oxygen sensing in type-1 cells:

In Chapters 3 and 4, I studied the effects of Gq-coupled receptors and PLC signalling molecules on the hypoxia signalling cascade in type-1 cells. In Chapter 3, hypoxia-evoked $[Ca^{2+}]i$ rise was found to be sensitive to alterations in Gq-coupled receptors, PLC, DAG, and PKC levels. However, when I examined the hypoxic inhibition of TASK channels, I found that it was exclusively sensitive to PLC and DAG. The reason for this discrepancy is unclear; however, it is possible that the observed $Ca^{2+}$ effects of Gq and PKC

inhibition were mediated by mechanisms independent of TASK channels (e.g., $Ca^{2+}$ channels). For example, the PKC inhibitor calphostin C has been shown to inhibit cardiac L-type $Ca^{2+}$ channels (Hartzell and Rinderknecht, 1996). Taking together, these findings emphasise the importance of PLC and DAG in the hypoxia signalling cascade in type-1 cells. Nevertheless, there is still the matter of how DAG integrates into the acute oxygen sensing process in type-1 cells.

It is worth noting that lipogenesis is known to be regulated in a tissue-specific manner and could be disrupted in excised patches (Wunderling et al., 2023). This could explain the lack of oxygen sensitivity of TASK channels when expressed in heterologous expression systems and in excised patches of type-1 cells (Buckler and Honore, 2004; Buckler, 2015). Furthermore, the triglyceride regeneration pathway is highly dependent on ATP; thus, it can be disrupted by reductions in ATP levels under hypoxic conditions. This can result in the accumulation of intermediates such as DAG (Sharma and Wolfrum, 2023). Interestingly, hypoxia has been shown to increase intracellular DAG levels in different cell types (Temes et al., 2004).

Based on the results of Chapters 3 and 4, I propose the following model for acute oxygen sensing in type-1 cells: Under hypoxic conditions, a reduction in $PO_2$ triggers a series of molecular events in type-1 cells. PLC inhibition by U73122 blocked the hypoxia-evoked $[Ca^{2+}]i$ rise, induced a strong activation of TASK channels, and prevented any additional effect in response to hypoxia (Figures 3.4 and 4.4). These observations indicate the presence of constitutive PLC activity in type-1 cells. Considering that DAG metabolism by DAGK is ATP-dependent, a reduction in $PO_2$ levels would diminish DAG metabolism, resulting in DAG build-up. This inhibits TASK channels and depolarises type-1 cells. This is supported by the observation that inhibiting DAGK activity induced a robust inhibition of TASK channels and prevented any additional

effect in response to hypoxia (Figure 4.8). Conversely, under normoxic conditions, adequate ATP levels sustain DAGK activity. This prevents DAG accumulation, preserves the activity of TASK channels, and hyperpolarizes type-1 cells (Figure 4.13).

**Figure 4.13 Proposed model for acute oxygen sensing in the carotid body type-1 cell**

Under hypoxic conditions, the reduction in ATP levels inhibits DAGK activity which results in the accumulation of PLC-produced DAG. DAG, in turn, inhibits TASK channels leading to type-1 cell depolarization. In contrast, under normoxic conditions, PLC-produced DAG would be continuously metabolised by DAGK. This prevents the accumulation of DAG and maintains the activity of TASK channels. Panel A depicts the activity of TASK channels under normoxic conditions and summarizes the effects of inhibiting PLC with U73122 (indicated by red arrows) and inhibiting DAGK with D5919 (indicated by green arrows). Panel B illustrates the impact of hypoxia on DAG metabolism and the subsequent inhibition of TASK channels and depolarization of type-1 cell. The effects of hypoxia are indicated by red arrows.

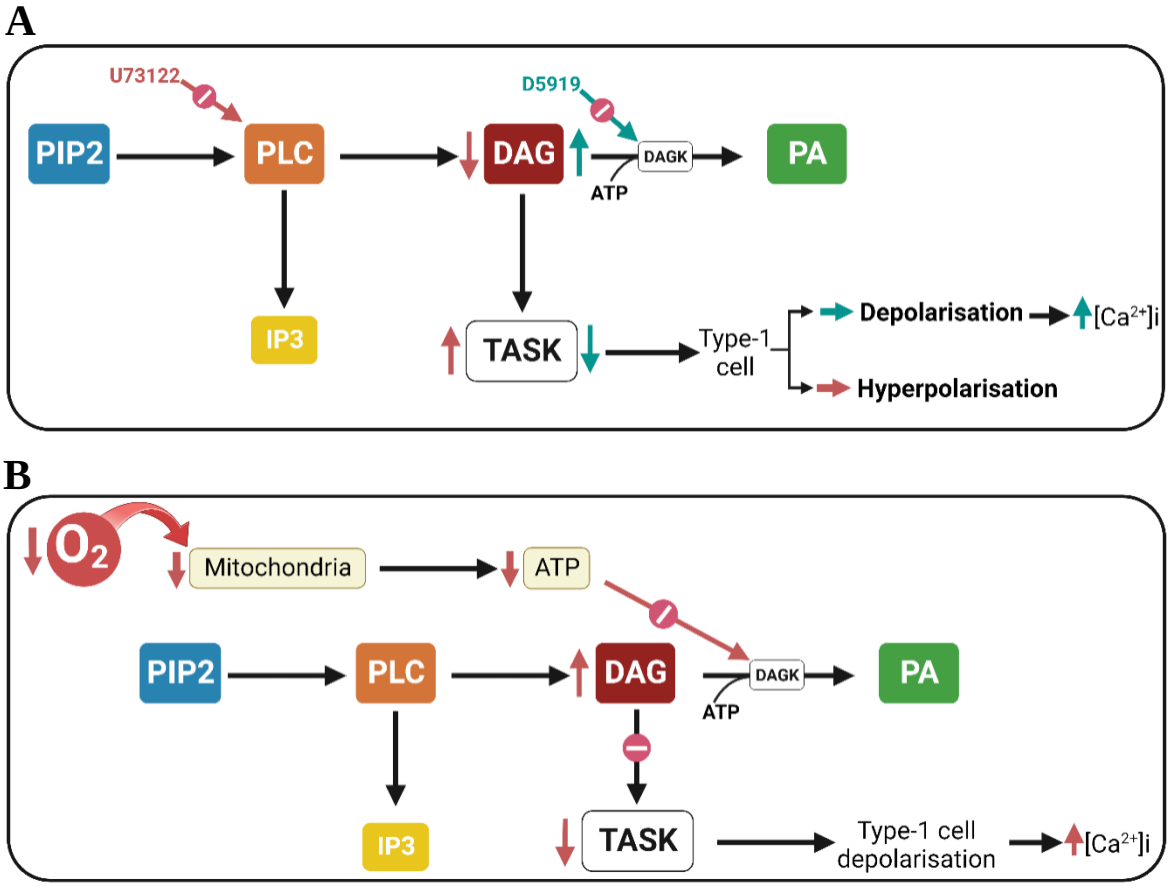

### 4.4.2 Limitations and technical challenges:

In this study, I investigated the role of Gq-coupled receptors and PLC signalling molecules in the regulation of TASK channels in type-1 cells. This was achieved by applying pharmacological agents targeting these signalling molecules and measuring the effects of these agents on the baseline activity of TASK channels as well as hypoxia- and muscarinic agonist-induced inhibition of these channels. The technical limitations of this chapter are similar to those previously outlined in Chapter 3, Section 5.

### 4.4.3 Suggestions for future research:

Several questions remain unanswered: Does $PO_2$ affect the production of DAG in type-1 cells? How do signalling molecules associated with PLC alter the gating of TASK channels? How do mitochondria, the plasma membrane, and PLC signalling molecules interact within type-1 cells to sustain the baseline activity of TASK channels?

The ability to detect and respond to changes in oxygen is crucial for the survival of both prokaryotic and eukaryotic species. Therefore, multiple pathways are likely to be involved in acute oxygen sensing (Prabhakar, 2006). I believe that it is crucial to develop experimental tools to dissect oxygen sensing pathways, analyse the regulation of each signalling pathway, and study their interactions. This will help us understand how these pathways function and identify potential upregulation or downregulation under different conditions. Future experiments may involve a genetic mouse model with a TH-conditional DAGK knock out. Another area of research may involve constructing a dose-response curve that delineates the effects of different concentrations of DAGK

inhibitors on the responses of carotid body type-1 cells to diverse hypoxic levels.

# Chapter. 5 The role of PLC signalling in mediating the effects of metabolic inhibitors on TASK channels in the carotid body type-1 cell

## 5.1 Introduction

Despite numerous proposed theories, the precise mechanism by which type-1 cells transduce a decrease in oxygen levels into the release of neurotransmitters remains elusive. Among the various explanations put forward, two main theories initially gained prominence: the membrane theory and the metabolic theory. The first to gain prominence was the metabolic theory, which proposed that the oxygen sensor was the mitochondrion. This hypothesis was supported by many studies demonstrating that all (membrane-permeant) inhibitors of oxidative phosphorylation are potent stimulants of the carotid body (Anichkov and Belen'kii, 1963; Duchen and Biscoe, 1992a, b; Heymans et al., 1931; Krylov and Anichkov, 1968; Mills and Jobsis, 1971).

This theory was followed in the 1990s by the membrane theory, which proposed that chemotransduction in type-1 cells takes place through electrophysiological events occurring in their plasma membrane, with all essential elements for oxygen sensing thought to be localised within the plasma membrane. Through their collective functioning, they trigger the depolarization of type-1 cells in response to changes in oxygen levels (Rakoczy and Wyatt, 2018).

This strictly membrane theory was soon challenged by studies conducted in excised patches of type-1 cells. Such studies have revealed that TASK channels rapidly rundown and lose their sensitivity to oxygen after patch excision. This observation suggests that TASK channels are not inherently oxygen sensitive and that cellular constituents are crucial for their functionality (Buckler, 2015; Buckler and Honore, 2004; Williams and Buckler, 2004). Consequently, an oxygen sensor/pathway is necessary to confer oxygen sensitivity to TASK channels in type-1 cells.

With the observations that, firstly, a wide range of metabolic inhibitors inhibit TASK channels in type-1 cells (Turner and Buckler, 2013b; Williams and Buckler, 2004; Wyatt and Buckler, 2004); and secondly, that the effects of metabolic inhibitors and hypoxia on TASK channel activity are mutually exclusive, our current model of oxygen sensing blends both metabolic and membrane theories. In this model, mitochondrial metabolism acts as the oxygen sensor signalling to TASK channels, which is the common point where hypoxia and metabolic inhibitors converge (Buckler, 2012, 2015; Wyatt and Buckler, 2004). There is, however, a missing link: how do mitochondria signal to TASK channels? Considering that all types of metabolic inhibitors inhibit TASK channels and/or stimulate the carotid body, the only obvious common denominator is ATP.

Whilst TASK channels in the excised patch are ATP sensitive, there is no known nucleotide binding site in the primary sequence of TASK channels, and there are no reports of cloned TASK1 or TASK3 channels being MgATP-sensitive (Buckler, 2015). This suggests that ATP must work through some membrane delimited, ATP sensitive signalling pathway.

As extensively discussed in Chapters 3 and 4, the regulation of TASK channels in type-1 cells involves signalling molecules associated with PLC activity. The research presented in these chapters has provided substantial data supporting the involvement of DAG in the hypoxia signalling cascade within type-1 cells. Previous studies have shown that DAG directly inhibits TASK channels, and the metabolism of DAG is known to be ATP-dependent (Sormann et al., 2022; Han et al., 2008; Wike et al., 2014). Specifically, diacyl glycerol kinases (DAGKs) use ATP to phosphorylate DAG to produce phosphatidic acid, thus terminating the function of DAG as a second messenger (Ma et al., 2019). I have shown (in Chapter 4) that type-1 cells appear to generate DAG constitutively via PLC. Therefore, I proposed that when metabolic function is

inhibited, there is a decrease in ATP levels, causing a decrease in DAGK activity, which leads to the accumulation of PLC-generated DAG. This accumulation of DAG could subsequently inhibit TASK channels. Therefore, DAG could play a critical role as a signalling molecule, bridging the gap between cellular metabolism and the regulation of TASK channel activity in type-1 cells.

To test this hypothesis, experiments were designed in which a PLC inhibitor was administered prior to the application of metabolic inhibitors such as FCCP or cyanide. The purpose of this approach was to reduce constitutive DAG production. Thus, I sought to examine whether the inhibitory effects of these metabolic poisons on TASK channels were, at least partly, attributed to the accumulation of PLC-generated DAG.

Note that I have chosen to use two inhibitors of ATP production (cyanide and FCCP), which have diametrically opposed effects upon the electron transport chain. The significance of this will be discussed in the final chapter.

## 5.2 Methods

### Cell isolation:

For the extended procedure, refer to Chapter 2, Section 2.1.1. Briefly, the carotid body bifurcations were dissected from rat pups (P11-P14). They were then digested enzymatically and mechanically, which led to a single cell suspension. Primary cell cultures were plated onto coverslips pre-treated with poly-D-lysine and incubated for 2 hours. Recordings took place within 5-6 hours of plating.

### Electrophysiology:

Cell-attached recordings were performed using an Axopatch 200B (Molecular Devices LLC, Sunnyvale, US). Sylgard-coated and fire-polished borosilicate pipettes (Harvard Apparatus Ltd., Kent, UK) were used. For the extended procedures, refer to Chapter 2. In summary, coverslips containing isolated type-1 cells were placed in the recording chamber and continuously superfused with a warmed Tyrode solution. Tyrode solutions were continuously bubbled with normoxic (5% $CO_2$, balance air) or hypoxic gas mixtures (5% $CO_2$, in balance $N_2$). For solutions containing NaCN, it should be noted that the solutions were bubbled for approximately 15 minutes prior to the addition of NaCN. NaCN was freshly added just before use, and the solutions were maintained under an atmosphere of 5% $CO_2$ and 95% air. Cyanide is highly volatile, and its concentration in solutions can rapidly decrease from 2 mM to 300 µM within one hour (Wyatt and Buckler, 2004). To overcome this problem, cyanide-containing solutions were replaced every 30-60 minutes. This approach ensured

that the cyanide concentration remained within the desired range throughout the experiment.

Seal formation was attempted with a borosilicate pipette containing a high $K^+$ solution (140 mM), 10 mM TEA, and 5 mM 4-AP (to block other $K^+$ channels). Upon the formation of a good seal (> 5 GΩ), the Tyrode solution was switched to a high $K^+$ solution, and a positive pipette potential of +100 mV was applied. Voltage clamp protocol, data acquisition, and data analysis were performed using Spike 10 software (Cambridge Electronics Design, Cambridge, UK). The background $K^+$ channel of type-1 cells exhibited inward currents with brief flickering openings under the recording conditions of this study.

**Experimental protocol for the measurements of TASK channels activity in type-1 cells:**

Channel activity analysis involved 20-second segments of recordings taken at least 10 seconds after any solution exchange. The quantification of single channel activity is defined by nPopen, which is the product of the number of channels in the patch and the probability of a channel being open at any given time. To determine nPopen, an all-point histogram was constructed using a 20-second segment of data, to identify the primary conductance state. A 50% opening threshold was then set for the nPopen analysis. Changes in channel activity were reported as an increase or decrease in nPopen values relative to the control.

**Drugs:**

Following cell identification, type-1 cells were subjected to superfusion with the Tyrode solution, both in the presence and absence of the drug under

investigation, using the cells as their own controls. NaCN and FCCP were applied to the cells over a duration of 20-30 seconds, whereas U73122 was applied for 40-50 seconds, and a similar wash period followed the exposure to allow any reversible effects to subside. All drugs were appropriately reconstituted prior to dissolution in Tyrode solution. Collagenase was obtained from Worthington. Trypsin, culture media, U73122, FCCP, and NaCN were obtained from Sigma/Aldrich. The concentrations of the administered drugs were determined either based on the EC50 values specific to each drug, prior usage in similar studies, or a combination of both approaches.

**Statistical analysis of TASK channel recordings:**

N numbers represent individual recordings obtained from distinct cells on different coverslips. The percentage change in nPopen was determined using the following formula:
Percentage change = ((nPopen under Condition A - nPopen under Control) / nPopen under Control) * 100
Mean normalised nPopen values were utilised to determine statistical significance using Student's t-test. A p-value of less than 0.05 was taken as statistically significant.

## 5.3 Results

### 5.3.1 The role of DAG in mediating cyanide-induced inhibition of TASK channel in type-1 cell

In this chapter, I investigated the effects of a classical cytochrome oxidase inhibitor (cyanide) and an uncoupler of the mitochondria (FCCP) on TASK channel activity in acutely isolated type-1 cells. The principal objective was to determine whether inhibiting constitutive PLC activity blocks or attenuates the inhibitory effects of these metabolic inhibitors on TASK channel.

In all cells, upon formation of a GΩ seal and switching to a high $K^+$ Tyrode, a brief (<20sec) hypoxic stimulus was applied first to confirm the health, identity, and oxygen sensitivity of the cell. Only cells that responded to this with inhibition of channel activity were further investigated. The TASK channel activity observed under the recording conditions indicated in the methods section (pipette +100 mV, 140 mM $K^+$, and 100 mM $K^+$ in Tyrode) resulted in brief flickery openings, which were observed as inward currents. Under these conditions, most all-points histograms typically displayed a single but broad peak, indicating one main open state, which previous research has suggested represents the heterodimeric TASK-1/3 channel predominant in rat type-1 cells (Kim et al., 2009a; Turner and Buckler, 2013b).

Application of 200 μM NaCN resulted in a substantial and reversible inhibition of channel activity, as defined by nPopen, with a decrease of 49.6 ± 2.5% that recovered rapidly after switching to normal Tyrode solution (see Figures 5.1A, B, and D, red bar, n = 8; $p<0.001$). Subsequently, the PLC inhibitor U73122 (5 μM) was applied, resulting in a significant activation of channel activity by 113.2 ± 7.9% (see Figures 5.2A, B, and D; blue bar, n = 8; $p<0.001$). Subsequently, NaCN was applied in the presence of U73122,

resulting in a pronounced and reversible inhibition of channel activity by 44.6 ± 4.1% (n=8; $p<0.001$). Notably, and contrary to expectations, U73122 had no significant effect on NaCN-induced inhibition (n=8; p=0.31, see Figures 5.1A, B, and D, compare red bar to green bar). Analysis of all-point histogram revealed that NaCN caused a decrease in the frequency of all open channel current amplitudes, which remained unaffected by the application of U73122 (see Figure 5.1C). These results demonstrate that the inhibitory effects of cyanide on TASK channels appear to be independent of PLC signalling and its downstream effects on DAG levels. However, data from this experiment also show that the U73122-induced excitation of TASK channels observed under normal conditions was absent in the presence of cyanide (see Figure 5.1, compare blue bar to green bar, n = 8, p =0.001 compared to control).

**Figure 5.1 U73122 had no effect on NaCN induced inhibition of TASK channels in rat carotid body type-1 cell** Representative single-channel recording showing the effect of NaCN (200 µM), U73122 (5 µM), and the co-application of NaCN plus U73122 over approximately 3.5 minutes **(A)** and 1.6 minutes **(B)**. A superimposition of all-points histograms obtained from 20-second segments of recordings during the application of various solutions: control, NaCN, U73122, and NaCN plus U73122. The bin width for the histogram was set at 0.1 pA **(C)**. The percentage change in nPopen is compared under different conditions: NaCN, U73122, and NaCN plus U73122, relative to the control. The data are presented as means ± S.E.M **(D)**. The traces were recorded with a pipette potential of +100 mV, 140 mM $K^+$ in pipette solution and 100 mM $K^+$ in Tyrode solution.

The horizontal bar in A represents a timescale of 30 seconds, and the vertical bar indicates a 5 pA current; whereas in B, the horizontal bar represents a timescale of 0.05 seconds, and the vertical bar indicates a 10 pA current. Statistical significance was evaluated utilizing a paired Student's t-test.

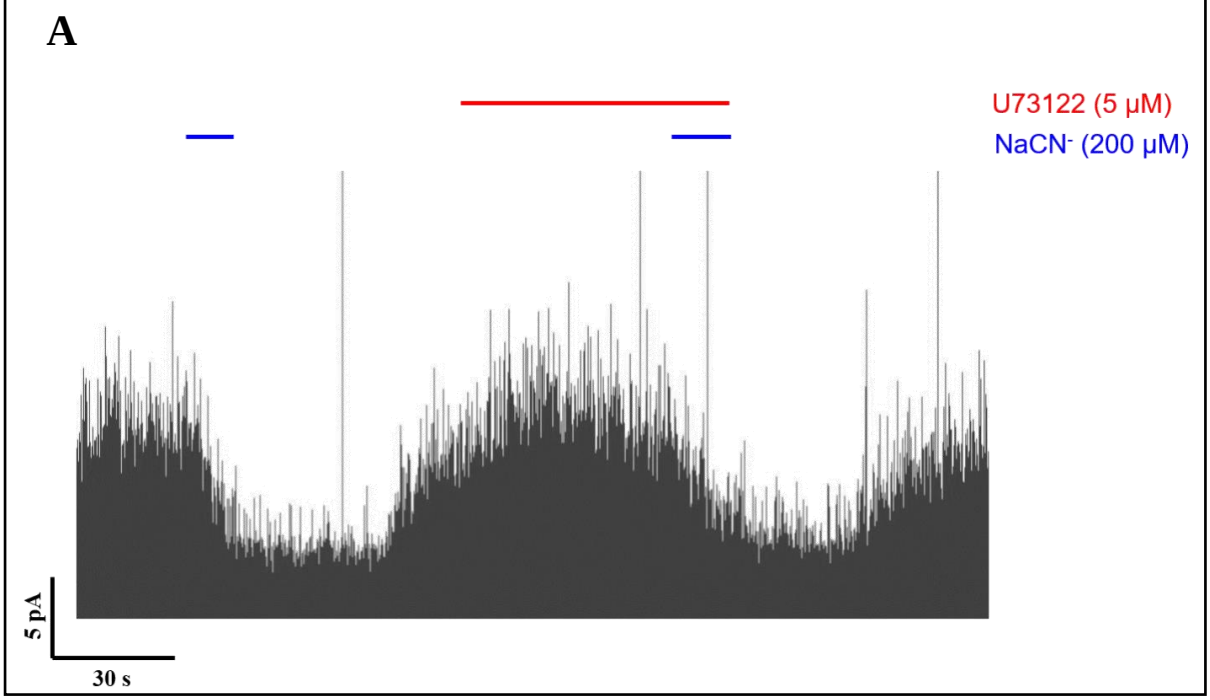

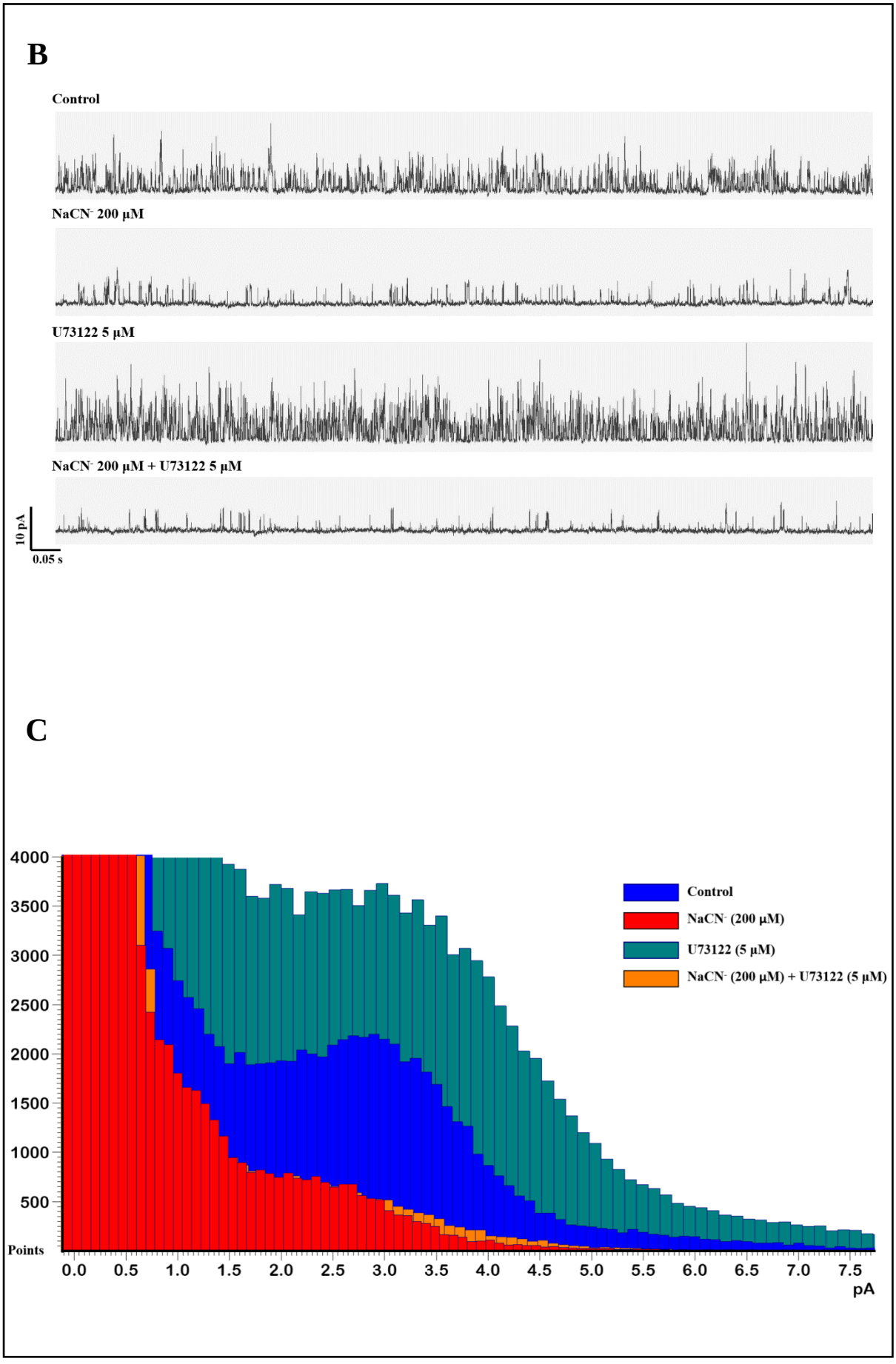
B
Control
NaCN- 200 µM
U73122 5 µM
NaCN- 200 µM + U73122 5 µM
10 pA
0.05 s
C
4000
3500
3000
2500
2000
1500
1000
500
Points
0.0
0.5
1.0
1.5
2.0
2.5
3.0
3.5
4.0
4.5
5.0
5.5
6.0
6.5
7.0
7.5
pA
Control
NaCN- (200 µM)
U73122 (5 µM)
NaCN- (200 µM) + U73122 (5 µM)

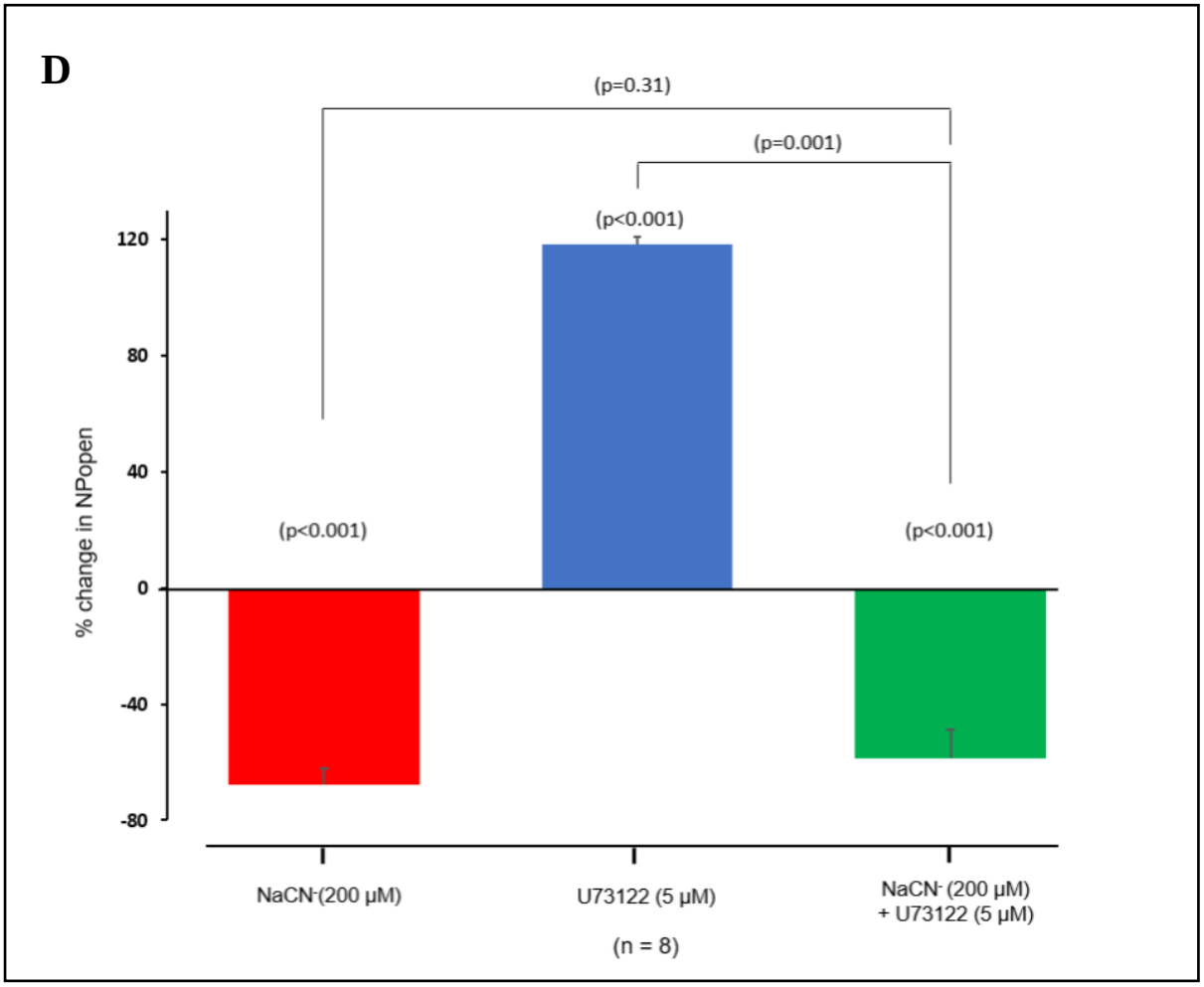
D
(p=0.31)
(p=0.001)
(p<0.001)
120
80
40
0
-40
-80
% change in NPopen
(p<0.001)
(p<0.001)
NaCN- (200 µM)
U73122 (5 µM)
NaCN- (200 µM)
+ U73122 (5 µM)
(n = 8)

### 5.3.2 The role of DAG in mediating FCCP-induced inhibition of TASK channel in type 1 cell

To further investigate the impact of mitochondrial inhibitors in conditions where DAG production is reduced by a PLC inhibitor, FCCP and U73122 were applied to acutely isolated type-1 cells. FCCP is an effective uncoupler of mitochondrial oxidative phosphorylation. It disrupts the proton gradient across the inner membrane of mitochondria and interferes with ATP production. The application of 1 μM FCCP induced a substantial and reversible inhibition of channel activity, as defined by nPopen by 67 ± 7.5% (see Figures 5.2A and D, red bar, n = 8, $p<0.001$). Figures 5.2A and B provide an illustrative example of a multichannel patch, showing that FCCP reduced both multiple and single channel opening events, evident from the decrease in frequency across all levels of channel current in the all-points histogram (Figure 5.2C). Upon removing FCCP, the background $K^+$ channel activity rapidly returned to normal levels. Next, I applied the PLC inhibitor U73122 (5 μM), which induced a significant activation of channel activity by 103.2 ± 11.8% (see Figures 5.2A and B, blue bar, n=8, $p<0.001$). Subsequently, FCCP was applied in the presence of U73122, leading to an inhibition of channel activity by 58.9 ± 6.5% (see Figures 5.2 A, B, and D, green bar). Notably, U73122 had no effect on the FCCP induced inhibition of channel activity (n=8, p=0.11). As with cyanide, however, the response to U73122 (blue bar) was ablated in the presence of FCCP (green bar), see Figure 5.2 (n=8, p=0.001 compared to control).

**Figure 5.2 U73122 had no effect on FCCP-induced inhibition of TASK channels in rat carotid body type-1 cell** Representative single channel recording showing the effect of FCCP (1 µM), U73122 (5 µM) and the co-application of FCCP and U73122 over approximately 3.5 minutes **(A)** and 1.6 minutes **(B)**. A superimposition of all-points histograms obtained from 20-second segments of recordings during the application of various solutions: control, FCCP, U73122, and FCCP plus U73122. The bin-width for the histogram was set at 0.1 pA **(C)**. The percentage change in nPopen is compared under different conditions: FCCP, U73122, and FCCP plus U73122, relative to the control. The data are presented as means ± S.E.M **(D)**. The traces were recorded with a pipette potential of +100 mV, 140 mM $K^+$ in pipette solution and 100 mM $K^+$ in Tyrode solution.

The horizontal bar in A represents a timescale of 30 seconds, and the vertical bar indicates a 5 pA current; whereas in B, the horizontal bar represents a timescale of 0.05 seconds, and the vertical bar indicates a 10 pA current. Statistical significance was evaluated utilizing a paired Student's t-test.

**A**

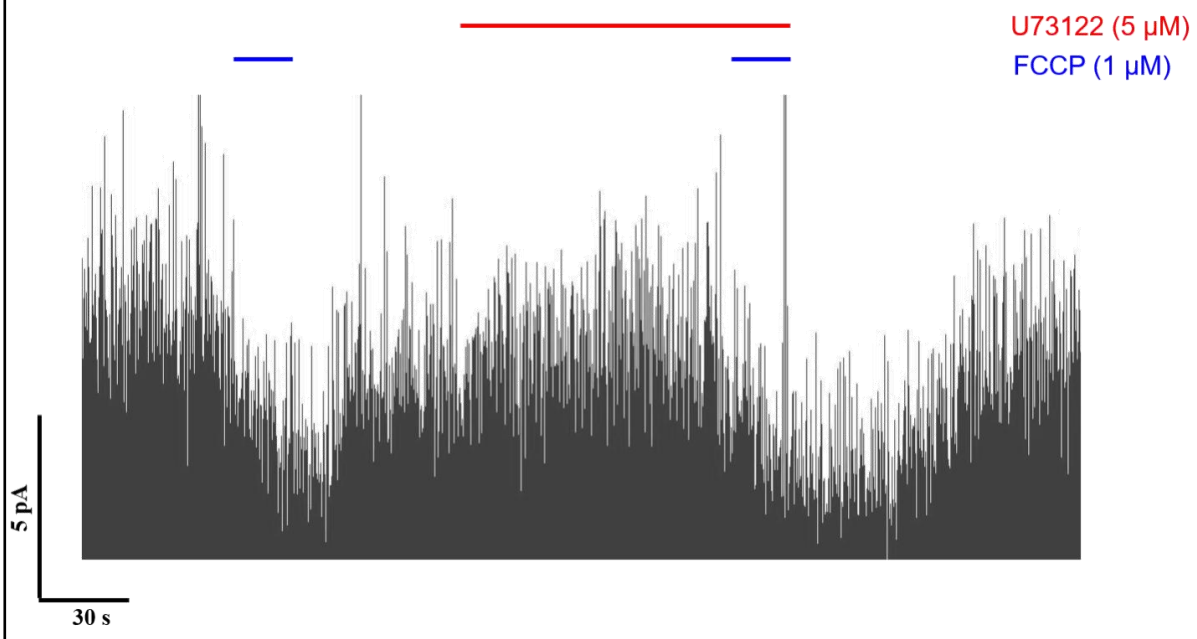

**B**

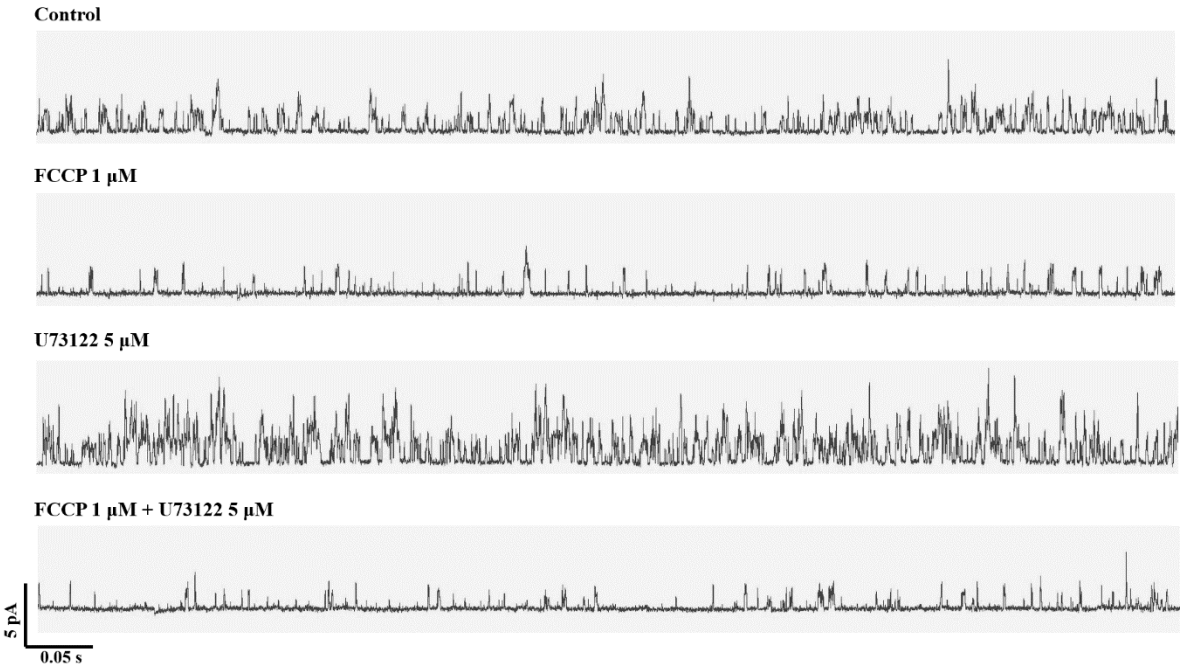
Control
FCCP 1 µM
U73122 5 µM
FCCP 1 µM + U73122 5 µM
5 pA
0.05 s

**C**

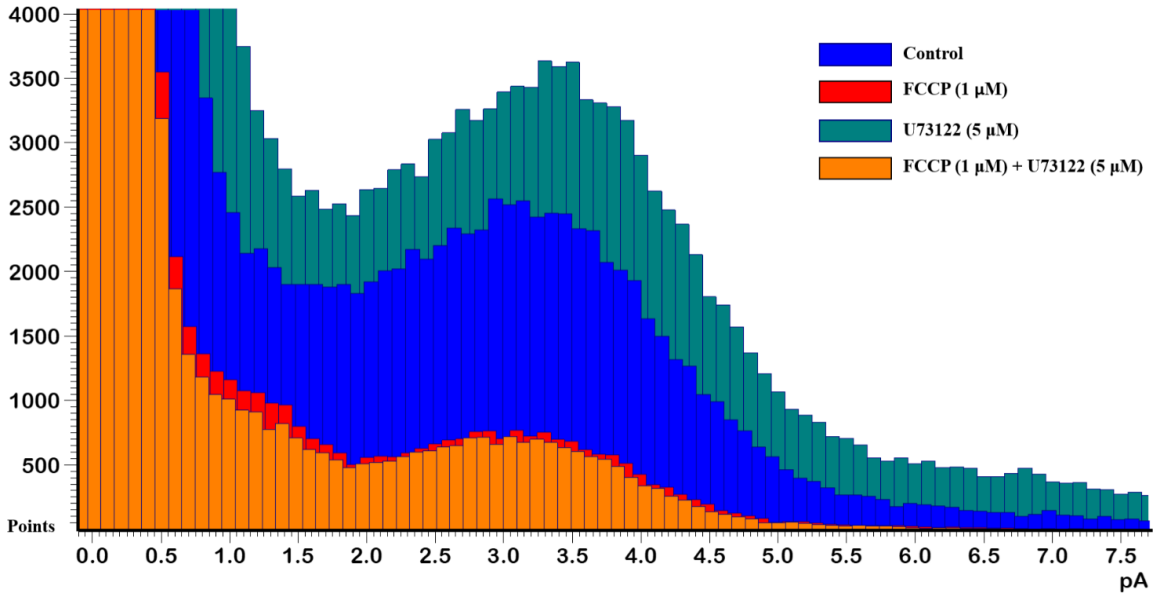
4000
3500
3000
2500
2000
1500
1000
500
Points
0.0
0.5
1.0
1.5
2.0
2.5
3.0
3.5
4.0
4.5
5.0
5.5
6.0
6.5
7.0
7.5
pA
Control
FCCP (1 µM)
U73122 (5 µM)
FCCP (1 µM) + U73122 (5 µM)

**D**

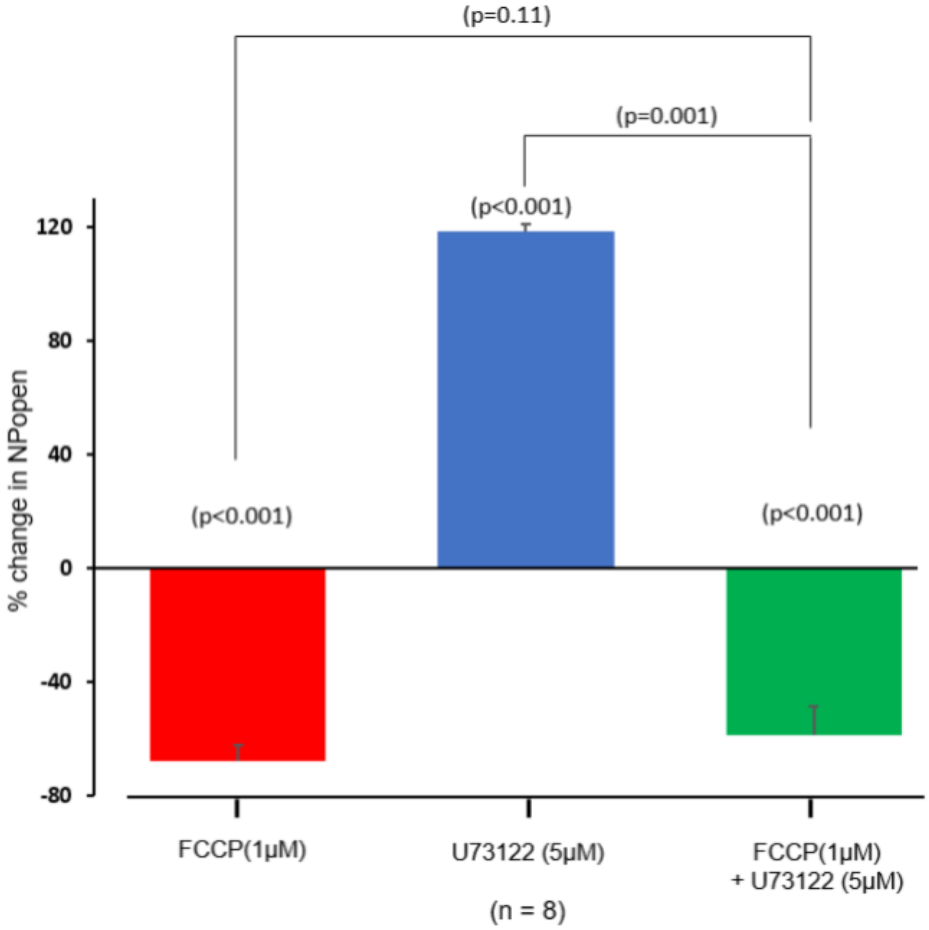
(p=0.11)
(p=0.001)
(p<0.001)
120
80
40
0
-40
-80
% change in NPopen
(p<0.001)
(p<0.001)
FCCP(1μM)
U73122 (5μM)
FCCP(1μM)
+ U73122 (5μM)
(n = 8)

## 5.4 Discussion

The data presented in this chapter further confirm the effects of mitochondrial inhibitors on TASK channel activity in carotid body type-1 cells and suggest that these effects are independent of PLC activity.

The findings described in Chapters 3 and 4 indicate the considerable influence of changes in both PLC and DAG levels on the hypoxia signalling cascade in type-1 cells. Previous research has demonstrated that DAG directly inhibits TASK channels in excised patches (Sormann et al., 2022; Wike et al., 2014). Because DAGK activity is ATP-dependent, I hypothesised that DAG accumulation may mediate the inhibitory effects of metabolic inhibitors on TASK channels (Ma et al., 2019). Inhibiting the metabolic activity of type-1 cells would reduce DAGK activity, causing a buildup of DAG inside the cells and, as a result, inhibiting TASK channels.

However, the findings presented in this chapter suggest that the actions of metabolic inhibitors on TASK channels remain largely unaffected by reductions in PLC activity. This was demonstrated by evaluating the impact of two mitochondrial inhibitors, FCCP and cyanide, on TASK channels under two different experimental conditions: normal conditions and conditions in which PLC activity was inhibited by the application of U73122. Under control conditions, inhibition of PLC activity, which subsequently reduced DAG levels, resulted in significant activation of TASK channels, confirming that TASK channels are sensitive to intracellular DAG levels. However, despite this sensitivity to DAG, it was observed that the inhibition of TASK channels by metabolic inhibitors remained unaffected by PLC inhibition. These findings suggest that the inhibition of TASK channels in response to metabolic inhibitors is mediated primarily by a non-PLC dependent pathway and that this pathway

dominates over any PLC dependent pathway (note, in the presence of metabolic inhibitors, U73122 has no effect on nPopen).

Although PLC serves as a crucial enzyme in DAG production, it is essential to acknowledge the existence of alternative pathways for DAG synthesis that operate independently of PLC activity. For instance, phospholipase D (PLD) can hydrolyse phosphatidylcholine to generate DAG. Additionally, phosphatidate phosphatase can convert phosphatidic acid into DAG (Eichmann and Lass, 2015). These, in addition to other pathways, provide flexibility and redundancy in DAG signalling allowing the maintenance of sufficient levels of DAG even when one pathway is compromised. The simplest interpretation of our findings is that, despite inhibiting PLC, accumulation of DAG produced through these alternative mechanisms may be adequate to mediate the inhibitory effects of cyanide and FCCP on TASK channels. The mechanisms of DAG synthesis and metabolism will be considered further in the final chapter of this thesis.

Another possible interpretation is that the inhibitory impact of cyanide and FCCP on TASK channels may not be attributable to DAG signalling but rather to an alternative pathway. Considering that cyanide and FCCP are potent metabolic poisons, it is likely that they have broader effects on cellular processes beyond the inhibition of DAG metabolism. The potential presence of other pathways and any interaction with DAG signalling will also be considered in the final chapter.

In conclusion, the data presented in this chapter indicate that PLC-produced DAG is not involved in the inhibition of TASK channels by metabolic inhibitors in type-1 cells.

### 5.4.1 Limitations and technical challenges:

In addition to the technical limitations discussed in Chapters 3 and 4, maintaining stable cyanide concentrations in gas-bubbled solutions was a challenge in this study. Refer to Methods, Section 5.2.

# Chapter. 6 Interactions between DAG and halothane with TASK channels in the carotid body type-1 cell

## 6.1 Introduction

Anaesthesia-induced respiratory depression is a well-known side effect of volatile anaesthetics, such as halothane. These agents suppress the ventilatory response to hypoxia and hypercapnia, resulting in a reduction in respiratory activity (Hirshman et al., 1977; Knill & Gelb, 1978; Idle et al., 1999). The mechanisms underlying the suppression of the ventilatory response involve the interaction of volatile anaesthetics with various targets in the central nervous system (CNS) and peripheral chemoreceptors. The sensitivity of the carotid body to hypoxia and hypercapnia is attenuated by volatile anaesthetics (Davies et al., 1982). Given that normal carotid body hypoxic and hypercapnic responses involve the modulation of TASK channels, research was undertaken by this laboratory to explore the actions of volatile anaesthetics on TASK channels in type-1 cells. Initially, halothane was identified as a powerful stimulant of background TASK-like $K^+$ currents in the carotid body and other tissues (Berg et al., 2004; Buckler et al., 2000; Putzke et al., 2007; Pandit et al., 2010). Subsequent investigations have revealed that both halothane and isoflurane can activate TASK channels and suppress hypoxia-evoked $[Ca^{2+}]i$ entry in carotid body type-1 cells (Pandit and Buckler, 2010).

As discussed in previous chapters, in addition to hypoxia and volatile anaesthetics, PLC signalling molecules have been shown to regulate TASK. Furthermore, I demonstrated in previous chapters that PLC signalling molecules, particularly DAG, play a role in regulating the baseline activity of TASK channels in type-1 cells and their sensitivity to hypoxia.

Previous research has emphasised the significant role of the VLRFMT region in TASK channels, demonstrating its involvement in various regulatory processes. This region has been identified as crucial for TASK channel

activation by anaesthetics and inhibition by receptor-mediated signalling (Patel et al., 1999; Tally & Bayliss, 2002; Veale et al., 2007). The fact that the same region is involved in both pathways suggests a shared molecular mechanism driving these regulatory effects. Additionally, it has been shown that the same region is also essential for DAG inhibition of TASK channels (Sörmann et al., 2022; Wike et al., 2014). Interestingly, the VLRMT region is contained in the closed structure of the recently identified "X-gate" in TASK channels (Rodstrom et al., 2019). Collectively, these findings emphasise the significance of this region in controlling the regulatory responses of TASK channels to various inputs.

Halothane and DAG have been found to affect TASK channel activity in excised patches, indicating that these substances have a direct effect on these channels (Patel et al., 1999; Wike et al., 2014; Sormann et al., 2022).

Franks and Lieb postulated in 1982 that endogenous ligands, such as neurotransmitters or other signalling molecules, may occupy the same binding sites on sensitive proteins that anaesthetics target. Therefore, the presence of these endogenous ligands may compete with anaesthetic compounds for the occupancy of these binding sites. This competition can affect the overall response to anaesthetics by influencing the degree of the anaesthetic effect.

The evidence supporting the significance of the VLRFMT motif in both halothane-induced activation and DAG-mediated inhibition of TASK channels, along with the direct effects of both halothane and DAG on these channels, gives rise to an intriguing hypothesis. It suggests that these molecules may compete for a shared region or binding site on the channel protein, potentially causing reciprocal modulation of channel activity. Consequently, the net effect on channel activity depends on the relative concentrations of these substances.

In this chapter, I looked for evidence of interactions between halothane and DAG in type-1 cells TASK channels. To accomplish this, I used two distinct concentrations of halothane (1 and 2%), along with three different concentrations of the DAG analogue DiC8 (0.75, 1.25, and 5 μM). Then, I compared the effect of halothane (1 and 2%) on TASK channels under control conditions to its effect when it was applied in the presence of different concentrations of DiC8 (0.75, 1.25, or 5 μM). My objective in utilising these mixtures was to determine whether there is a competition between DAG (DiC8) and halothane at the level of single channel binding site.

## 6.2 Methods

All experiments were performed in accordance with the UK Animals (Scientific Procedures) Act, 1986.

**Cell isolation:**

For the extended procedure, refer to Chapter 2, Section 2.1.2. Briefly, the carotid body bifurcations were dissected from rat pups (P11-P14). The dissected carotid body bifurcations were subjected to both enzymatic and mechanical digestion to obtain a single cell suspension. Primary cell cultures were plated onto coverslips pretreated with poly-D-lysine and incubated for 2 hours. Recordings took place within 5-6 hours of plating.

**Electrophysiology:**

Cell-attached recordings were performed using an Axopatch 200B (Molecular Devices, LLC, Sunnyvale, US). Sylgard-coated and fire-polished borosilicate pipettes (Harvard Apparatus Ltd., Kent, UK) were used. For the extended procedures, refer to Chapter 2, Section 2.8. In short, coverslips containing isolated type-1 cells were placed in the recording chamber and continuously superfused with a warmed Tyrode solution. Tyrode solutions were continuously bubbled with either normoxic (5% $CO_2$, balance air), hypoxic (5% $CO_2$, balance $N_2$), or anaesthetic gas mixtures (halothane 1-2% in 5% $CO_2$, balance air).

Seal formation was attempted with a borosilicate pipette containing a high $K^+$ solution (140 mM), 10 mM TEA, and 5 mM 4-AP (to block other $K^+$ channels). Upon the formation of a good seal (> 5 GΩ), the Tyrode solution was switched

to a high $K^+$ solution. Then, a positive pipette potential of +100 mV was applied.
Voltage clamp protocol, data acquisition, and data analysis were performed using Spike 10 software (Cambridge Electronics Design, Cambridge, UK).
The background $K^+$ channel of type-1 cells exhibited inward currents with brief, flickering openings under the recording conditions of this study.

**Drugs:**

Following cell identification, type-1 cells were subjected to superfusion with the Tyrode solution, both in the presence and absence of the drug under investigation, using the cells as their own controls. The drugs were applied to cells for a duration of 50-60 seconds, and a similar wash period followed the exposure to allow any reversible effects to subside. All drugs were appropriately reconstituted prior to dissolution in Tyrode solution. DiC8 and halothane were obtained from Sigma-Aldrich. The effects of both DiC8 and halothane were reversible, and channel activity rapidly returned to baseline levels upon removal of these agents. The concentrations of the administered drugs were determined either based on the EC50 values specific to each drug, prior usage in similar studies, or a combination of both approaches.

**Anaesthetic delivery**

Our laboratory has previously designed a system for precise anaesthetic delivery in a recording chamber with a constant flow of solutions. The primary purpose of this system is to minimise concentration loss while the anaesthesia travels from the vaporiser to the recording chamber and to maintain a relatively stable concentration during the experiment (Huskens et al., 2016). The

halothane concentration in the gas phase above the bubbling solutions was continuously monitored using an infrared analyser (Capnomac Ultima, Datex, Sevenoaks, UK). The concentrations of halothane used in this study fall within the range that is clinically relevant (Huskens, 2015).

**Experimental protocol for the measurements of TASK channels activity in type-1 cells:**

Channel activity analysis involved 20-second segments of recordings taken at least 10 seconds after any solution exchange. Quantification of single channel activity was defined by nPopen, which represents the product of the number of channels in the patch and the probability that a channel is open at any given time. nPopen analysis starts with the construction of an all-points frequency histogram to determine the main conductance state. Then, a 50% opening threshold was set for the nPopen analysis.

**Statistical analysis of TASK channel recordings:**

Data are presented as mean ± SD. Halothane concentrations are expressed as % delivered, where 1% halothane equates to 0.24 mM (Franks and Lieb, 1993).

N numbers denote separate recordings from a distinct cell/s on different coverslips. The percentage change in nPopen was determined using the following formula:

Percentage change = ((nPopen under Condition A - nPopen under Control) / nPopen under Control) * 100

Therefore, if an agent had no effect on channel activity, the change in channel activity relative to the control would be 0%.

In Figure 6.3 the nPopen values for the combined responses of DiC8 and halothane were normalized to the halothane (1% and 2%) responses in control (with no DiC8). Mean normalised nPopen values were used to assess statistical significance by student's t-test. A P value $< 0.05$ was taken as statistically significant. Where more than two groups were compared, an ANOVA test was used.

The concentration-response relationships were plotted, and lines of best fit were constructed using non-linear least squares regression with GraphPad PRISM version 10 software. The fitting was performed based on a simple ligand binding equation.

## 6.3 Results

### 6.3.1 Effects of DAG on TASK channel activity in type-1 cell

A brief hypoxic stimulus (<20 sec) was applied first to confirm the identity of the cell. Only cells that responded to this with inhibition of channel activity were selected for further study. The TASK channel activity observed under the recording conditions indicated in the methods section (pipette +100 mV, 140 mM $K^+$, and 100 mM $K^+$ in Tyrode) resulted in brief flickery openings, which were observed as inward currents. Under these conditions, most all-points histograms typically displayed a single but broad peak, indicating one main open state, which previous research has suggested represents the heterodimeric TASK-1/3 channel predominant in rat type-1 cells (Kim et al., 2009a; Turner and Buckler, 2013b).

The effect of DiC8 on TASK channel activity in type-1 cells was studied at concentrations ranging from 5 to 0.75 µM. Application of 5, 1.25, and 0.75 µM DiC8 induced a dose-dependent reversible inhibition of channel activity, as defined by nPopen in cell-attached patches (DiC8 concentration: % inhibition of channel activity: 5 µM: 74.5 ± 6.3, n = 9, $p<0.001$; 1.25 µM: 49.3 ± 3.4, n = 9, $p<0.001$; 0.75 µM: 34 ± 3.2, n=9=, $p<0.001$; see Figure 6.1A). In Figure 6.1B, representative all-point histograms are presented, demonstrating the dose-dependent inhibition of channel activity by DiC8. Note the reduction in channel activity across all conductance levels. The concentration dependency of DiC8-induced inhibition of the TASK channel is shown in Figure 6.1C, which was confirmed with an ANOVA test ($p<0.001$). A curve fitting of a hyperbola suggests a $K_d$ for the effect of DiC8 of 1.187 µM and a Bmax of 93.98% inhibition. Collectively, these findings further confirm the effects of DiC8 on TASK channel activity in type-1 cells and its concentration dependence.

**Figure 6.1 DAG induced inhibition of TASK channels activity in rat carotid body type-1 cell** Representative single-channel recordings showing the effect of DiC8 (5 (i), 1.25 (ii), 0.75 (iii) μM) over approximately 0.8 second. Note that traces were obtained from different cells at each concentration **(A)**. A representative all-points histogram was generated from a 20-second segment of recordings obtained during superfusion with either control or varying concentrations of DiC8 (5 μM (i), 1.25 μM (ii), and 0.75 μM (iii)). The bin width used for the histogram was set to 0.1 pA **(B)**. Concentration response of DiC8 (5, 1.25 and 0.75 μM) on rat type-1 cell TASK channel activity defined as percentage inhibition in nPopen relative to the control. The curve is fitted by non-linear least squares regression to a variable slope model, R square of 0.8559, Bmax of 93.98 and $K_d$ of 1.187 μM **(C)**. Data are mean ± S.E.M; n=9 for each concentration. The traces were recorded with a pipette potential of +100 mV, 140 mM $K^+$ in pipette solution and 100 mM $K^+$ in Tyrode solution.

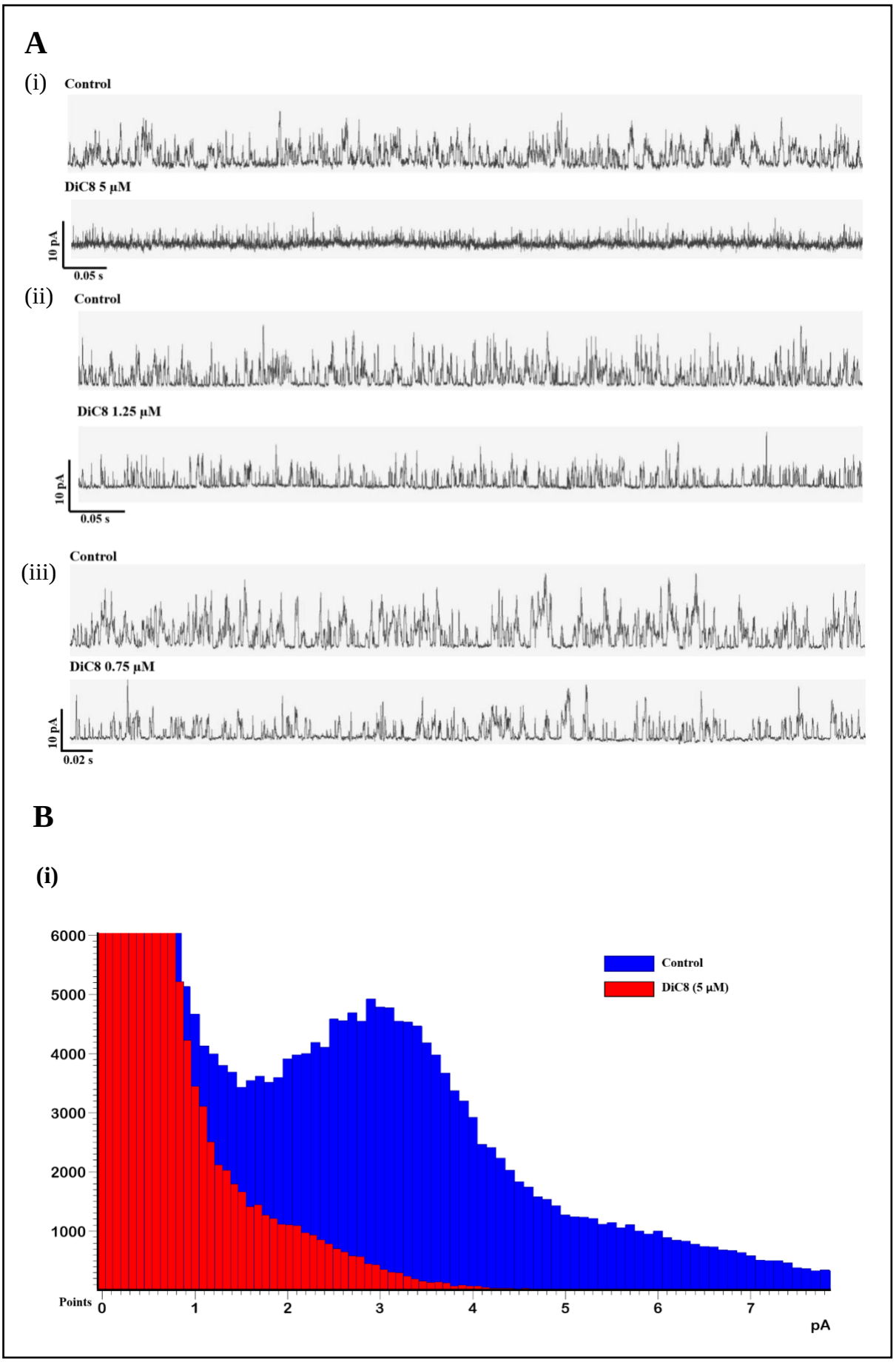
A
(i)
Control
DiC8 5 µM
10 pA
0.05 s
(ii)
Control
DiC8 1.25 µM
10 pA
0.05 s
(iii)
Control
DiC8 0.75 µM
10 pA
0.02 s
B
(i)
6000
5000
4000
3000
2000
1000
Points
0
1
2
3
4
5
6
7
pA
Control
DiC8 (5 µM)

(ii)

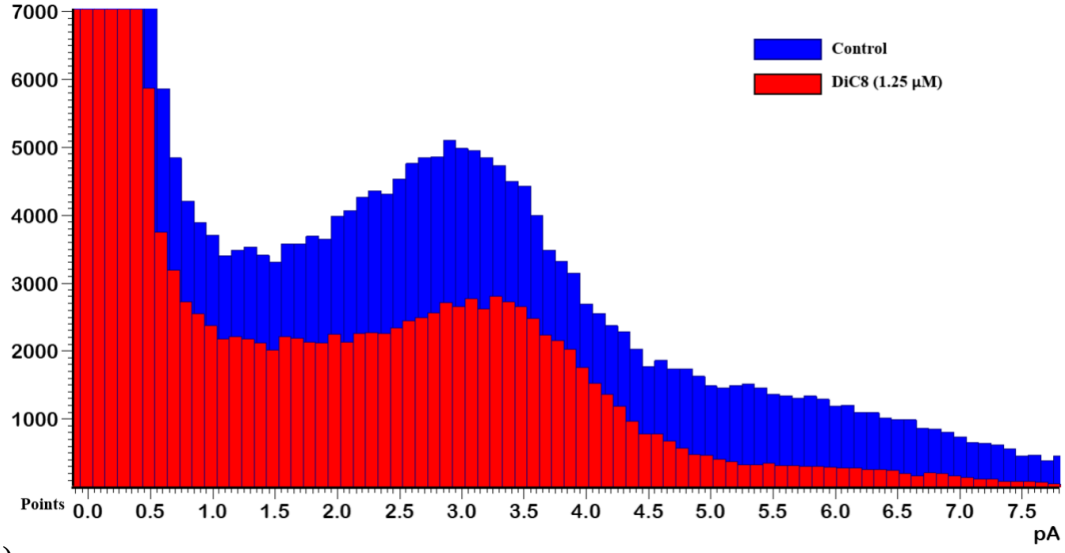
Control
DiC8 (1.25 µM)
7000
6000
5000
4000
3000
2000
1000
Points
0.0 0.5 1.0 1.5 2.0 2.5 3.0 3.5 4.0 4.5 5.0 5.5 6.0 6.5 7.0 7.5
pA

(iii)

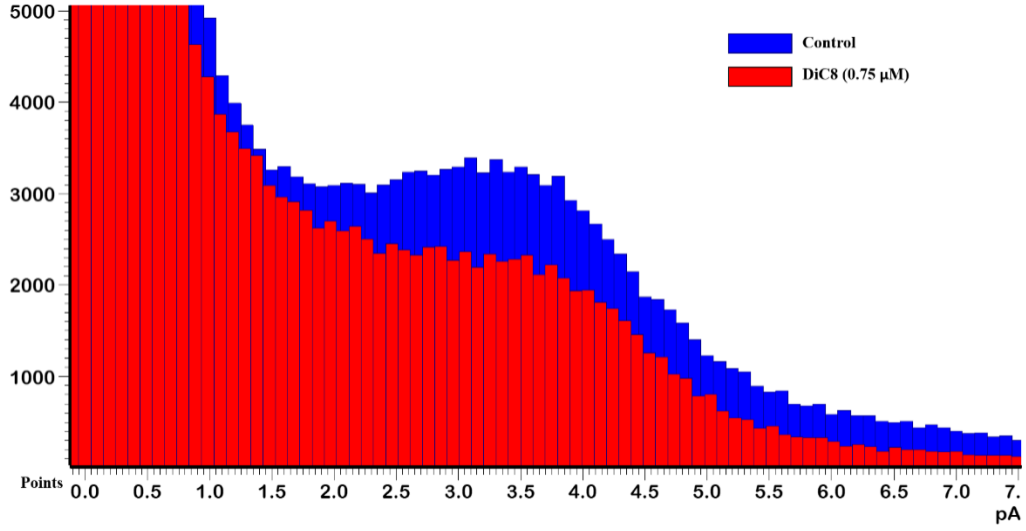
Control
DiC8 (0.75 µM)
5000
4000
3000
2000
1000
Points
0.0 0.5 1.0 1.5 2.0 2.5 3.0 3.5 4.0 4.5 5.0 5.5 6.0 6.5 7.0 7.
pA

**C**

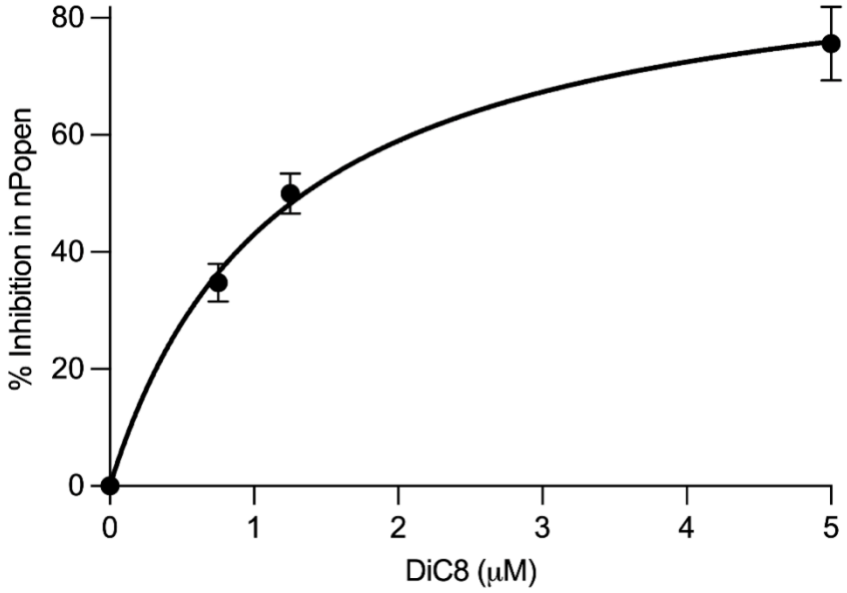
% Inhibition in nPopen
80
60
40
20
0
0 1 2 3 4 5
DiC8 (µM)

### 6.3.2 The combined effects of DAG and halothane on TASK channel activity in type-1 cell

Subsequently, I examined the combined effects of DiC8 and halothane on background TASK channel activity in acutely isolated rat carotid body type-1 cells. First, halothane (1% and 2%) was applied, which elicited a concentration-dependent increase in channel activity in cell-attached patches (see Tables 6.1, n= 27).

These 27 recordings were conducted in 3 groups (9 recordings per group), each with a different concentration of DiC8 (5, 1.25, and 0.75 μM). Once channel activity returned to baseline following halothane application, DiC8 (5, 1.25, and 0.75 μM) was applied for ~60 sec then halothane (1% and 2%) was applied in the presence of DiC8.

Application of 5 μM DiC8 completely blocked the activation of channel activity by 1% and 2% halothane. This can be observed in the representative traces depicted in Figure 6.2A (i) and B (i) (n = 9). In two different experiments, the concentration of DiC8 was reduced to 1.25 and 0.75 μM which resulted in a dose-dependent suppression of the effects of 1% and 2% halothane on channel activity, refer to Tables 6.1 and 6.2. Representative traces showing the inhibitory effects of DiC8 (1.25 and 0.75 μM) on halothane (1 and 2%) are shown in Figure 6.2A (ii and iii) and B (ii and iii).

**Table 6.1 Normalised TASK channels activity, as defined by nPopen in control and in the presence of different combinations of DiC8 (5, 1.25, and 0.75 µM) and halothane (1% and 2%)** Statistical significance was assessed by a two-way ANOVA test, which revealed a statistically significant interaction between DiC8 and halothane on channel activity [F (6, 96) = 26.52, P<0.001]. N= 27 for halothane (1% and 2%) in the control (without DiC8) and 9 for the other groups.

| DiC8 (µM) | No halothane | 1% halothane | 2% halothane |
|---|---|---|---|
| **0** | 1 | 1.48 ± 0.06 | 2.29 ± 0.07 |
| **0.75** | 0.66 ± 0.03 | 1.12 ± 0.02 | 2.06 ± 0.08 |
| **1.25** | 0.50 ± 0.03 | 1.03 ± 0.02 | 1.71 ± 0.09 |
| **5** | 0.23 ± 0.06 | 0.25 ± 0.06 | 0.24 ± 0.05 |

**Table 6.2 TASK channels activity, as defined by nPopen normalised to channel activity in control and in the presence of 1% and 2% halothane**

| DiC8 (µM) | No halothane | 1% halothane | 2% halothane |
|---|---|---|---|
| **0** | 1 | 1 | 1 |
| **0.75** | 0.66 ± 0.03 | 0.80 ± 0.04 | 0.91 ± 0.04 |
| **1.25** | 0.50 ± 0.03 | 0.67 ± 0.04 | 0.75 ± 0.03 |
| **5** | 0.23 ± 0.06 | 0.25 ± 0.06 | 0.24 ± 0.05 |

**Figure 6.2 Effects of DiC8 (5, 1.25, 0.75 µM) on halothane (1% and 2%) induced activation of TASK channels in rat carotid body type-1 cell**

Representative single-channel recordings showing the effect of DiC8, halothane (1 and 2%), and halothane plus DiC8 5 (i), 1.25 (ii) and 0.75 µM (iii) over approximately 8 minutes **(A)**. Data from same recordings over 0.6 seconds intervals under control condition, in the presence of halothane (1 and 2%) and when halothane and DiC8 5 (i), 1.25 (ii) and 0.75 (iii) µM were coapplied **(B)**. The traces were recorded with a pipette potential of +100 mV, 140 mM $K^+$ in pipette solution and 100 mM $K^+$ in Tyrode solution.

The horizontal bar in A represents a timescale of 30-40 seconds, and the vertical bar indicates a 5pA current; whereas in B, the horizontal bar represents a timescale of 0.05 seconds, and the vertical bar indicates a 10 pA current.

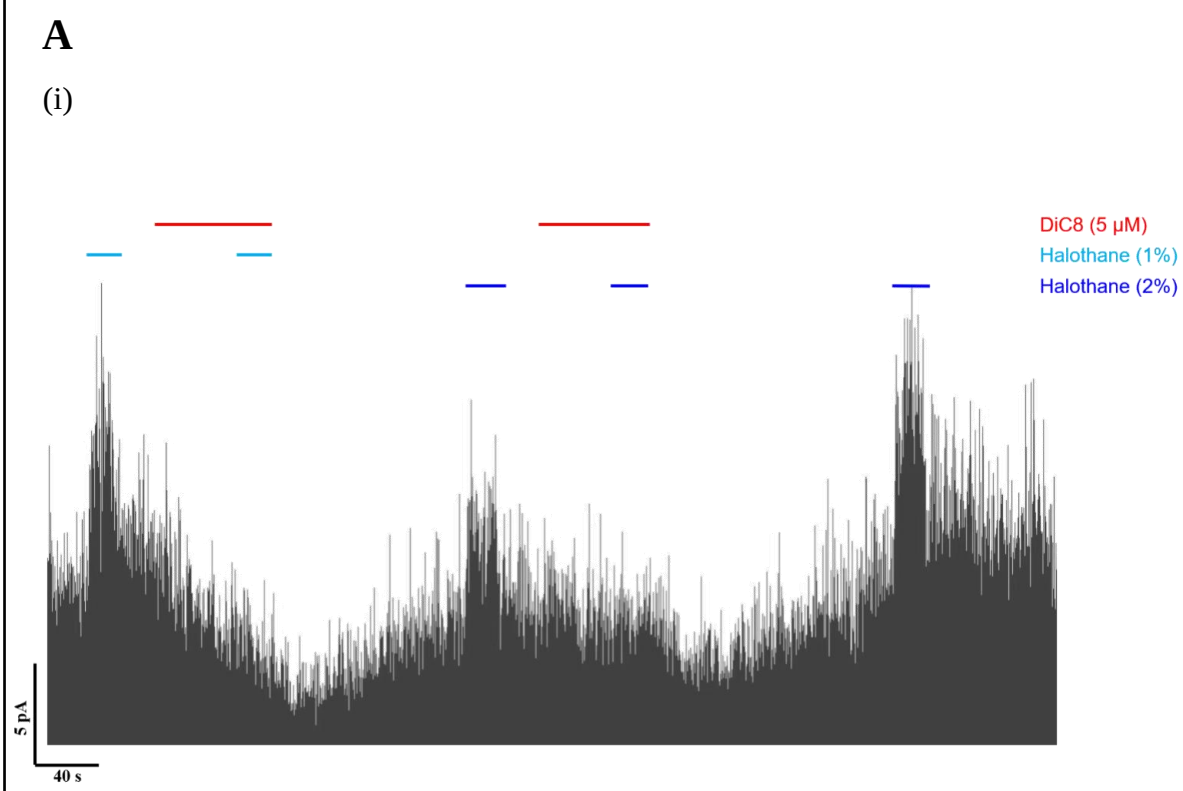

(ii)

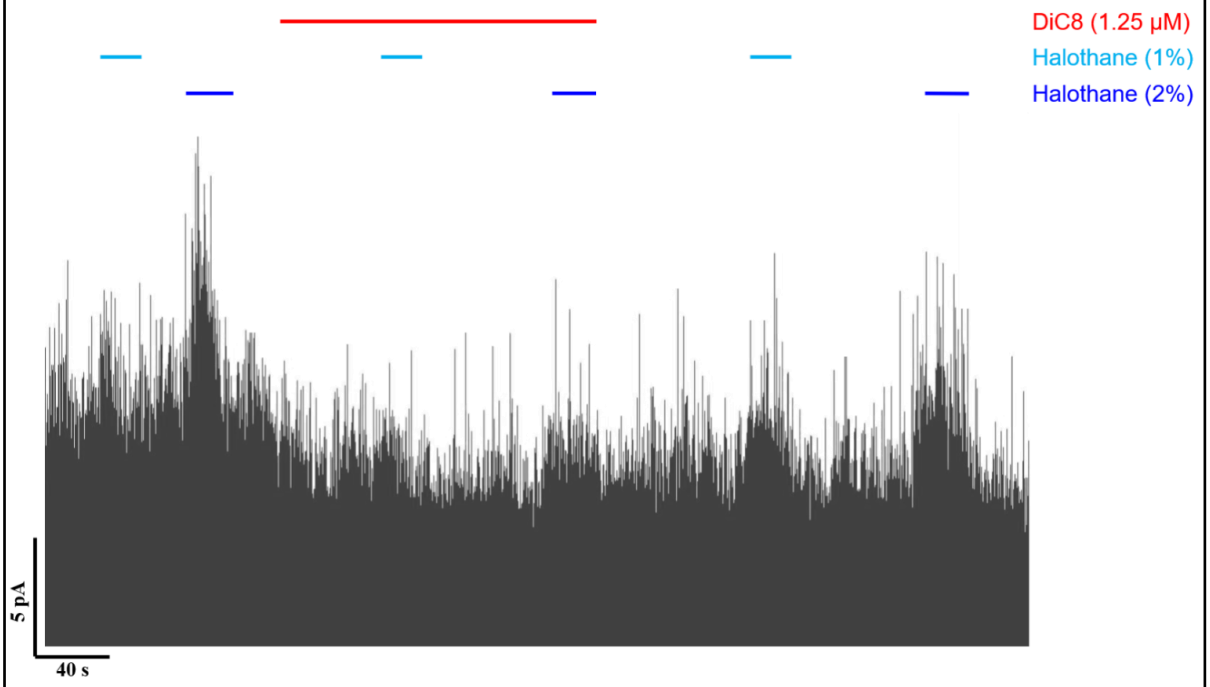
DiC8 (1.25 μM)
Halothane (1%)
Halothane (2%)
5 pA
40 s

(iii)

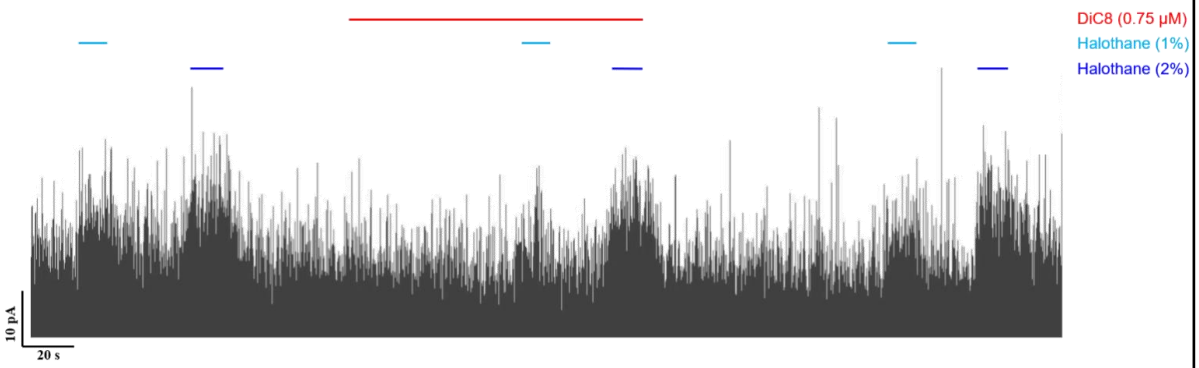
DiC8 (0.75 μM)
Halothane (1%)
Halothane (2%)
10 pA
20 s

**B**

(i)

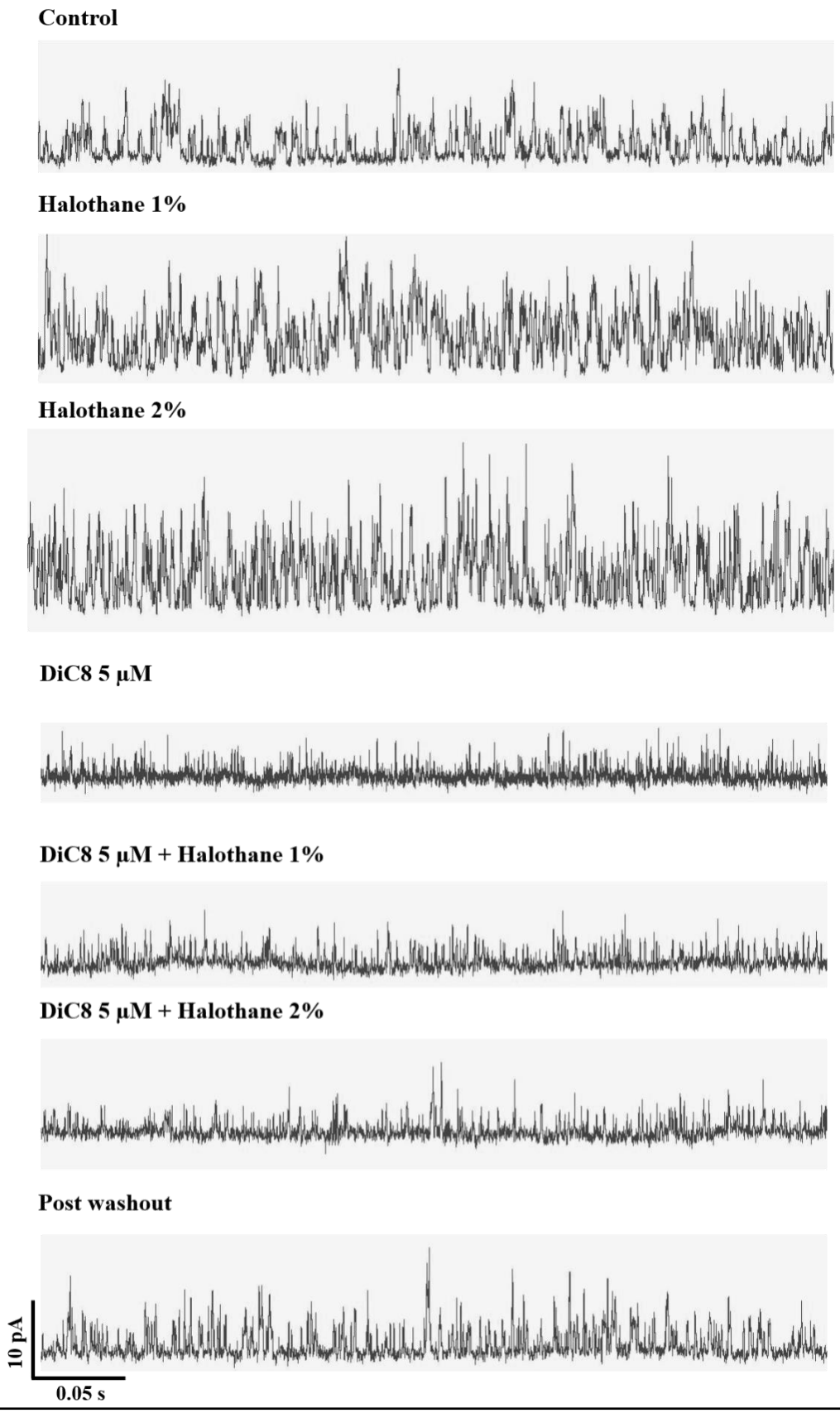
Control
Halothane 1%
Halothane 2%
DiC8 5 µM
DiC8 5 µM + Halothane 1%
DiC8 5 µM + Halothane 2%
Post washout
10 pA
0.05 s

(ii)

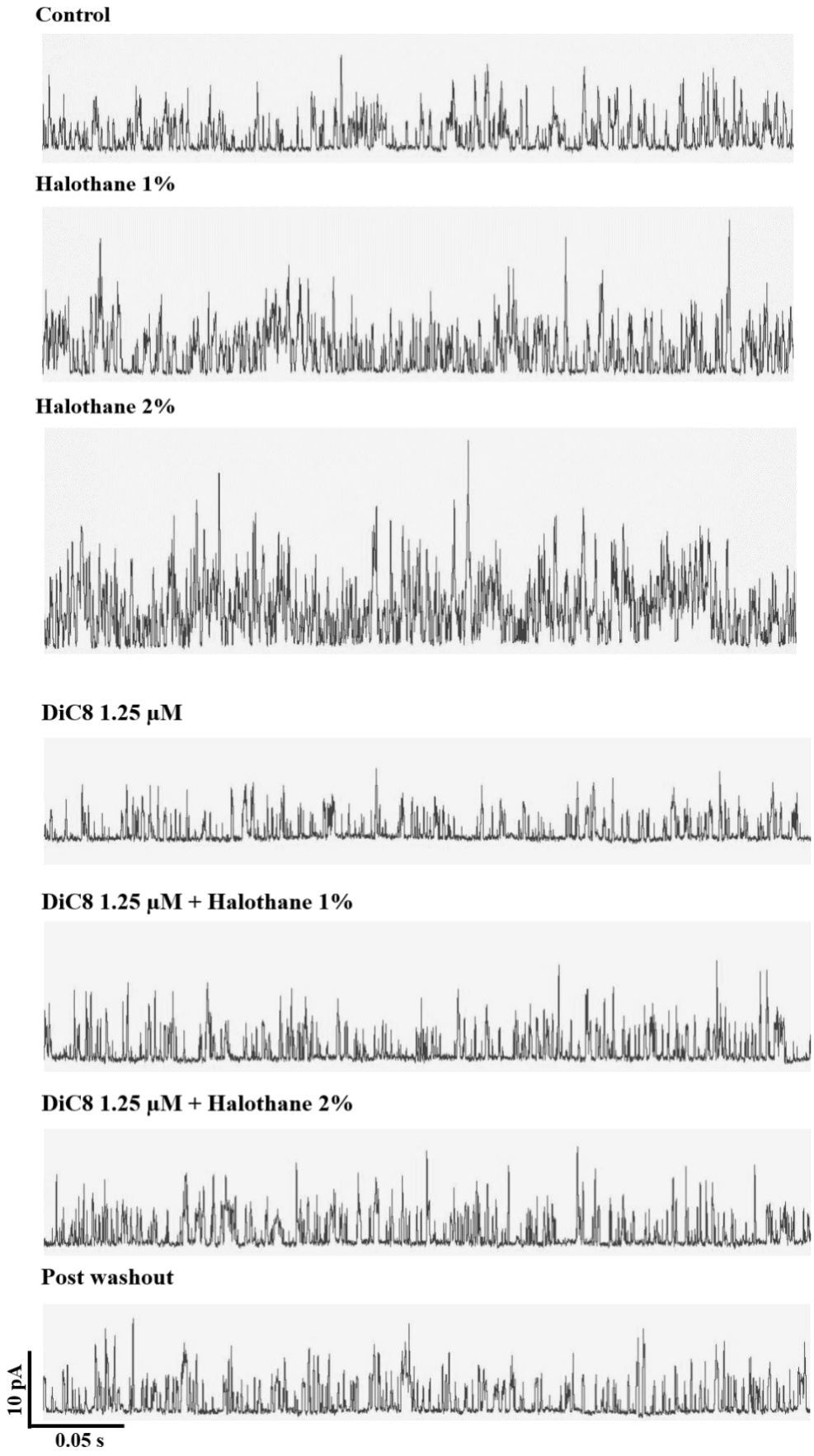
Control
Halothane 1%
Halothane 2%
DiC8 1.25 µM
DiC8 1.25 µM + Halothane 1%
DiC8 1.25 µM + Halothane 2%
Post washout
10 pA
0.05 s

(iii)

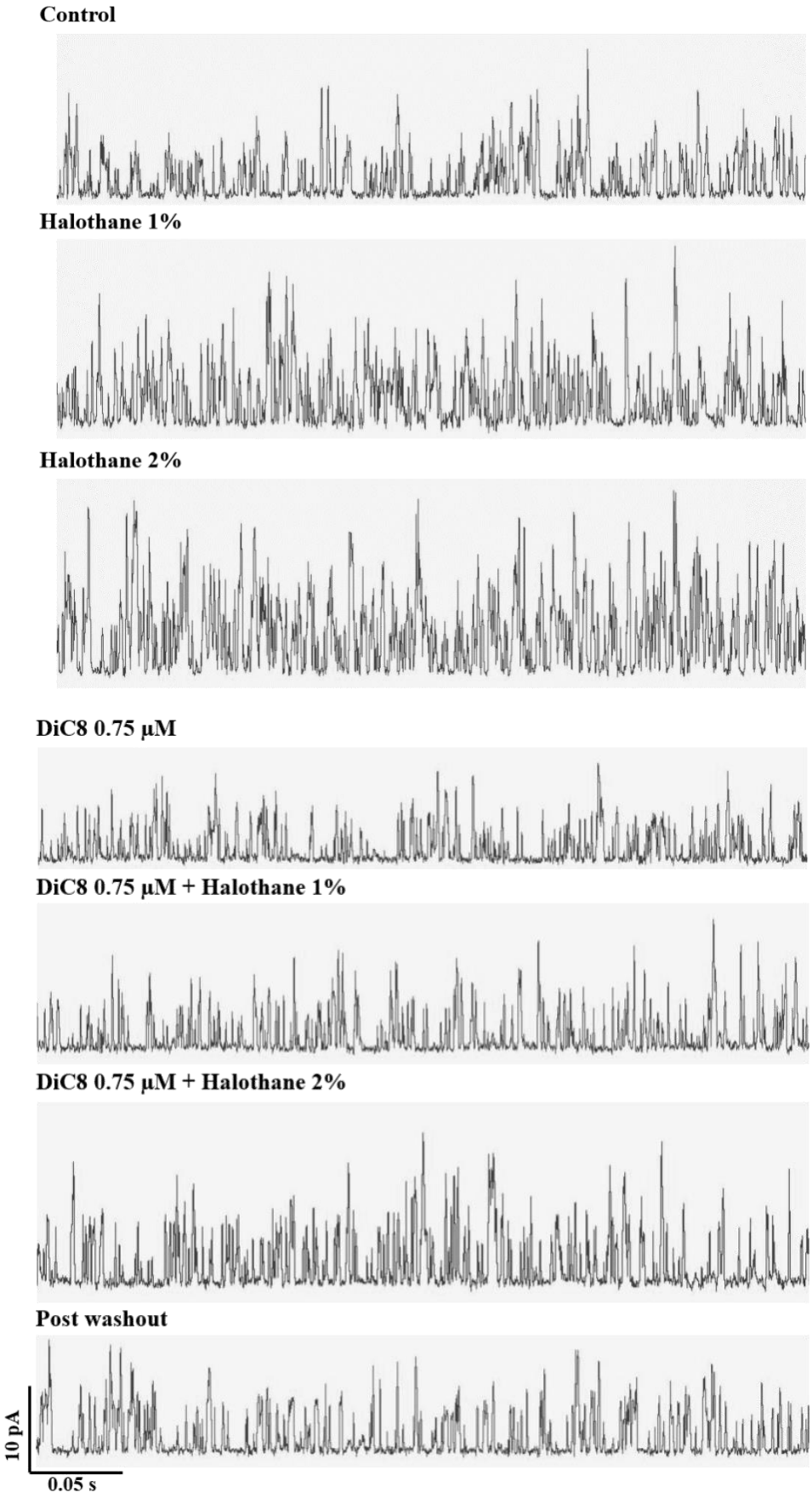
Control
Halothane 1%
Halothane 2%
DiC8 0.75 µM
DiC8 0.75 µM + Halothane 1%
DiC8 0.75 µM + Halothane 2%
Post washout
10 pA
0.05 s

### 6.3.3 Effects of halothane on the DiC8-induced inhibition of TASK channels in type-1 cells

Figure 6.3 depicts a dose-response curve for the percentage inhibition of channel activity, as defined by normalised nPopen, following the application of DiC8 in three conditions: control (without halothane) and the presence of 1% and 2% halothane, with a total of 27 data points and an average of 9 recordings per concentration. Applications of halothane (1 and 2%) increased the EC50 of DiC8 from 0.9406 μM (in control with no halothane) to 1.591 μM with 1% halothane and 2.188 μM with 2% halothane. Collectively, these findings suggest that halothane and DAG exhibit reciprocal modulation of the TASK channel, with one compound promoting channel activation and the other promoting channel inhibition. The net effect on channel activity is therefore dependent on the concentrations of these two compounds.

**Figure 6.3 Effects of halothane on the DiC8 induced inhibition of TASK channel in type-1 cells** The x-axis represents the concentrations of DiC8 in μM, while the y-axis shows the percentage inhibition in normalized channel activity as defined by nPopen under three conditions: DiC8, DiC8 plus 1% halothane, and DiC8 plus 2% halothane. Note, the data with 1% and 2% halothane were normalized to the halothane response in control (without DiC8).

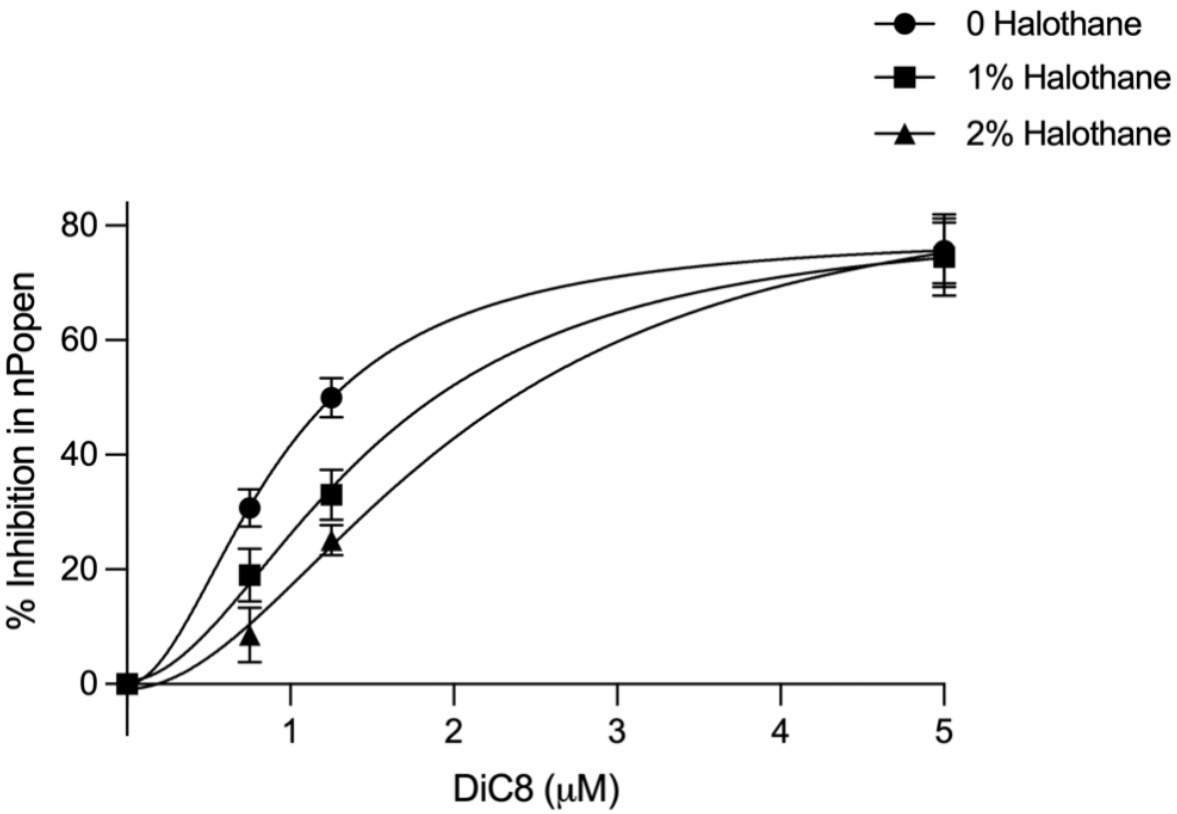

## 6.4 Discussion

The findings presented in this chapter show that DiC8 exerts concentration-dependent inhibition of TASK channels in type-1 cells and acts as an antagonist, counteracting halothane-induced activation of these channels.

To confirm the findings of Chapter 4 regarding the inhibitory effect of DiC8 on TASK channels, I conducted a comprehensive analysis of its effect at varying concentrations (0.75, 1.25, and 5 μM). The results presented in this chapter revealed that DiC8 inhibited TASK channel activity in a concentration-dependent manner. This is consistent with earlier studies that reported the regulation of TASK channels by DAG in native cells and heterologous expression models (Sormann et al., 2022; Wike et al., 2014).

My research has uncovered a significant interaction between DiC8 and halothane on TASK channels in type-1 cells. Halothane was first recognised as a potent activator of the background TASK-like potassium current in various tissues, including the carotid body (Buckler et al., 2000; Berg et al., 2004; Putzke et al., 2007; Pandit et al., 2010). Additionally, halothane was shown to inhibit hypoxia-induced $[Ca^{2+}]i$ rise in carotid body type-1 cells (Pandit et al., 2010). Here, I investigated the effects of three different concentrations of DiC8 (0.75, 1.25, and 5 μM) on the halothane-induced activation of TASK channels. At 5 μM, DiC8 completely blocked the effects of halothane on TASK channels. The level of suppression of the halothane-induced activation of TASK channels decreased as lower concentrations of DiC8 were used. Figure 6.3 depicts the combined effects of DiC8 (0.75, 1.25, and 5 μM) and halothane (1% and 2%), and shows that the EC50 of DiC8 increases when applied with halothane, suggesting a competitive antagonistic interplay between these two compounds, which will be discussed in the general discussion chapter.

In summary, the results presented in this chapter demonstrate that DiC8 inhibits TASK channels in type-1 cells in a reversible dose-dependent manner and reduces halothane-induced activation of these channels. These results improve our understanding of the complicated interactions between DiC8, halothane, and TASK channels and may help us understand cellular responses to anaesthesia. Additionally, the findings described in this chapter have the potential to facilitate the design of anaesthetic agents with fewer side effects on ventilation, thereby enhancing the safety of volatile anaesthetics.

### 6.4.1 Limitations and technical challenges:

Handling volatile anaesthetics in conventional delivery systems, such as perfusion rigs, presents a number of challenges (see Chapter 2, Section 2.5). Thus, minimising the reduction in anaesthetic concentration becomes more challenging. Refer to Methods, Section 6.2.

### 6.4.2 Suggestions for future research:

On the basis of the findings presented in this chapter, I propose some additional experiments that would enhance our understanding of the interaction between DAG, halothane, and TASK channels in type 1 cells. Initially, it would be valuable to explore how DAG impacts the effects of other anaesthetics on TASK channels to determine if its effects are limited to halothane or extend to other anaesthetics. Furthermore, investigating the impact of inhibitors that target DAG metabolism on the activation of the TASK channel by halothane and other anaesthetics may aid in understanding the interactions between endogenous DAG levels and anaesthetic agents.

# Chapter 7. Discussion

## 7.1 Main findings

This thesis explores the regulatory mechanisms governing the activity of TASK channels in type-1 cells of the rat carotid body, particularly in response to hypoxia, Gq/11-coupled receptors, and ATP. It also investigates the impact of volatile anaesthetics as significant modulators of TASK channels, highlighting their potential clinical implications. Additionally, this thesis seeks to address the question as to whether there might be a common signalling pathway mediating all these effects. More specifically, I suggest that, ultimately, lipid signalling may be central to all these forms of TASK channel regulation.

I started by examining the effect of $G_{q/11}$ and PLC signalling molecules on intracellular $Ca^{2+}$ signalling as well as hypoxia and muscarinic agonist-evoked $[Ca^{2+}]i$ rise in type-1 cells. Next, I directly examined the effects of these signalling molecules on the activity of TASK channels in type-1 cells, first in the cell-attached and then in the inside-out configuration. The last two chapters of this thesis investigate the interactions between PLC signalling molecules and two other known regulators of TASK channels: metabolic poisons (or ATP) and halothane. This thesis has achieved its primary goal and revealed that $G_{q/11}$ and PLC signalling molecules are involved in the regulation of carotid body type-1 cells.

In Chapter 3, I presented evidence demonstrating the effects of $G_{q/11}$ receptors and PLC signalling molecules on $Ca^{2+}$ signalling in type-1 cells, specifically in response to hypoxia and muscarinic stimulation. The results presented in this chapter suggest that $G_{q/11}$ receptors and PLC signalling molecules play a significant role in the regulation of $Ca^{2+}$ signalling within type-1 cells, particularly in response to hypoxia.

In Chapter 4, I directly examined the effects of $G_{q/11}$ receptors and PLC signalling molecules on TASK channel activity in type-1 cells. My results are essentially comparable with those described in Chapter 3, although I found that inhibiting $G_{q/11}$ receptors had no effect on the baseline activity of TASK channels or the hypoxic inhibition of these channels. Therefore, the effects of $G_{q/11}$ inhibition on hypoxia-evoked $[Ca^{2+}]i$ entry do not involve TASK channels and are likely to be mediated by other mechanisms (e.g., $Ca^{2+}$ channels). On the other hand, PLC signalling molecules, particularly DAG, showed consistent effects on both hypoxia-evoked $[Ca^{2+}]i$ rise and hypoxia-induced inhibition of TASK channels. It is worth noting that among the downstream signalling molecules of PLC that are studied in this thesis, DAG stands out as the only signalling molecule that consistently affected both hypoxia-induced $[Ca^{2+}]i$ rise and hypoxia-induced inhibition of TASK channels in type-1 cells. This suggests that DAG is the key signalling molecule that mediates the PLC regulation of TASK channels.

U73122, a PLC inhibitor that reduces DAG production, activated TASK channels under normoxic conditions and blocked the inhibition of these channels under hypoxia (Figure 4.3). In contrast, m-3m3fbs, a PLC activator that increases DAG production, inhibited TASK channels under normoxic conditions and prevented any additional inhibition in response to hypoxia (Figure 4.5). These findings emphasise the importance of PLC and DAG in the regulation of TASK channels. Moreover, bypassing PLC and directly increasing intracellular DAG levels by the application of DiC8 (a DAG analogue) resulted in $Ca^{2+}$ oscillations in normoxia and an augmented hypoxia-evoked $[Ca^{2+}]i$ rise (Figure 3.8). Correspondingly, patch clamp studies in Chapters 4 and 6 demonstrated direct (dose dependent) inhibition of TASK channels by DiC8 (Figures 4.7 and 6.1). I also observed that increasing intracellular DAG levels by applying a DAG analogue or a DAGK inhibitor inhibited TASK channels

and prevented any additional inhibition in response to hypoxia (Figure 4.8). These data suggest that there is constitutive DAG production (by PLC), and DAG phosphorylation (by DAGK). Under resting conditions, this would appear to maintain sufficient DAG to slightly inhibit TASK channel activity (as testified by the increase in TASK activity in the presence of U73122). The data also demonstrate that PLC activation or DAG inhibition can cause a level of TASK channel inhibition comparable to that observed in hypoxia. Consequently, responses to hypoxia could theoretically be mediated by either PLC activation or DAGK inhibition (See Chapter 4, section 4.4).

Our examination of the effect of PLC inhibition on TASK channel activity in excised patches of type-1 cells yielded unexpected findings. PLC inhibition had no effect on the decline in TASK channel activity after patch excision. Moreover, DAGK inhibition did not have any discernible impact on the reactivation of TASK channels by MgATP after patch excision. Nonetheless, there are two possible explanations for these observations. First, in addition to PLC, DAG can be generated by different reactions that take place at different cellular compartments, including the endoplasmic reticulum, Golgi network, lipid droplets, and plasma membrane. These reactions involve the activity of different enzymes, such as PAPs, sphingomyelin synthase (SMS), and monoacylglycerol-O-transferase (MGAT) (Tafesse et al., 2006; Prentki and Madiraju, 2008; Eichmann and Lass, 2015). Thus, the accumulation of DAG produced through these mechanisms could mediate the inhibition of TASK channels in excised patches of type-1 cells. Second, it is possible that MgATP induced a strong activation of DAGK, which impaired the efficacy of the applied DAGK inhibitor. As a result, MgATP may activate DAGK despite the presence of the inhibitor. Furthermore, in addition to DAGK, DAG can be metabolised by other mechanisms. For example, DAG lipases (DAGLs), particularly DAGLα which is located at the plasma membrane, metabolise DAG

to generate monoacylglycerol and a free fatty acid (Eichmann and Lass, 2015). Thus, DAG metabolism by these alternative pathways may mediate MgATP activation of TASK channels by reducing membrane-associated DAG levels.

Despite these observations, which cast doubt on DAG's direct involvement in the regulation of TASK channel in type-1 cells, it is worth considering that DAG, as evidenced by its effect on both hypoxia-evoked $[Ca^{2+}]i$ entry and hypoxia-induced inhibition of TASK channels, is the signalling molecule responsible for conferring oxygen sensitivity to these channels. In this setting, a critical question arises: How does DAG integrate into the acute oxygen sensing process in type-1 cells? In Chapter 4, I proposed a model for acute oxygen sensing in type-1 cells. To validate this model, measurements of intracellular DAG levels under hypoxic and normoxic conditions are required.

To further examine the role of DAG in regulating the activity of TASK channels, I expanded my investigations to include two additional well-known regulators of TASK channels: ATP and halothane. By investigating the effects of ATP and halothane on TASK channels in conjunction with DAG, I aimed to examine the interaction and potential convergence of these signalling pathways.

Chapter 5 investigates the effects of PLC inhibition and the consequent reduction in DAG production on FCCP- and cyanide-induced inhibition of TASK channels in type-1 cells. It has been established that TASK channels are inhibited by FCCP and cyanide. Intriguingly, their effects on TASK channels are mutually exclusive with hypoxia, indicating that they share a common underlying mechanism (Wyatt and Buckler, 2004; Turner and Buckler, 2013b). Nevertheless, despite various hypotheses proposed, the precise link between metabolic function and TASK channel activity remains elusive. Considering that the metabolism of DAG is ATP-dependent, I hypothesised that DAG may

serve as a crucial intermediary, linking metabolic function to TASK channel activity in type-1 cells. However, the results presented in Chapter 5 demonstrate that the application of the PLC inhibitor U73122 had no effect on FCCP- or cyanide-induced inhibition of TASK channels. This suggests that PLC-produced DAG is not involved in mediating the effects of metabolic inhibitors on TASK channels. One plausible explanation for these findings is that despite PLC inhibition, DAG could still be produced by PLC-independent mechanisms (e.g. PAPs). Interestingly, PAPs' activity is $Mg^{2+}$-dependent; this raises the possibility that $Mg^{2+}$ released by the net hydrolysis of MgATP in response to metabolic inhibitors could directly activate PAPs (Varas et al., 2007; Wu and Carman, 1994). Furthermore, the reduction in ATP levels secondary to the application of metabolic inhibitors would reduce ATP-dependent DAGK activity (Han et al., 2008; Ma et al., 2019; Varas et al., 2007). These two mechanisms would increase intracellular DAG levels secondary to metabolic inhibition, resulting in TASK channels inhibition (Figure 7.1). This may explain the lack of effects of metabolic inhibitors on TASK channels in excised patches of type-1 cells where cytosolic factors are not preserved (Williams and Buckler, 2004).

It is worth noting that cyanide and FCCP occluded the activation of TASK channels by U73122 (Figures 5.1 and 5.2); therefore, if TASK channels activation by U73122 is mediated by a reduction in intracellular DAG levels, this could easily be antagonised by DAG production via activation of PAPs by cyanide and FCCP. The observation that U73122 blocked hypoxia-induced TASK channel inhibition but had no effect on both FCCP- and NaCN-induced inhibition of these channels can be explained by the fact that hypoxia resulted in a smaller increase in free cytosolic $Mg^{2+}$ within type-1 cells compared to NaCN and mitochondrial uncouplers (Varas et al., 2007). Consequently, it is not anticipated that a profound activation of PAPs would occur in response to

hypoxia. Therefore, inhibiting PLC activity was adequate to inhibit DAG production and subsequently block the hypoxia-induced inhibition of TASK channels. Considering these possibilities, it is also essential to explore other potential mechanisms that could mediate the effects of metabolic inhibitors on TASK channels.

The mitochondria of type-1 cells exhibit an unusually high $PO_2$ threshold and display a distinct profile of mitochondrial gene expression (Mills and Jobsis, 1972; Duchen and Biscoe, 1992; Buckler and Turner, 2013b; Fernández-Agüera et al., 2015; Zhou et al., 2016; Gao et al., 2017; Moreno-Domínguez et al., 2020). These features suggest that type-1 cells have specialised adaptations in their mitochondrial function to support their role in oxygen sensing.

ROS and NADH, two mitochondrial-related signalling molecules, have been implicated in acute $O_2$ sensing in type-1 cells (Fernández-Agüera et al., 2015; Arias-Mayenco et al., 2018). Considering that the effects of mitochondrial inhibitors and hypoxia on TASK channels in type-1 cells are mutually exclusive, it is plausible that the effects of cyanide and FCCP on TASK channels are mediated by ROS and NADH. However, TASK channels in type-1 cells were insensitive to ROS (Papreck et al., 2012). Furthermore, it is worth noting that TASK channels are inhibited by both electron transport inhibitors and uncouplers, as illustrated in Figures 5.1 and 5.2, despite their opposing effects on $NAD^+$/NADH. Inhibition of mitochondrial electron transport by cyanide decreases, and uncoupling the mitochondria with FCCP increases $NAD^+$/NADH. Hence, the involvement of alterations in $NAD^+$/NADH in mediating TASK channel inhibition by metabolic inhibitors appears to be improbable, as suggested by previous studies (Duchen and Biscoe, 1992a; Wyatt and Buckler, 2004). A role for ROS seems equally improbable given that TASK channel inhibition can be maintained even in the complete

absence of oxygen (Buckler and Vaughan-Jones, 1994a; Buckler and Turner, 2013).

Therefore, the inhibition of TASK channels by metabolic inhibitors is most likely to be attributed to a decline in ATP levels. To create a physiologically active form, ATP bonds to $Mg^{2+}$. It is thought that a substantial amount of intracellular ATP and $Mg^{2+}$ exist in the form of MgATP complexes. Interestingly, MgATP has been shown to directly activate TASK channels in type-1 cells. Additionally, it has been reported that hypoxia, which inhibits these channels, reduces intracellular MgATP levels (Williams and Buckler, 2004; Varas et al., 2007). This sensitivity to MgATP prompts the question of whether mitochondrial inhibitors might inhibit TASK channels by reducing MgATP levels. Plausible mechanisms for this include a direct effect of MgATP on these channels or reductions in MgATP-dependent signalling molecules. The absence of known nucleotide binding sites in the primary sequence of TASK channels and the lack of reports of cloned TASK1 or TASK3 being sensitive to MgATP suggest that the impact of MgATP on these channels is likely mediated by an intermediate signalling molecule (Buckler, 2015). One particularly well-accepted MgATP-dependent signalling molecule involved in the regulation of TASK channels is DAG. This dependency arises from the requirement of MgATP for DAG metabolism (Badola and Sanders, 1997). Despite our findings not conclusively proofing the involvement of DAG in mediating the actions of metabolic inhibitors on TASK channels, they do suggest a model that explains the mechanism of action of metabolic inhibitors. More research is needed to understand the role of DAG in mediating the effects of metabolic inhibitors on TASK channels in type 1 cells, which will be discussed in Section 7.2.

In Chapter 6, I presented novel findings demonstrating the effect of DAG on the baseline activity of TASK channels in type-1 cells and on the activation of these channels by halothane. I demonstrated that the DAG analogue DiC8

inhibited TASK channels in a reversible and dose-dependent manner and decreased the halothane-induced activation of these channels.

It has been established that TASK channels in excised patches can be modulated by halothane and DAG, suggesting that these two agents may directly affect TASK channels (Patel et al., 1999; Sormann et al., 2022; Wike et al., 2014). Furthermore, it has been demonstrated that the VLRFMT region of TASK channels is essential for both anaesthetics-induced activation and DAG-induced inhibition of these channels (Tally and Bayliss, 2002; Wike et al., 2014). Based on these findings, the results presented in Chapter 6 further support the hypothesis that anaesthetics and endogenous ligands may compete for the same binding site or interact via overlapping signalling pathways (Franks and Lieb, 1982; Tally and Bayliss, 2002). Additionally, the observation that DiC8 inhibited the halothane-induced activation of TASK channels raises the possibility that this activation may simply result from displacing DAG, thereby disinhibiting TASK channels.

In conclusion, this thesis has shed light on the complex mechanisms that control the activity of TASK channels in type-1 cells in response to hypoxia, $G_{q/11}$-coupled receptors, ATP, and volatile anaesthetics. The collective findings from these investigations suggest that DAG may serve as a crucial signalling molecule that effectively regulates the activity of TASK channels in response to various endogenous and exogenous stimuli (Figure 7.2).

**Figure 7.1 Metabolic inhibitors regulation of TASK channels in type-1 cell**

The schematic presentation depicts the potential regulatory pathways influenced by metabolic inhibitors. These inhibitors can inhibit TASK channels through two distinct mechanisms. First, they raise cytosolic $Mg^{2+}$ levels, triggering the activation of PAPs, which in turn, generates DAG. Second, metabolic inhibitors reduce ATP levels, which in turn diminish DAGK activity. These dual mechanisms ultimately result in the accumulation of DAG, leading to the inhibition of TASK channels.

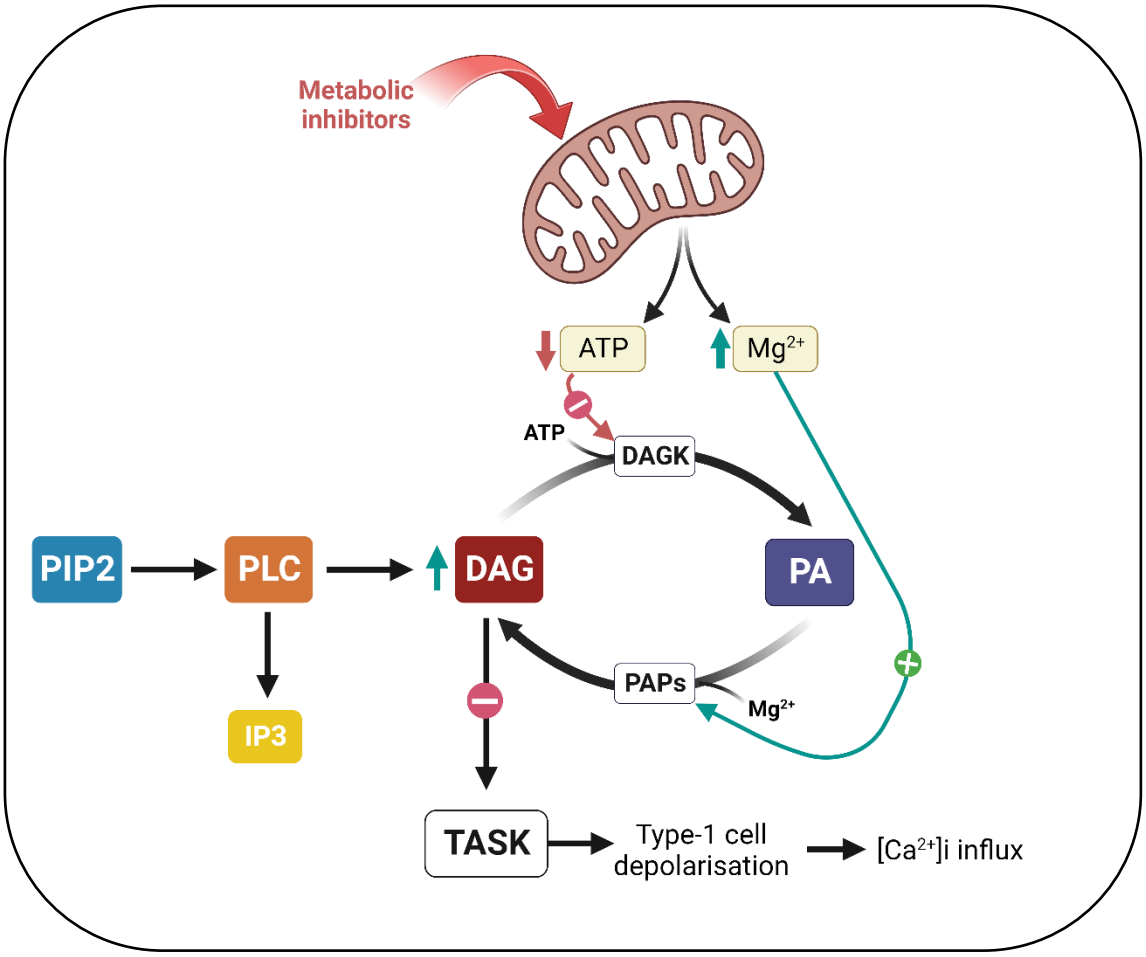

**Figure 7.2 Regulation of TASK channels in type-1 cells by hypoxia, metabolic Inhibitors, and anaesthetics**

The schematic presentation depicts the potential regulatory pathways influenced by hypoxia, metabolic inhibitors, and volatile anaesthetics. I propose that these well-known regulators of TASK channels converge on a common signalling pathway, with DAG playing a crucial role. Hypoxia can activate DAG production mechanisms (possibly PAPs) and/or inhibit DAGK activity. These two mechanisms result in DAG accumulation which inhibits TASK channels in response to reductions in $PO_2$ levels. On the other hand, metabolic inhibitors could inhibit TASK channels through two mechanisms. They increase free cytosolic $Mg^{2+}$ levels which activates PAPs resulting in an elevation in intracellular DAG levels. Additionally, by reducing ATP levels, metabolic inhibitors may reduce DAGK activity. These two mechanisms result in DAG accumulation which inhibits TASK channels. Conversely, volatile anaesthetics, such as halothane activate TASK channels by competing with DAG for a shared binding site within the channel.

Red arrows represent signalling pathways activated by hypoxia. Blue arrows represent signalling pathways triggered by metabolic inhibitors. The green arrow represents signalling pathways induced by volatile anaesthetics. HRE: hypoxia-response element.

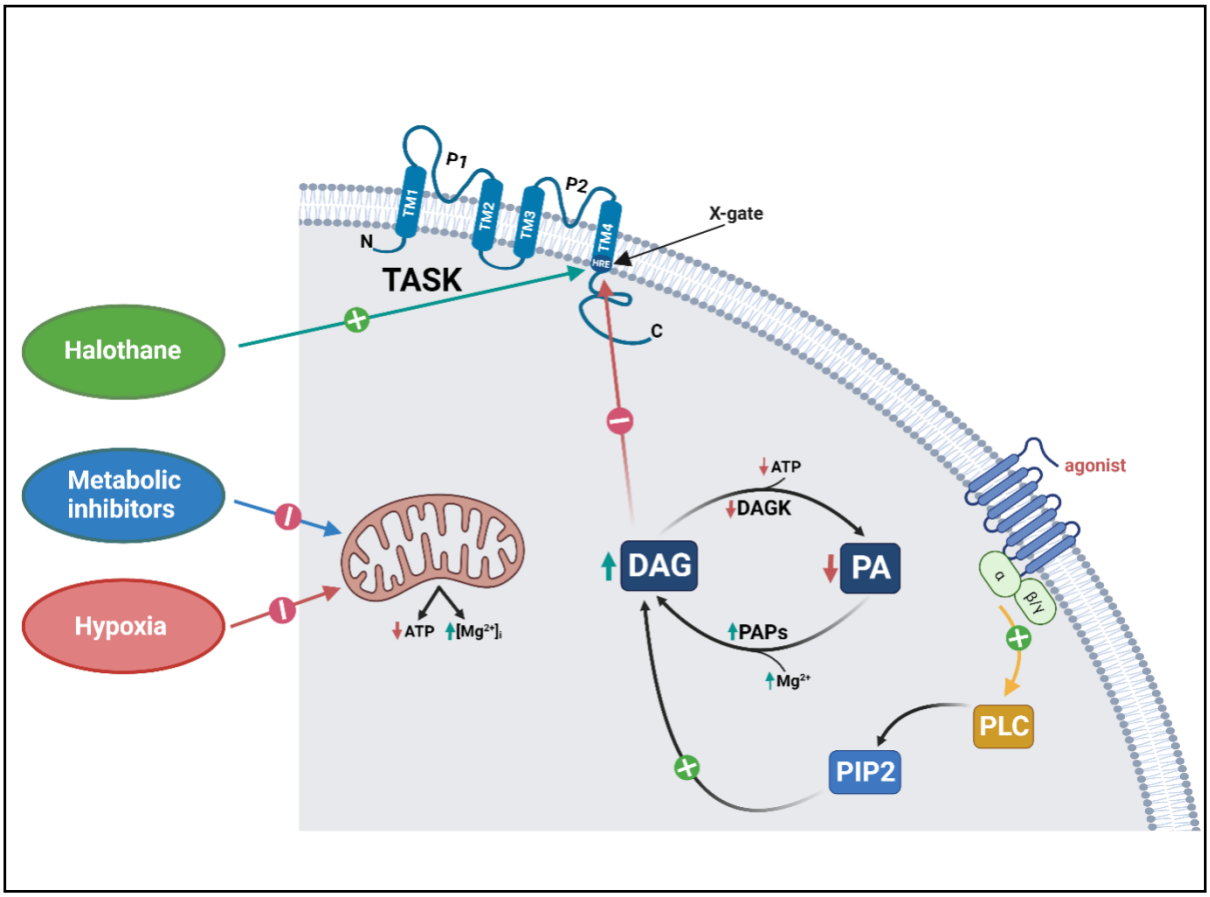
P1
P2
TM1
TM2
TM3
TM4
N
C
X-gate
TASK
Halothane
Metabolic inhibitors
Hypoxia
ATP
[Mg2+]i
ATP
DAGK
DAG
PA
PAPs
Mg2+
agonist
α
β/γ
PLC
PIP2

## 7.2 Future work:

The findings presented in this thesis have provided important insights into the role of $G_{q/11}$ receptors and PLC signalling molecules in the control of $Ca^{2+}$ signalling and TASK channel activity in type-1 cells. Several questions, however, remain unresolved. It is critical to determine whether hypoxia activates DAG production mechanisms (e.g., PAPs) in type-1 cells. This can start by looking at the effects of PAPs inhibitors (e.g., propranolol) on hypoxia-evoked $[Ca^{2+}]i$ rise and TASK channels inhibition in type-1 cells (Meier et al., 1998). Further research is needed to investigate the possibility of cross-talk between DAG and other signalling pathways involved in oxygen sensing (e.g., ROS, AMPK, and LKB1).

Another area of research may involve genetic mouse models that disrupt DAG metabolism. Such models have been used to investigate the relationship between disruptions in DAG metabolism and various metabolic disorders, such as insulin resistance (Eichmann and Lass, 2015). Furthermore, a significant progression would involve the development of mice lacking DAG-binding sites within TASK channels. Examining the hypoxic ventilatory response (HVR) in these mice could offer crucial insights into the relationship between DAG signalling and chemoreceptors function.

To further investigate the relationship between metabolic inhibitors, MgATP levels, and TASK channels activity in type-1 cells, additional experiments are warranted. One technique may involve investigating the effects of metabolic inhibition on intracellular DAG levels. Another approach may involve examining the effects of metabolic inhibitors on TASK channels under elevated MgATP levels. If this blocks the inhibition of these channels by metabolic inhibitors, then the next step would be to apply a cocktail of inhibitors targeting DAG-metabolism under elevated MgATP conditions before

the application of metabolic inhibitors. These experiments can help determine whether the effects of metabolic inhibitors on TASK channels are mediated by reductions in MgATP levels and whether this is mediated by the activation of DAGK.

As established in my work, the competitive antagonism between DiC8 and halothane offers valuable insights into the molecular processes underlying the regulation of TASK channels by anaesthetic agents. Another aspect to consider is the possibility of developing strategies to alter DAG signals to minimise the effects of halothane on TASK channels. This has the potential to reduce the negative effects of volatile anaesthetics on breathing. Future research may also involve investigating the interactions between DAG and other volatile anaesthetics, such as isoflurane, to determine whether the effects of DAG are specific to halothane or extend to other anaesthetics. Further research may also involve examining the effects of halothane on TASK channels under conditions where DAG production is completely inhibited by the application of a cocktail of inhibitors targeting both PLC and PAPs activity.

Understanding how $G_{q/11}$ receptors, PLC signalling, particularly DAG, and TASK channels interact has the potential to elucidate the mechanisms underlying type-1 cells responses to hypoxia and other endogenous and exogenous stimuli.

# Appendix A

# Effects of endocytosis inhibitors on carotid body type-1 cell intracellular calcium and TASK channel responses to hypoxia and muscarinic stimulation

# 1. Introduction

As previously discussed in Chapter 1, ion channels can be inhibited by a change in their gating mechanisms or by a reduction in their surface expression (Wickman and Clapham, 1995). One proposed mechanism for the regulation of TASK channels by GPCRs is internalisation.

Internalisation of TASK1 channels in response to the activation of the muscarinic M1 receptor or TrkA, a receptor for nerve growth factor, was reported in adrenal medullary cells and its cloned cell line PC12. Dynasore, a dynamin inhibitor, reduced the inhibitory effects of muscarinic stimulation on the TASK 1 channel and prevented the translocation of TASK-like immunoreactive material from the plasma membrane to the cytoplasm (Matsuoka et al., 2013; Matsuoka and Inoue, 2017; Inoue et al., 2020). This implies that the internalisation of TASK1 by muscarinic stimulation depends on a clathrin-mediated mechanism.

Furthermore, the internalisation of TASK1 channels in response to muscarinic stimulation was shown to be PLC-PKC dependent. Inhibition of either PLC or PKC activity prevented TASK1 internalisation, emphasising the importance of the PLC-PKC pathway in mediating TASK1 internalisation. Once activated, PKC activates the non-receptor tyrosine kinase, Src, which phosphorylates a tyrosine residue at the C-terminus of TASK1. This phosphorylation induces a conformational change in the C-terminus of TASK1, exposing a dileucine motif downstream of the fourth transmembrane domain. This enables the binding of the adaptor protein AP-2 to the dileucine motif, which triggers clathrin-dependent endocytosis (Inoue et al., 2020). In contrast, the TASK3 channel has not been shown to internalise upon muscarinic

stimulation because its C-terminus lacks tyrosine phosphorylation sites (Matsuoka and Inoue, 2017).

This study investigated the involvement of TASK channel internalisation in mediating the hypoxic response of type-1 cells. To achieve this, we used two specific inhibitors of endocytosis, dynasore and MiTMAB. Dynasore and MiTMAB are well-known and widely used endocytosis inhibitors. They specifically target the GTPase activity of dynamin, a key protein involved in clathrin-mediated endocytosis. By blocking dynamin function, dynasore and MiTMAB effectively inhibit the formation of clathrin-coated vesicles and the internalisation of membrane proteins (Hill et al., 2004, 2005; Macia et al., 2006).

I started by examining the effects of dynasore and MiTMAB on $Ca^{2+}$ signalling as well as hypoxia- and muscarinic agonist-evoked $[Ca^{2+}]i$ rise in type-1 cells. Next I examined the effects of endocytosis inhibitors on TASK channel activity in these cells.

## 2. Methods

All experiments were performed in accordance with the UK Animals (Scientific Procedures) Act, 1986.

**Cell isolation:**

For the extended procedure refer to Chapter 2, Section 2.1.1. Briefly, carotid body bifurcations were dissected from neonatal rat pups (P11-P14). They were then digested enzymatically and mechanically which led to a single cell suspension. Primary cell cultures were plated onto coverslips pre-treated with poly-D-lysine and incubated for 2 hours. Recordings took place within 5-6 hours of plating.

**Electrophysiology:**

Cell-attached recordings were performed using an Axopatch 200B (Molecular Devices LLC, Sunnyvale, US). Sylgard-coated and fire-polished borosilicate pipettes (Harvard Apparatus Ltd., Kent, UK) were used. For the extended procedures, refer to Chapter 2. In short, coverslips containing isolated type-1 cells were placed in the recording chamber and continuously superfused with a warmed Tyrode solution. Tyrode solutions were continuously bubbled with normoxic (5% $CO_2$, balance air) or hypoxic gas mixture (5% $CO_2$, balance $N_2$). Seal formation was attempted with a borosilicate pipette containing a high $k^+$ solution (140 mM). Upon the formation of a good seal (> 5 GΩ), the Tyrode solution was switched to a high $K^+$ solution. Then a positive pipette potential of +100 mV was applied. Voltage clamp protocol, data acquisition, and data

analysis were performed using Spike 10 software (Cambridge Electronics Design, Cambridge, UK).
The background $K^+$ channel of type-1 cells exhibited inward currents with brief, flickering openings under the recording conditions of this study.

**Calcium imaging;**

The detailed method of calcium imaging is described in Chapter 2, Section 2.7. Indo-1 dye was excited by bialkali photomultiplier tubes (PMT) at 340 ± 5 nm and recorded at 405 and 495 nm. The PMT output was transmitted to a current to voltage converter then digitized by spike software (CED, Cambridge, UK).

The $Ca^{2+}$ transient was determined by calculating the absolute difference between the mean $[Ca^{2+}]i$ during control conditions and the average $[Ca^{2+}]i$ during exposure to hypoxia, methacholine chloride, and endocytosis inhibitors. This calculation was also performed for the combined application of endocytosis inhibitors with hypoxia or methacholine chloride, where the absolute difference between $[Ca^{2+}]i$ during hypoxia or methacholine chloride exposure and $[Ca^{2+}]i$ during the combined application of endocytosis inhibitors with hypoxia or methacholine chloride was computed. The statistical significance of the differences between the means of the responses was evaluated using student's t-tests. A p-value $<0.05$ was taken as statistically significant.

**Experimental protocol for the measurements of TASK channels activity in type-1 cells:**

Channel activity analysis involved 20-second segments of recordings, taken at least 10 seconds after any solution exchange. Quantification of single channel activity was defined by nPopen, which represents the product of the number of channels in the patch and the probability of a channel being open at any given time. To determine nPopen, an all-point histogram was constructed using a 20-second segment of data to identify the primary conductance state. A 50% opening threshold was then set for the nPopen analysis. Changes in channel activity were reported as either an increase or decrease in nPopen values relative to the control. The percentage change in nPopen was determined using the following formula:
Percentage change = ((nPopen under Condition A - nPopen under Control) / nPopen under Control) * 100

**Drugs:**

Following cell identification, type-1 cells were subjected to superfusion with Tyrode solution, both in the presence and absence of the drug under investigation, using the cells as their own controls. The drugs were applied to cells for a duration of 50-60 seconds, and a similar wash period followed the exposure to allow any reversible effects to subside. All drugs were appropriately reconstituted prior to dissolution in Tyrode solution. Collagenase was obtained from Worthington. Trypsin, culture media, dynasore, and MiTMAB were obtained from Sigma/Aldrich. The concentrations of the administered drugs were determined either based on the EC50 values specific to each drug, prior usage in similar studies, or a combination of both approaches.

**Statistical analysis of TASK channels recordings:**

N numbers denote separate recordings from a distinct cell/s on different coverslips. Mean normalised nPopen values were used to assess statistical significance by student t-tests. p value $< 0.05$ was taken as statistically significant.

# 3. Results

In this study, type-1 cells were identified based on visual inspection. Initially, individual cells or small clusters consisting of 2-3 cells with an approximate diameter of 5 μm were selected for further analysis. A short (>20 second) hypoxic stimulation was used to validate the cells' identity as type-1 cells. Cells that showed a distinctive rise in intracellular calcium levels $[Ca^{2+}]i$ in response to hypoxic challenge were selected for further examination.

## 3.1 Effects of endocytosis inhibitors on type-1 cells hypoxia and methacholine chloride evoked $[Ca^{2+}]i$ rise

We conducted a series of experiments using two selective inhibitors targeting dynamin to evaluate the effect of endocytosis inhibitors on hypoxia- and methacholine chloride (300 μM)-evoked $[Ca^{2+}]i$ rise. Dynasore and MiTMAB were applied to acutely isolated type-1 cells in two sets of experiments. Dynasore, a widely used dynamin inhibitor, was applied at a concentration of 60 μM. Dynasore had no effect on baseline levels of $[Ca^{2+}]i$ but completely blocked hypoxia and methacholine chloride (300 μM) evoked $[Ca^{2+}]i$ rise ($n=19$, $p<0.001$, $n=7$, $p=0.003$ respectively; see Figures 1A and B).

In addition to its inhibitory effects on hypoxia and methacholine chloride evoked $[Ca^{2+}]i$ rise, dynasore also exhibited an inhibitory effect on the high $K^+$ (100 mM)-evoked $[Ca^{2+}]i$ rise in type-1 cells. This suggests that dynasore may have some off-target effects on calcium signalling pathways beyond its specific inhibition of dynamin-mediated endocytosis.

To evaluate the specificity of the effects of dynasore, we conducted an additional experiment to investigate its impact on ML 365, a specific pore-blocker of TASK channels. ML365 (1 µM) induced a strong-reversible rise in intracellular $[Ca^{2+}]i$ from 55.17 ± 4.8 to 533.2 ± 103.5 nM (see Figures 1 A (iii) and B (iii), n= 10, $p<0.001$). Upon removal of ML365, $[Ca^{2+}]_i$ rapidly returned to baseline. Dynasore inhibited ML 365 induced $[Ca^{2+}]_i$ rise by 77.9 ± 9% (see Figures 1 A (iii) and B (iii), n=10, p=0.002). This implies that dynasore could have either caused a broad inhibition of $Ca^{2+}$ signalling or potentially enhanced the surface expression of TASK channels under normal conditions.

To further investigate the effects of endocytosis inhibitors on $Ca^{2+}$ responses in type-1 cells, we applied another specific inhibitor of endocytosis, MiTMAB. MiTMAB, known for its ability to interfere with endocytic processes, was applied at a concentration of 30 µM. Interestingly, we observed that MiTMAB also had no effect on baseline $[Ca^{2+}]i$ levels. However, it significantly inhibited the hypoxia-evoked rise in $[Ca^{2+}]i$ (see Figures 2 A and B: $\Delta$ $[Ca^{2+}]i$ hypoxia vs. hypoxia plus MiTMAB: 519.4 ± 195.5 vs. 41.9 ± 13.9 nM; n = 10, $p < 0.001$). MiTMAB had no effect on the high $K^+$ evoked $[Ca^{2+}]i$ rise, and its effect on hypoxia was irreversible, suggesting a specific effect on the hypoxia-induced $[Ca^{2+}]i$ rise and a sustained interference with endocytic processes.

**Figure 1: Effects of dynasore (60 µM) on [$Ca^{2+}$]i in type-1 cells.** Recordings of **[**$Ca^{2+}$] in isolated type-1 cells showing responses to hypoxia (i), methacholine chloride (300 µM) (ii), and ML 365 (1µM) (iii) in control and in the presence dynaosre **(A)**. Quantitative effects of dynasore on hypoxia (i), ML 365 (ii), and methacholine chloride (iii) evoked [$Ca^{2+}$]i rise. Note that dynasore inhibited the high $K^+$ (100 mM) evoked [$Ca^{2+}$]i rise. N numbers denote separate recordings from a distinct cell/s on different coverslips. Error bars indicate S.E.M. The signal was saturated in response to high $K^+$, resulting in an abrupt truncation of the signal.

**A**

(i)

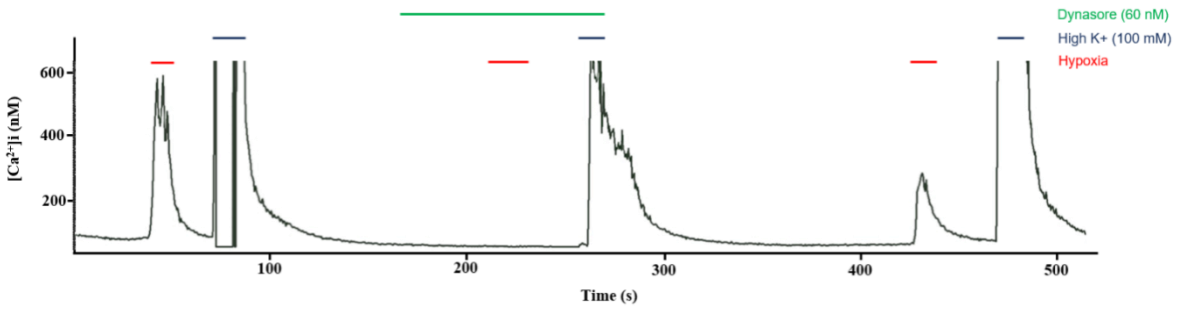


(ii)

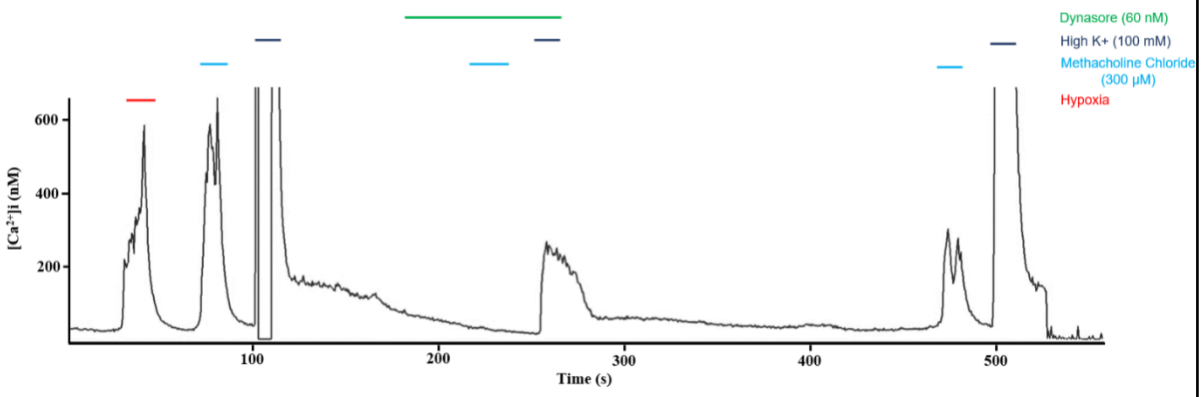

(iii)

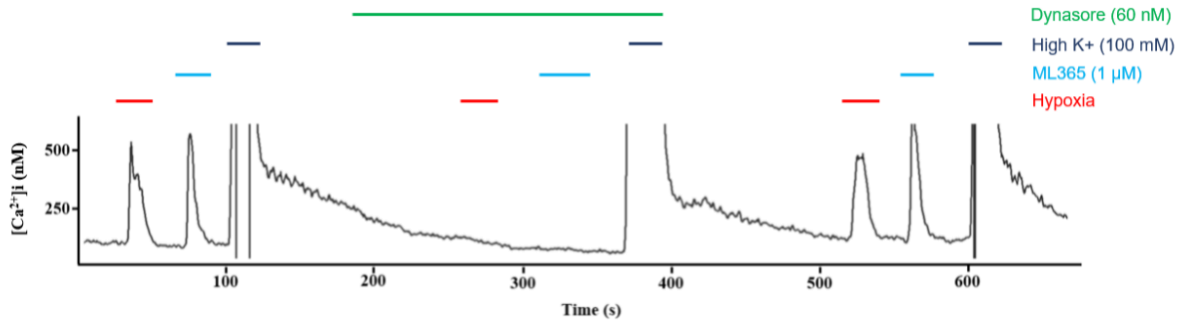
Dynasore (60 nM)
High K+ (100 mM)
ML365 (1 µM)
Hypoxia
[Ca2+]i (nM)
500
250
100
200
300
400
500
600
Time (s)

**B**

(i)

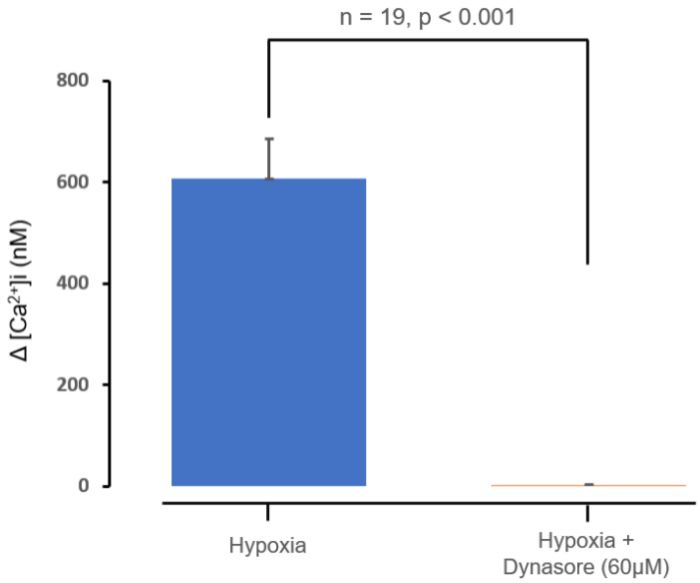
n = 19, p < 0.001
800
600
400
200
0
Δ [Ca2+]i (nM)
Hypoxia
Hypoxia +
Dynasore (60µM)

(ii)

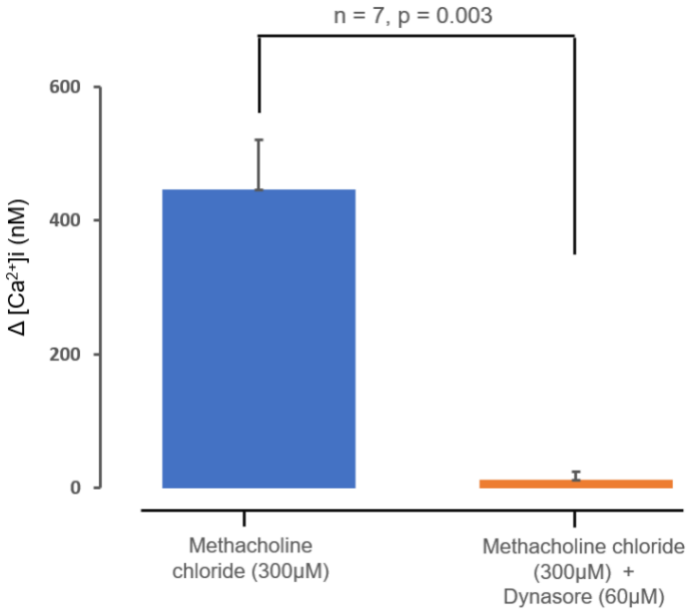
n = 7, p = 0.003
600
400
200
0
Δ [Ca2+]i (nM)
Methacholine
chloride (300µM)
Methacholine chloride
(300µM) +
Dynasore (60µM)

(ii)

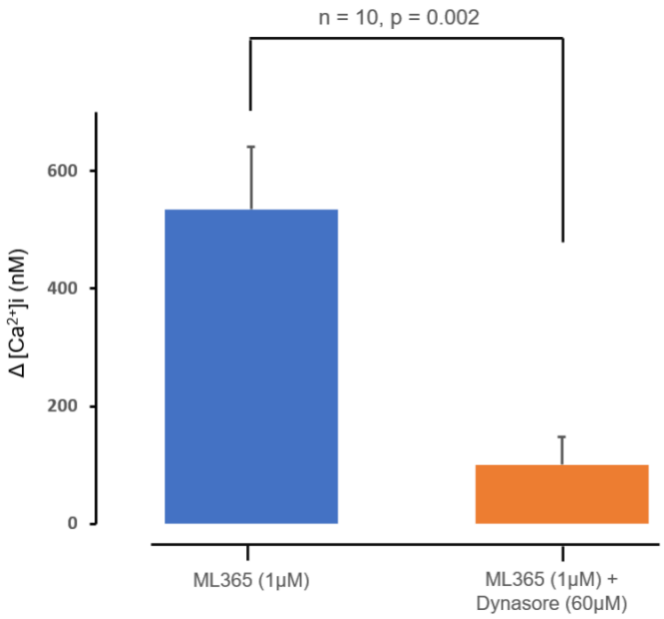
n = 10, p = 0.002
600
400
200
0
Δ [Ca2+]i (nM)
ML365 (1μM)
ML365 (1μM) +
Dynasore (60μM)

**Figure 2: Effects of MiTMAB (30 µM) on [$Ca^{2+}$]i in type-1 cells.** Recordings of **[**$Ca^{2+}$] in isolated type-1 cells showing responses to hypoxia in control and in the presence of MiTMAB **(A)**. Quantitative effects of MiTMAB on hypoxia evoked [$Ca^{2+}$]i. N numbers denote separate recordings from a distinct cell/s on different coverslips. Error bars indicate S.E.M. The signal was saturated in response to high $K^+$, resulting in an abrupt truncation of the signal.

**A**

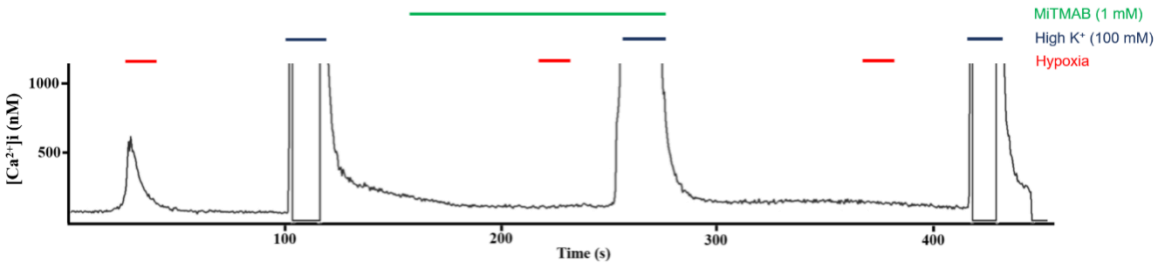


**B**

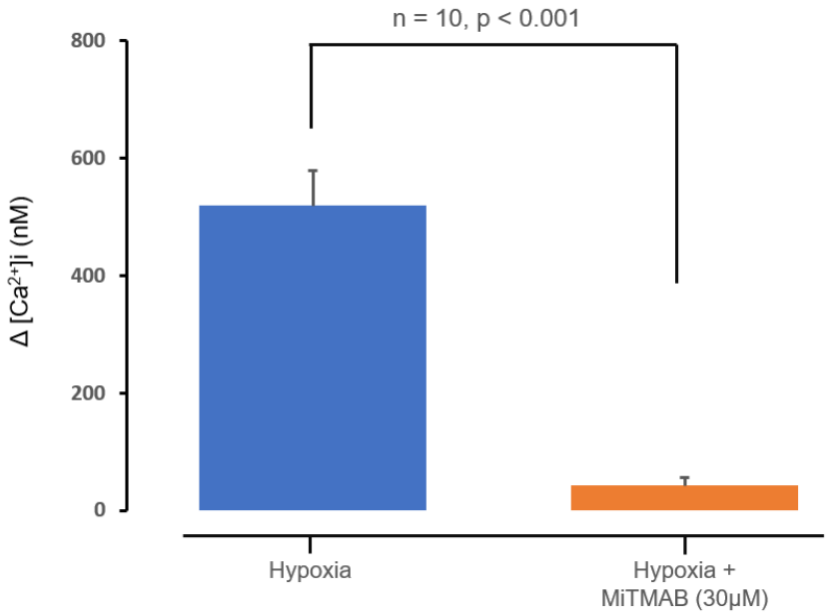

## 3.2 Effects of endocytosis inhibitors on TASK channels activity in rat carotid body type-1 cells

In this study, I performed cell-attached patch clamp recordings on a total of nine acutely isolated type-1 cells. The classification of cells as type-1 cells was based on their response to hypoxia, characterised by the inhibition of background TASK-like $K^+$ currents. Only cells that exhibited this specific response to a brief hypoxic stimulus were included in this study.

Unexpectedly, the administration of dynasore (60 µM) and MiTMAB (30 µM) resulted in a moderate and reversible inhibition of TASK channel activity in type-1 cells. Dynasore caused a reduction of 48.2 ± 4% (n=5, p=0.03), while MiTMAB resulted in a decrease of 42.1 ± 5.7% (n=4, p=0.03) in channel activity. Representative traces demonstrating the effects of dynasore and MiTMAB on TASK channels are shown in Figure 3A. Figure 3B (i and ii) displays representative all-points histograms illustrating the impact of dynasore and MiTMAB on channel activity. It is notable that both dynasore and MiTMAB led to a reduction in the frequency of channel currents at all levels. These findings were surprising as they deviated from the anticipated response of simple endocytosis inhibitors, suggesting the possibility of off-target effects induced by these agents. Consequently, we did not pursue further examination of their effects on TASK channels.

**Figure 3 Effects of dynasore (60 µM) and MiTMAB (30 µM) on TASK channels activity in rat carotid body type-1 cell.**

Three representative traces of single-channel recordings for control (top trace), dynasore (i) or MiTMAB (ii) (middle trace), and post washout (bottom trace) **(A)**. Representative all-points histogram from the same recordings, control in blue and dynasore (i) or MiTMAB (ii) in red. Histogram was generated from a selected 20s of both control and dynasore and MiTMAB application. Bin-width was 0.1 pA **(B)**. Comparison of the inhibitory effects of dynaosre (i) and MiTMAB (ii) on channel activity. Data are expressed as percentage changes in nPopen in the presence of dynasore or MiTMAB relative to the control (means ± SEM) **(C)**. The traces are recorded with a pipette potential of +100 mV, 140 mM $K^+$ in pipette solution and 100 mM $K^+$ in Tyrode solution.

Bar shows 0.02-0.05 s timescale; vertical bar shows 10 pA current.

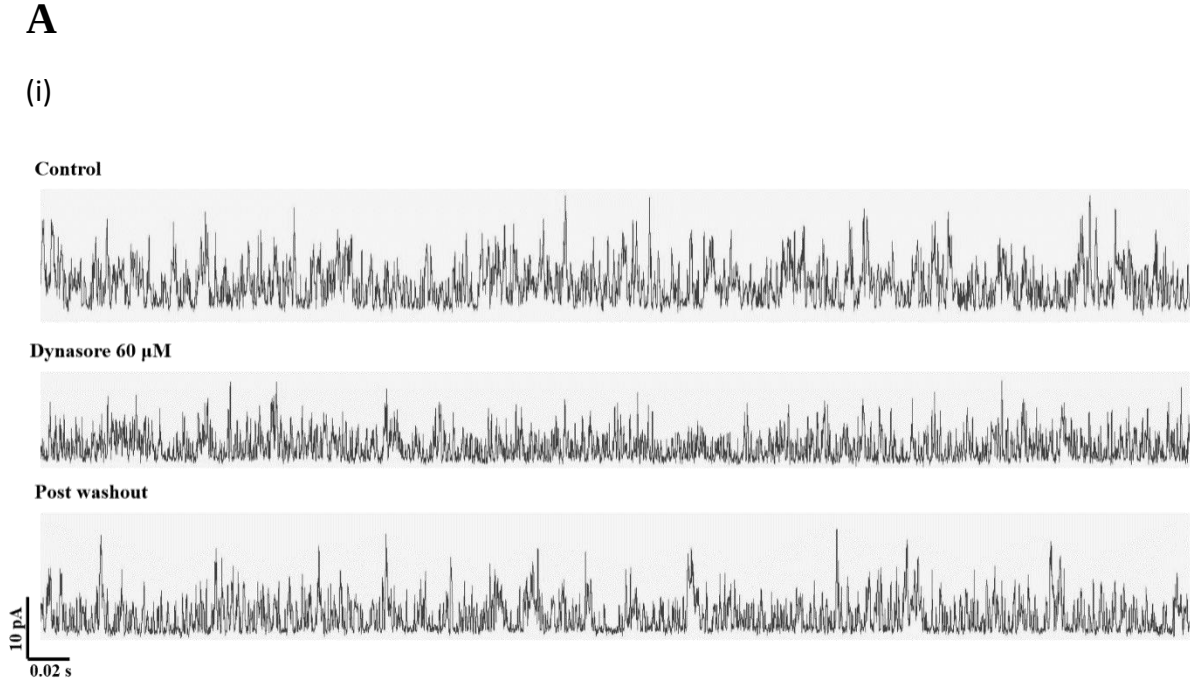

(ii)

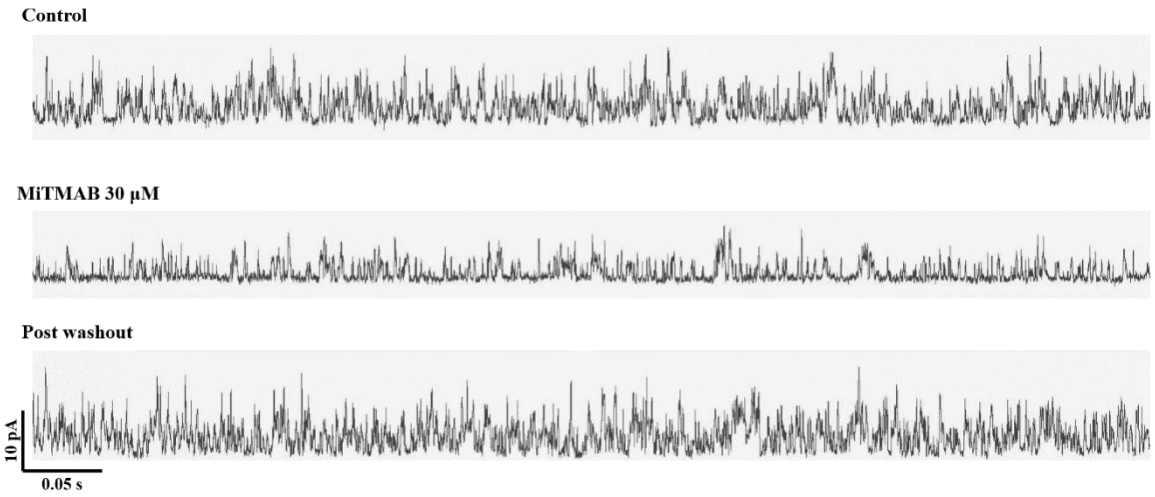
Control
MiTMAB 30 µM
Post washout
10 pA
0.05 s

**B**

(i)

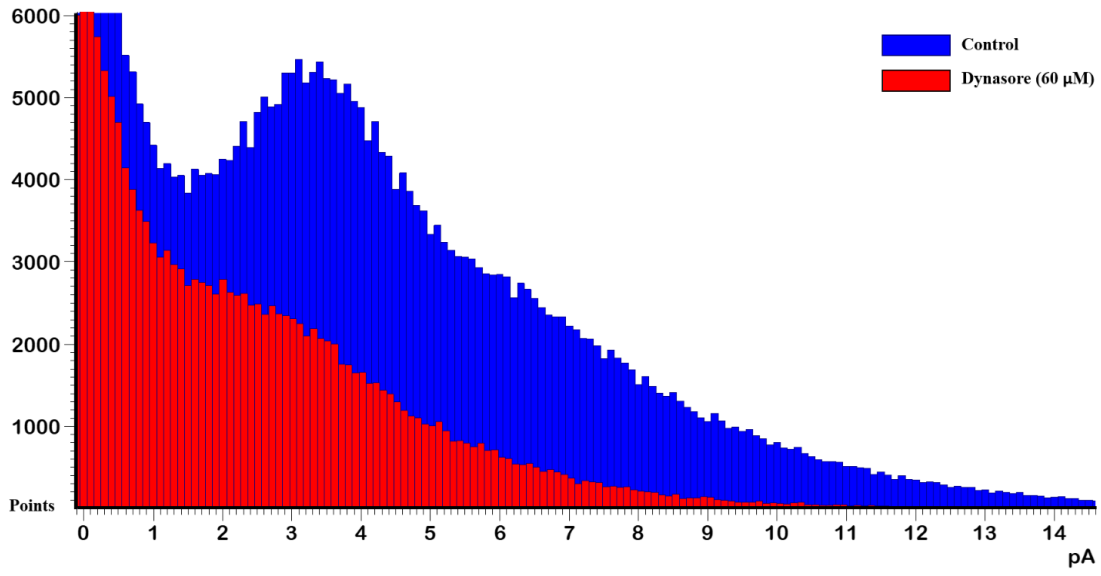
6000
5000
4000
3000
2000
1000
Points
0
1
2
3
4
5
6
7
8
9
10
11
12
13
14
pA
Control
Dynasore (60 µM)

(ii)

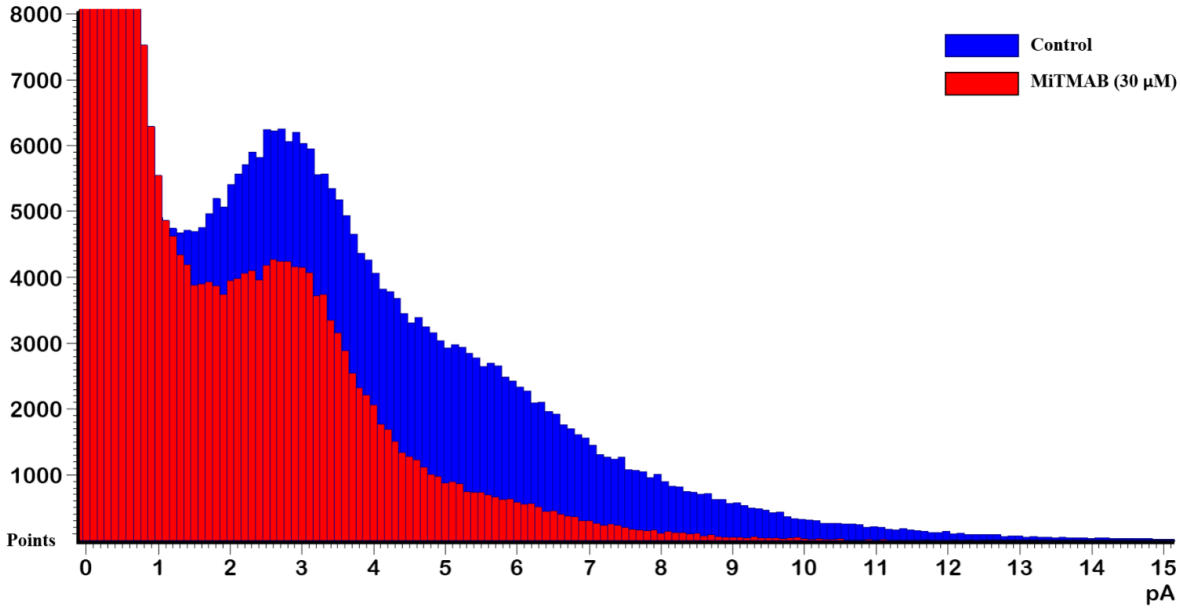
8000
7000
6000
5000
4000
3000
2000
1000
Points
0 1 2 3 4 5 6 7 8 9 10 11 12 13 14 15
pA
Control
MiTMAB (30 µM)

**C**

(i)

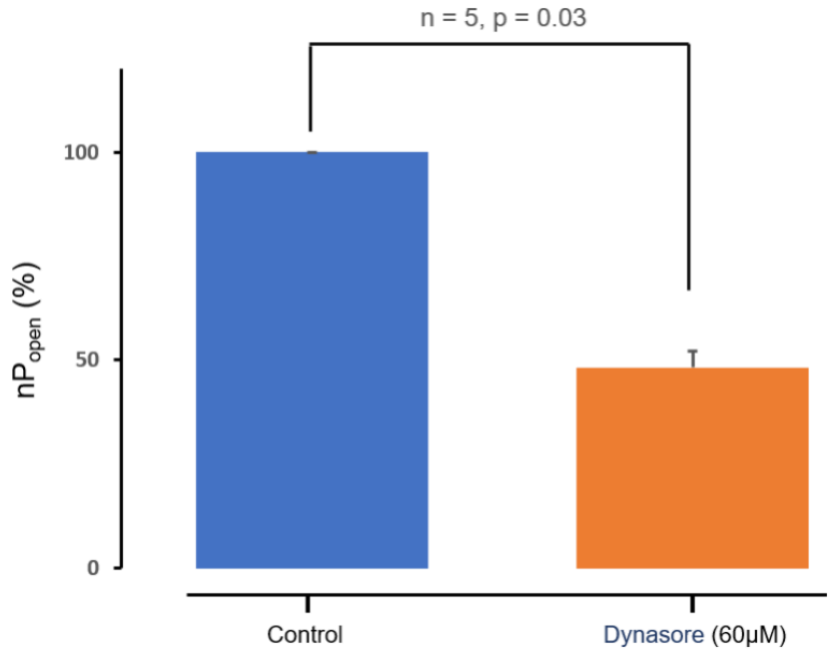
n = 5, p = 0.03
100
50
0
nP$_{open}$ (%)
Control
Dynasore (60µM)

(ii)

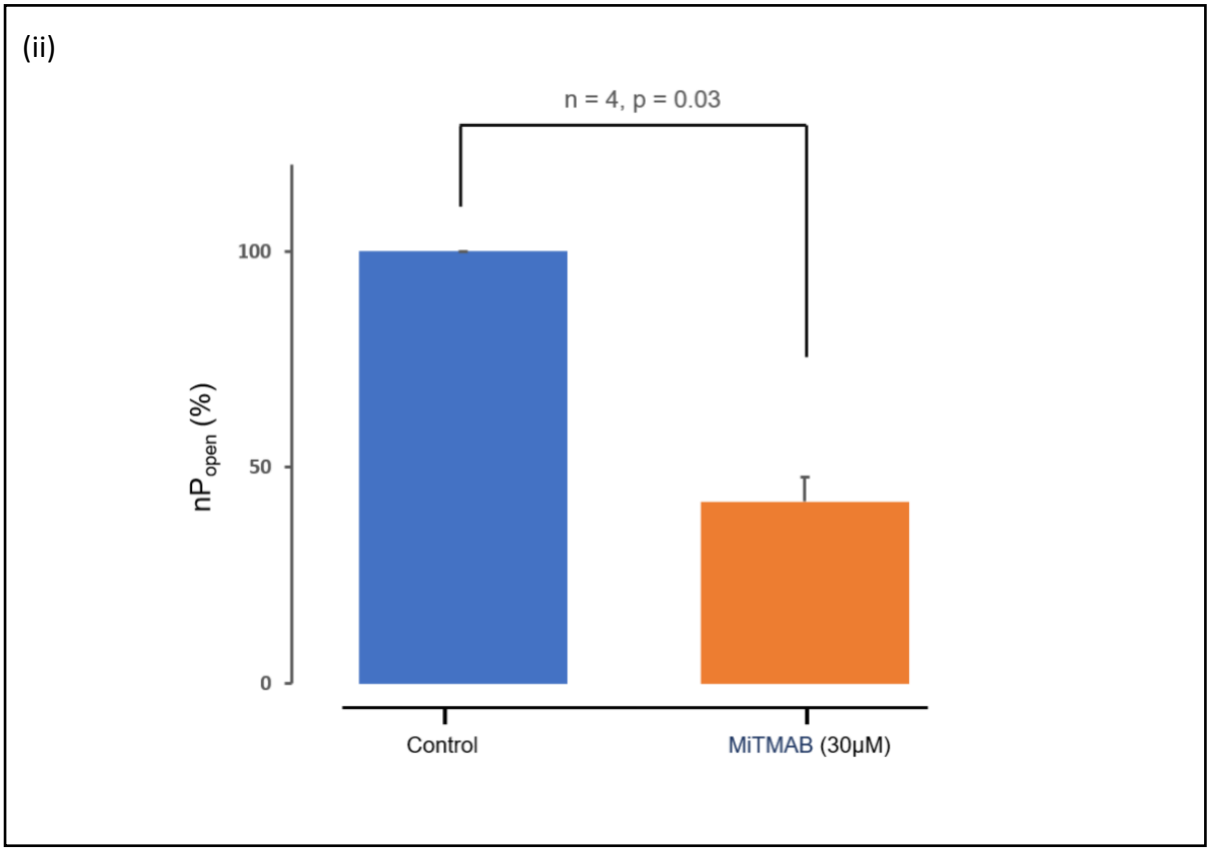

# 4. Discussion

The findings of this chapter demonstrate that dynasore and MiTMAB both blocked hypoxia and methacholine chloride-evoked $[Ca^{2+}]i$ rise and inhibited TASK channels activity in carotid body type-1 cells. These observations, and others, are, however, difficult to reconcile with a model in which Gq-protein coupled receptors and hypoxia simply regulate the surface expression of TASK channels by controlling endocytosis. Firstly, dynamin may be involved in a number of different cellular processes not just endocytosis, and secondly, there is increasing concern over the specificity of some of the drugs used in studying dynamin function. This poses challenges in interpreting the observed results and necessitates further investigation and clarification as to the precise mechanisms of action of these drugs.

My study revealed that both dynasore and MiTMaB effectively blocked hypoxia- and methacholine chloride-evoked $[Ca^{2+}]i$ rise in type-1 cells. This is consistent with the involvement of internalisation of ion channels in mediating the effects of muscarinic agonists, as previously suggested by Matuoka and Inoue (2017). However, it is noteworthy that dynasore also inhibited the $Ca^{2+}$ response to high $K^+$, suggesting a broader impact on $Ca^{2+}$ signalling. Moreover, dynasore inhibited the $Ca^{2+}$ response to ML 365, a specific pore blocker of TASK channels, suggesting that dynasore may increase the surface expression of TASK channels under resting conditions or exert a non-specific depressive effect on $Ca^{2+}$ signalling in type-1 cells. These findings indicate that the effects of dynasore cannot be solely attributed to a simple inhibition of endocytosis and that additional mechanisms may be involved. Indeed, measurement of TASK channel activity in cell attached patches demonstrated a paradoxical inhibition of channel activity in the presence of dynasore.

Previous studies have reported the potential side effects of dynasore. Preta et al. (2015) found that apart from its inhibitory effects on dynamin GTPase activity, dynasore can also have broader impacts on cellular processes such as cholesterol metabolism, lipid raft organization, and actin dynamics.

As a dynamin inhibitor, dynasore can also affect the activity of the dynamin-related protein-1 (Dpr1) at the mitochondrial membrane. Dpr1 is a key protein involved in regulating mitochondrial fission (Reddy et al., 2014). The activity of this protein has been shown to be inhibited by the application of dynasore, which affects mitochondrial function and ROS production (Gao et al., 2013). Furthermore, dynasore has been shown to maintain cellular ATP content in stressed cardiomyocytes (Gao et al., 2013). Additional effects of dynasore include direct effects on $Ca^{2+}$ channels (Ahmed et al., 2023).

Another unexplained finding of this study is that MiTMAB exhibited an irreversible inhibitory effect on hypoxia-evoked $[Ca^{2+}]i$ entry in type-1 cells while not affecting high $K^+$ evoked $[Ca^{2+}]i$ rise. These results could support the involvement of ion channel endocytosis in mediating hypoxia-evoked $[Ca^{2+}]i$ rise in type-1 cells. However, as with dynasore, MiTMAB also inhibited TASK channels activity in cell attached patches, which contradicts the expectation that inhibition of endocytosis should increase cell surface expression of TASK channels. Taking together, these findings suggest that MiTMAB may have additional effects independent of its role in inhibiting endocytosis.

MiTMAB was initially identified through a screening process aimed at identifying molecules with inhibitory effects on dynamin (Hill et al., 2004, 2005). MiTMAB specifically inhibits the GTPase activity of dynamin, a key protein involved in the formation and scission of clathrin-coated vesicles during endocytosis. By impairing dynamin's GTPase activity, MiTMAB prevents the internalisation of membrane proteins and induces changes in membrane

dynamics. These, in turn, have downstream effects on various cellular processes, including cell signalling, receptor trafficking, and surface expression of ion channels. Similar to many other drugs, MiTMAB is associated with its own set of side effects. Notably, studies have demonstrated that MiTMAB reduce $Ca^{2+}$ entry in chromaffin cells, suggesting a potential impact on $Ca^{2+}$ channels (Quan et al., 2007).

Another issue pertaining to the effects of both dynasore and MiTMAB arises from the methodological approach used in this study. The formation of a cell-attached patch can potentially disrupt the normal endocytosis process; therefore, evaluating the effects of endocytosis inhibitors in this context does not necessarily reflect the role of ion channel internalisation under normal conditions. Additionally, these inhibitors might decrease single channel activity while simultaneously increasing the number of ion channels on the cell surface. Consequently, perforated patch whole cell recordings may be a more effective method for evaluating ion channels internalisation.

In conclusion, this study investigated the impact of endocytosis inhibitors on $Ca^{2+}$ responses and TASK channels activity of type-1 cell. However, the observed side effects of the pharmacological agents used in this study have hindered my ability to draw definitive conclusions regarding the involvement of ion channel endocytosis in the hypoxia signalling cascade in type-1 cells.

### 4.1 Suggestions for future research:

Because dynasore and MiTMAB exhibited off-target effects in this study, it would be valuable to explore the effects of other more specific endocytosis inhibitors on type-1 cell responses in perforated whole cell patch clamp recordings. Additionally, monitoring the real-time dynamics of ion channel

endocytosis in response to hypoxia using live-cell imaging techniques can provide valuable insights into the temporal and spatial aspects of endocytic processes in type-1 cells.

# References


Acker, Helmut. (1994). Cellular Oxygen Sensors. Annals of the New York Academy of Sciences, 718(1), 3-12.

Ahmed, A., Trezza, A., Gentile, M., Paccagnini, E., Panti, A., Lupetti, P., Spiga, O., Bova, S., & Fusi, F. (2023). Dynamin-independent $Ca_V1.2$ and $K_{Ca}1.1$ channels regulation and vascular tone modulation by the mitochondrial fission inhibitors dynasore and dyngo-4a. European journal of pharmacology, 951, 175786.

Allen A. M. (1998). Angiotensin AT1 receptor-mediated excitation of rat carotid body chemoreceptor afferent activity. The Journal of physiology, 510 ( Pt 3)(Pt 3), 773–781.

Andres-Enguix, Isabelle, Caley, Alex, Yustos, Raquel, Schumacher, Mark A., Spanu, Pietro D., Dickinson, Robert, Maze, Mervyn, and Franks, Nicholas P. (2007). Determinants of the anesthetic sensitivity of two-pore domain acid-sensitive potassium channels: molecular cloning of an anesthetic-activated potassium channel from Lymnaea stagnalis. Journal of Biological Chemistry, 282(29), 20977-20990.

Anichkov, S.V. & Belen'kü, M.L. (1963) Pharmacology of the Carotid Body Chemoreceptors, Pergamon Press, Oxford.

Arias-Mayenco, I., González-Rodríguez, P., Torres-Torrelo, H., Gao, L., Fernández-Agüera, M. C., Bonilla-Henao, V., Ortega-Sáenz, P., & López-Barneo, J. (2018). Acute $O_2$ Sensing: Role of Coenzyme $QH_2$/Q Ratio and Mitochondrial ROS Compartmentalization. Cell metabolism, 28(1), 145–158.e4.

Badola, P., & Sanders, C. R., 2nd (1997). Escherichia coli diacylglycerol kinase is an evolutionarily optimized membrane enzyme and catalyzes direct phosphoryl transfer. The Journal of biological chemistry, 272(39), 24176–24182.

Bairam, A., Joseph, V., Lajeunesse, Y., & Kinkead, R. (2006). Developmental pattern of M1 and M2 muscarinic gene expression and receptor levels in cat carotid body, petrosal and superior cervical ganglion. Neuroscience, 139(2), 711–721.

Barbé, C., Al-Hashem, F., Conway, A. F., Dubuis, E., Vandier, C., & Kumar, P. (2002). A possible dual site of action for carbon monoxide-mediated chemoexcitation in the rat carotid body. The Journal of Physiology, 543(3), 933-945.

Barnett, S, Mulligan, E, Wagerle, L. C, & Lahiri, S. (1988). Measurement of carotid body blood flow in cats by use of radioactive microspheres. Journal of Applied Physiology, 65(6), 2484-2489.

Bayliss, Douglas A, Talley, Edmund M, Sirois, Jay E, & Lei, Qiubo. (2001). TASK-1 is a highly modulated pH-sensitive ‘leak’ K channel expressed in brainstem respiratory neurons. Respiration Physiology, 129(1), 159-174.

Berg, Allison P, Talley, Edmund M, Manger, Jules P, & Bayliss, Douglas A. (2004). Motoneurons Express Heteromeric TWIK-Related Acid-Sensitive K (TASK) Channels Containing TASK-1 (KCNK3) and TASK-3 (KCNK9) Subunits. The Journal of Neuroscience, 24(30), 6693-6702.

Bernardini, A., Brockmeier, U., Metzen, E., Berchner-Pfannschmidt, U., Harde, E., Acker-Palmer, A., Papkovsky, D., Acker, H., & Fandrey, J. (2015). Type I cell ROS kinetics under hypoxia in the intact mouse carotid body

ex vivo: a FRET-based study. American journal of physiology. Cell physiology, 308(1), C61–C67.

Besana, Alessandra, Barbuti, Andrea, Tateyama, Miyuki A., Symes, Aviva J., Robinson, Richard B., & Feinmark, Steven J. (2004). Activation of Protein Kinase C ϵ Inhibits the Two-pore Domain K Channel, TASK-1, Inducing Repolarization Abnormalities in Cardiac Ventricular Myocytes. The Journal of Biological Chemistry, 279(32), 33154-33160.

Biscoe, T. J., Bradley, G. W., & Purves, M. J. (1970). The relation between carotid body chemoreceptor discharge, carotid sinus pressure and carotid body venous flow. The Journal of Physiology, 208(1), 99-120.

Bista, P., Pawlowski, M., Cerina, M., Ehling, P., Leist, M., Meuth, P., Aissaoui, A., Borsotto, M., Heurteaux, C., Decher, N., Pape, H. C., Oliver, D., Meuth, S. G., & Budde, T. (2015). Differential phospholipase C-dependent modulation of TASK and TREK two-pore domain K+ channels in rat thalamocortical relay neurons. The Journal of physiology, 593(1), 127–144.

Boroda, S., Niccum, M., Raje, V., Purow, B. W., & Harris, T. E. (2017). Dual activities of ritanserin and R59022 as DGKα inhibitors and serotonin receptor antagonists. Biochemical pharmacology, 123, 29–39.

Boyd, D. F., Millar, J. A., Watkins, C. S., & Mathie, A. (2000). The role of Ca2+ stores in the muscarinic inhibition of the K+ current IK(SO) in neonatal rat cerebellar granule cells. The Journal of physiology, 529 Pt 2(Pt 2), 321–331.

Brohawn, Stephen G. (2015). How ion channels sense mechanical force: Insights from mechanosensitive K2P channels TRAAK, TREK1, and TREK2. Annals of the New York Academy of Sciences, 1352(1), 20-32.

Brohawn, Stephen G., Campbell, Ernest B., & MacKinnon, Roderick. (2013). Domain-swapped chain connectivity and gated membrane access in a Fab-mediated crystal of the human TRAAK $K^+$ channel. Proceedings of the National Academy of Sciences - PNAS, 110(6), 2129-2134.

Brohawn, Stephen G., Campbell, Ernest B., & MacKinnon, Roderick. (2014). Physical mechanism for gating and mechanosensitivity of the human TRAAK K channel. Nature (London), 516(7529), 126-130.

Brohawn, Stephen G., Del Mármol, Josefina, & MacKinnon, Roderick. (2012). Crystal Structure of the Human K2P TRAAK, a Lipid-and Mechano-Sensitive $K^+$ Ion Channel. Science (American Association for the Advancement of Science), 335(6067), 436-441.

Buckler KJ, Honore E (2005) The lipid-activated two-pore domain K+ channel TREK-1 is resistant to hypoxia: implication for ischaemic neuroprotection. Journal Of Physiology, 562, 213-222.

Buckler KJ, Vaughan-Jones RD (1993) Effects of acidic stimuli on intracellular calcium in isolated type I cells of the neonatal rat carotid body. Pflügers Archiv - European Journal Of Physiology, 425, 22-27.

Buckler KJ, Vaughan-Jones RD (1994a) Effects of hypoxia on membrane potential and intracellular calcium in rat neonatal carotid body type I cells. Journal of Physiology, 476, 423-428.

Buckler KJ, Vaughan-Jones RD (1994b) Effects of hypercapnia on membrane potential and intracellular calcium in rat carotid body type I cells. Journal Of Physiology, 478, 157-171.

Buckler, K J. (1997). A novel oxygen-sensitive potassium current in rat carotid body type I cells. The Journal of Physiology, 498(Pt 3), 649-662.

Buckler, K. J., & Honoré, E. (2005). The lipid-activated two-pore domain K+ channel TREK-1 is resistant to hypoxia: implication for ischaemic neuroprotection. The Journal of physiology, 562(Pt 1), 213–222.

Buckler, K. J., & Vaughan-Jones, R. D. (1998). Effects of mitochondrial uncouplers on intracellular calcium, pH and membrane potential in rat carotid body type I cells. The Journal of Physiology, 513(3), 819-833.

Buckler, K. J., Williams, B. A., & Honore, E. (2000). An oxygen-, acid-and anaesthetic-sensitive TASK-like background potassium channel in rat arterial chemoreceptor cells. The Journal of physiology, 525(Pt 1), 135.

Buckler, K., & Honoré, E. (2004). Molecular strategies for studying oxygen-sensitive K+ channels. In Methods in enzymology (Vol. 381, pp. 233-256). Academic Press.

Buckler, Keith J. (2015). TASK channels in arterial chemoreceptors and their role in oxygen and acid sensing. Pflügers Archiv, 467(5), 1013-1025.

Buckler, Keith J., & Turner, Philip J. (2013). Oxygen sensitivity of mitochondrial function in rat arterial chemoreceptor cells. The Journal of Physiology, 591(14), 3549-3563.

Buckler, Keith. (2012). Effects of exogenous hydrogen sulphide on calcium signalling, background (TASK) K channel activity and mitochondrial function in chemoreceptor cells. Pflugers Archiv : European Journal of Physiology, 463, Pflugers Archiv : European journal of physiology, 2012, Vol.463.

Campanucci, Verónica A, & Nurse, Colin A. (2007). Autonomic innervation of the carotid body: Role in efferent inhibition. Respiratory Physiology & Neurobiology, 157(1), 83-92.

Carpenter, E., & Peers, C. (1997). Swelling- and cAMP-activated Cl- currents in isolated rat carotid body type I cells. The Journal of Physiology, 503(Pt 3), 497-511.

Carpenter, Elisabeth, & Peers, Chris. (2001). A standing Na conductance in rat carotid body type I cells. Neuroreport, 12(7), 1421-1425.

Chang, A. J., Kim, N. S., Hireed, H., de Arce, A. D., Ortega, F. E., Riegler, J., Madison, D. V., & Krasnow, M. A. (2018). Chang et al. reply. Nature, 561(7724), E41.

Chang, A. J., Ortega, F. E., Riegler, J., Madison, D. V., & Krasnow, M. A. (2015). Oxygen regulation of breathing through an olfactory receptor activated by lactate. Nature, 527(7577), 240-244.

Chemin, J., Girard, C., Duprat, F., Lesage, F., Romey, G., & Lazdunski, M. (2003). Mechanisms underlying excitatory effects of group I metabotropic glutamate receptors via inhibition of 2P domain K+ channels. The EMBO journal, 22(20), 5403-5411.

Chen, Xiangdong, Talley, Edmund M., Patel, Nitin, Gomis, Ana, McIntire, William E., Dong, Biwei, Viana, Félix, Garrison, James C., and Bayliss, Douglas A. (2006). Inhibition of a background potassium channel by Gq protein α-subunits. Proceedings of the National Academy of Sciences, 103(9), 3422-3427.

Coburn, Craig A., Luo, Yunfu, Cui, Mingxiang, Wang, Jiabing, Soll, Richard, Dong, Jingchao, Hu, Bin, Lyon, Michael A., Santarelli, Vincent P., Kraus, Richard L., Gregan, Yun, Wang, Yi, Fox, Steven V., Binns, Jacquelyn, Doran, Scott M., Reiss, Duane R., Tannenbaum, Pamela L., Gotter, Anthony L., Meinke, Peter T., and Renger, John J. (2012). Discovery of a pharmacologically active antagonist of the two-pore-

domain potassium channel K2P9. 1 (TASK-3). ChemMedChem, 7(1), 123-133.

Conde, S. V., Monteiro, E. C., Rigual, R., Obeso, A., & Gonzalez, C. (2012). Hypoxic intensity: a determinant for the contribution of ATP and adenosine to the genesis of carotid body chemosensory activity. Journal of applied physiology (Bethesda, Md. : 1985), 112(12), 2002–2010.

Conway, Kevin E., and Cotten, Joseph F. (2012). Covalent modification of a volatile anesthetic regulatory site activates TASK-3 (KCNK9) tandem-pore potassium channels. Molecular pharmacology, 81(3), 393-400.

Cotten, J. F. (2013). TASK-1 (KCNK3) and TASK-3 (KCNK9) tandem pore potassium channel antagonists stimulate breathing in isoflurane anesthetized rats. Anesthesia and analgesia, 116(4).

Czirják, G., & Enyedi, P. (2002). Formation of functional heterodimers between the TASK-1 and TASK-3 two-pore domain potassium channel subunits. Journal of Biological Chemistry, 277(7), 5426-5432.

Czirják, G., Petheo, G. L., Spät, A., & Enyedi, P. (2001). Inhibition of TASK-1 potassium channel by phospholipase C. American Journal of Physiology-Cell Physiology, 281(2), C700-C708.

Czirják, Gábor, & Enyedi, Péter. (2003). Ruthenium Red Inhibits TASK-3 Potassium Channel by Interconnecting Glutamate 70 of the Two Subunits. Molecular Pharmacology, 63(3), 646-652.

Czirják, Gábor, Fischer, Tamás, Spät, András, Lesage, Florian, & Enyedi, Péter. (2000). TASK (TWIK-related acid-sensitive K channel) is expressed in glomerulosa cells of rat adrenal cortex and inhibited by angiotensin II. Molecular Endocrinology (Baltimore, Md.), 14(6), 863-874.

Dallas, M.L., Scragg, J.L., Wyatt, C.N., Ross, F., Hardie, D.G., Evans, A.M., & Peers, C. (2009). Modulation of O2 Sensitive K Channels by AMP-activated Protein Kinase. In Advances in Experimental Medicine and Biology (Vol. 648, Advances in Experimental Medicine and Biology, pp. 57-63). Dordrecht: Springer Netherlands.

Daly, M. (1997). Peripheral arterial chemoreceptors and respiratory-cardiovascular integration (Monographs of the Physiological Society ; 46). Oxford: Clarendon.

Daly, M. De Burgh, Lambertsen, C. J., & Schweitzer, A. (1954). Observations on the volume of blood flow and oxygen utilization of the carotid body in the cat. The Journal of Physiology, 125(1), 67-89.

Dasso, L. L., Buckler, K. J., & Vaughan-Jones, R. D. (1997). Muscarinic and nicotinic receptors raise intracellular Ca2+ levels in rat carotid body type I cells. The Journal of physiology, 498 ( Pt 2)(Pt 2), 327–338.

Davies, R.O., Edwards Jr, M.W., & Lahiri, S. (1982). Halothane depresses the response of carotid body chemoreceptors to hypoxia and hypercapnia in the cat. Anesthesiology (Philadelphia), 57(3), 153-159.

De Kock, L.L, & Dunn, A.E.G. (1966). AN ELECTRON MICROSCOPE STUDY OF THE CAROTID BODY. Cells, Tissues, Organs, 64(1-3), 163-178.

De Kock, L.L. (1954). THE INTRA-GLOMERULAR TISSUES OF THE CAROTID BODY. Cells, Tissues, Organs, 21(2), 101-116.

Decher, Niels, Rinné, Susanne, Bedoya, Mauricio, Gonzalez, Wendy, & Kiper, Aytug K. (2021). Molecular Pharmacology of K2P Potassium Channels. Cellular Physiology and Biochemistry, 55(3), 87-107.

Decher, Niels, Wemhöner, Konstantin, Rinné, Susanne, Netter, Michael F, Zuzarte, Marylou, Aller, Maria I, Kaufmann, Susann G, Li, Xian Tao, Meuth, Sven G, Daut, Jürgen, Sachse, Frank B, and Maier, Sebastian K.G. (2011). Knock-out of the potassium channel TASK-1 leads to a prolonged QT interval and a disturbed QRS complex. Cellular Physiology and Biochemistry, 28(1), 77-86.

Ding, Yanfeng, Li, Yu-Long, & Schultz, Harold D. (2011). Role of blood flow in carotid body chemoreflex function in heart failure. The Journal of Physiology, 589(1), 245-258.

Dong, Yin Yao, Pike, Ashley C. W., Mackenzie, Alexandra, McClenaghan, Conor, Aryal, Prafulla, Dong, Liang, Quigley, Andrew, Grieben, Mariana, Goubin, Solenne, Mukhopadhyay, Shubhashish, Ruda, Gian Filippo, Clausen, Michael V., Cao, Lishuang, Brennan, Paul E., Burgess-Brown, Nicola A., Sansom, Mark S. P., Tucker, Stephen J., and Carpenter, Elisabeth P. (2015). K2P channel gating mechanisms revealed by structures of TREK-2 and a complex with Prozac. Science, 347(6227), 1256-1259.

Duchen, M R, & Biscoe, T J. (1992). Mitochondrial function in type I cells isolated from rabbit arterial chemoreceptors. The Journal of Physiology, 450(1), 13-31.

Duchen, M R, & Biscoe, T J. (1992). Relative mitochondrial membrane potential and [Ca2 ]i in type I cells isolated from the rabbit carotid body. The Journal of Physiology, 450(1), 33-61.

Duchen, M.R., Caddy, K.W.T., Kirby, G.C., Patterson, D.L., Ponte, J., & Biscoe, T.J. (1988). Biophysical studies of the cellular elements of the rabbit carotid body. Neuroscience, 26(1), 291-311.

Duprat, Fabrice, Lesage, Florian, Fink, Michel, Reyes, Roberto, Heurteaux, Catherine, & Lazdunski, Michel. (1997). TASK, a human background K channel to sense external pH variations near physiological pH. The EMBO Journal, 16(17), 5464-5471.

Eichmann, T. O., & Lass, A. (2015). DAG tales: the multiple faces of diacylglycerol—stereochemistry, metabolism, and signaling. Cellular and Molecular Life Sciences, 72, 3931-3952.

Emerling, Brooke M., Viollet, Benoit, Tormos, Kathryn V., & Chandel, Navdeep S. (2007). Compound C inhibits hypoxic activation of HIF-1 independent of AMPK. FEBS Letters, 581(29), 5727-5731.

Enyedi, P., & Czirják, G. (2010). Molecular background of leak K+ currents: two-pore domain potassium channels. Physiological reviews, 90(2), 559-605.

Evans, A. Mark, Mustard, Kirsteen J.W., Wyatt, Christopher N., Peers, Chris, Dipp, Michelle, Kumar, Prem, Kinnear, Nicholas P., and Hardie, D. Grahame. (2005). Does AMP-activated protein kinase couple inhibition of mitochondrial oxidative phosphorylation by hypoxia to calcium signaling in O2-sensing cells?. Journal of Biological Chemistry, 280(50), 41504-41511.

Fagerlund, Malin Jonsson, Kåhlin, Jessica, Ebberyd, Anette, Schulte, Gunnar, Mkrtchian, Souren, & Eriksson, Lars I. (2010). The human carotid body: Expression of oxygen sensing and signaling genes of relevance for anesthesia. Anesthesiology (Philadelphia), 113(6), 1270-1279.

Felippe, I. S. A., Zera, T., da Silva, M. P., Moraes, D. J. A., McBryde, F., & Paton, J. F. R. (2023). The sympathetic nervous system exacerbates

carotid body sensitivity in hypertension. Cardiovascular research, 119(1), 316–331.

Fernández-Agüera, M. Carmen, Gao, Lin, González-Rodríguez, Patricia, Pintado, C. Oscar, Arias-Mayenco, Ignacio, García-Flores, Paula, García-Pergañeda, Antonio, Pascual, Alberto, Ortega-Sáenz, Patricia, and López-Barneo, José. (2015). Oxygen sensing by arterial chemoreceptors depends on mitochondrial complex I signaling. Cell metabolism, 22(5), 825-837.

Flaherty, D. P., Simpson, D. S., Miller, M., Maki, B. E., Zou, B., Shi, J., Wu, M., McManus, O. B., Aubé, J., Li, M., & Golden, J. E. (2014). Potent and selective inhibitors of the TASK-1 potassium channel through chemical optimization of a bis-amide scaffold. Bioorganic & medicinal chemistry letters, 24(16), 3968–3973.

Franks, N. P., & Lieb, W. R. (1982). Molecular mechanisms of general anaesthesia. Nature, 300(5892), 487–493

Gao, D., Zhang, L., Dhillon, R., Hong, T. T., Shaw, R. M., & Zhu, J. (2013). Dynasore protects mitochondria and improves cardiac lusitropy in Langendorff perfused mouse heart. PloS one, 8(4), e60967.

Gao, L., Bonilla-Henao, V., García-Flores, P., Arias-Mayenco, I., Ortega-Sáenz, P., & López-Barneo, J. (2017). Gene expression analyses reveal metabolic specifications in acute $O_2$ -sensing chemoreceptor cells. The Journal of physiology, 595(18), 6091–6120.

Goldstein, S. A., Bayliss, D. A., Kim, D., Lesage, F., Plant, L. D., & Rajan, S. (2005). International Union of Pharmacology. LV. Nomenclature and molecular relationships of two-P potassium channels. Pharmacological reviews, 57(4), 527-540.

Goldstein, S. A., Bockenhauer, D., O'Kelly, I., & Zilberberg, N. (2001). Potassium leak channels and the KCNK family of two-P-domain subunits. Nature Reviews Neuroscience, 2(3), 175-184.

Gonzalez, Constancio, Almaraz, Laura, Obeso, Ana, & Rigual, Ricardo. (1994). Carotid body chemoreceptors: From natural stimuli to sensory discharges. Physiological Reviews, 74(4), 829-898.

Guigas, B., Taleux, N., Foretz, M., Detaille, D., Andreelli, F., Viollet, B., & Hue, L. (2007). AMP-activated protein kinase-independent inhibition of hepatic mitochondrial oxidative phosphorylation by AICA riboside. Biochemical Journal, 404(3), 499-507.

Gurney, A. M., Osipenko, O. N., MacMillan, D., McFarlane, K. M., Tate, R. J., & Kempsill, F. E. J. (2003). Two-pore domain K channel, TASK-1, in pulmonary artery smooth muscle cells. Circulation research, 93(10), 957-964.

Han, G. S., O'Hara, L., Siniossoglou, S., & Carman, G. M. (2008). Characterization of the yeast DGK1-encoded CTP-dependent diacylglycerol kinase. The Journal of biological chemistry, 283(29), 20443–20453.

Hansen, J. T., Brokaw, J., Christie, D., & Karasek, M. (1982). Localization of enkephalin-like immunoreactivity in the cat carotid and aortic body chemoreceptors. The Anatomical record, 203(3), 405–410.

Hartzell, H. C., & Rinderknecht, A. (1996). Calphostin C, a widely used protein kinase C inhibitor, directly and potently blocks L-type Ca channels. The American journal of physiology, 270(5 Pt 1), C1293–C1299.

Heath, D., Edwards, C., & Harris, P. (1970). Post-mortem size and structure of the human carotid body. Thorax, 25(2), 129–140.

Hess A. (1975). Hyposensitivity of deafferented receptor cells in the rat carotid body. Brain research, 98(2), 348–353.

Heymans, C., & Bouckaert, J. J. (1930). Sinus caroticus and respiratory reflexes: I. Cerebral blood flow and respiration. Adrenaline apnœa1. The Journal of physiology, 69(2), 254.

Hill, T. A., Odell, L. R., Quan, A., Abagyan, R., Ferguson, G., Robinson, P. J., & McCluskey, A. (2004). Long chain amines and long chain ammonium salts as novel inhibitors of dynamin GTPase activity. Bioorganic & medicinal chemistry letters, 14(12), 3275–3278.

Hill, T., Odell, L. R., Edwards, J. K., Graham, M. E., McGeachie, A. B., Rusak, J., Quan, A., Abagyan, R., Scott, J. L., Robinson, P. J., & McCluskey, A. (2005). Small molecule inhibitors of dynamin I GTPase activity: development of dimeric tyrphostins. Journal of medicinal chemistry, 48(24), 7781–7788.

Hirshman, C. A., McCullough, R. E., Cohen, P. J., & Weil, J. V. (1977). Depression of hypoxic ventilatory response by halothane, enflurane and isoflurane in dogs. British Journal of Anaesthesia, 49(10), 957-963.

Holmes, Andrew P., Swiderska, Agnieszka, Nathanael, Demitris, Aldossary, Hayyaf S., Ray, Clare J., Coney, Andrew M., & Kumar, Prem. (2022). Are Multiple Mitochondrial Related Signalling Pathways Involved in Carotid Body Oxygen Sensing? Frontiers in Physiology, 13, 908617.

Hopwood, S. E., & Trapp, S. (2005). TASK-like K+ channels mediate effects of 5-HT and extracellular pH in rat dorsal vagal neurones in vitro. The Journal of Physiology, 568(1), 145-154.

Horowitz, L. F., Hirdes, W., Suh, B. C., Hilgemann, D. W., Mackie, K., & Hille, B. (2005). Phospholipase C in living cells: activation, inhibition, Ca2+ requirement, and regulation of M current. The Journal of general physiology, 126(3), 243-262.

Humble, E., & Berglund, L. (1991). Stimulation and inhibition of the activity of rat liver cytosolic phosphatidate phosphohydrolase by various phospholipids. Journal of lipid research, 32(11), 1869–1872.

Huskens, N. (2015). Novel interactions of volatile anaesthetics on O2 sensing and TASK channels in carotid body type-1 cells.

Huskens, N., O'Donohoe, P., Wickens, J. R., McCullagh, J. S., Buckler, K. J., & Pandit, J. J. (2016). A method for continuous and stable perfusion of tissue and single cell preparations with accurate concentrations of volatile anaesthetics. Journal of Neuroscience Methods, 258, 87-93.

Ide, T., Sakurai, Y., Aono, M., & Nishino, T. (1999). Contribution of peripheral chemoreception to the depression of the hypoxic ventilatory response during halothane anesthesia in cats. The Journal of the American Society of Anesthesiologists, 90(4), 1084-1091.

Inoue, M., Matsuoka, H., Harada, K., Mugishima, G., & Kameyama, M. (2020). TASK channels: channelopathies, trafficking, and receptor-mediated inhibition. Pflügers Archiv-European Journal of Physiology, 472, 911-922.

Jackson, A. P., Timmerman, M. P., Bagshaw, C. R., & Ashley, C. C. (1987). The kinetics of calcium binding to fura-2 and indo-1. FEBS letters, 216(1), 35-39.

Jiménez-Gómez, B., Ortega-Sáenz, P., Gao, L., González-Rodríguez, P., García-Flores, P., Chandel, N., & López-Barneo, J. (2023). Transgenic NADH dehydrogenase restores oxygen regulation of breathing in mitochondrial complex I-deficient mice. Nature Communications, 14(1), 1172.

Jones, S. A., Morton, M. J., Hunter, M., & Boyett, M. R. (2002). Expression of TASK-1, a pH-sensitive twin-pore domain K+ channel, in rat myocytes. American Journal of Physiology-Heart and Circulatory Physiology, 283(1), H181-H185.

Kadamur, G., & Ross, E. M. (2013). Mammalian phospholipase C. Annual review of physiology, 75, 127-154.

Karschin, Christine, Wischmeyer, Erhard, Preisig-Müller, Regina, Rajan, Sindhu, Derst, Christian, Grzeschik, Karl-Heinz, Daut, Jürgen, and Karschin, Andreas. (2001). Expression pattern in brain of TASK-1, TASK-3, and a tandem pore domain K+ channel subunit, TASK-5, associated with the central auditory nervous system. Molecular and Cellular Neuroscience, 18(6), 632-648.

Kettunen, Petronella, Hess, Dietmar, & Manira, Abdeljabbar El. (2003). MGluR1, But Not mGluR5, Mediates Depolarization of Spinal Cord Neurons by Blocking a Leak Current. Journal of Neurophysiology, 90(4), 2341-2348.

Kholwadwala, D., & Donnelly, D. F. (1992). Maturation of carotid chemoreceptor sensitivity to hypoxia: in vitro studies in the newborn rat. The Journal of physiology, 453, 461–473.

Kim, D., Cavanaugh, E. J., Kim, I., & Carroll, J. L. (2009). Heteromeric TASK-1/TASK-3 is the major oxygen-sensitive background K+ channel in rat carotid body glomus cells. The Journal of physiology, 587(12), 2963-2975.

Kim, D., Kang, D., Martin, E. A., Kim, I., & Carroll, J. L. (2014). Effects of modulators of AMP-activated protein kinase on TASK-1/3 and intracellular Ca2+ concentration in rat carotid body glomus cells. Respiratory physiology & neurobiology, 195, 19-26.

Kim, I., Yang, D. J., Donnelly, D. F., & Carroll, J. L. (2009). Fluoresceinated peanut agglutinin (PNA) is a marker for live O 2 sensing glomus cells in rat carotid body. Arterial Chemoreceptors: Arterial Chemoreceptors, 185-190.

Kim, Y., Bang, H., & Kim, D. (2000). TASK-3, a new member of the tandem pore K+ channel family. Journal of Biological Chemistry, 275(13), 9340-9347.

Kim, I., Fite, L., Donnelly, D. F., Kim, J. H., & Carroll, J. L. (2015). Possible Role of TRP Channels in Rat Glomus Cells. Advances in experimental medicine and biology, 860, 227–232.

Kim, D., Kim, I., Wang, J., White, C., & Carroll, J. L. (2015). Hydrogen sulfide and hypoxia-induced changes in TASK (K2P3/9) activity and intracellular Ca(2+) concentration in rat carotid body glomus cells. Respiratory physiology & neurobiology, 215, 30–38.

Kiper, A. K., Rinné, S., Rolfes, C., Ramírez, D., Seebohm, G., Netter, M. F., González, W., & Decher, N. (2015). Kv1.5 blockers preferentially inhibit TASK-1 channels: TASK-1 as a target against atrial fibrillation and obstructive sleep apnea?. Pflugers Archiv : European journal of physiology, 467(5), 1081–1090.

Knill, R. L., & Gelb, A. W. (1978). Ventilatory responses to hypoxia and hypercapnia during halothane sedation and anesthesia in man. Anesthesiology, 49(4), 244-251.

Kréneisz, O., Benoit, J. P., Bayliss, D. A., & Mulkey, D. K. (2009). AMP-activated protein kinase inhibits TREK channels. The Journal of physiology, 587(24), 5819-5830.

Krylov, S.A. and Anichkov, S.V. (1968). In Arterial Chemoreceptors, R.W. Torrance (ed.), Oxford, Blackwell, pp. 103–113.

Kumar, P., Pearson, S. and Gu, Y. (2006), A role for TRP channels in carotid body chemotransduction?. The FASEB Journal, 20: A1229-A1229.

Kumar, P., & Prabhakar, N. R. (2012). Peripheral chemoreceptors: function and plasticity of the carotid body. Comprehensive Physiology, 2(1), 141–219.

Larkman, P. M., & Perkins, E. M. (2005). A TASK-like pH-and amine-sensitive 'leak'K+ conductance regulates neonatal rat facial motoneuron excitability in vitro. European Journal of Neuroscience, 21(3), 679-691.

Lever JD, Lewis PR, Boyd JD (1959) Observations on the fine structure and histochemistry of the carotid body in the cat and rabbit. Journal Of Anatomy, 93, 478-490.

Lewis, A., Hartness, M. E., Chapman, C. G., Fearon, I. M., Meadows, H. J., Peers, C., & Kemp, P. J. (2001). Recombinant hTASK1 is an O2-

sensitive K+ channel. Biochemical and biophysical research communications, 285(5), 1290-1294.

Li Wu, BAUER, Claudia S, ZHEN, Xiao-Guang, Cheng Xie, & YANG, Jian. (2002). Dual regulation of voltage-gated calcium channels by PtdIns(4,5)P2. Nature (London), 419(6910), 947-952.

Linden, A. M., Sandu, C., Aller, M. I., Vekovischeva, O. Y., Rosenberg, P. H., Wisden, W., & Korpi, E. R. (2007). TASK-3 knockout mice exhibit exaggerated nocturnal activity, impairments in cognitive functions, and reduced sensitivity to inhalation anesthetics. Journal of Pharmacology and Experimental Therapeutics, 323(3), 924-934.

Linden, Anni-Maija, Aller, M. Isabel, Leppä, Elli, Vekovischeva, Olga, Aitta-Aho, Teemu, Veale, Emma L., Mathie, Alistair, Rosenberg, Per, Wisden, William, and Korpi, Esa R. (2006). The in vivo contributions of TASK-1-containing channels to the actions of inhalation anesthetics, the α2 adrenergic sedative dexmedetomidine, and cannabinoid agonists. The Journal of Pharmacology and Experimental Therapeutics, 317(2), 615-626.

Lindner, M., Leitner, M. G., Halaszovich, C. R., Hammond, G. R., & Oliver, D. (2011). Probing the regulation of TASK potassium channels by PI (4, 5) P2 with switchable phosphoinositide phosphatases. The Journal of Physiology, 589(13), 3149-3162.

Lingelem, A. B. D., Kavaliauskiene, S., Halsne, R., Klokk, T. I., Surma, M. A., Klose, C., Skotland, T., & Sandvig, K. (2021). Diacylglycerol kinase and phospholipase D inhibitors alter the cellular lipidome and endosomal sorting towards the Golgi apparatus. Cellular and molecular life sciences : CMLS, 78(3), 985–1009.

Litosch, I. (2016). Decoding Gαq signaling. Life sciences, 152, 99-106.

Lolicato, M., Riegelhaupt, P. M., Arrigoni, C., Clark, K. A., & Minor, D. L. (2014). Transmembrane helix straightening and buckling underlies activation of mechanosensitive and thermosensitive K2P channels. Neuron, 84(6), 1198-1212.

Lopes, C. M., Rohács, T., Czirják, G., Balla, T., Enyedi, P., & Logothetis, D. E. (2005). PIP2 hydrolysis underlies agonist-induced inhibition and regulates voltage gating of two-pore domain K+ channels. The Journal of physiology, 564(1), 117-129.

Lopez-Barneo J, Lopez-Lopez JR, Urena J, Gonzalez C (1988) Chemotransduction in the carotid body: K+ current modulated by pO2 in type I chemoreceptor cells. Science, 241, 580-582.

López-Barneo, J., Macías, D., Platero-Luengo, A., Ortega-Sáenz, P., & Pardal, R. (2016). Carotid body oxygen sensing and adaptation to hypoxia. Pflügers Archiv-European Journal of Physiology, 468, 59-70.

López-Barneo, J., Pardal, R., & Ortega-Sáenz, P. (2001). Cellular mechanism of oxygen sensing. Annual review of physiology, 63(1), 259-287.

López-López, J. R., Gonzalez, C., & Perez-Garcia, M. T. (1997). Properties of ionic currents from isolated adult rat carotid body chemoreceptor cells: effect of hypoxia. The Journal of Physiology, 499(2), 429-441.

Lopez-Lopez, J., González, C., Urena, J., & López-Barneo, J. (1989). Low pO2 selectively inhibits K channel activity in chemoreceptor cells of the mammalian carotid body. The Journal of general physiology, 93(5), 1001-1015.

Ludbrook J. (1990). Cardiovascular reflexes from cardiac sensory receptors. Australian and New Zealand journal of medicine, 20(4), 597–606.

Ma, Q., Gabelli, S. B., & Raben, D. M. (2019). Diacylglycerol kinases: Relationship to other lipid kinases. Advances in biological regulation, 71, 104–110.

Macia, Ehrlich, M., Massol, R., Boucrot, E., Brunner, C., & Kirchhausen, T. (2006). Dynasore, a Cell-Permeable Inhibitor of Dynamin. Developmental Cell, 10(6), 839–850.

MacMillan S, Holmes AP, Dallas ML, Mahmoud AD, Shipston MJ, Peers C, Hardie DG, Kumar P, Evans AM. (2022). LKB1 is the gatekeeper of carotid body chemosensing and the hypoxic ventilatory response. Commun Biol 5:642

Mahmoud, A. D., Lewis, S., Juričić, L., Udoh, U. A., Hartmann, S., Jansen, M. A., Ogunbayo, O. A., Puggioni, P., Holmes, A. P., Kumar, P., Navarro-Dorado, J., Foretz, M., Viollet, B., Dutia, M. B., Marshall, I., & Evans, A. M. (2016). AMP-activated Protein Kinase Deficiency Blocks the Hypoxic Ventilatory Response and Thus Precipitates Hypoventilation and Apnea. American journal of respiratory and critical care medicine, 193(9), 1032–1043.

Mathie, A., Al-Moubarak, E., & Veale, E. L. (2010). SYMPOSIUM REVIEW: Gating of two pore domain potassium channels. The Journal of physiology, 588(17), 3149-3156.

Matsuoka, H., & Inoue, M. (2017). Molecular mechanism for muscarinic M1 receptor-mediated endocytosis of TWIK-related acid-sensitive K+ 1

channels in rat adrenal medullary cells. The Journal of Physiology, 595(22), 6851-6867.

Matsuoka, H., Harada, K., Nakamura, J., & Inoue, M. (2013). Nerve growth factor-induced endocytosis of TWIK-related acid-sensitive K+ 1 channels in adrenal medullary cells and PC12 cells. Pflügers Archiv-European Journal of Physiology, 465, 1051-1064.

McDonald, D. M. (1981). Peripheral chemoreceptors: structure-function relationships of the carotid body. Regulation of breathing, 17(pt 1), 105-319.

McDonald, D. M., & Blewett, R. W. (1981). Location and size of carotid body-like organs (paraganglia) revealed in rats by the permeability of blood vessels to Evans blue dye. Journal of neurocytology, 10(4), 607–643.

McDonald, D. M., & Larue, D. T. (1983). The ultrastructure and connections of blood vessels supplying the rat carotid body and carotid sinus. Journal of neurocytology, 12(1), 117–153.

McDonald, D. M., & Mitchell, R. A. (1981). The neural pathway involved in efferent inhibition of chemoreceptors in the cat carotid body. The Journal of comparative neurology, 201(3), 457–476.

McDonald, D.M., & Mitchell, R.A. (1975). The innervation of glomus cells, ganglion cells and blood vessels in the rat carotid body: A quantitative ultrastructural analysis. Journal of Neurocytology, 4, 177-230.

Meier, K. E., Gause, K. C., Wisehart-Johnson, A. E., Gore, A. C., Finley, E. L., Jones, L. G., Bradshaw, C. D., McNair, A. F., & Ella, K. M. (1998). Effects of propranolol on phosphatidate phosphohydrolase and mitogen-

activated protein kinase activities in A7r5 vascular smooth muscle cells. Cellular signalling, 10(6), 415–426.

Meuth, S. G., Budde, T., Kanyshkova, T., Broicher, T., Munsch, T., & Pape, H. C. (2003). Contribution of TWIK-related acid-sensitive K+ channel 1 (TASK1) and TASK3 channels to the control of activity modes in thalamocortical neurons. Journal of Neuroscience, 23(16), 6460-6469.

Michal, P., Lysíková, M., & Tucek, S. (2001). Dual effects of muscarinic M(2) acetylcholine receptors on the synthesis of cyclic AMP in CHO cells: dependence on time, receptor density and receptor agonists. British journal of pharmacology, 132(6), 1217–1228.

Millar, J. A., Barratt, L., Southan, A. P., Page, K. M., Fyffe, R. E., Robertson, B., & Mathie, A. (2000). A functional role for the two-pore domain potassium channel TASK-1 in cerebellar granule neurons. Proceedings of the National Academy of Sciences, 97(7), 3614-3618.

Miller, A. N., & Long, S. B. (2012). Crystal structure of the human two–pore domain potassium channel K2P1. Science, 335(6067), 432-436.

Mills, E., & Jöbsis, F. F. (1972). Mitochondrial respiratory chain of carotid body and chemoreceptor response to changes in oxygen tension. Journal of neurophysiology, 35(4), 405–428.

Milsom, W. K., & Burleson, M. L. (2007). Peripheral arterial chemoreceptors and the evolution of the carotid body. Respiratory physiology & neurobiology, 157(1), 4–11.

Mkrtchian, S., Kåhlin, J., Ebberyd, A., Gonzalez, C., Sanchez, D., Balbir, A., Kostuk, E. W., Shirahata, M., Fagerlund, M. J., & Eriksson, L. I. (2012). The human carotid body transcriptome with focus on oxygen sensing and

inflammation--a comparative analysis. The Journal of physiology, 590(16), 3807–3819.

Moreno-Domínguez, A., Ortega-Sáenz, P., Gao, L., Colinas, O., García-Flores, P., Bonilla-Henao, V., Aragonés, J., Hüttemann, M., Grossman, L. I., Weissmann, N., Sommer, N., & López-Barneo, J. (2020). Acute $O_2$ sensing through HIF2α-dependent expression of atypical cytochrome oxidase subunits in arterial chemoreceptors. Science signaling, 13(615), eaay9452.

Musset, B., Meuth, S. G., Liu, G. X., Derst, C., Wegner, S., Pape, H. C., Budde, T., Preisig-Müller, R., & Daut, J. (2006). Effects of divalent cations and spermine on the K+ channel TASK-3 and on the outward current in thalamic neurons. The Journal of physiology, 572(Pt 3), 639–657.

Nurse C. A. (2014). Synaptic and paracrine mechanisms at carotid body arterial chemoreceptors. *The Journal of physiology*, *592*(16), 3419–3426.

Nurse, C. A., Leonard, E. M., & Salman, S. (2018). Role of glial-like type II cells as paracrine modulators of carotid body chemoreception. Physiological genomics, 50(4), 255–262.

O'Donohoe, P. B., Huskens, N., Turner, P. J., Pandit, J. J., & Buckler, K. J. (2018). A1899, PK-THPP, ML365, and Doxapram inhibit endogenous TASK channels and excite calcium signalling in carotid body type-1 cells. Physiological reports, 6(19), e13876.

Olschewski, A., Li, Y., Tang, B., Hanze, J., Eul, B., Bohle, R. M., Wilhelm, J., Morty, R. E., Brau, M. E., Weir, E. K., Kwapiszewska, G., Klepetko, W., Seeger, W., & Olschewski, H. (2006). Impact of TASK-1 in human pulmonary artery smooth muscle cells. Circulation research, 98(8), 1072–1080.

Ortega-Sáenz, P., & López-Barneo, J. (2020). Physiology of the carotid body: from molecules to disease. Annual review of physiology, 82, 127-149.

Ortega-Sáenz, P., Pardal, R., García-Fernández, M., & López-Barneo, J. (2003). Rotenone selectively occludes sensitivity to hypoxia in rat carotid body glomus cells. The Journal of physiology, 548(3), 789-800.

Ortega-Sáenz, P., Pascual, A., Gómez-Díaz, R., & López-Barneo, J. (2006). Acute oxygen sensing in heme oxygenase-2 null mice. The Journal of general physiology, 128(4), 405–411.

Ortiz, F. C., & Varas, R. (2010). Muscarinic modulation of TASK-like background potassium channel in rat carotid body chemoreceptor cells. Brain research, 1323, 74-83.

Pandit, J. J. (2002). The variable effect of low-dose volatile anaesthetics on the acute ventilatory response to hypoxia in humans: a quantitative review. Anaesthesia, 57(7), 632-643.

Pandit, J. J., Winter, V., Bayliss, R., & Buckler, K. J. (2010). Differential effects of halothane and isoflurane on carotid body glomus cell intracellular Ca 2+ and background K+ channel responses to hypoxia. In New Frontiers in Respiratory Control: XIth Annual Oxford Conference on Modeling and Control of Breathing (pp. 205-208). Springer New York.

Pandit, Jaideep J, Huskens, Nicky, O'Donohoe, Peadar B, Turner, Philip J, & Buckler, Keith J. (2020). Competitive Interactions between Halothane and Isoflurane at the Carotid Body and TASK Channels. Anesthesiology (Philadelphia), 133(5), 1046-1059.

Pang, D. S., Robledo, C. J., Carr, D. R., Gent, T. C., Vyssotski, A. L., Caley, A., Zecharia, A. Y., Wisden, W., Brickley, S. G., & Franks, N. P. (2009). An unexpected role for TASK-3 potassium channels in network oscillations with implications for sleep mechanisms and anesthetic action. Proceedings of the National Academy of Sciences of the United States of America, 106(41), 17546–17551.

Papreck, J. R., Martin, E. A., Lazzarini, P., Kang, D., & Kim, D. (2012). Modulation of K 2P 3.1 (TASK-1), K 2P 9.1 (TASK-3), and TASK-1/3 heteromer by reactive oxygen species. Pflügers Archiv-European Journal of Physiology, 464, 471-480.

Pardal, R., Ortega-Sáenz, P., Durán, R., & López-Barneo, J. (2007). Glia-like stem cells sustain physiologic neurogenesis in the adult mammalian carotid body. Cell, 131(2), 364-377.

Patel, A. J., Honoré, E., Lesage, F., Fink, M., Romey, G., & Lazdunski, M. (1999). Inhalational anesthetics activate two-pore-domain background K+ channels. Nature neuroscience, 2(5), 422-426.

Peng, Y. J., Gridina, A., Wang, B., Nanduri, J., Fox, A. P., & Prabhakar, N. R. (2020). Olfactory receptor 78 participates in carotid body response to a wide range of low $O_2$ levels but not severe hypoxia. Journal of neurophysiology, 123(5), 1886–1895.

Peng, Y. J., Nanduri, J., Wang, N., Kumar, G. K., Bindokas, V., Paul, B. D., Chen, X., Fox, A. P., Vignane, T., Filipovic, M. R., & Prabhakar, N. R. (2023). Hypoxia sensing requires $H_2S$-dependent persulfidation of olfactory receptor 78. Science advances, 9(27), eadf3026.

Peng, Y. J., Raghuraman, G., Khan, S. A., Kumar, G. K., & Prabhakar, N. R. (2011). Angiotensin II evokes sensory long-term facilitation of the carotid

body via NADPH oxidase. Journal of applied physiology (Bethesda, Md. : 1985), 111(4), 964–970.

Perrier, J. F., Alaburda, A., & Hounsgaard, J. (2003). 5-HT1A receptors increase excitability of spinal motoneurons by inhibiting a TASK-1-like K+ current in the adult turtle. The Journal of physiology, 548(2), 485-492.

Piechotta, P. L., Rapedius, M., Stansfeld, P. J., Bollepalli, M. K., Ehrlich, G., Andres-Enguix, I., Fritzenschaft, H., Decher, N., Sansom, M. S., Tucker, S. J., & Baukrowitz, T. (2011). The pore structure and gating mechanism of K2P channels. The EMBO journal, 30(17), 3607–3619.

Pietruschka F (1974) Cytochemical demonstration of catecholamines in cells of the carotid body in primary tissue culture. Cell And Tissue Research, 151, 317-321.

Platero-Luengo, A., González-Granero, S., Durán, R., Díaz-Castro, B., Piruat, J. I., García-Verdugo, J. M., Pardal, R., & López-Barneo, J. (2014). An O2-sensitive glomus cell-stem cell synapse induces carotid body growth in chronic hypoxia. Cell, 156(1-2), 291–303.

Prabhakar, N. R. (2006). O2 sensing at the mammalian carotid body: why multiple O2 sensors and multiple transmitters?. Experimental physiology, 91(1), 17-23.

Prabhakhar, N. R., & Joyner, M. J. (2015). Tasting arterial blood: what do the carotid chemoreceptors sense?. Frontiers in physiology, 5, 524.

Prentki, Marc, & Madiraju, S. R. Murthy. (2008). Glycerolipid Metabolism and Signaling in Health and Disease. Endocrine Reviews, 29(6), 647-676.

Preta, G., Cronin, J. G., & Sheldon, I. M. (2015). Dynasore - not just a dynamin inhibitor. Cell communication and signaling : CCS, 13, 24.

Putzke, C., Hanley, P. J., Schlichthörl, G., Preisig-Müller, R., Rinné, S., Anetseder, M., Eckenhoff, R., Berkowitz, C., Vassiliou, T., Wulf, H., & Eberhart, L. (2007). Differential effects of volatile and intravenous anesthetics on the activity of human TASK-1. American journal of physiology. Cell physiology, 293(4), C1319–C1326.

Putzke, C., Wemhöner, K., Sachse, F. B., Rinné, S., Schlichthörl, G., Li, X. T., Jaé, L., Eckhardt, I., Wischmeyer, E., Wulf, H., Preisig-Müller, R., Daut, J., & Decher, N. (2007). The acid-sensitive potassium channel TASK-1 in rat cardiac muscle. Cardiovascular research, 75(1), 59–68.

Quan, A., McGeachie, A. B., Keating, D. J., van Dam, E. M., Rusak, J., Chau, N., Malladi, C. S., Chen, C., McCluskey, A., Cousin, M. A., & Robinson, P. J. (2007). Myristyl trimethyl ammonium bromide and octadecyl trimethyl ammonium bromide are surface-active small molecule dynamin inhibitors that block endocytosis mediated by dynamin I or dynamin II. Molecular pharmacology, 72(6), 1425–1439.

Rajan, S., Wischmeyer, E., Liu, G. X., Preisig-Muller, R., Daut, J., Karschin, A., & Derst, C. (2000). TASK-3, a novel tandem pore domain acid-sensitive K+ channel: an extracellular histidine as pH sensor. Journal of Biological Chemistry, 275(22), 16650-16657.

Rakoczy, R. J., & Wyatt, C. N. (2018). Acute oxygen sensing by the carotid body: a rattlebag of molecular mechanisms. The Journal of physiology, 596(15), 2969–2976.

Reddy P. H. (2014). Inhibitors of mitochondrial fission as a therapeutic strategy for diseases with oxidative stress and mitochondrial dysfunction. Journal of Alzheimer's disease : JAD, 40(2), 245–256.

Renigunta, V., Schlichthörl, G., & Daut, J. (2015). Much more than a leak: structure and function of K 2P-channels. Pflügers Archiv-European Journal of Physiology, 467, 867-894.

Rigual, R., Gonzalez, E., Fidone, S., & Gonzalez, C. (1984). Effects of low pH on synthesis and release of catecholamines in the cat carotid body in vitro. Brain research, 309(1), 178–181

Rjasanow, A., Leitner, M. G., Thallmair, V., Halaszovich, C. R., & Oliver, D. (2015). Ion channel regulation by phosphoinositides analyzed with VSPs—PI (4, 5) P2 affinity, phosphoinositide selectivity, and PI (4, 5) P2 pool accessibility. Frontiers in pharmacology, 6, 127.

Rödström, K. E. J., Kiper, A. K., Zhang, W., Rinné, S., Pike, A. C. W., Goldstein, M., Conrad, L. J., Delbeck, M., Hahn, M. G., Meier, H., Platzk, M., Quigley, A., Speedman, D., Shrestha, L., Mukhopadhyay, S. M. M., Burgess-Brown, N. A., Tucker, S. J., Müller, T., Decher, N., & Carpenter, E. P. (2020). A lower X-gate in TASK channels traps inhibitors within the vestibule. Nature, 582(7812), 443–447.

Rong, W., Gourine, A. V., Cockayne, D. A., Xiang, Z., Ford, A. P., Spyer, K. M., & Burnstock, G. (2003). Pivotal role of nucleotide P2X2 receptor subunit of the ATP-gated ion channel mediating ventilatory responses to hypoxia. The Journal of neuroscience: the official journal of the Society for Neuroscience, 23(36), 11315–11321.

Sampson, S.R. (1972). Mechanism of efferent inhibition of carotid body chemoreceptors in the cat. Brain Research, 45(1), 266-270.

Schiekel, J., Lindner, M., Hetzel, A., Wemhöner, K., Renigunta, V., Schlichthörl, G., Decher, N., Oliver, D., & Daut, J. (2013). The inhibition of the potassium channel TASK-1 in rat cardiac muscle by endothelin-1 is mediated by phospholipase C. Cardiovascular research, 97(1), 97–105.

Sharma, A. K., & Wolfrum, C. (2023). Lipid cycling isn't all futile. Nature metabolism, 5(4), 540–541.

Shirahata, M., Hirasawa, S., Okumura, M., Mendoza, J. A., Okumura, A., Balbir, A., & Fitzgerald, R. S. (2004). Identification of M1 and M2 muscarinic acetylcholine receptors in the cat carotid body chemosensory system. Neuroscience, 128(3), 635–644.

Sirois, J. E., Lei, Q., Talley, E. M., Lynch, C., & Bayliss, D. A. (2000). The TASK-1 two-pore domain K+ channel is a molecular substrate for neuronal effects of inhalation anesthetics. Journal of Neuroscience, 20(17), 6347-6354.

Sirois, J. E., Lynch III, C., & Bayliss, D. A. (2002). Convergent and reciprocal modulation of a leak K+ current and Ih by an inhalational anaesthetic and neurotransmitters in rat brainstem motoneurones. The Journal of physiology, 541(3), 717-729.

Slingo, M. E. (2013). The role of the hypoxia-inducible pathway in metabolism and cardiopulmonary physiology (Doctoral dissertation, University of Oxford).

Smith, R. J., Sam, L. M., Justen, J. M., Bundy, G. L., Bala, G. A., & Bleasdale, J. E. (1990). Receptor-coupled signal transduction in human polymorphonuclear neutrophils: effects of a novel inhibitor of phospholipase C-dependent processes on cell responsiveness. The Journal of pharmacology and experimental therapeutics, 253(2), 688–697.

Sörmann, Janina, Schewe, Marcus, Proks, Peter, Jouen-Tachoire, Thibault, Rao, Shanlin, Riel, Elena B., Agre, Katherine E., Begtrup, Amber, Dean, John, Descartes, Maria, Fischer, Jan, Gardham, Alice, Lahner, Carrie, Mark, Paul R., Muppidi, Srikanth, Pichurin, Pavel N., Porrmann, Joseph, Schallner, Jens, Smith, Kirstin, Straub, Volker, Vasudevan, Pradeep, Willaert, Rebecca, Carpenter, Elisabeth P., Rödström, Karin E. J., Hahn, Michael G., Müller, Thomas, Baukrowitz, Thomas, Hurles, Matthew E., Wright, Caroline F., and Tucker, Stephen J. (2022). Gain-of-function mutations in KCNK3 cause a developmental disorder with sleep apnea. Nature Genetics, 54(10), 1534-1543.

Steinberg, E. A., Wafford, K. A., Brickley, S. G., Franks, N. P., & Wisden, W. (2015). The role of k2p channels in anaesthesia and sleep. Pflügers Archiv-European Journal of Physiology, 467, 907-916.

Streit, A. K., Netter, M. F., Kempf, F., Walecki, M., Rinné, S., Bollepalli, M. K., Preisig-Müller, R., Renigunta, V., Daut, J., Baukrowitz, T., Sansom, M. S., Stansfeld, P. J., & Decher, N. (2011). A specific two-pore domain potassium channel blocker defines the structure of the TASK-1 open pore. The Journal of biological chemistry, 286(16), 13977–13984.

Summers, B. A., Overholt, J. L., & Prabhakar, N. R. (2000). Augmentation of L-type calcium current by hypoxia in rabbit carotid body glomus cells: evidence for a PKC-sensitive pathway. Journal of neurophysiology, 84(3), 1636–1644.

Suh, B. C., Inoue, T., Meyer, T., & Hille, B. (2006). Rapid chemically induced changes of PtdIns (4, 5) P2 gate KCNQ ion channels. Science, 314(5804), 1454-1457.

Swiderska, A., Coney, A. M., Alzahrani, A. A., Aldossary, H. S., Batis, N., Ray, C. J., Kumar, P., & Holmes, A. P. (2021). Mitochondrial Succinate Metabolism and Reactive Oxygen Species Are Important but Not Essential for Eliciting Carotid Body and Ventilatory Responses to Hypoxia in the Rat. Antioxidants (Basel, Switzerland), 10(6), 840.

Tafesse, Fikadu Geta, Ternes, Philipp, & Holthuis, Joost C.M. (2006). The Multigenic Sphingomyelin Synthase Family. The Journal of Biological Chemistry, 281(40), 29421-29425.

Talley, E. M., & Bayliss, D. A. (2002). Modulation of TASK-1 (Kcnk3) and TASK-3 (Kcnk9) potassium channels: volatile anesthetics and neurotransmitters share a molecular site of action. Journal of Biological Chemistry, 277(20), 17733-17742.

Talley, E. M., Lei, Q., Sirois, J. E., & Bayliss, D. A. (2000). TASK-1, a two–pore domain K+ channel, is modulated by multiple neurotransmitters in motoneurons. Neuron, 25(2), 399-410.

Temes, E., Martín-Puig, S., Aragonés, J., Jones, D. R., Olmos, G., Mérida, I., & Landázuri, M. O. (2004). Role of diacylglycerol induced by hypoxia in the regulation of HIF-1α activity. Biochemical and biophysical research communications, 315(1), 44-50.

Thompson, C. M. (2010). Presynaptic Regulation of Carotid Body Type I Cells by Histaminergic and Muscarinic Receptors (Doctoral dissertation, Wright State University).

Tietze, D., Kaufmann, D., Tietze, A. A., Voll, A., Reher, R., König, G., & Hausch, F. (2019). Structural and Dynamical Basis of G Protein Inhibition by YM-254890 and FR900359: An Inhibitor in Action. Journal of chemical information and modeling, 59(10), 4361–4373.

Torres-Torrelo, Hortensia, Ortega-Sáenz, Patricia, Macías, David, Omura, Masayo, Zhou, Ting, Matsunami, Hiroaki, Johnson, Randall S., Mombaerts, Peter, and López-Barneo, José. (2018). The role of Olfr78 in the breathing circuit of mice. Nature (London), 561(7724), E33-E40.

Turner, P. J., & Buckler, K. J. (2013). Oxygen and mitochondrial inhibitors modulate both monomeric and heteromeric TASK-1 and TASK-3 channels in mouse carotid body type-1 cells. The Journal of physiology, 591(23), 5977-5998.

Ureña, J., López-López, J., González, C., & López-Barneo, J. (1989). Ionic currents in dispersed chemoreceptor cells of the mammalian carotid body. The Journal of general physiology, 93(5), 979-999.

Varas, R., Wyatt, C. N., & Buckler, K. J. (2007). Modulation of TASK-like background potassium channels in rat arterial chemoreceptor cells by intracellular ATP and other nucleotides. The Journal of physiology, 583(2), 521-536.

Veale, E. L., Kennard, L. E., Sutton, G. L., MacKenzie, G., Sandu, C., & Mathie, A. (2007). Gαq-mediated regulation of TASK3 two-pore domain potassium channels: the role of protein kinase C. Molecular pharmacology, 71(6), 1666-1675.

Verna, A. (1979). Ultrastructure of the carotid body in the mammals. International Review of Cytology, 60, 271-330.

Wang, J P. (1996). U-73122, an aminosteroid phospholipase C inhibitor, may also block Ca2 influx through phospholipase C-independent mechanism in neutrophil activation. Naunyn-Schmiedeberg's Archives of Pharmacology, 353(6), 599-605.

Wang, Z. Z., Stensaas, L. J., Dinger, B. G., & Fidone, S. J. (1995). Nitric oxide mediates chemoreceptor inhibition in the cat carotid body. Neuroscience, 65(1), 217–229.

Wang, J., Hogan, J. O., Wang, R., White, C., & Kim, D. (2017). Role of cystathionine-γ-lyase in hypoxia-induced changes in TASK activity, intracellular [$Ca^{2+}$] and ventilation in mice. Respiratory physiology & neurobiology, 246, 98–106.

Weir, E. K., López-Barneo, J., Buckler, K. J., & Archer, S. L. (2005). Acute oxygen-sensing mechanisms. New England Journal of Medicine, 353(19), 2042-2055.

Weis, W. I., & Kobilka, B. K. (2018). The molecular basis of G protein–coupled receptor activation. Annual review of biochemistry, 87, 897-919.

Wickman, K, & Clapham, D. E. (1995). Ion channel regulation by G proteins. Physiological Reviews, 75(4), 865-885.

Wilke, Bettina U., Lindner, Moritz, Greifenberg, Lea, Albus, Alexandra, Kronimus, Yannick, Bünemann, Moritz, Leitner, Michael G., and Oliver, Dominik. (2014). Diacylglycerol mediates regulation of TASK potassium channels by Gq-coupled receptors. Nature communications, 5(1), 5540.

Williams, B. A., & Buckler, K. J. (2004). Biophysical properties and metabolic regulation of a TASK-like potassium channel in rat carotid body type 1 cells. American Journal of Physiology-Lung Cellular and Molecular Physiology, 286(1), L221-L230.

Wu, W. I., & Carman, G. M. (1994). Regulation of phosphatidate phosphatase activity from the yeast Saccharomyces cerevisiae by nucleotides. The Journal of biological chemistry, 269(47), 29495–29501.

Wunderling, Zurkovic, J., Zink, F., Kuerschner, L., & Thiele, C. (2023). Triglyceride cycling enables modification of stored fatty acids. Nature Metabolism, 5(4), 699–709.

Wyatt, C. N., & Buckler, K. J. (2004). The effect of mitochondrial inhibitors on membrane currents in isolated neonatal rat carotid body type I cells. The Journal of physiology, 556(1), 175-191.

Wyatt, Christopher N., Mustard, Kirsty J., Pearson, Selina A., Dallas, Mark L, Atkinson, Lucy, Kumar, Prem, Peers, Chris, Hardie, D. Grahame, and Evans, A. Mark. (2007). AMP-activated protein kinase mediates carotid body excitation by hypoxia. Journal of Biological Chemistry, 282(11), 8092-8098.

Xia, Hui Jun, & Yang, Guang. (2005). Inositol 1,4,5-trisphosphate 3-kinases: Functions and regulations. Cell Research, 15(2), 83-91

Xu, J., Tse, F. W., & Tse, A. (2003). ATP triggers intracellular Ca2+ release in type II cells of the rat carotid body. The Journal of physiology, 549(3), 739-747.

Yadav, V. R., Song, T., Joseph, L., Mei, L., Zheng, Y. M., & Wang, Y. X. (2013). Important role of PLC-γ1 in hypoxic increase in intracellular calcium in pulmonary arterial smooth muscle cells. American journal of physiology. Lung cellular and molecular physiology, 304(3), L143–L151.

Yamamoto, Y., & Taniguchi, K. (2006). Expression of tandem P domain K+ channel, TREK-1, in the rat carotid body. The journal of histochemistry and cytochemistry : official journal of the Histochemistry Society, 54(4), 467–472.

Yokoyama, T., Nakamuta, N., Kusakabe, T., & Yamamoto, Y. (2015). Serotonin-mediated modulation of hypoxia-induced intracellular calcium responses in glomus cells isolated from rat carotid body. Neuroscience letters, 597, 149–153.

Zhang, M., & Nurse, C. A. (2000). Does endogenous 5-HT mediate spontaneous rhythmic activity in chemoreceptor clusters of rat carotid body?. *Brain research*, *872*(1-2), 199–203.

Zhang, M., Fearon, I. M., Zhong, H., & Nurse, C. A. (2003). Presynaptic modulation of rat arterial chemoreceptor function by 5-HT: role of K+ channel inhibition via protein kinase C. The Journal of physiology, 551(Pt 3), 825–842.

Zhang, M., & Nurse, C. A. (2004). CO2/pH chemosensory signalling in co-cultures of rat carotid body receptors and petrosal neurons: role of ATP and ACh. Journal of neurophysiology, 92(6), 3433–3445.

Zhou, T., Chien, M. S., Kaleem, S., & Matsunami, H. (2016). Single cell transcriptome analysis of mouse carotid body glomus cells. The Journal of Physiology, 594(15), 4225-4251.